The pre-nucleation of zeolites: a theoretical approach

José Miguel Mora Fonz

Centre for Theoretical and Computational Chemistry
Department of Chemistry,

University College London

London, December 2006

A thesis submitted for the degree of Doctor of Philosophy

ProQuest LLC
789 East Eisenhower Parkway
P.O. Box 1346
Ann Arbor, MI 48106-1346

I, José Miguel Mora Fonz, confirm that the work presented in this thesis is my own. Where information has been derived from other sources, I confirm that this has been indicated in the thesis.

London, December 2006

ABSTRACT

The reactions and clusters involved in the first stage of nucleation of high silica zeolites are studied using computational methods. A method is developed which gives accurate energetics compared with experiment. Characteristic thermodynamical properties (enthalpy, entropy and Gibbs free energy) for the reactions of silicates up to 12 silicon atoms are presented. The silicate geometry and energy were calculated with a standard density functional method (DFT): BLYP/DNP//BLYP/DNP. A DFT simulated annealing is performed before the geometry optimisation, to avoid local minima. Solvation is modelled with a continuum dielectric method (COSMO), and in some cases with explicit water molecules; the thermodynamical properties (including Zero Point Energy Correction) are calculated with standard statistical mechanical methods.

High accuracy in deprotonation energies could be obtained with the model employed. The results reveal the crucial role of high pH in creating anionic silicate species, which can condense linearly, while solvation offers a stable environment for those anions. The important cyclic condensations, which produce the ring structures present in every zeolite crystal, are driven by a large positive change in the entropy. pH and temperature in some cases allow selective condensations. However, uniquely, 4-ring species are found to be very stable under most of the conditions considered (pH and temperature).

The conditions for the specific cyclization of important ring structures including three, four, five and double-four rings is discussed. The interaction between silicate clusters and water molecules is investigated and an important silicate-silicate interaction is found which could be responsible for the driving force to form silicate aggregates, a crucial step in zeolite synthesis.

CONTENTS

LIST OF FIGURES

LIST OF TABLES

ACKNOWLEDGMENTS

I want to thank to the following people for their support during my PhD.

A mi familia: Mamá, Papá, Arturo, Lupita y David, gracias por haber caminado conmigo, por todo el cariño y apoyo que me dieron. Durante mi doctorado, su constante presencia domingo a domingo, mantuvo mi corazón feliz y el espíritu en alto.

A todos mis amigos allá en México, que a pesar de la distancia estuvieron presentes durante estos años: Karen Cárdenas, Araceli Azuara, Righel Morales, Mariana Prieto, Erika Cisneros, Nadia Silvestry, Tania Blanco, Lisset Montaño y Laura Sierra. A todos ustedes mi sincera gratitud.

During my PhD, here in London, I made very good friends that showed me their support in completing this PhD: Isabel Cortes, Italia Boliver, Nancy López, Gabriel Olarte, Guayana Páez, Carmen Torres, Ben Goerz, María Gómez, Eve Arnera, Antonio Torrisi, Said Hamad, Ricardo Grau and all the friends in room 105, Clare Bishop, Davy Adriaens, Bevan Sharma, Dimitris and Fedor Goumanns. Thanks to Laura Fortunato and especially to my rescuer friend Viky Martzoukou.

The most challenging moments in completing my PhD were easier because you were there always when I needed you; Rinita, all my love to you. You and Ana gave me love and tenderness, thank you.

To my supervisors, Prof. Richard Catlow and Dr. Dewi Lewis my deepest gratitude for all the advise, guidance, permanent encouragement and support in this early stage of my scientific career.

To all the institutions that supported me in this scientific enterprise: Consejo Nacional de Ciencia y Tecnología (CONACYT, México), University College London (UCL), Secretaría de Educación Pública (SEP) and Universidad Juárez Autónoma de Tabasco (UJAT).

1 INTRODUCTION

Zeolites have extensive applications, including petrochemical catalysis, fine chemical synthesis, gas separation and ion exchange, which have stimulated a wide range of studies in recent years. An increasingly important fundamental area of the field concerns the development of a better understanding of the nucleation and growth of zeolites, where knowledge of the mechanism of zeolite synthesis can assist to the design of new materials.

The nucleation and growth of zeolites and other microporous solids continues to pose many questions[1, 2]. Whilst the very general features of self-assembly via condensation polymerization are understood for siliceous systems, the conditions under which both natural and synthetic zeolites form are so complex, that they are difficult to characterize experimentally. Thus, whilst the species initially present in silicate gels can be characterized by NMR with some certainty,[3-5] their charge state is more difficult to probe[6]. Similarly, although scattering methods can tentatively identify larger species,[7, 8] (which may be possibly nuclei) the relative stability and lifetime of the smallest clusters, significant in zeolitic structures, such as 4-membered rings, remain unclear. Furthermore, in the post-nucleation regime, there is much debate as to what species are responsible for crystal growth: small oligomers or larger sub-units. Indeed, it has been suggested that the growth of silicalite-1 (MFI zeolite) is controlled by a unique nanocluster[9], although there is some debate about this proposal[10]. In contrast, characterization of zeolite surfaces suggests that much smaller units are responsible for surface growth[11].

1.1 Objectives

The understanding of silicate (including zeolites) genesis is of primary importance, since nucleation will dictate the structural arrangement in the growing crystal and form the subsequent final crystalline material. However, in the past decades, since the synthesis of the first non-natural zeolite, the elucidation of how the first silicate structures form during hydrothermal synthesis has proved to be a challenging issue[1, 12]. In this work, we will address the problem of nucleation of pure siliceous zeolites, from a theoretical point of view, using a range of computational chemistry techniques. The methods and the results are relevant to a wide range of silicates, although the focus here is on zeolites. The aim of this work is to survey the structures and reactions that occur in the first stages of the nucleation of a zeolite. Two aspects are considered in detail in this computational study: the effects of solvation, and of the high pH in the synthesis solution. Specifically, the objectives are to:

- develop a method to study the nucleation process,
- evaluate the different geometrical conformations for the clusters analysed and their influence on nucleation,
- study the thermochemistry of the deprotonation and condensation (polymerization vs. cyclization and specific cyclizations) reactions,
- rationalize the effect of the pH and solvation on the reactions involved in nucleation,
- examine the hydrogen bonding within the silicate clusters and between silicate clusters and water molecules.

A brief introduction to zeolites and to hydrothermal synthesis will be presented: a more detailed account of these subjects is left to the current extensive literature[1, 12-15]. Previous studies (both theoretical and experimental) for the description of clusters and reactions in the nucleation of zeolites will also be reviewed in this introductory chapter.

1.2 Zeolites

Zeolite science was initially a branch of mineralogy. However, the widespread application of zeolites has been the main driving force behind attempts at synthesising novel materials, leading to the considerable growth in the number of unique structures

discovered[1, 16]. This section reviews the structure, properties and applications of this fascinating class of solids.

1.2.1 The nature of zeolites

Zeolites are an important class of technological materials and are the focus of intense research in different fields of science and technology[17, 18]. These crystalline materials are aluminosilicates with a microporous structures[1].

Although the composition of the framework is, in general, limited to a few elements, zeolites show a surprisingly high variety of structures. In addition, a large array of isomorphous materials can be formed which can be considered as zeolite analogues (or zeotypes) for example, AlPOs (aluminophosphates) and SAPOs (silicoaluminophosphates). The basic building unit is a tetrahedral TO_4 (where T is Si, Al, etc.), which links via bridging oxygen atoms to form a three-dimensional framework (Figure 1). The aluminium (if present) substitutes for the silicon in a tetrahedral position and hence requiring some form of charge compensation, typically alkali metal cations in the cavities. The three-dimensional arrangement of these tetrahedral units forms unique structures, which have channels and cages of molecular size. Examples of some zeolite structures can be seen in Figure 1. A comprehensive account of all known zeolitic frameworks, is given in the publications of the International Zeolite Association[16, 19]. However, the number of zeolitic frameworks known to date is only a small subset of all

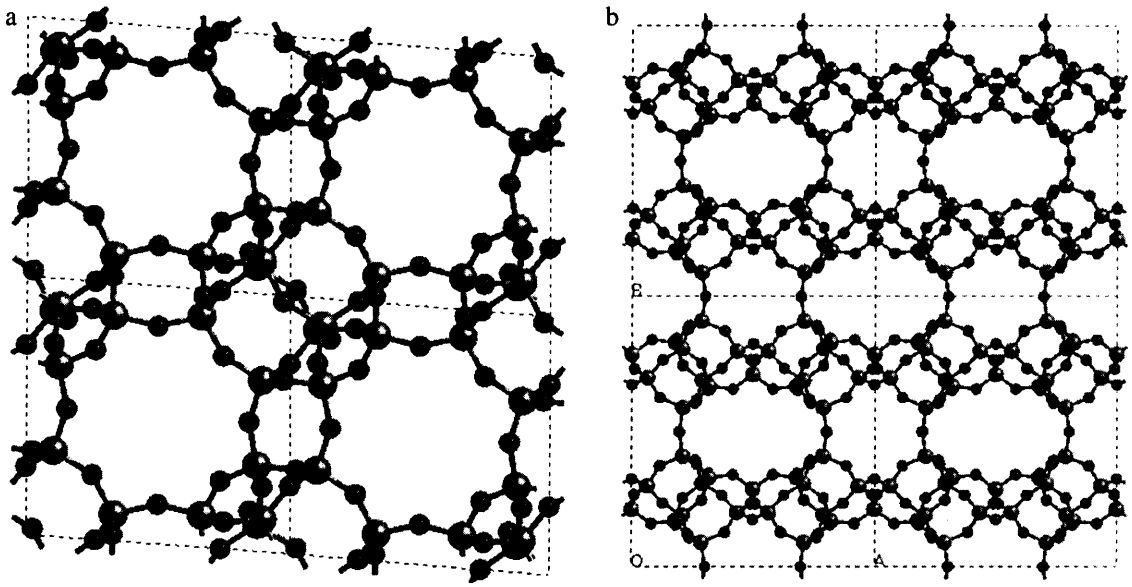

Figure 1 Examples of zeolitic structures, (a) Chabazite and (b) Clinoptilolite. Si atoms are in tetrahedral position.

possible structures: many thousands of hypothetical structures have been elucidated[20-24]. It is therefore clearly necessary to understand better how zeolites are formed.

The properties of zeolites including acidity, ion exchange and molecular sieving, enable them to be used in a large variety of industrial applications, such as: gas separation, adsorption[17, 18], catalytic cracking, catalytic reforming[25], ion exchange and fine chemicals synthesis. In addition to these typical and extensively studied applications of zeolites, new applications of microporous materials are emerging, for example, as insulators with low dielectric constant in microchip devices, hosts for metals in medical diagnosis, hosts for laser dyes, and templates for porous carbons[26]. This large variety of important applications of zeolites provides further incentive for the detailed study of their formation and a first step to this is to explore with molecular detail the nucleation process during synthesis.

The first natural zeolite was discovered in the XVIIIth century[27], and in the middle of XXth century the first synthetic zeolites were prepared[28]. Since then, the number of synthetic zeolites has been increased, some resembling natural zeolites, but others with new structures unknown in nature. Moreover, new elements have been incorporated into the zeolite framework such as Ti, P, Fe, V, Cr, Mn, Zn[2], expanding the possible applications for these materials; indeed 25 elements are known as main components for their structures[29]. Synthetic zeolites are prepared by hydrothermal methods, which are discussed in more detail in the next section.

1.2.2 Hydrothermal synthesis

In hydrothermal synthesis[17], sources of Si, Al, water, alkaline base and sometimes an organic cation or molecule (such as tetrametylammonium) react in a batch process at a temperature between 80°C and 200°C, for a time ranging between minutes and days[13, 19][i]. A diagram showing the essential features of such syntheses is presented in the Figure 2.

The lower part of the Figure 2 shows, in simple and schematic terms, the chemical processes occurring inside the autoclave, at a molecular level. The first reaction is the fundamental dimerization reaction, where two monomers will condense into a dimer (and a water molecule expelled as a by-product). Next, in some way, linear silicates will

[i] The F^- could be used as mineralizing agent instead of the OH^-[1]. However, in this thesis only the latter is considered.

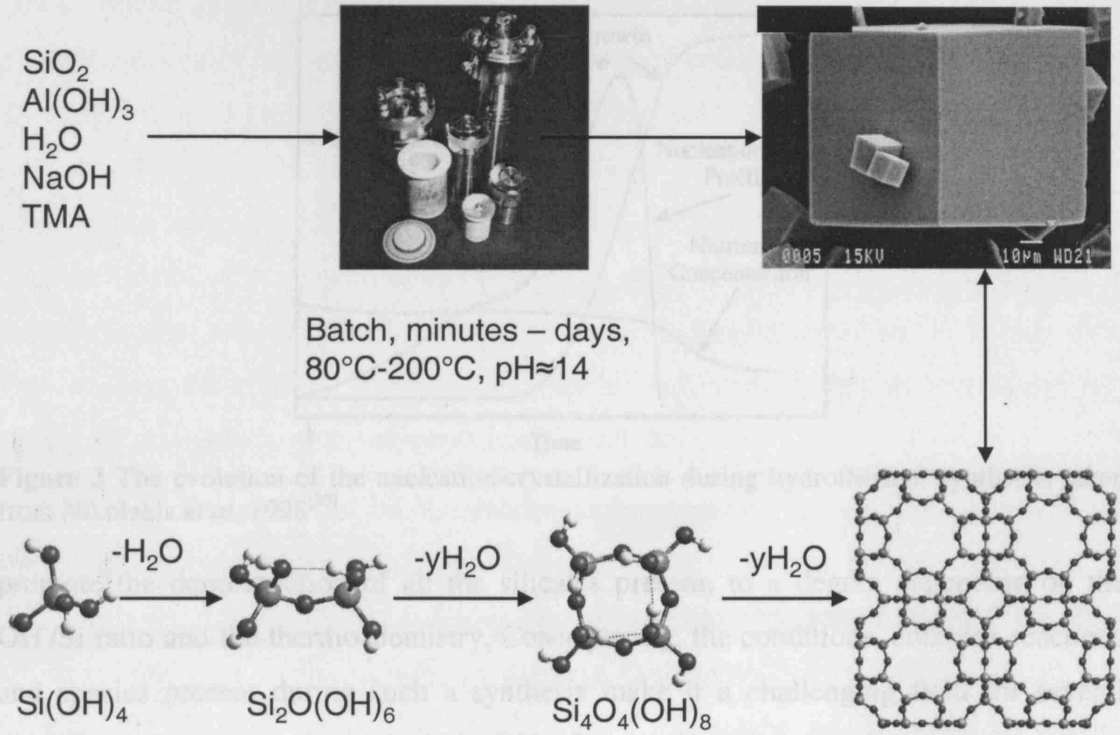

Figure 2 A general schematic representation of the hydrothermal synthesis of zeolites.

react to produce cyclic structures such as the four-member ring shown. This step is necessary because the final zeolite frameworks contain ring structures, as shown in the example of zeolite A in the diagram. In the final part of hydrothermal synthesis, rapid crystallization happens, where condensation of silicates finally produces the zeolite structure.

During synthesis, several reactions and species are formed: first an induction period involving the slow formation of seed structures (nucleation), followed by a rapid crystal growth to form the final crystalline zeolitic structure. A basic description of the changes with time for the main participants in the hydrothermal synthesis of zeolites (nucleus and crystal), is shown in Figure 3. The well-known s-shaped curve for crystal growth is observed, with a long induction period followed by fast crystallization.

There are two global mechanisms proposed: a solution mediated process and a hydrogel reconstruction in a heterogeneous setting[2] (discussed later).

Hydrothermal synthesis is a nucleation-crystallization process involving liquid, amorphous, and crystalline solid phases[1]. The possible clusters present in the solution are numerous, and the high pH (12.6 – 14[19]) conditions present during the synthesis,

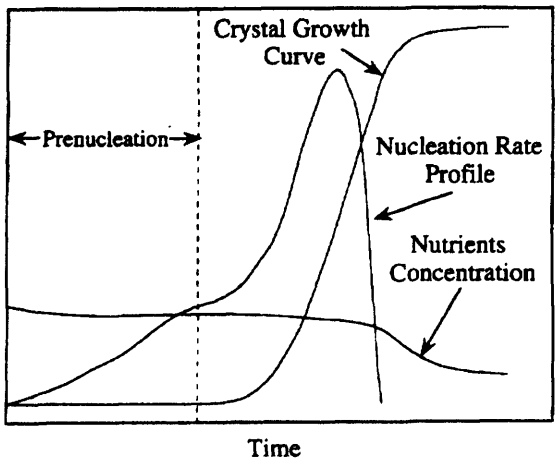

Figure 3 The evolution of the nucleation-crystallization during hydrothermal synthesis, taken from Nikolakis *et al*, 1998[30].

promote the deprotonation of all the silicates present, to a degree depending on the OH^-/Si ratio and the thermochemistry. Consequently, the conditions, complex reactions and species present during such a synthesis make it a challenging field for several disciplines and one that is particularly difficult to study experimentally.

1.2.3 Zeolite nucleation

Some of the silicate clusters present in solution at the pre-nucleation phase of synthesis have been identified using NMR spectroscopy[3, 5, 31-33]. However, the precise charge state of these species is more difficult to determine[ii] and furthermore, the reactions involved in forming these clusters are very difficult to study experimentally. Some authors have suggested structures which are believed to be the building blocks in silicalite-1[9, 35-37], although this proposal has raised considerable debate[3, 4, 10]. Scattering methods have identified larger structures (ca. 2.8 nm) considered primary units in the Si-MFI system[7, 8], although their precise structure is unknown. Given these experimental difficulties, computational methods provide an alternative method to gain key insights into the formation of the pre-nucleation species – probing areas that are beyond current experimental methods and hence providing evidence for the mechanisms of zeolite nucleation and subsequent crystal growth[38].

Thus, over the past few years a number of investigations into the structural chemistry of small silicate species have been performed. As will be discussed in greater detail below, Pereira *et al*[39, 40] studied neutral silicate structures with up to five silicon atoms using

[ii] Though, mass spectrometry can provide information of the charge of some clusters[34]

Local Density Approximation (LDA) methods. However, one of the outcomes of the methods chosen in this work – essentially a limit of computer technology at the time – was that linear condensation reactions were favoured over the formation of cyclic species a conclusion at odds with the formation of crystalline zeolites. Lewis *et al*[41], using more approximate molecular mechanics methods, identified the key role of templating molecules in preventing the collapse of large hydrophobic silicate clusters in the presence of solvent. However, here, no reactions can be modelled. Thus, it is clear that whilst such methods can provide valuable information they cannot adequately reflect the complexity of the experimental conditions.

In this work, therefore, we build a method suitable to the more general study of the formation of small silicate species, fundamental to the nucleation of pure silica zeolites. The structures of these species and their related energetic and thermodynamic properties are calculated with methods based on Density Functional Theory (DFT). But we also consider the effect of water using the COSMO [42-44] (conductor-like screening model) solvation approach together with explicit water molecules. The high pH of synthesis will also be accounted for by the study of deprotonated species.

Although limited, the experimental results under the complex hydrothermal synthesis, will provide stringent checks on the accuracy of the results in this work, and will provide a larger framework in which to interpret our results.

1.2.4 Experimental identification of nanoparticles

To unveil a detailed mechanism of hydrothermal zeolitic synthesis, several experimental techniques have been applied, including XRD, NMR, EXAFS, SAXS, WAXS, IR/Raman, electron microscopy, TEM, AFM, mass spectrometry and light scattering[4, 34, 41, 45]. With this range of techniques it is possible to elucidate some of the clusters and reactions present during nucleation, although the complexity of the problem often imposes considerable uncertainty[3, 10].

From studies of silicalite-1 (MFI) it is suggested that both the nucleation and crystal growth are solution mediated processes, even if an amorphous gel phase is present[46]. X-ray scattering techniques (SAXS, WAXS, USAXS) have shown that alkalinity has a major role in the formation of colloidal aggregates in the synthesis of high silica zeolites[46-48]. At high alkalinity no aggregates form, whilst a colloidal phase is seen at

lower alkalinity; the transition is at $Si/OH^- = 2.65$[47]. However, these particles do not participate directly in nucleation nor are they a pre-requisite for it, and may therefore be a source of nutrients through dissolution of silicate ions.

In the synthesis of high silicas, nanometre sized particles have been identified and considered to be primary building units precursors in the nucleation and crystal growth[7, 8, 49]. In the case of Si-MFI, this primary unit is found to be a 2.8 nm diameter particle, in Si-BEA 2.6 nm and 1.5 nm in Si-MTW. Therefore, it is suggested that the primary units are unique to each zeolite topology. The Si-MFI primary unit (2.8 nm) is independent of the structure-directing agent, alkalinity, silica source, and temperature. The existence of primary units involved in the nucleation and crystallisation stages is without doubt important, because it could lead to the idea of a common nucleation-crystallisation mechanism for high-silica zeolites.

In another series of experiments on Si-MFI[9, 35, 36, 50-52], a unique particle believed to be a primary building unit has been postulated. The principal difference with the work mentioned above is that in the former, the analysis is *in-situ*, whereas in the latter *ex-situ* techniques are used. A cluster with a specific structure, called first a "nanoslab" and later a "nanoblock", has been assigned as the building unit, with dimensions 1.3 x 4.0 x 4.0 nm[36]. Smaller cluster precursors to this nanoslab, have also been identified[51] and a mechanism was proposed for the self-assembly of these nanoslabs to produce tablets and afterwards a crystal[50, 51]. However the proposed cluster structures, including the nanoslab and the self-assembly mechanism have been criticised[3, 4], due to the possible over interpretation of the IR and NMR data.

For particles smaller than 2.8 nm, there are numerous ^{29}Si NMR studies that reveal some of the small structures present in aqueous silicate solutions[3, 32, 33, 56]. The species found in solution, as illustrated in Figure 4, include among others 3- and 4-membered rings, double-4-rings and others clusters involving either 3- or 4-membered rings, or a combination of both.

In Figure 5 the so-called "Secondary Building Units" are shown[16]. Using only these units is possible to build all the known zeolitic frameworks with a tiling process. However, they are not necessarily implicated in the nucleation-growth process of the zeolites.

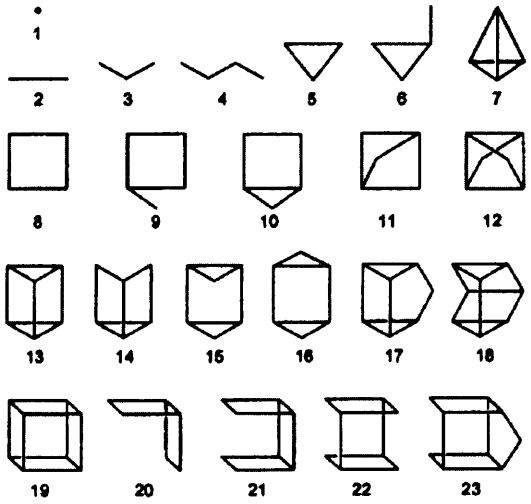

Figure 4 Silicate cluster structures found by ^{29}Si NMR, each line represents a Si-O-Si linkage. Image taken from the work of Knight and Kinrade[3][iii].

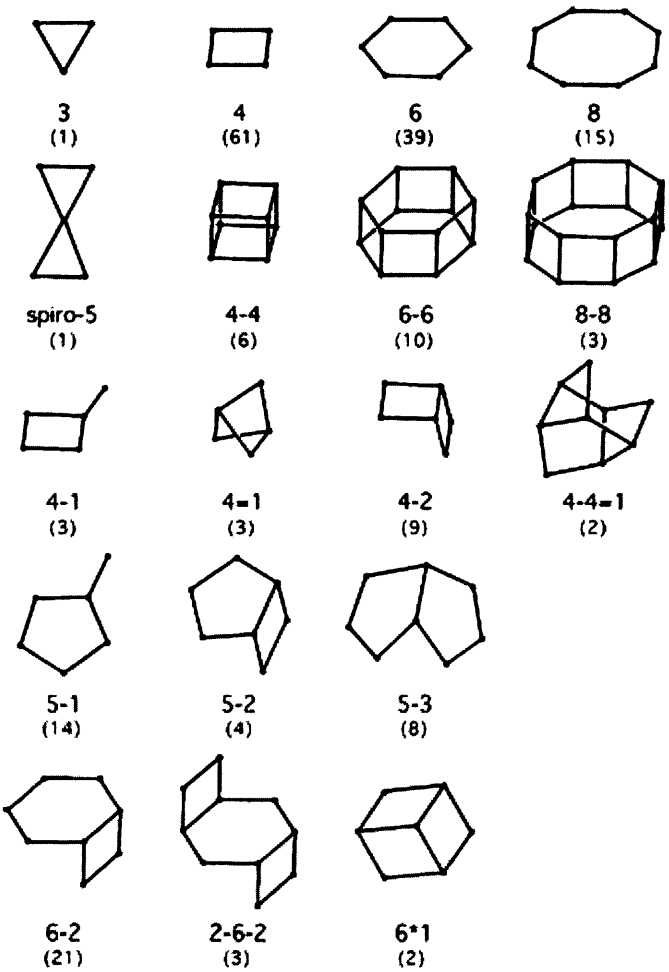

Figure 5 The Secondary Building Units (SBU) [16].

[iii] The reference from the work of Knight and Kinrade is used frequently in this thesis. Figure 4 taken from this work, is a summary of several papers[32, 33, 53-55]. These clusters were detected in a recent work[5].

1.2.5 Proposed condensation mechanisms in silicates

Clusters are formed through a condensation reaction producing a Si-O-Si siloxane linkage. The simplest processes involve the direct condensation reaction of monomer ($Si(OH)_4$) species. Typical reactions include:

$$2Si(OH)_4 \leftrightarrow Si_2O(OH)_6 + H_2O, \qquad 3Si(OH)_4 \leftrightarrow Si_3O_2(OH)_8 + 2H_2O. \tag{1.1}$$

Felmy *et al.*[6] studied these sort of reactions under basic conditions (pH > 10), the following ionic reactions were proposed by them, applying a thermodynamical model to experimental data,

$$2H_3SiO_4^- \leftrightarrow Si_2O_3(OH)_4^{2-} + H_2O, \tag{1.2}$$

$$3H_3SiO_4^- \leftrightarrow Si_3O_5(OH)_5^{3-} + 2H_2O. \tag{1.3}$$

Another mechanism was proposed by Gittleman *et al.*[57], where the secondary product is OH^- instead of H_2O:

$$\equiv SiOH + SiO_4H_{(4-n)}^{n-} \leftrightarrow \equiv SiOSiO3H_{(3-n)}^{(n-1)-} + OH^-, \tag{1.4}$$

$$\equiv SiO^- + \equiv SiOH \leftrightarrow \equiv SiOSi\equiv + OH^-. \tag{1.5}$$

The first of these reactions (producing OH^-) is considered the route to small clusters, whilst the second reaction allows the products of the first reaction to condense into larger particles.

A more detailed mechanism, considered by Lickiss[58], describes the formation of siloxanes, in reactions catalyzed by both acid and base. The important feature of this mechanism is the proposal of the formation of a base (or acid) catalyzed intermediate involving all of the reactants, *i.e.* the two silanols and the base (or acid). The mechanisms are as follows for the base and acid catalyzed reaction respectively:

$$\equiv SiOH + :B \leftrightarrow \equiv SiO^- \cdots B^+H, \equiv SiOH + \equiv SiO^- \cdots B^+H \leftrightarrow \equiv SiOSi\equiv + (HB)^+(OH)^-, \tag{1.6}$$

$$\equiv SiOH + HA \leftrightarrow \equiv SiO^+H_2 \cdots A^-, \equiv SiOH + \equiv SiO^+H_2 \cdots A^- \leftrightarrow \equiv SiOSi\equiv + H_3O^+ \cdots A^-. \tag{1.7}$$

In this thesis, we will focus on the mechanism for the neutral and anionic silicate cluster reactions producing a larger silicate and water.

1.2.6 Modelling nucleation

As noted earlier, molecular modelling, including quantum mechanical (QM) calculations provide one of the more promising classes of technique for understanding the mechanism of zeolite nucleation and the species involved. However, the high computational requirements for these QM calculations still limit their use to some tens of atoms. Nevertheless, the constant increase in computing power is now allowing calculations that are more precise and that describe larger species[59].

An analysis of the smallest silicate clusters of up to 5 Si has already been performed by Pereira *et al*[39, 40]. The structure, charge distribution, and energy were studied in these clusters principally with a local Density Functional Theory (DFT) model BHL/DNP. The strong hydrogen bonds, present in most of the clusters, were found to have a major role in the conformation and energy, mainly when calculating the clusters *in vacuo*. The formation of these intramolecular hydrogen bonds leads to linear silicate clusters being more stable when "curved" rather than straight, *i.e.* enhancing the intramolecular H-bonding. This work also suggests that the charges involved in the clusters have a strong effect on the reaction energy.

The effect of solvation and the role of structure-directing agents was studied by Lewis *et al.*[41, 60], with a molecular mechanics model. The presence of water was treated explicitly by "soaking" the clusters studied in spherical droplets of water. The results revealed a role for the template other than just acting as a structure-directing agent *i.e.* a stabilizing agent, preventing the collapse of the early void structures. They also found that a strong charge-mediated interaction between the template and the clusters is necessary to keep them spatially close together during which time the silicate clusters may condense.

The above work and other earlier work[61-64], is among the most extensive calculations reported on silicate clusters for zeolite nucleation. With these antecedents, there is a firm basis for understanding some of the most important aspects of the nucleation of high silica zeolites *i.e.* cluster structures (especially stable conformations), templating, and solvation. However, the applicability is limited by the level of theory, cluster size and the assumptions employed.

2 THEORETICAL METHODS

We have seen, during the last 20 years, a dramatic expansion in the applications of computational chemistry techniques to a vast range of different chemical problems, and no more so than in zeolite science[40, 60, 65-67]. Indeed, possibly more so than any other field of material chemistry, computational methods have proven to be a very successful tool in understanding, with atomic detail, key aspects of the chemistry of zeolites[1, 12] and can be considered almost a routine complement to experimental work.

This chapter provides a brief introduction to the theoretical methods used in this thesis. In particular, the advantages and disadvantages of various methods are highlighted and discussed.

2.1 Computational Chemistry

Computational methods, allow us to calculate the geometries and properties of chemical systems at a molecular level. The principal and most common properties, which can be calculated with molecular modelling, are:

- The total energy of a system with a specific geometric arrangement.
- The energy minimized structure for a set of atoms.

Other properties, which may be obtained, are:

- Molecular Orbitals
- Transition States
- Multipole Moments
- Atomic charges
- Vibrational frequencies

- IR and Raman Spectra
- NMR properties

Further analysis of these calculated properties also allows us to determine, for example, bond and reaction energies, reaction pathways and thermodynamical properties[68].

With the properties available from these computational methods and notwithstanding the limitations on the number of atoms due to computer restrictions, there is a vast spectrum of molecular systems, which can be studied using these techniques. For zeolites, this range of systems goes from periodic crystal structures to single silicate molecules and ions: the latter are the subject of this thesis.

Computational methods provide us with a complement to experimental methods, especially, as with the rapid development of faster computers, more complex and larger systems can be analysed. Indeed, and more importantly, they provide a means to study systems under conditions that are difficult to probe in the laboratory and allow the study of properties that cannot be assessed experimentally. Computational methods should, however, always where possible be used together with experiment.

Of course, we must not forget the limitations of these methods. Firstly, we must consider the approximation made in constructing our model, as most models in science are of an approximate nature. The number of atoms that can be handled range from small numbers to millions, depending of the task and the method employed. The accuracy of the results also depends on the properties and the method used, and in some cases very precise results require a huge computational effort, only available with high-end computing resources.

In the next sections we will give a brief introduction to the computational methods used in this thesis: a more complete description of the methodology are available elsewhere[68-73]. We first present methods based on interatomic potentials or forcefields, then electronic structure methods, including *ab initio*[iv] (principally Hartree-Fock) and Density Functional Theory (DFT). The approaches for modelling solvation will also be introduced. Finally, some of the principles of Statistical Mechanics will be presented.

[iv] *Ab Initio* means in Latin "from the beginning"

2.1.1 Force Field Methods

Force field methods do not attempt to solve the Schrödinger equation for the system; rather they use parameterised expressions for the potential energy of the system as a function of the nuclear coordinates (or quantities that depend on the latter such as bond length and as angles). Such methods have been widely applied to solids and liquids[74]. In the account which follows, we consider "molecular mechanics", *i.e.* the application of these methods to molecules.

These methods take as an input a predefined array of bonds connecting all the atoms and express the energy of the system as a function of atomic coordinates. Each atom is defined depending on the bonds and atoms surrounding it, *e.g.* carbon atoms in an ethene, ethyne or methanol will be all different. The energy expression is parameterised either by fitting to experimental data (*e.g.* molecular structures and infrared frequencies) or to quantum mechanical calculations[75].

The total energy of a system, in the molecular mechanics methods, is described as a sum of terms, some of which account for the energy necessary to distort in the system[73]; others refer to non-bonded interactions. The typical terms in this description are:

$$E_{FF} = E_{str} + E_{bend} + E_{tors} + E_{vdw} + E_{el} + E_{cross}. \qquad (2.1)$$

E_{str} = Energy to stretch a bond

E_{bend} = Energy to bend an angle

E_{tors} = Torsional energy around a bond

$E_{vdw} + E_{el}$ = Non-bonded atom-atom energy

E_{cross} = Coupling between E_{str}, E_{bend} and E_{tors}

Molecular mechanics provides a very cheap[v] way to determine the potential energy surface of a system, and can calculate systems containing thousands of atoms in a short time. However, as these methods do not treat the electrons explicitly, reactions involving bond formation or breaking cannot be treated. Another limitation is that only systems, which have been suitably parameterized, can be investigated. These methods are, however, a widely and routinely used tool in computational chemistry.

[v] "Cheap" and "expensive" methods are relative terms which refers to the computational effort need, *i.e.* the time necessary for a particular task on a defined computer arrangement.

2.1.1.1 Minimization

In this section, we will present an introduction to the application of energy minimization to generate the lowest energy configurations[73, 75, 76]. These methods can be used in both forcefields and quantum mechanical applications. Energy minimization and molecular dynamics methods are applied in investigating the silicate systems presented later.

The potential energy surface represents the energy with respect to the coordinates of a system. For a system with N atoms, the energy is a function of 3N coordinates (or 3N-6 internal coordinates, when it is described by a Z-matrix).

The position on the potential energy surface where displacements from that point increase the energy of the system is known as a minimum. In a complex system, there will be several of these points. However, the minimum with the lowest energy is defined as the global minimum. Identification of global minima is a major challenge; and indeed there is no way to have complete certainty that the minimum found is a global minimum.

In a system with several minima, the lowest point in the potential energy surface connecting two minima is defined as a saddle point and this structure is the transition state between the minima.

A minimum can be formally defined as the point at which all the first derivatives of the energy function with respect to the coordinate variables $\boldsymbol{R}_1$, $\boldsymbol{R}_2$,..., $\boldsymbol{R}_n$ are zero; while at a minimum, the second derivatives of the energy will be all positive, *i.e.*:

$$\frac{\partial E}{\partial \boldsymbol{R}_i} = 0, \quad \frac{\partial^2 E}{\partial \boldsymbol{R}^2_i} > 0. \tag{2.2}$$

If there is an analytical expression for the energy with respect to the coordinates, the solution in principle could be obtained analytically. However, in most cases, numerical methods are applied to find the energy minimum.

There are several such methods, and the one chosen will depend on the geometrical characteristics of the system and the forcefield or electronic structure method used. For example, the minimization of a system with few tens of atoms will be practically performed with a numerical method, which includes matrix inversion. However, a system with thousand of atoms is not suitable to such a method. As well, a numerical

minimization method, which requires several steps, and a similar number of calculations of the energy, is much slower with an electronic structure method; but this method could be more appropriate for a forcefield.

Minimization methods can be classified into those, which require the calculation of the first derivative or second derivative of the energy with respect to the coordinates, and those which does not require derivatives. The derivatives can be calculated analytically or numerically; the first approach is more desirable, because the result is exact and is calculated faster; however this is not always practical[75].

A non-derivative method is the sequential univariate method. In this method, a coordinate is chosen from which two new structures are calculated changing that coordinate, from these three points a parabola is fitted. The minimum in the parabola is found and the structure is changed to this point. The same procedure is performed for each one of the coordinates in the system. This method could be slow to converge, for example when there is coupling between coordinates.

The derivative methods are more frequently used in minimization of systems with less than a hundred of atoms. The basic strategy is to follow the direction of the first derivative since this direction is certainly towards a minimum. However, there is no guarantee that this is the global minimum, as explained before. The magnitude of the derivative is related to the steepness of the curve in the region being analysed.

The steepest descent method uses the first derivative to find the minimum. The direction of the next step in this numerical method is given with the unit vector (s_k),

$$s_k = \frac{-g_k}{|g_k|}, \tag{2.3}$$

where (g_k) is the gradient (first derivative) of the energy with respect to the position coordinates. This method can take too many steps if the minimum is in a long narrow valley; but the method is well suited to start a minimization, where the minimum could be far from the initial point.

Another method, which uses first derivatives is the conjugate gradient algorithm. This method differentiates from the previous one in having non-orthogonal directions for each step, which has a better performance in long narrow valleys. To calculate the

direction in every step, the method uses the information of the gradient and the direction of the previous step.

A set of methods used commonly in minimization of structures with electronic structure are the Newton-Raphson and its variants. These methods employ the second derivative of the energy, which gives information of the curvature of the potential energy surface. This method requires the calculation of the inverse of the Hessian matrix, which is the matrix of the second derivatives of the energy with respect to the coordinates. This step is generally only affordable for a small number of atoms (less than a hundred), which is one of its weakness. There are several modifications to the Newton-Raphson method, which focus on changing the way of calculating the expensive step of the Hessian matrix and its inverse. For example, some methods uses the same Hessian matrix in several steps, others move one atom in each interaction, which simplifies greatly the Hessian matrix.

2.1.1.2 Dynamics

Molecular dynamics is used to simulate dynamics at the atomic and molecular level explicitly, using the Newton's laws of motion[73-76]. These forces (***F***) are a consequence of an inter-particle potential ***V(R)***,

$$\boldsymbol{F} = -\frac{d\boldsymbol{V}(\boldsymbol{R})}{d\boldsymbol{R}}. \tag{2.4}$$

For each particle, Newton's second law of motion can be expressed as:

$$\frac{d^2\boldsymbol{R}_i}{dt^2} = \frac{\boldsymbol{F}_i}{m_i}. \tag{2.5}$$

From the last equation, the velocity and position for each particle can be obtained,

$$\frac{d\boldsymbol{R}_i}{dt} = \left(\frac{\boldsymbol{F}_i}{m_i}\right)t + c_1, \tag{2.6}$$

$$\boldsymbol{R}_i = \boldsymbol{u}_i + \frac{1}{2}\boldsymbol{a}_i t^2 + c_2, \tag{2.7}$$

where, m is mass, t is time, c_1 and c_2 are the integration constants. In order to compute these variables (acceleration, velocity and position) the last equations can be approximated as Taylor series expansions,

$$\boldsymbol{R}_i(t+\Delta t) = \boldsymbol{R}_i(t) + \boldsymbol{u}_i\Delta t + \frac{1}{2}\boldsymbol{a}_i\Delta t^2 + \ldots, \tag{2.8}$$

$$\boldsymbol{u}_i(t+\Delta t) = \boldsymbol{u}_i(t) + \boldsymbol{a}_i\Delta t + \frac{1}{2}\boldsymbol{b}_i\Delta t^2 + \ldots, \tag{2.9}$$

$$\boldsymbol{a}_i(t+\Delta t) = \boldsymbol{a}_i(t) + \boldsymbol{b}_i\Delta t + \frac{1}{2}\boldsymbol{c}_i\Delta t^2 + \ldots. \tag{2.10}$$

In the computation of the latter equations errors are derived from the truncation of the Taylor series. However, some methods have been developed to minimize these errors, especially the Verlet algorithm and its variation the Leapfrog Verlet.

A typical molecular dynamics simulation starts with a minimization to allow all the particles to relax and avoid local strains. After the minimization, the system is heated to the desired temperature, which is done gradually. The temperature (T) is calculated from the kinetic energy of all the particles,

$$\frac{1}{2}\sum_i m_i u_i^{\,2} = \frac{3}{2}Nk_BT\,, \tag{2.11}$$

where k_B is the Boltzmann constant and N is the number of particles. To start the simulation the initial velocities for all the particles are assigned randomly (the randomness assures that there are no local high-temperature spots in the system). After the first step, the position, velocity and acceleration for all the particles can be calculated from the truncated Taylor series presented before. Once the desired temperature is reached, a period of equilibration is left to guarantee the stability of the system. The final step of the simulation is the production run, where all the desired properties are calculated. These properties will depend on the selected ensemble, being typical the microcanonical and canonical ensemble (constant energy and temperature respectively).

2.1.2 Electronic Structure Methods

Electronic structure methods, in contrast to force field techniques, apply the laws of quantum mechanics[68, 70, 72]. The basis of these methods is the attempt to solve the Schrödinger equation, which can only be solved exactly for the simplest atom and molecule: the hydrogen atom and H_2^+. Therefore, to solve the equation for other systems requires approximations, which we will discuss in detail in this section.

Ab initio methods differ from empirical or semiempirical quantum mechanical methods in that they avoid the use of empirically parameterised terms. They are, however, the most expensive techniques in computational chemistry and, in most cases, only some hundreds of atoms can be treated.

We now present the fundamentals, which underpin *ab initio* methods and show some of the assumptions necessary to find solutions, and also indicate the limitations of these methods.

As noted the primary equation in all electronic structure methods is the Schrödinger equation:

$$H\Psi(\boldsymbol{r},t) = \frac{ih}{2\pi}\frac{\partial\Psi(\boldsymbol{r},t)}{\partial t}, \tag{2.12}$$

where H is the Hamiltonian of the system. The equation represents a description of a system in terms of the wavefunction (Ψ), for which the probability distribution is given by $|\Psi|^2$. Solution of this equation enables us to obtain the energy of the system and other properties.

If we consider that the potential $\boldsymbol{V}$ (see eq. (2.14)) in the Halmintonian of equation (2.12) is independent of time we obtain the time-independent Schrödinger equation (2.13). Equation (2.13) is an eigenvalue equation, where $\boldsymbol{H}$ is the Hamiltonian and E (energy of the system) is the respective eigenvalue.

$$\boldsymbol{H}\Psi = E\Psi. \tag{2.13}$$

The Hamiltonian ($\boldsymbol{H}$) in the Schrödinger equation is,

$$\boldsymbol{H} = \boldsymbol{T}^{elec}(\boldsymbol{r}) + \boldsymbol{T}^{nucl}(\boldsymbol{R}) + \boldsymbol{V}^{nucl\text{-}elec}(\boldsymbol{R},\boldsymbol{r}) + \boldsymbol{V}^{elec}(\boldsymbol{r}) + \boldsymbol{V}^{nucl}(\boldsymbol{R}). \tag{2.14}$$

Here, the kinetic (T) and potential (V)[vi] terms for the electrons and nuclei are functions of the electron (r) and the nuclei coordinates (R).

An important approximation for the solution of the Schrödinger equation is to consider the nuclei fixed with respect to the electrons, because of the higher mass of the former, which is known as the Born-Oppenheimer approximation, which equates to zero the second term ($T^{nucl}(R)$) of equation (2.14). This Hamiltonian will then give the solution to the electronic wavefunction (Ψ^{elec}).

The wavefunction has boundary conditions, the first being that the electron has to be in some part of the space. So, if $|\Psi|^2$ is the probability density of the particle,

$$\int_{-\infty}^{+\infty} |c\Psi|^2 dv = n_{particles} , \tag{2.15}$$

which is known as the normalization condition. The second boundary condition relates to antisymmetry, which requires that the function changes the sign if two particles are interchanged:

$$f(i,j) = -f(j,i). \tag{2.16}$$

According to molecular orbital theory, the wavefunction can be formed from a combination of molecular orbitals, so:

$$\Psi(r) = \prod_i \Phi_i(r_i) . \tag{2.17}$$

However, in order to fulfil the antisymmetry condition, the wavefunction should be represented as a combination of molecular orbitals in a determinant,

$$\Psi(r) = \frac{1}{\sqrt{N!}} \det\left|\Phi_{a,\alpha}(r_1)\Phi_{a,\beta}(r_2)\ldots\Phi_{z,\beta}(r_N)\right| . \tag{2.18}$$

All *ab initio* methods have some approximations, which are mainly:

- The potential (V) in the Hamiltonian is independent of the time, $V \neq f(t)$ (and hence the Schrödinger equation is solved independent of the time).

[vi] The $V^{nucl\text{-}elec}$, V^{elec} and V^{nucl} are the potentials for the nuclear-electron attraction, electron-electron repulsion and nuclear-nuclear repulsion respectively.

- The nuclei are considered static with respect to the electrons, so the kinetic energy for the nuclei motion is zero in the Hamiltonian (Born-Oppenheimer approximation).
- In the majority of applications, the Schrödinger equation is solved in the non-relativistic form, so in atoms (mainly with high atomic number) where the electrons have velocities close to the speed of light, the solution is inaccurate, especially for core electrons. Relativistic methods are, however, used when studying systems with heavy atoms.

We now consider two main classes of *ab initio* (or first principles) methods: Hartree-Fock and Density Functional Theory.

2.1.2.1 Hartree-Fock Methods

2.1.2.1.1 Basis sets

The molecular orbitals in the *ab initio* methods are represented by a basis set[68], which normally comprises several atom-centred functions, *i.e.* each molecular orbital is composed of several basis functions,

$$\Phi_i = \sum_{\mu} c_{\mu i} \chi_{\mu}, \tag{2.19}$$

where the X_μ are the atomic orbital functions. Furthermore, each of the atomic basis functions is often a linear combination of primitive functions (commonly primitive Gaussians, g_p) which on substitution into the equation (2.19) produces:

$$\Phi_i = \sum_{\mu} c_{\mu i} \left(\sum_{p} d_{\mu p} g_p \right). \tag{2.20}$$

To solve the Schrödinger equation, we have to obtain the set of constants ($c_{\mu i}$), which are determined using the variational principle, which states that the energy calculated for a system will be always higher than that corresponding to the exact solution of its wavefunction. The Hartree-Fock theory uses this principle to find the constants $c_{\mu i}$, which leads to the matrix equation (Roothaan equations):

$$\boldsymbol{FC = SC\varepsilon}, \tag{2.21}$$

$$\det|\boldsymbol{F} - \varepsilon_a \boldsymbol{S}| = 0. \tag{2.22}$$

Each element in equation (2.21) is a matrix. $\boldsymbol{F}$ is the Fock matrix (formed with the Fock operator, f_1), which could be interpreted as the effect of the electrons fields on each orbital,

$$F_{ij} = \int \chi_i^*(1) f_1 \chi_j(1) dv, \tag{2.23}$$

$$S_{ij} = \int \chi_i^*(1) \chi_j(1) dv. \tag{2.24}$$

C is the matrix containing the constants $c_{\mu i}$; $\boldsymbol{S}$ is the matrix accounting for the overlap of the orbitals (2.24) and $\boldsymbol{\varepsilon}$ is the matrix that contains the energy of the system.

The Roothaan equations are solved iteratively (self-consistent) in the Hartree-Fock method. Figure 6 shows the procedure used.

The Hartree-Fock method is a mean field theory, because it approximates the many electron problem by a one electron problem, *i.e.* each electron interacts with the average filed of the rest of the electrons. In an attempt to account for electron correlation, methods known as post-Self Consistent Field (SCF) have been developed[68].

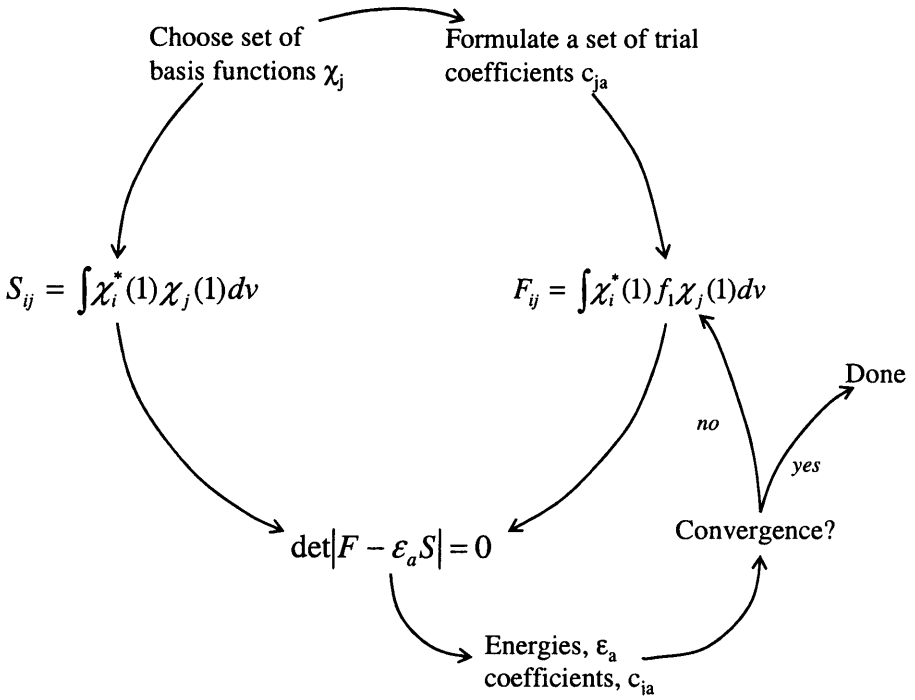

Figure 6 Self-consistent iteration in the Hartree-Fock *ab initio* method. Adapted from Atkins 2004[70]

Configuration Interaction (CI) methods take into account the mixing of the possible electronic states of the molecule. In its full form it is described by,

$$\Psi = b_0\Psi_0 + \sum_s b_s\Psi_s\,, \tag{2.25}$$

where the first part ($b_0\Psi_0$) is the Hartree-Fock level and the second part accounts for all the substitutions of virtual (excited states) for occupied orbitals.

A second post-SCF method is Moller-Plesset perturbation theory[68]. In this case, the higher excitations are added to the Hartree-Fock method, through perturbations to the Hamiltonian, for example,

$$\boldsymbol{H} = \boldsymbol{H_0} + \lambda \boldsymbol{V}. \tag{2.26}$$

An important issue in computational chemistry concerns the computing resources needed for a system. The scaling of the different methods is measured in terms of the number (N) of basis functions (X_μ) used, which depends directly from the selected basis set. Hartree-Fock methods scale formally as the fourth power of the basis functions (N^4), although in practice the scaling may be less severe. However, when electron correlation is considered the scaling is increased. The post-SCF methods based on the Moller-Plesset perturbation theory MP2 and MP4 scale to N^5 and N^7 respectively, while the Configuration Interaction methods CISD and CISD(T) scale formally as N^6 and N^8 respectively[75]. While for small systems the electron correlation methods are feasible, for larger ones this scaling make the methods prohibitive. Alternative and more accessible methods, which take in account electron correlation, are necessary.

2.1.3 Density Functional Theory

Density Functional Theory (DFT) differs from Hartree-Fock methods in that we solve for the electron density not the wave function ψ, and implicitly these methods take into account electron correlation[69]. Density Functional Theory methods have improved scaling compared with Hartree-Fock, which has encouraged their widespread use.

The electron density (ρ) on which Density Functional Theory is based, is calculated from the molecular orbitals (Φ_i):

$$\rho(r) = \sum_i |\Phi_i(r)|^2 . \tag{2.27}$$

Crucially, the energy is defined as a function of the electron density solely, which is at the same time a function of the position (functional), based on the Hohenberg-Kohn theorem[77]:

$$E = f[\rho(r)], \tag{2.28}$$

$$E(\rho) = E^T(\rho) + E^V(\rho) + E^J(\rho) + E^{XC}(\rho). \tag{2.29}$$

The kinetic electron interactions (E^T), the nuclei-electron (E^V) and electron-electron (E^J) potential are taken into account. However, the central term in DFT methods is the exchange-correlation (E^{XC}), which accounts for the exchange energy from the antisymmetry of wavefunction and the correlation in the movement of the electrons. In the simplest approximation, the exchange-correlation energy term is calculated approximately from the homogeneous electron gas density energy (ε^{XC}), also known as the local density approximation and can be separated into an exchange and a correlation term:

$$E^{XC}(\rho) = \int \rho(r) \varepsilon^{XC}[\rho(r)] dr , \tag{2.30}$$

$$E^{XC}(\rho) = E^X(\rho) + E^C(\rho). \tag{2.31}$$

Improvement of the description of the exchange-correlation energy can be made by making the functional dependent on the electron density and its gradient (ρ and $\nabla\rho$): so called gradient-corrected functionals. These have generally proved to be more successful.

The performance of Density Functional Theory methods is indeed crucially dependent on the exchange and correlations functionals. A very common exchange functional is the one formulated by Becke and a common correlation functional is that by Lee, Yang and Parr[78], which together produce the BLYP correlation-exchange functional ($E^{XC}(\rho)$).

The exchange part of the Hartree-Fock theory can be mixed with the exchange term in the Density Functional Theory, producing the hybrid functionals,

$$E_{hybrid}^{XC} = c_{HF} E_{HF}^{X} + c_{DFT} E_{DFT}^{XC}. \tag{2.32}$$

The c_{HF} and c_{DFT} are constants, which are fitted. A popular hybrid Density Functional Theory method is that of Becke three parameter functional, B3LYP[79, 80].

The molecular orbitals (Φ_i), the electron density (2.27) and finally the total energy (2.29) are obtained by solving the Kohn-Sham equations[81],

$$\left\{-\frac{\nabla^2}{2} - V_n + V_e + \mu^{XC}(\rho)\right\}\Phi_i = \varepsilon_i \Phi_i, \tag{2.33}$$

$$\mu^{XC} = \frac{\partial \rho \varepsilon^{XC}}{\partial \rho}. \tag{2.34}$$

Equation (2.33) could be rewritten into a form that resembles the Roothaan equations,

$$\boldsymbol{HC} = \boldsymbol{\varepsilon SC}. \tag{2.35}$$

Moreover, as for the Hartree-Fock techniques, this last equation is solved iteratively in a self-consistent procedure, which is shown in Figure 7.

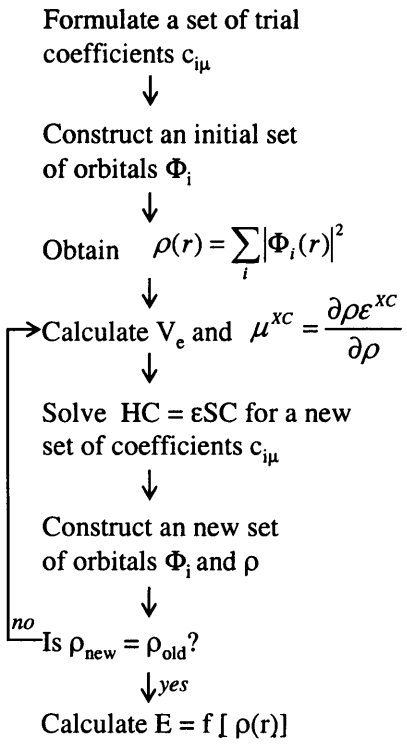

Figure 7 Self-consistent iteration in the Density Functional Theory methods.

The basis set, which define the molecular orbitals (Φ_i) can be numerical, rather than analytical (for example as the Gaussian type orbitals), which is the approach in the Dmol^3[82, 83] code used in this thesis. This procedure has some advantages, for example basis set superposition errors are minimized and an improved description of weak interactions (for example H-bonds) can be achieved[84, 85].

Density Functional Theory methods offer a good compromise between accuracy and computational cost. For example the B3LYP/6-31+G(d,p) has roughly twice the accuracy compared with MP2/6-31+G(d,p), both of which require roughly the same computer resources.

2.1.4 Modelling solvation

Modelling solvation is one of the most challenging issues in computational chemistry. The origins of the complexity of the problem are the large number of dynamical interactions of the solvent molecules with the molecular system being investigated, although many of the theoretical approaches use a continuum treatment of the solvent.

There are several approaches in modelling solvation[86]. For example, surrounding the molecule with a large number of solvent molecules treated using interatomic potentials and calculating the system with molecular mechanics or Monte Carlo methods. However, recently a method based on a conductor-like screening description of the solute molecule (COSMO[87]) has proved to give satisfactory results[43, 44].

The COSMO approach (a continuum solvation model[86]) to the treatment of the solvation of molecules relies on the "calculation of the dielectric screening charges and energies on a van der Waals-like molecular surface in the approximation of a conductor"[43].The calculation of such a dielectric screening can be embedded in a Self Consistent Field molecular orbital calculation such as Hartree-Fock or Density Functional Theory, which is a major strength of the method.

The COSMO method creates a cavity occupied by the solute (Figure 8). As a consequence of the charge distribution in the solute, a screening charge is created in the dielectric continuum. This ideal screening charge is calculated in the approximation of an ideal conductor. Under these ideal conditions the total potential (V_{tot}) on the surface is zero,

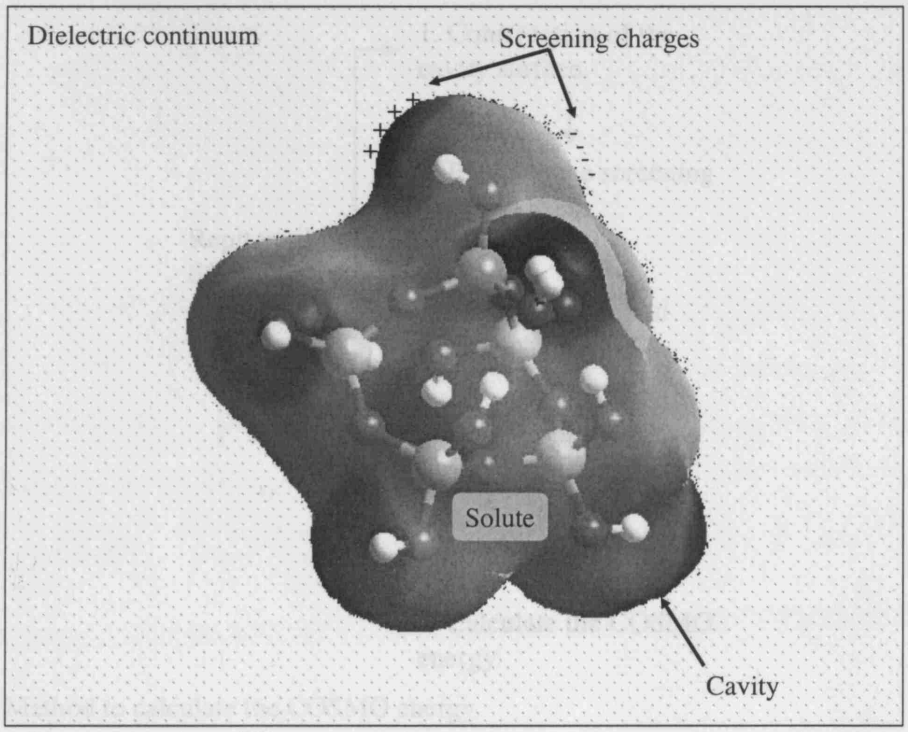

Figure 8 The COSMO model[88].

$$V_{tot} = BQ + Aq = V_{sol} + V_{pol} = 0, \tag{2.36}$$

where q are the solute charges and Q are the induced screening charges. B and A are Coulomb matrices. Now from the last equation the solute charges can be calculated,

$$q = -A^{-1}BQ, \tag{2.37}$$

and the real charges in a dielectric medium (ε) are evaluated with,

$$f(\varepsilon)\frac{\varepsilon - 1}{\varepsilon + 1/2}. \tag{2.38}$$

The COSMO method is differentiated from other continuum solvation models in considering the limiting case where the dielectric is an ideal conductor.

The cavity is created with the interpolation of spheres centred on the atoms of the molecule; the parts of the spheres lying inside the molecule are discarded (see Figure 8). The surface of the spheres is represented with a grid of points, which will carry the charge. A critical step in the COSMO method is the calculation of the cavity (which is based on the van der Waals radii of the atoms), since a great part of the accuracy of the

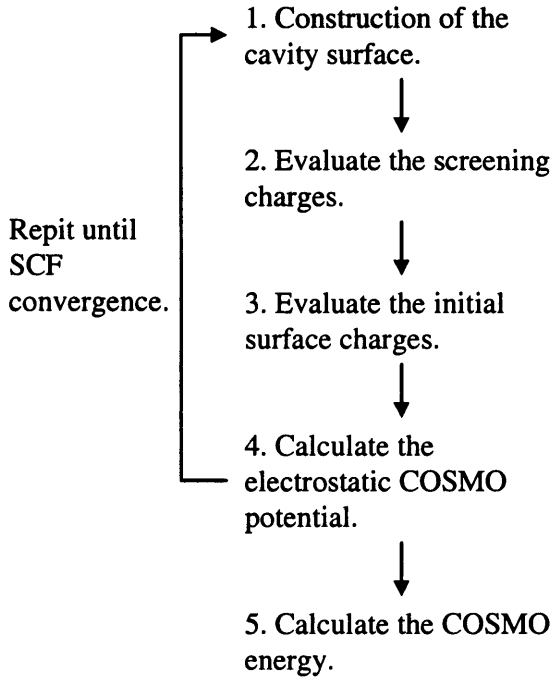

Figure 9 Method to calculate the COSMO energy.

method relies on it. However, in some cases some of the electron density of the solute reaches out of the cavity[44].

Figure 9 describes the COSMO methodology. The method has proved to give satisfactory results in calculating solvation energies, within 8 $kJmol^{-1}$ of the experimental results for neutral molecules[89]. It has also been shown that COSMO reproduces the trends in deprotonation energies in organic molecules[90]. However, as mentioned before, one important step in the COSMO method is the construction of the cavity, because the outlying charge error could be significant in continuum solvation models[44].

2.1.5 Statistical Mechanics

The energy calculated with ab initio or DFT methods is the electronic energy at 0K, for a static molecule. However, even at 0K there are vibrational motions, which have to be taken into account to compute the energy of the system. Calculating the energy at a (finite) higher temperature requires the application of Statistical Thermodynamics, which has at its core the calculation of the partition function (q). Once the partition function is calculated, thermodynamic properties can be determined; for example entropy, enthalpy and free energy[69, 91]. In particular, the entropy (S) and internal energy (E) are calculated with the following equations:

$$S = R\left(\ln(q_t q_e q_r q_v e) + T\left(\frac{\partial \ln q}{\partial T} \right)_V \right), \tag{2.39}$$

$$E = Nk_B T^2 \left(\frac{\partial \ln q}{\partial T} \right)_V . \tag{2.40}$$

Where "t", "e", "r" and "v" sub-indexes are the translational, electronic, rotational and vibrational contributions respectively to the partition function; R and k_B are the gas and Bolztmann constants; T, V and N are the temperature, volume and number of moles.

From the energy the heat capacity can be calculated with,

$$C_V = \left(\frac{\partial E}{\partial T} \right)_{N,V} . \tag{2.41}$$

Calculating the translational, electronic, rotational and vibrational contributions to the partition function allows us to obtain these contributions to the entropy, energy and heat capacity. However, it is important to mention that the partition function is constructed on the assumption of non-interacting particles.

The contribution from the translation to the partition function is given by,

$$q_t = \left(\frac{2\pi m k_B T}{h^2} \right) V . \tag{2.42}$$

Assuming a gas ideal behaviour the translational contribution can calculated from,

$$q_t = \left(\frac{2\pi m k_B T}{h^2} \right) \frac{k_B T}{P} . \tag{2.43}$$

With the last equation and equation (2.39), the translational entropy can now be evaluated as:

$$S_t = R\left(\ln\left[\left(\frac{2\pi m k_B T}{h^2} \right) \frac{k_B T}{P} \right] + \frac{5}{2} \right). \tag{2.44}$$

The respective translational contributions to the energy and heat capacity are given by using equation (2.43) into equations (2.40) and (2.41) respectively,

$$E_t = \frac{3}{2}RT, \tag{2.45}$$

$$C_{V,t} = \frac{3}{2}R. \tag{2.46}$$

The electronic partition function is obtained assuming that first electronic excitation energy is substantially greater than k_BT, and is expressed by,

$$q_e = \omega_0, \tag{2.47}$$

where ω is the degeneracy of the energy level. The entropy electronic contribution is then,

$$S_e = R(\ln \omega_0). \tag{2.48}$$

The corresponding energy and heat capacity are zero, because the electronic partition function in this case is independent of the temperature.

The rotational contribution to the partition function is calculated depending on whether the particle is linear or non-linear. For a linear particle the partition function is,

$$q_{r,linear} = \frac{1}{\sigma_r}\left(\frac{T}{\Theta_r}\right), \tag{2.49}$$

where σ_r is the symmetry number for rotation and $\Theta_r = h^2/8\pi^2 I k_B$ (with "I" being the moment of inertia).

Using the latter equation with the early definitions of entropy, energy and heat capacity (equations (2.39), (2.40) and (2.41) respectively), we obtain for a linear particle the following rotational contributions,

$$S_{r,linear} = R\left(\ln\left[\frac{1}{\sigma_r}\left(\frac{T}{\Theta_r}\right)\right] + 1\right), \tag{2.50}$$

$$E_{r,linear} = RT, \tag{2.51}$$

$$C_{V,r,linear} = R. \tag{2.52}$$

In the general case of a non-linear particle, the rotational partition function is given by,

$$q_{r,nonlinear} = \frac{\pi^{1/2}}{\sigma_r}\left(\frac{T^{3/2}}{(\Theta_{r,x}\Theta_{r,y}\Theta_{r,z})^{1/2}}\right). \tag{2.53}$$

With equations (2.39), (2.40), (2.41) and (2.53) we obtain for the entropy, energy and heat capacity,

$$S_{r,nonlinear} = R\left(\ln\left[\frac{\pi^{1/2}}{\sigma_r}\left(\frac{T^{3/2}}{(\Theta_{r,x}\Theta_{r,y}\Theta_{r,z})^{1/2}}\right)\right]+\frac{3}{2}\right), \tag{2.54}$$

$$E_{r,nonlinear} = \frac{3}{2}RT, \tag{2.55}$$

$$C_{V,r,nonlinear} = \frac{3}{2}R. \tag{2.56}$$

Finally, the vibrational motion contribution to the partition function is given as a product of each of the $3n_{atoms}$-6 vibrational modes, K, with a characteristic vibrational temperature, $\Theta_{v,K}=h\upsilon_K/k_B$,

$$q_v = \prod_K \frac{e^{-\Theta_{v,K}/2T}}{1-e^{-\Theta_{v,K}/2T}}. \tag{2.57}$$

Equation (2.57) is applied in equations (2.39), (2.40) and (2.41) to evaluate the vibrational entropy, energy and heat capacity,

$$S_v = R\sum_K\left(\frac{\Theta_{v,K}/T}{e^{\Theta_{v,K}/T}-1} - \ln(1-e^{-\Theta_{v,K}/T})\right), \tag{2.58}$$

$$E_v = R\sum_K \Theta_{v,K}\left(\frac{1}{2}+\frac{1}{e^{\Theta_{v,K}/T}-1}\right), \tag{2.59}$$

$$C_{V,v} = R\sum_{K} e^{\Theta_{v,K}/T}\left(\frac{\Theta_{v,K}/T}{e^{-\Theta_{v,K}/T}-1}\right)^2. \qquad (2.60)$$

From the latter equations for the entropy and energy, further thermodynamic properties can be derived[91], for example, the enthalpy (H) is calculated with the following expression,

$$H(T) = E_V(T) + E_r(T) + E_t(T) + RT. \qquad (2.61)$$

And the free energy of the system is then evaluated with,

$$G = H - TS. \qquad (2.62)$$

The equations presented in this section are the basis for the calculation of the thermodynamic properties presented later chapters of this thesis. We shall present later on the exact method used here, including the use of simulated annealing to avoid local minima.

3 METHODOLOGY FOR MODELLING SILICATE SPECIES IN AQUEOUS SOLUTION

The aim of this work is to analyse the key structures and mechanisms involved in zeolite nucleation using a computational approach.

To this end, we have developed a method using Density Functional Theory (DFT), which allows consideration of solvation, the high pH, and the temperature of hydrothermal synthesis. We shall demonstrate in the next chapters how the method performs by comparison to the few well-known quantitative data related to the chemistry of nucleation of zeolites, e.g. deprotonation of the monomer, dimer, and the free energy of dimerization. The current chapter will focus on a detailed account of the method. A Density Functional Theory method with a numerical basis set is chosen because of its good description of hydrogen bonds[84], together with the minimal Basis Set Superposition Errors (BSSE)[85] and the number of previous works modelling silicates with a similar level of theory[39, 40, 60].

All the calculations were performed with DMOL^3, version 2.2[82, 83, 92]. The structure manipulation and some of the analysis of the results were achieved with the visualization software Cerius^2 from Accelrys[88]. The procedures at each stage will now be discussed in more detail.

3.1 Simulated Annealing and geometry optimization

The initial geometry of the clusters considered was taken where appropriate directly from the crystal structure of a Chabazite zeolite, although some are suggested directly by the experimental results[3, 5, 31-33]. Most of the clusters studied are, however, common to the majority of zeolite frameworks.

The flexible nature of silicate clusters, and the number of atoms involved, results in a potential energy surface with many local minima. Thus, in order to avoid locating such local minima, we have employed a simulated annealing procedure illustrated diagrammatically in Figure 10, where the structures were first subjected to a procedure involving quantum molecular dynamics prior to the gas phase optimization. First, an optimization is carried out with a low-cost local DFT (PWC) method, and then a simulated annealing cycle is done with melting, molecular dynamics NVT and quenching steps. The molecular dynamics NVT stage is performed in 3000 steps of 0.46fs at 700K, using a minimal basis set (which uses one atomic orbital for each occupied orbital) and the PWC functional. The mass of all the atoms is set equal, so they have the same mobility and more conformations can be sampled. Finally, an optimization with the same level of theory as the first optimization is carried out.

This simulated annealing procedure will generate a structure closer to the global minima. A further optimization with a more precise DFT method will then find the structure in that energy minimum. However, there is no complete guarantee that a global minimum has been reached and there are no means to know whether the

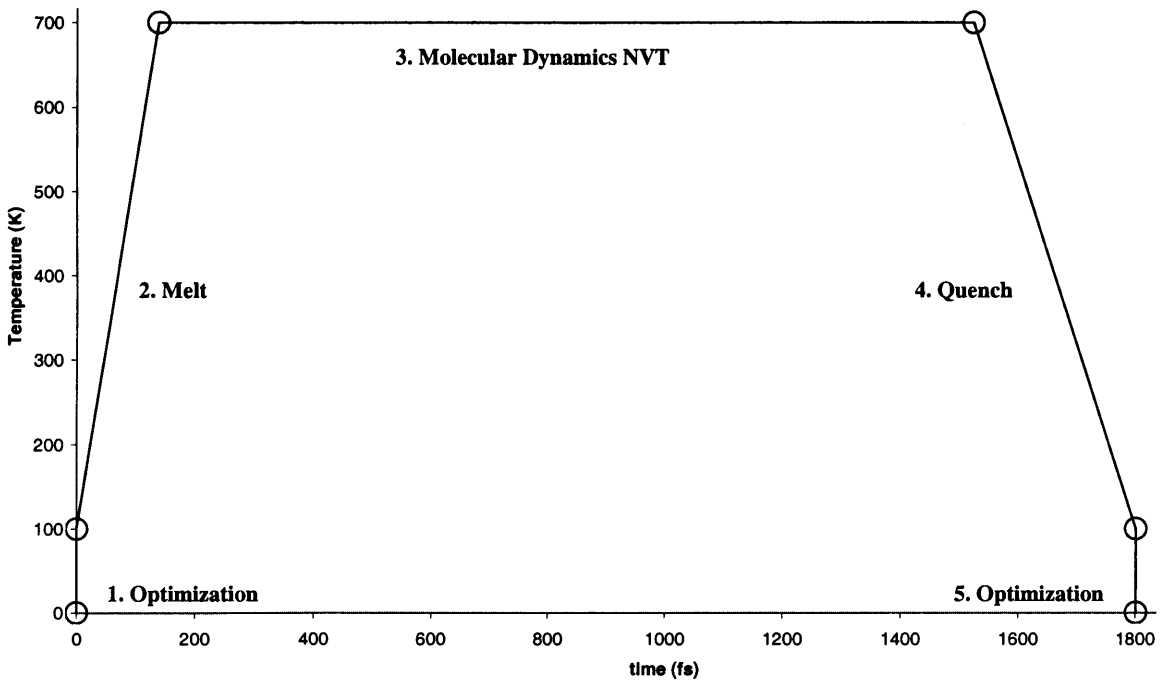

Figure 10 Schematic representation of the Simulated Annealing procedure followed in this work.

minimum found is global or local. Nevertheless, it is hoped that such approach applied together with chemical intuition will ensure that global minima are achieved for the majority of the clusters.

Using the structure obtained from simulated annealing as a starting point, a full optimization with a high level of theory is then carried out. A non-local DFT, with a double numerical basis set with polarization is used: BLYP/DNP//BLYP/DNP. The energy calculated after the geometry optimization is the electronic energy at 0K, without correction for the zero point energy (ZPE). To account for the vibrations present even at 0K, and to calculate thermodynamical properties *i.e.* enthalpy, entropy, and Gibbs free energy, a standard statistical mechanical method is applied. The translational, rotational, vibrational, and electronic contributions to the energy are taken into account in the statistical mechanical calculations[91]. The corrected energy for the temperature is then analyzed at 298K, as this is the temperature at which the raw material is mixed and the temperature at which experimental results are available, followed by an analysis at 450K a temperature typical of zeolite synthesis. Further analysis can also be performed at different temperatures as necessary.

The structure and its associated thermodynamic quantities obtained from the optimization method explained above, models the cluster in the gas phase without any kind of interaction with its surroundings. From here onwards, the structure generated by this step will be labelled the "gas phase" cluster, which is obviously an unrealistic representation of the clusters when in solution under hydrothermal synthesis conditions. Nevertheless, it is a first approximation, and some time ago was the only method available to model zeolites.[62] Indeed, it does give acceptable results in terms of bond lengths, angles and even NMR chemical shifts [68]. However, it is clear that in the hydrothermal synthesis of zeolites, two critical aspects are the solvent and the high pH present, as described in the section 1.2.2. Thus, in this work, an attempt will be made to incorporate their influence.

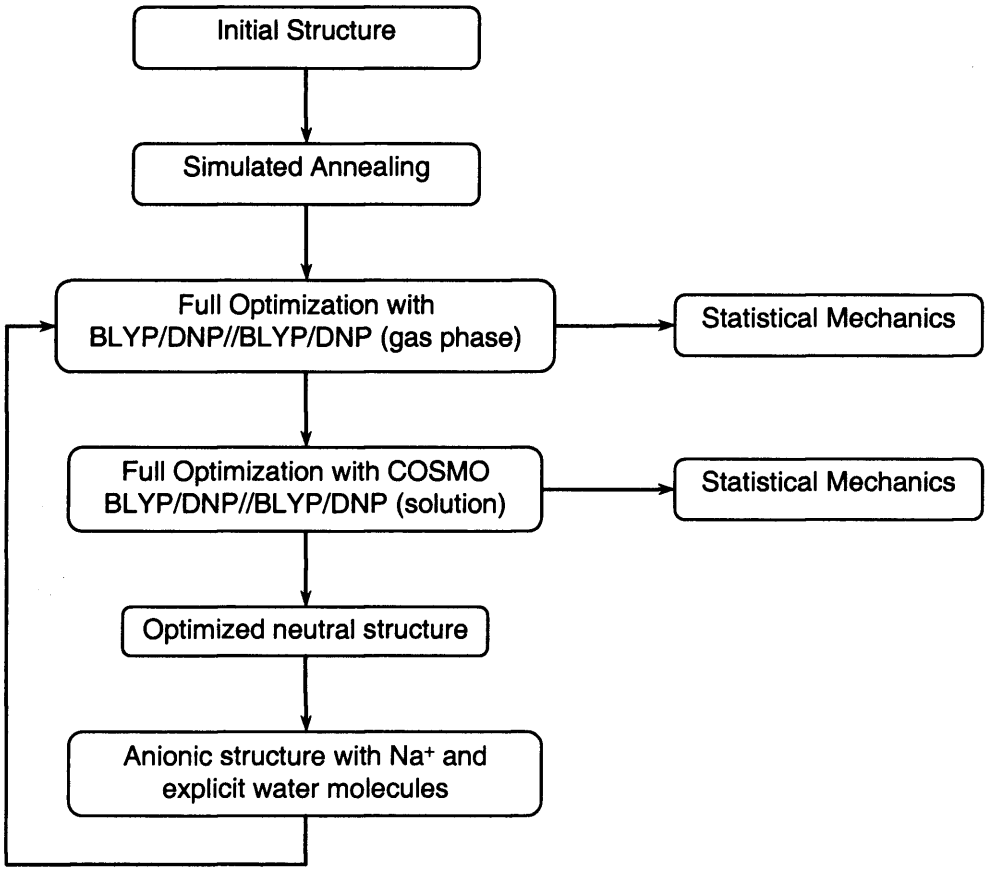

Figure 11 The general procedure developed in this work to model silicate clusters. The initial structure is neutral. The optimized structure in solution (COSMO) is used to generate the anion, which undergoes the same gas phase and solution optimization as the neutral cluster. Standard Statistical Mechanics calculations are performed for every optimized structure.

The complete strategy needed to analyse the clusters presented in this work is summarized in the Figure 11.

3.2 Models studied

Figure 12 shows the clusters studied in this work and how they could be related under synthesis conditions. Each arrow represents a single condensation, in the direction of the arrow and indicates the product; also formed is water, which is omitted for clarity. Some of the arrows in the lower part of the diagram refer to multiple condensations (*i.e.* where several siloxane bonds are formed). This diagram and the following images, Figures 9-38, present a synthesis of the clusters studied in this work, which could be used as a reference in the analysis of the following chapters. The structures of Figures 9-38 are the optimized results in COSMO solvation, obtained using the procedure outlined in this chapter.

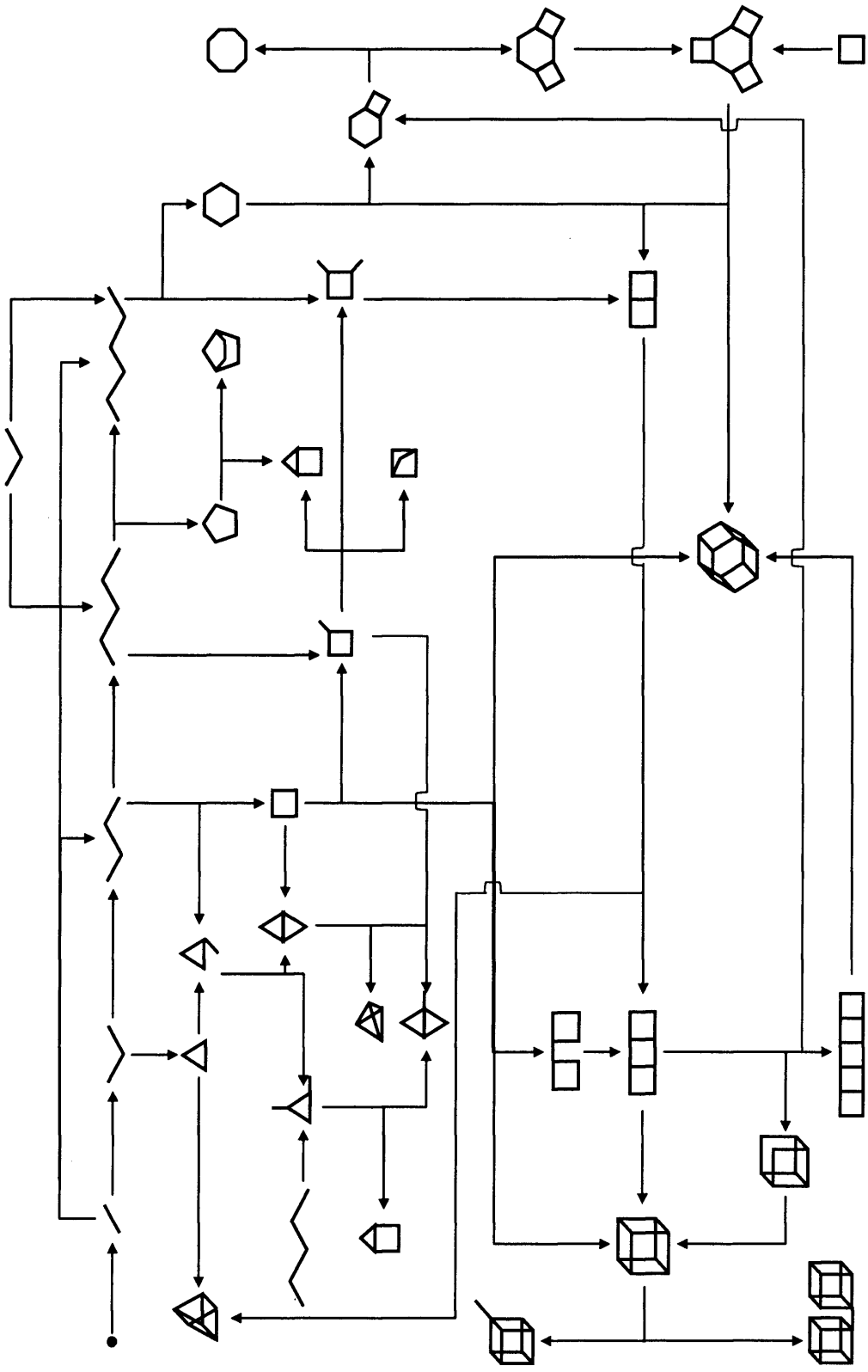

Figure 12 The relation of the clusters presented in Figures 9-38. The clusters are shown as a line diagram, where in each corner there is a silicon and in the middle of line there is an oxygen.

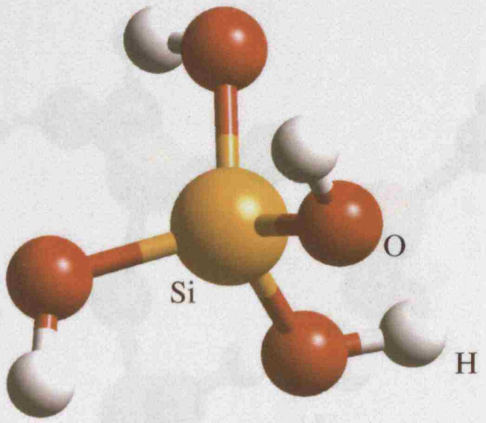

monomer $Si(OH)_4$

Figure 13 The monomer; its formula and symbol/line diagram used in Figure 12. The atom type is identified by an adjacent label. **The size of the spheres is always Si > O > H. Si always occupies a tetrahedral site. Note, these conventions are used in all the molecular graphics in this thesis.**

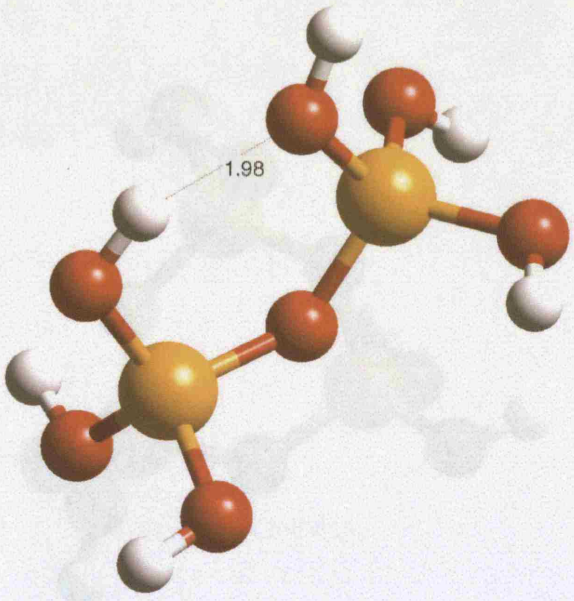

dimer $Si_2O(OH)_6$

Figure 14 The dimer. The H-bond (Å) is denoted by a dashed line as in all subsequent graphics.

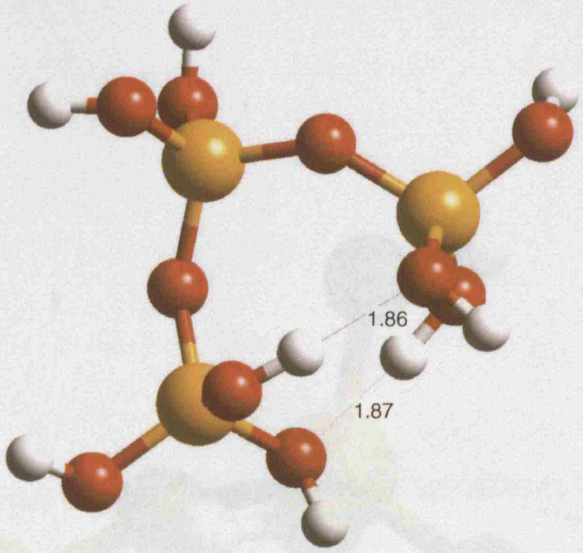

trimer $Si_3O_2(OH)_8$

Figure 16 The trimer.

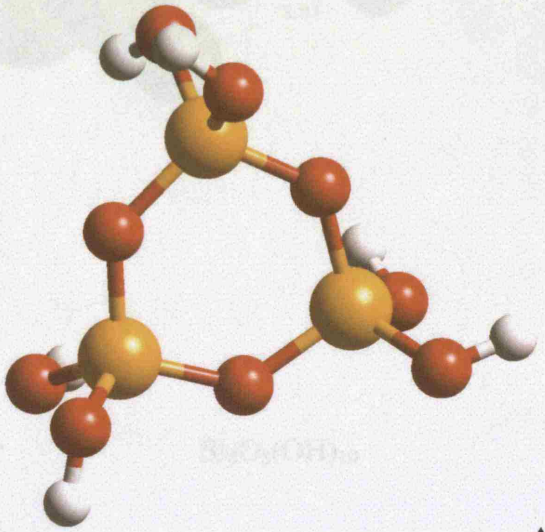

3-ring $Si_3O_3(OH)_6$

Figure 15 The 3-ring.

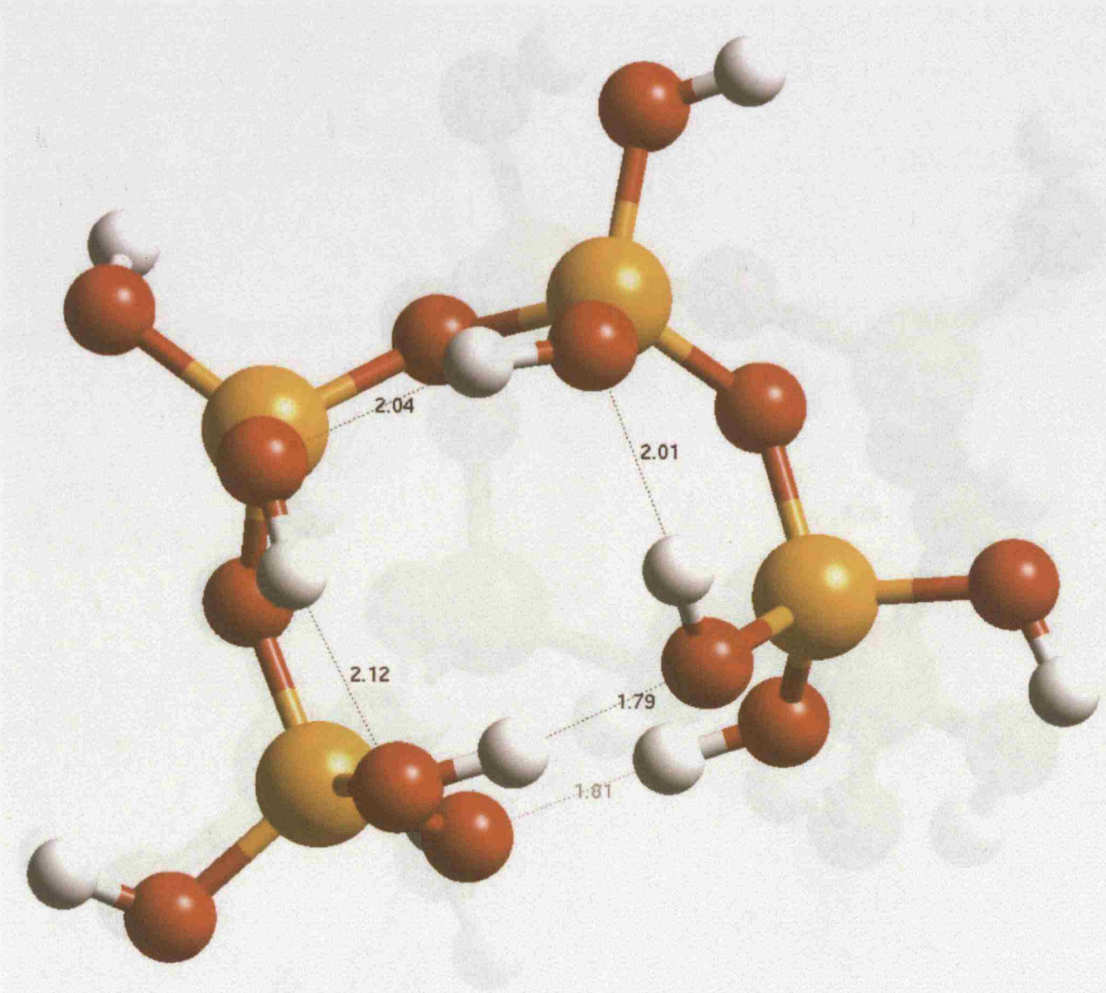

tetramer $Si_4O_3(OH)_{10}$

Figure 17 The tetramer.

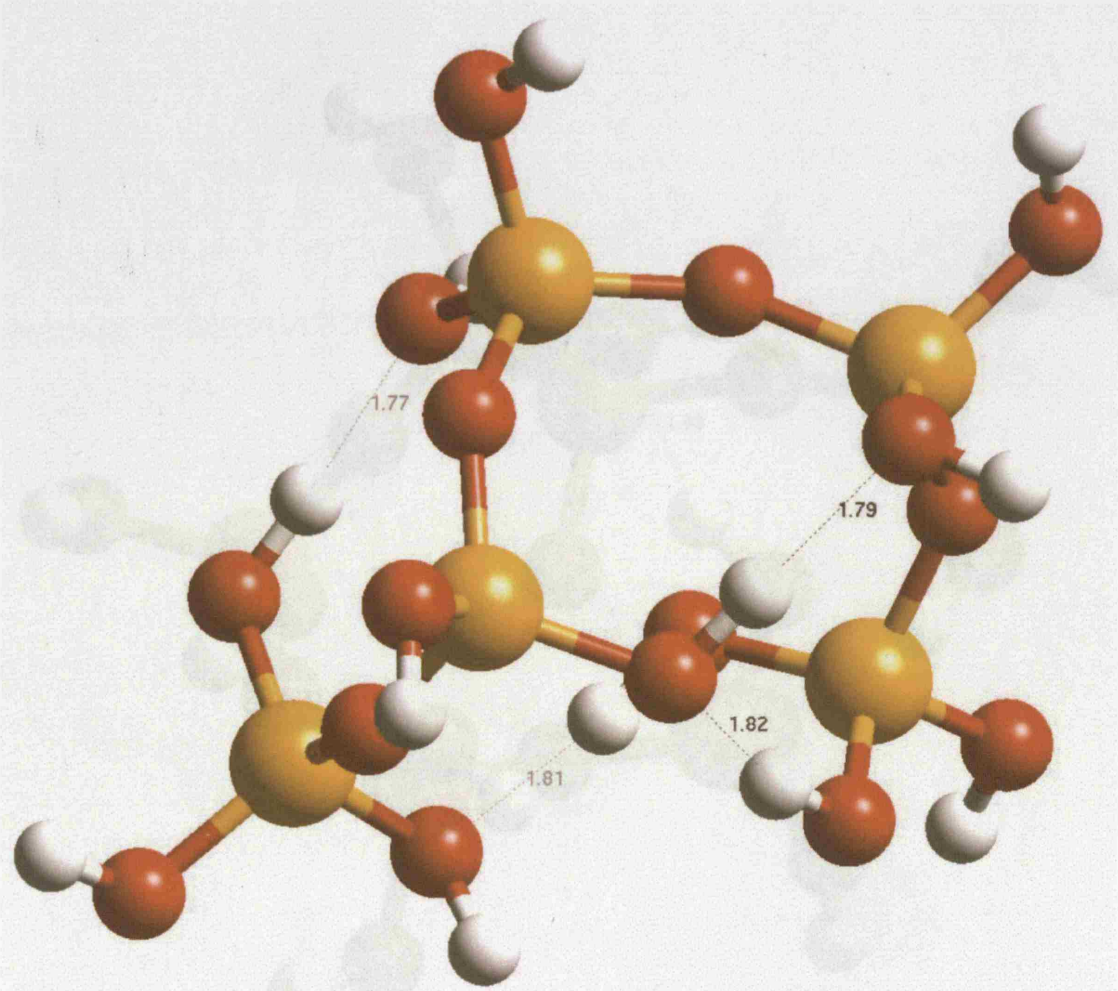

pentamer $Si_5O_4(OH)_{12}$

Figure 18 The pentamer.

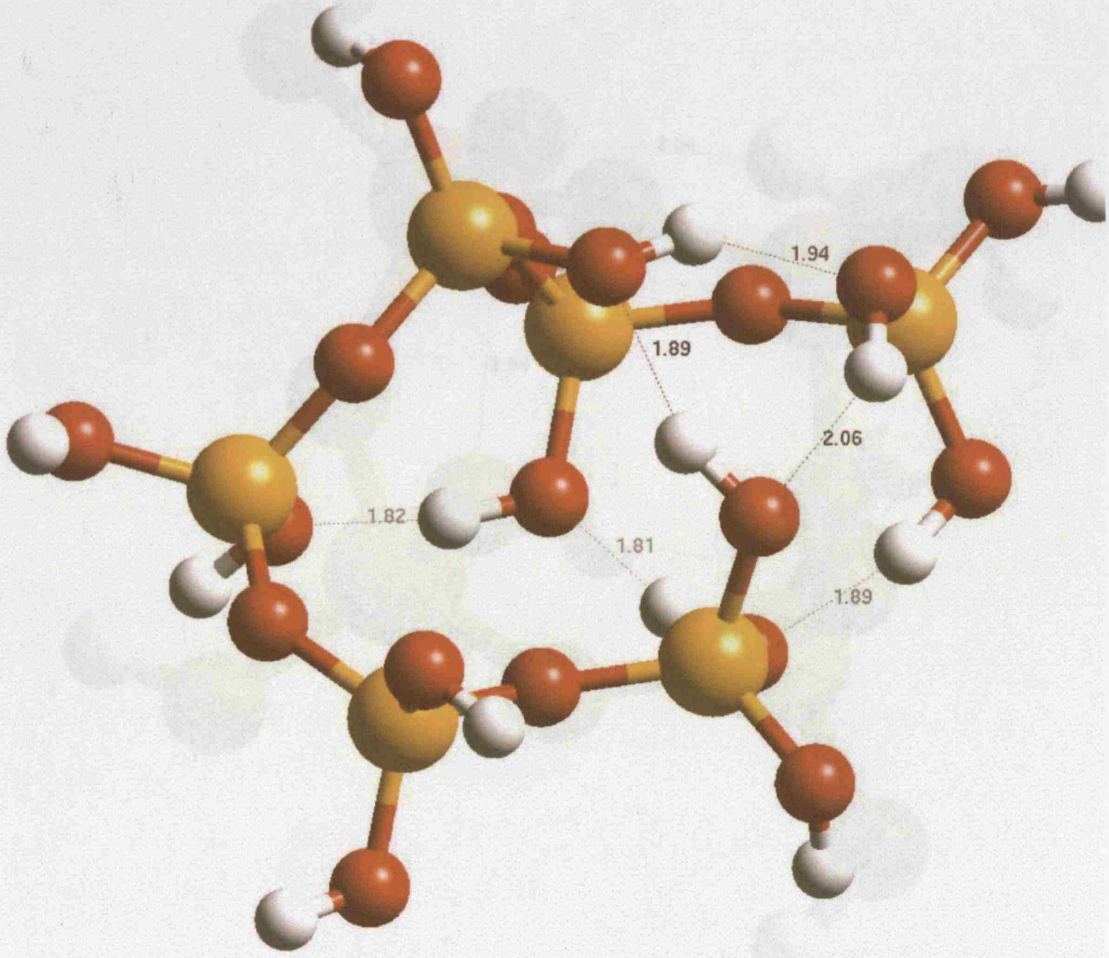

hexamer $Si_6O_5(OH)_{14}$

Figure 19 The hexamer.

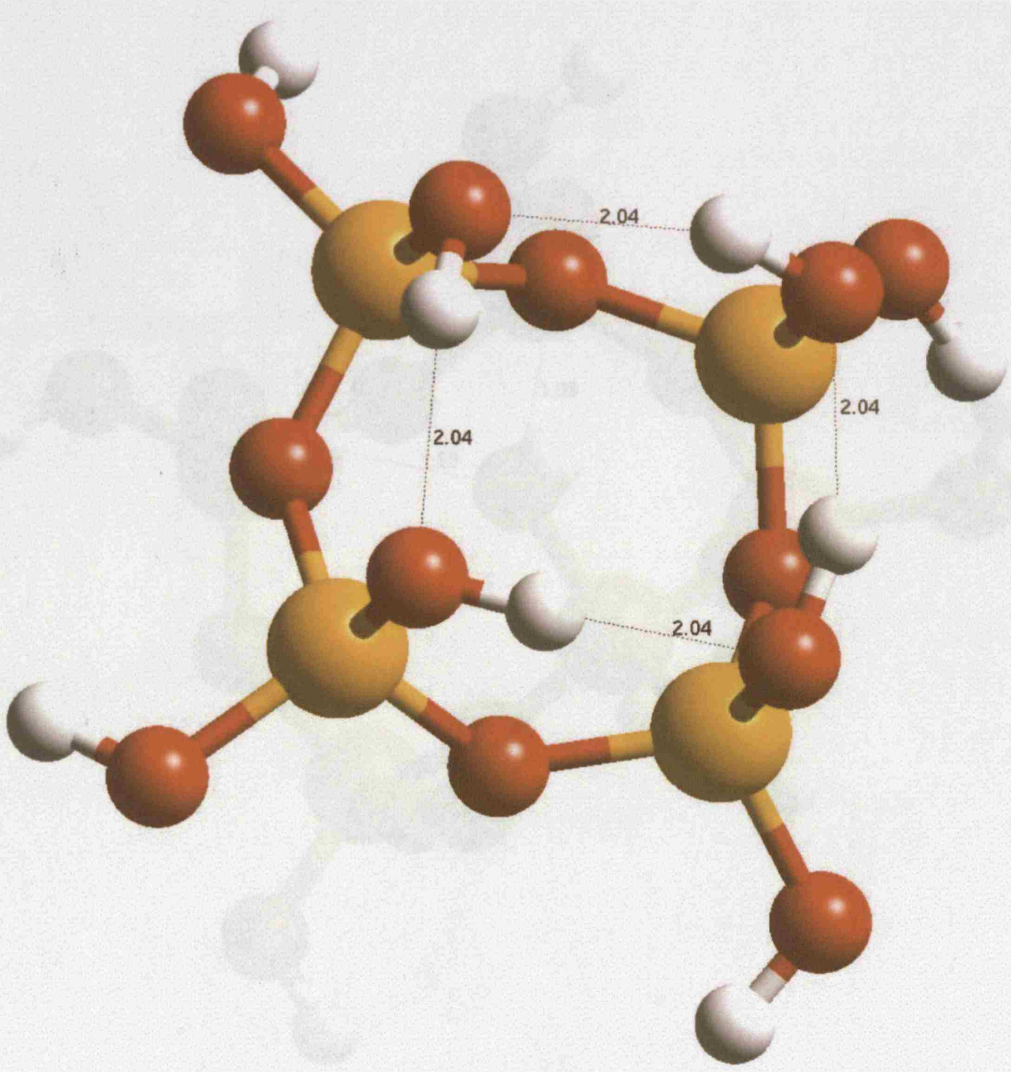

4-ring $Si_4O_4(OH)_8$

Figure 20 The 4-ring.

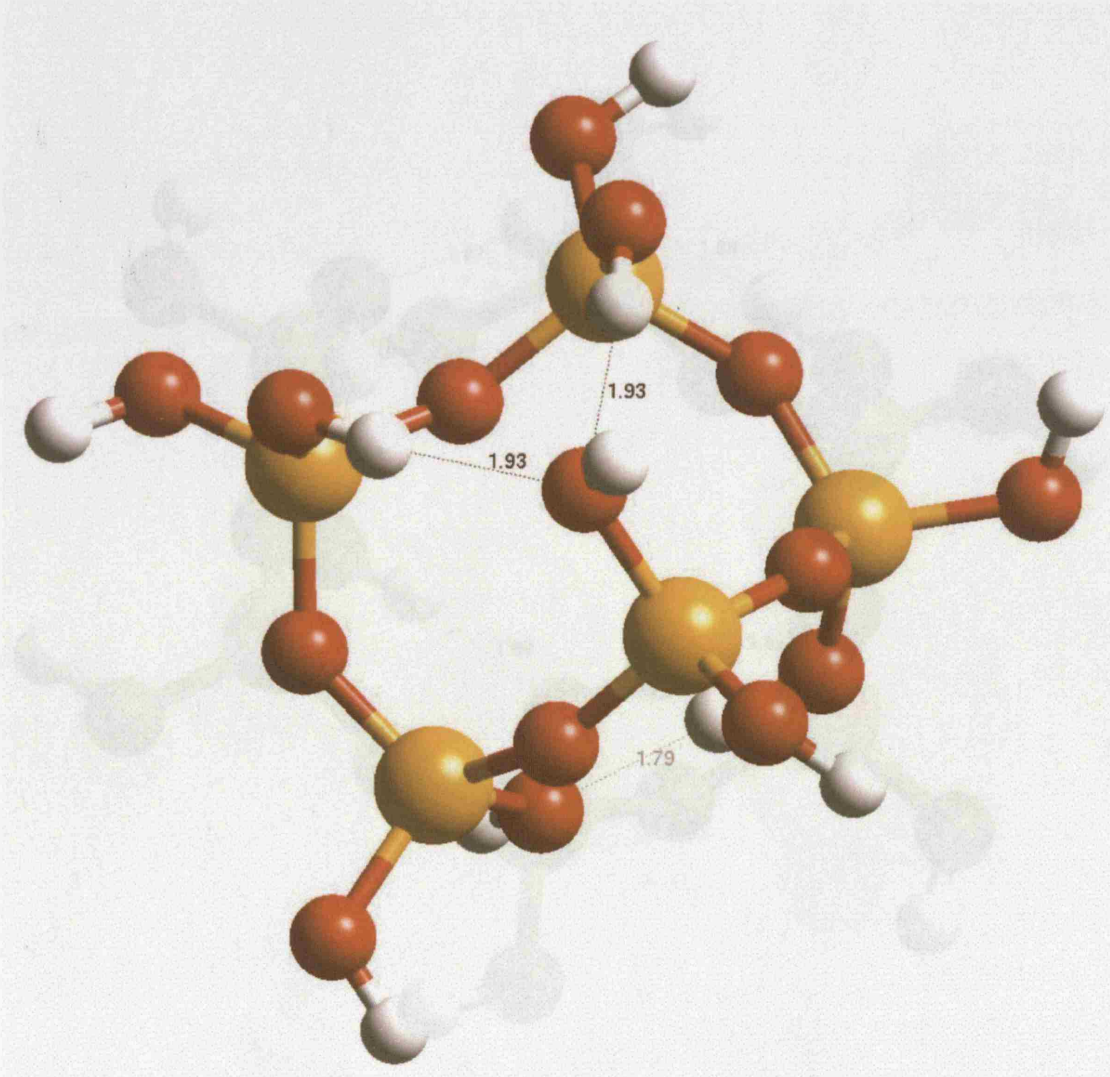

5-ring $Si_5O_5(OH)_{10}$ 

Figure 21 The 5-ring.

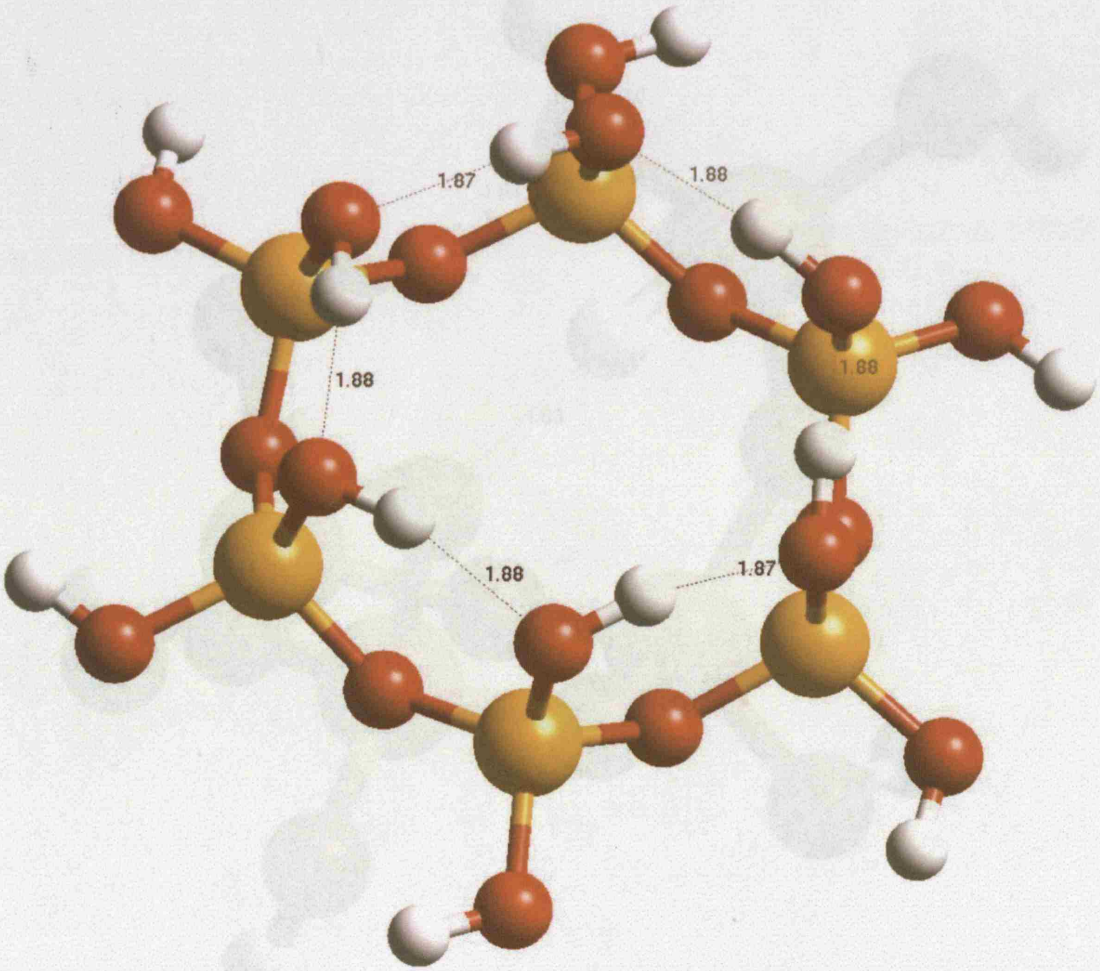

6-ring $Si_6O_6(OH)_{12}$ 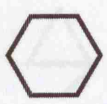

Figure 22 The 6-ring.

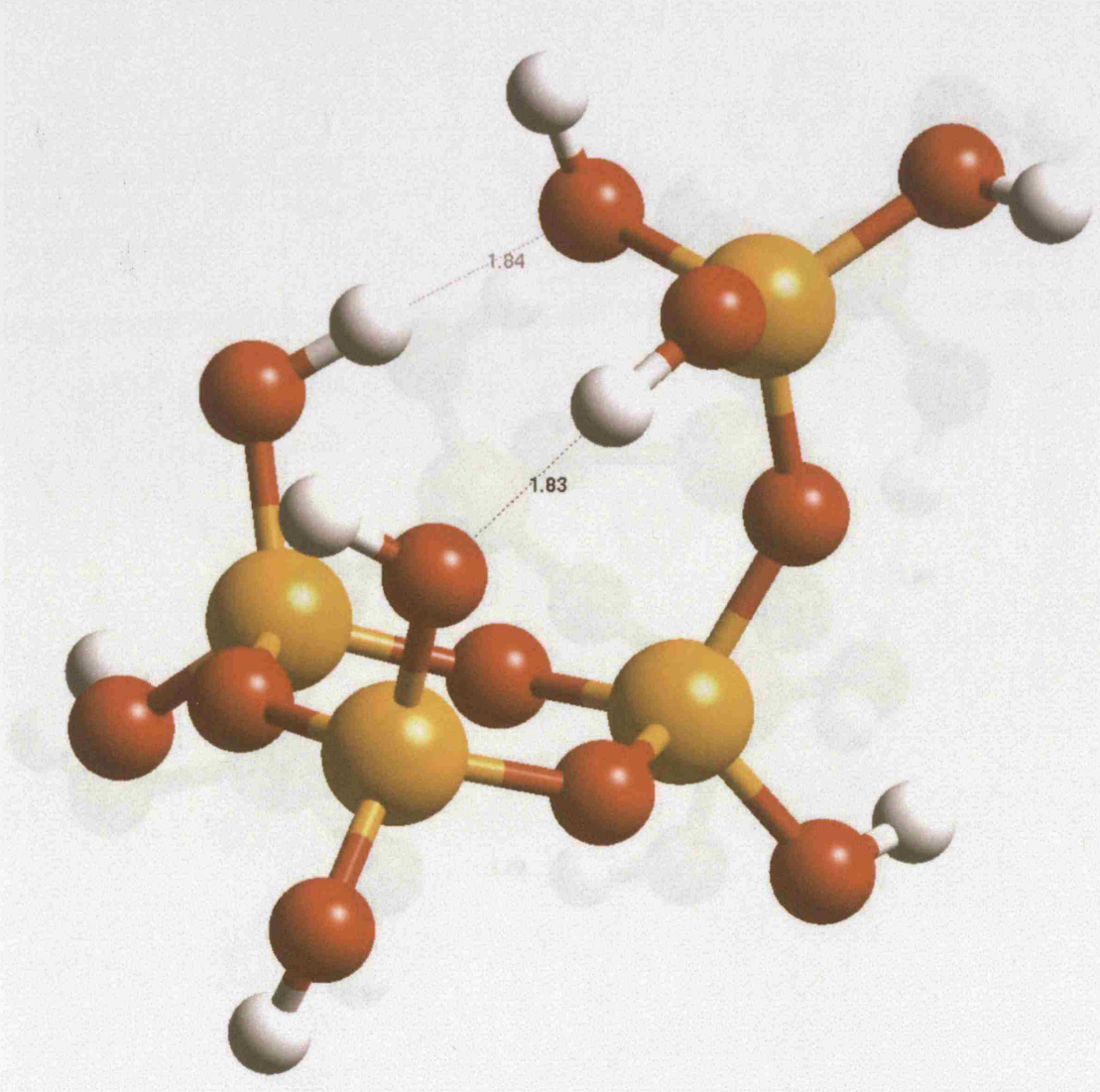

3-1-ring $Si_4O_4(OH)_8$

Figure 23 The 3-1-ring.

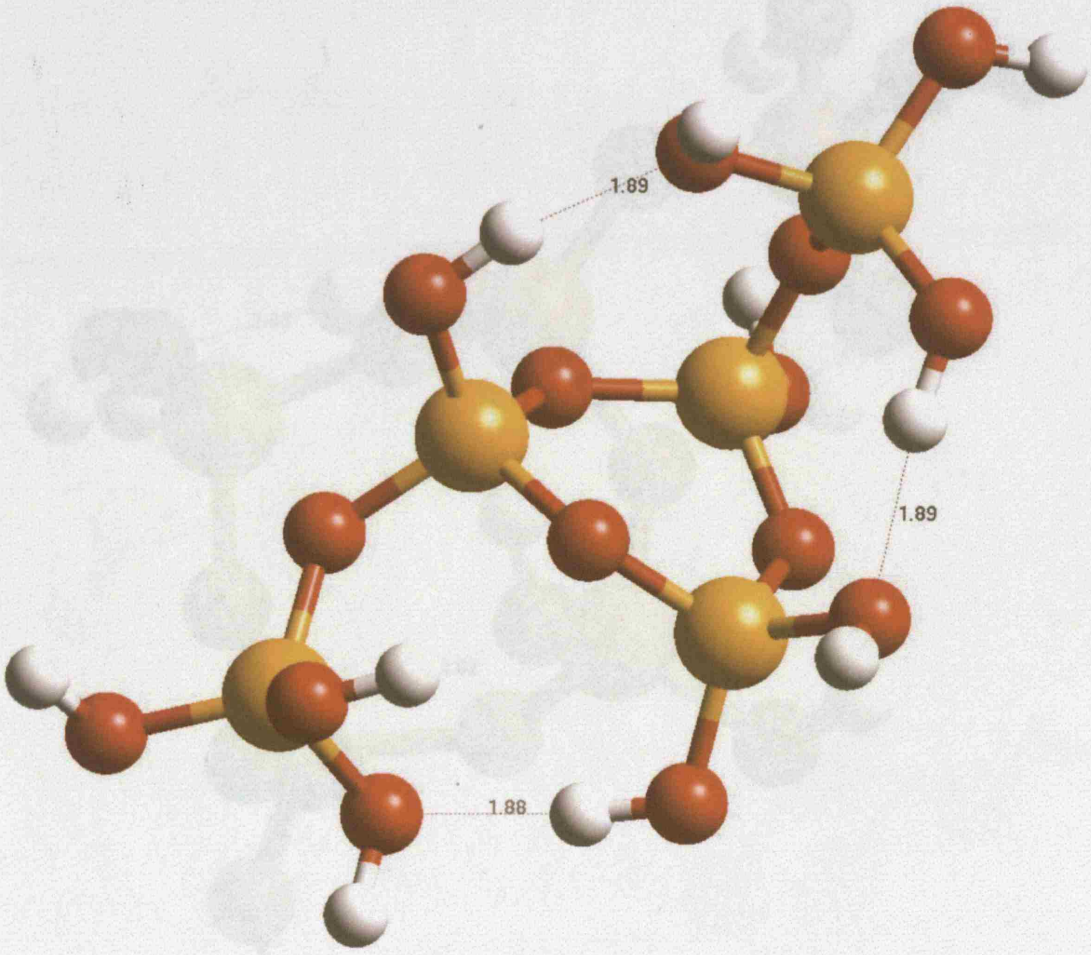

3-2-ring $Si_5O_5(OH)_{10}$

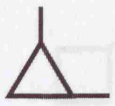

Figure 24 The 3-2-ring.

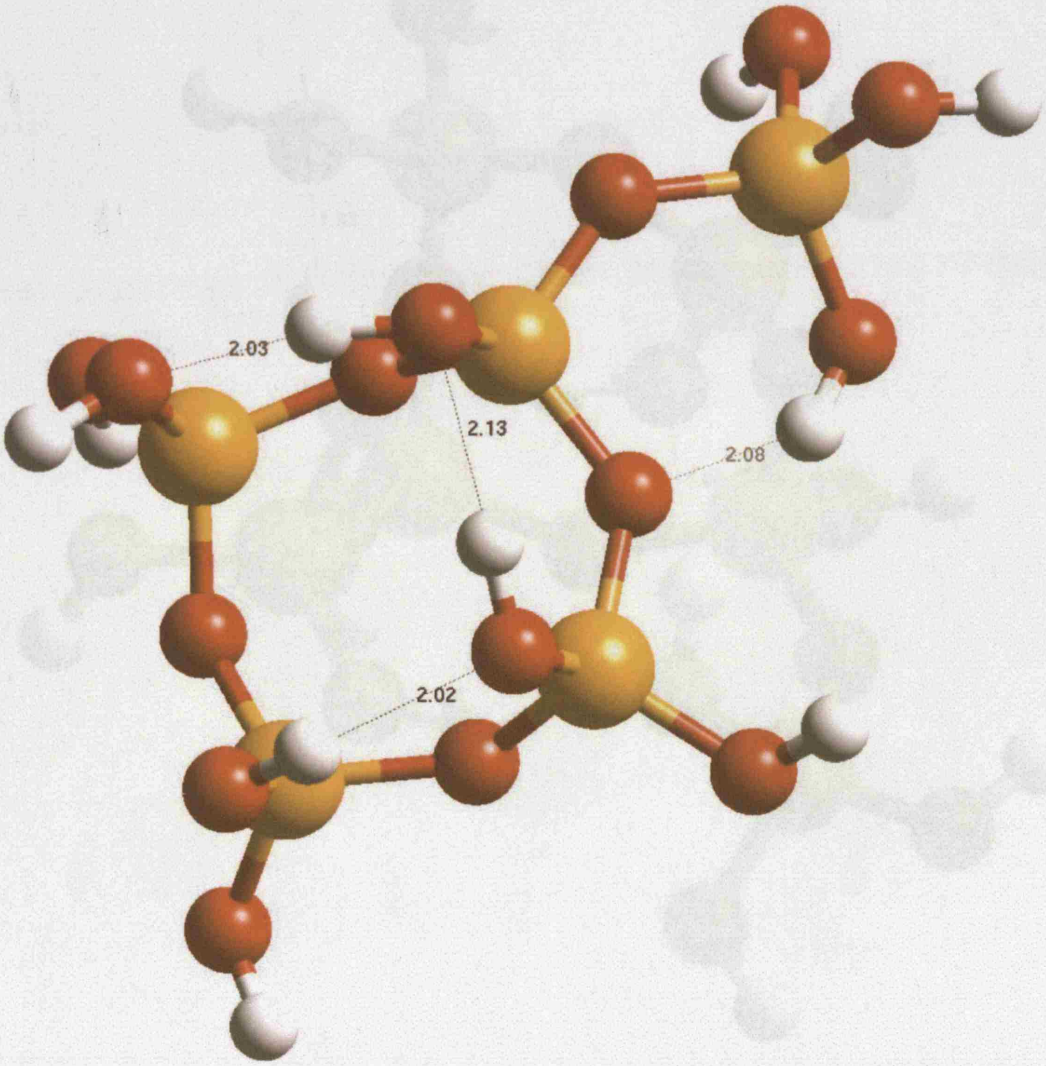

4-1-ring $Si_5O_5(OH)_{10}$

Figure 25 The 4-1-ring.

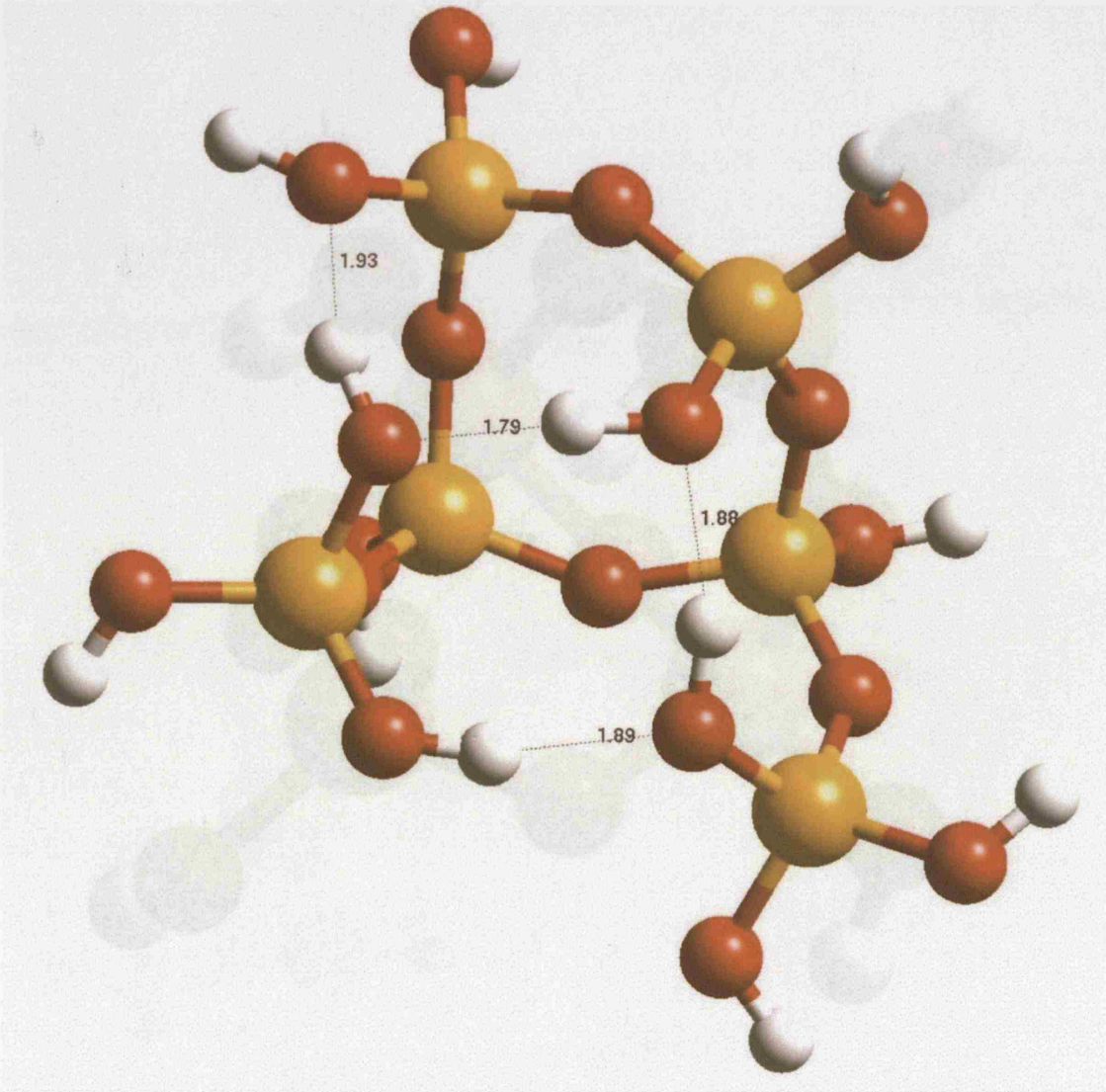

4-2-ring $Si_6O_6(OH)_{12}$

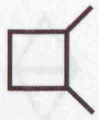

Figure 26 The 4-2-ring.

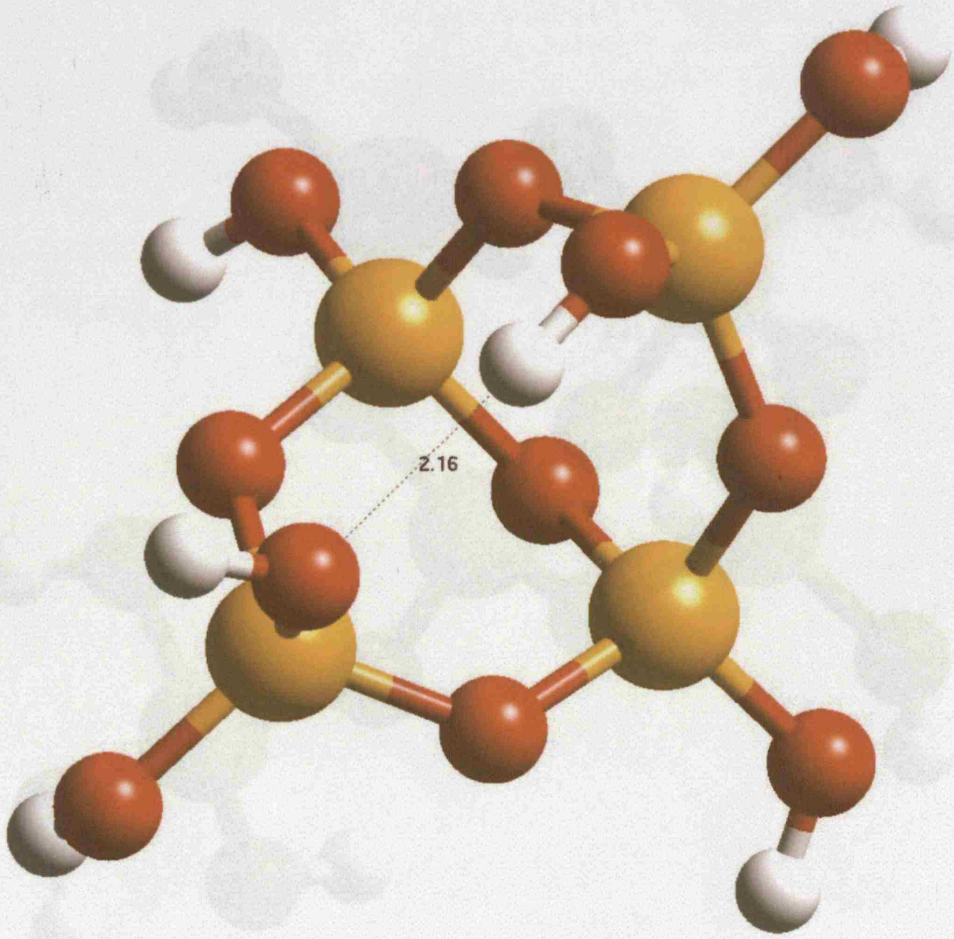

fused3-ring $Si_4O_5(OH)_6$

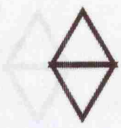

Figure 27 The fused3-ring.

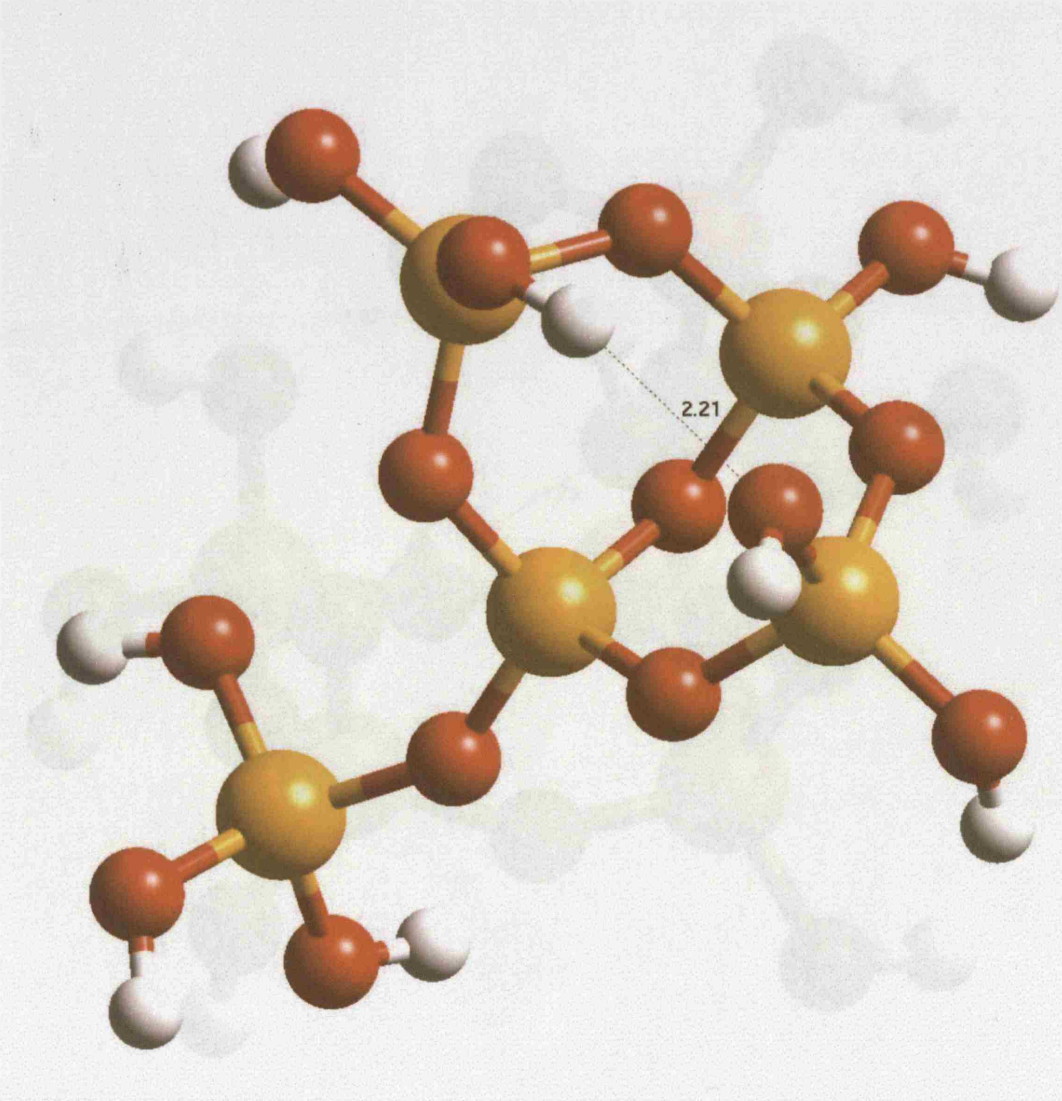

fused3-1-ring $Si_5O_6(OH)_8$

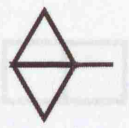

Figure 28 The fused3-1-ring.

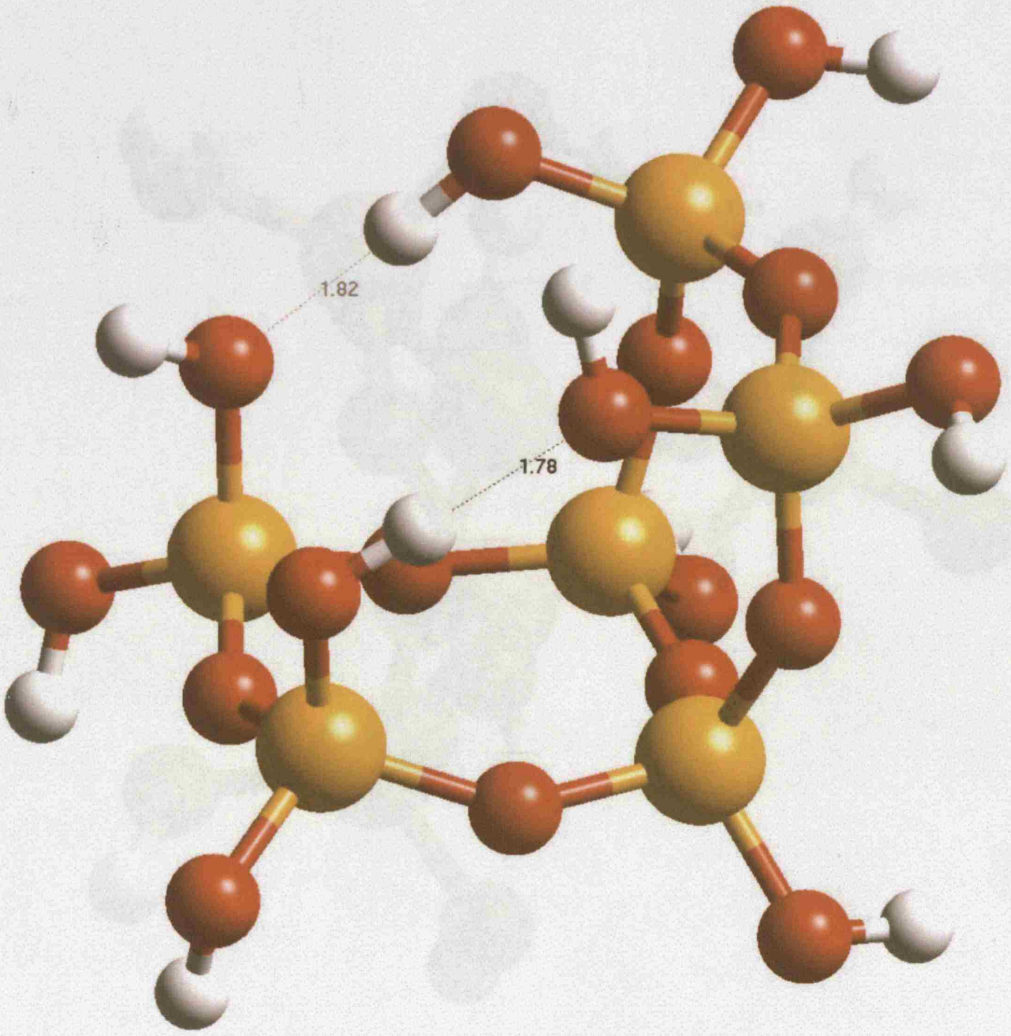

fused4-ring $Si_6O_6(OH)_{10}$

Figure 29 The fused4-ring.

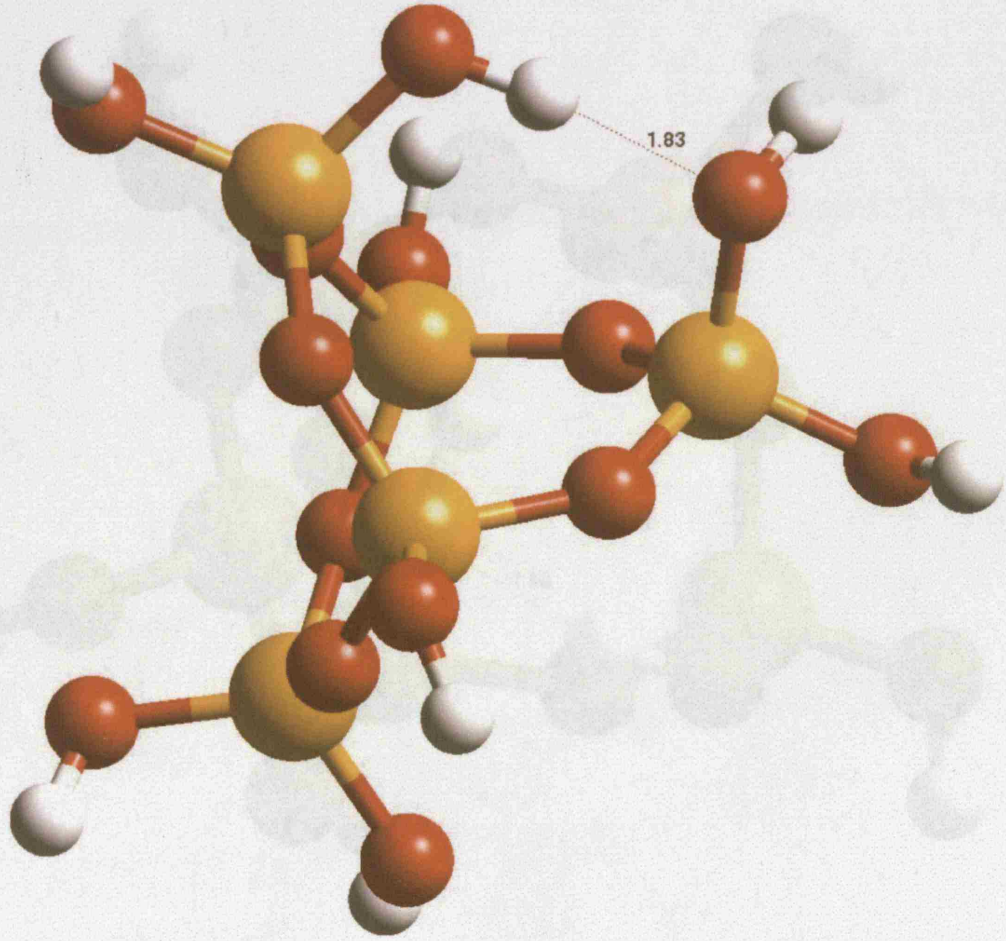

4-one-ring $Si_5O_6(OH)_8$

Figure 30 The 4-one-ring.

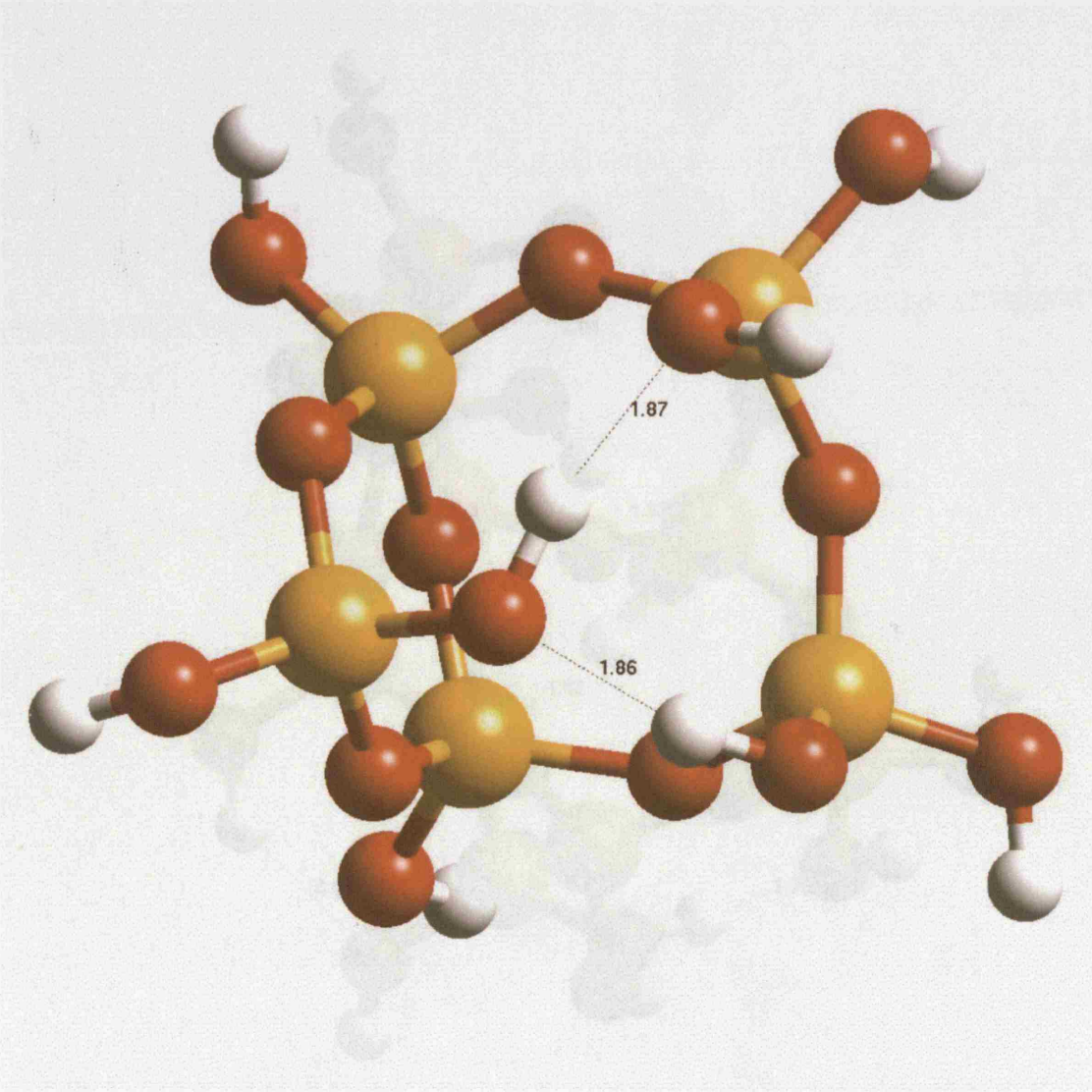

4-three-ring $Si_5O_6(OH)_8$

Figure 31 The 4-three-ring.

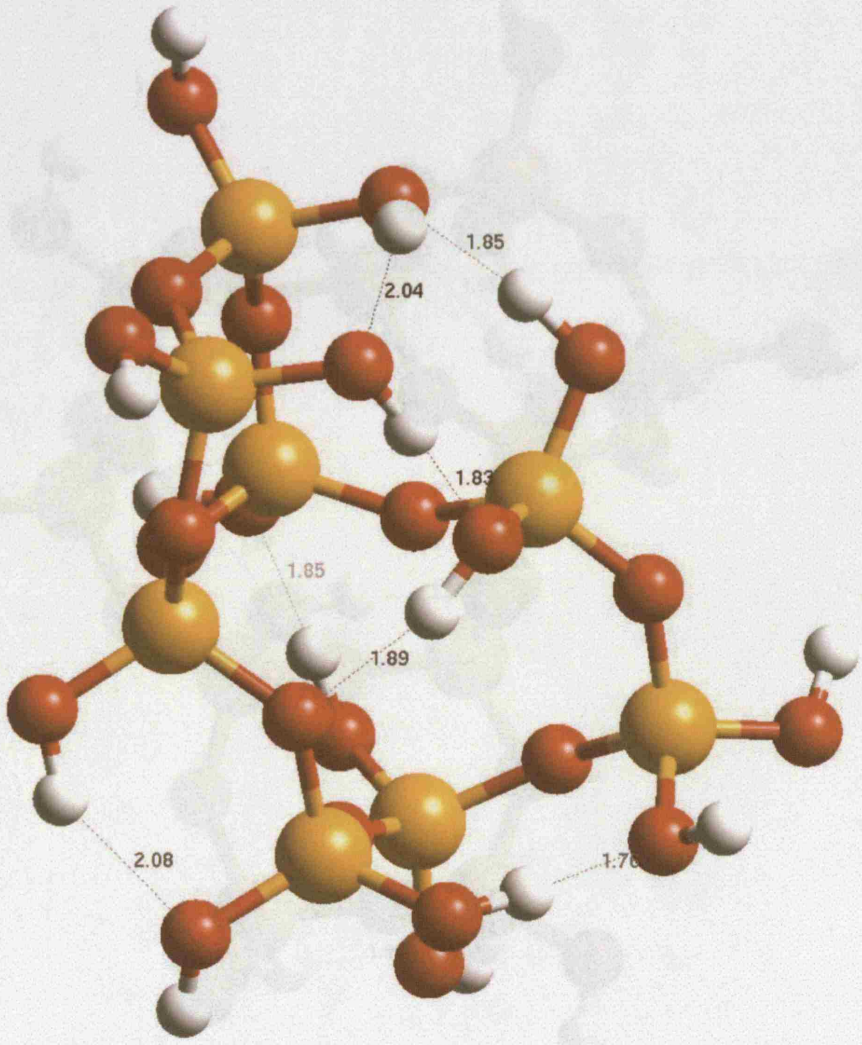

6-one4-ring $Si_8O_9(OH)_{14}$

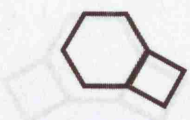

Figure 32 The 6-one4-ring.

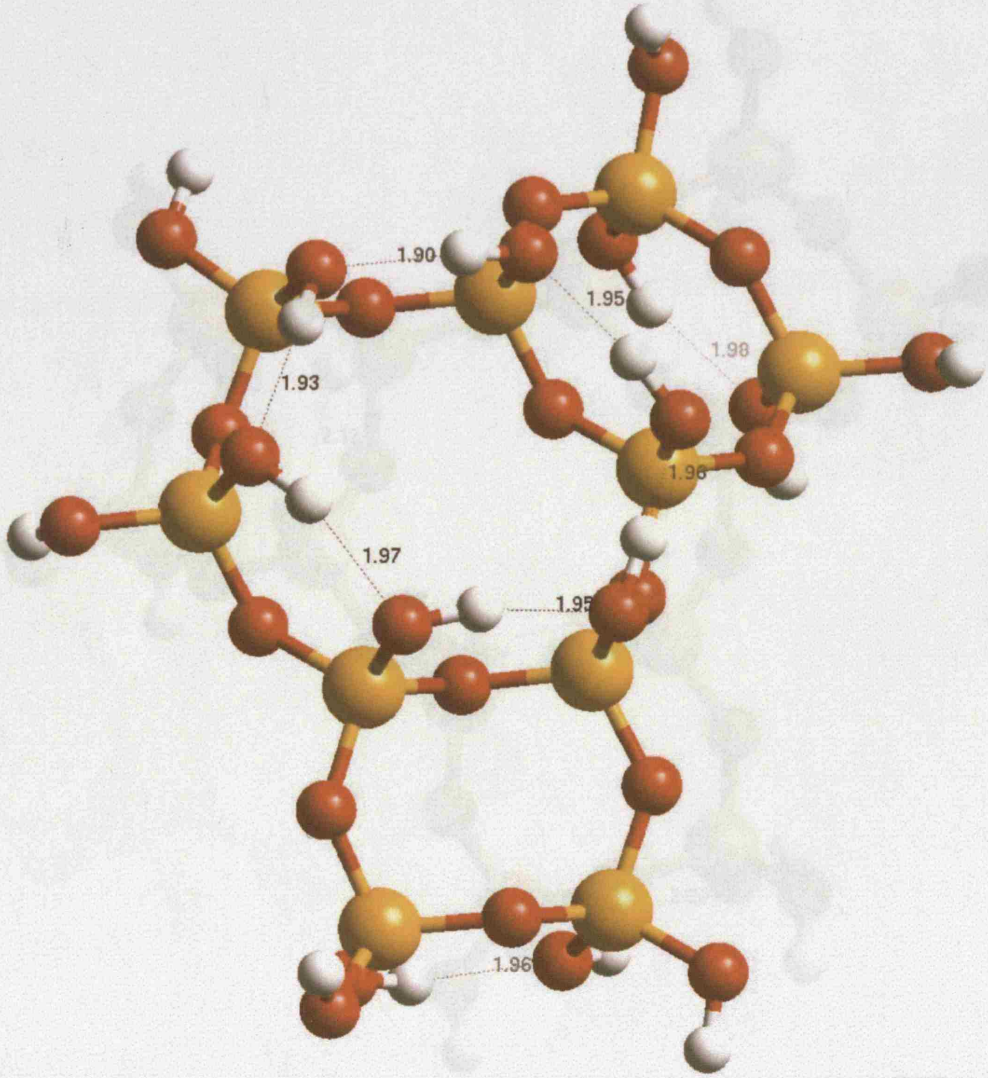

6-two4-ring $Si_{10}O_{12}(OH)_{16}$

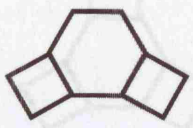

Figure 33 The 6-two4-ring.

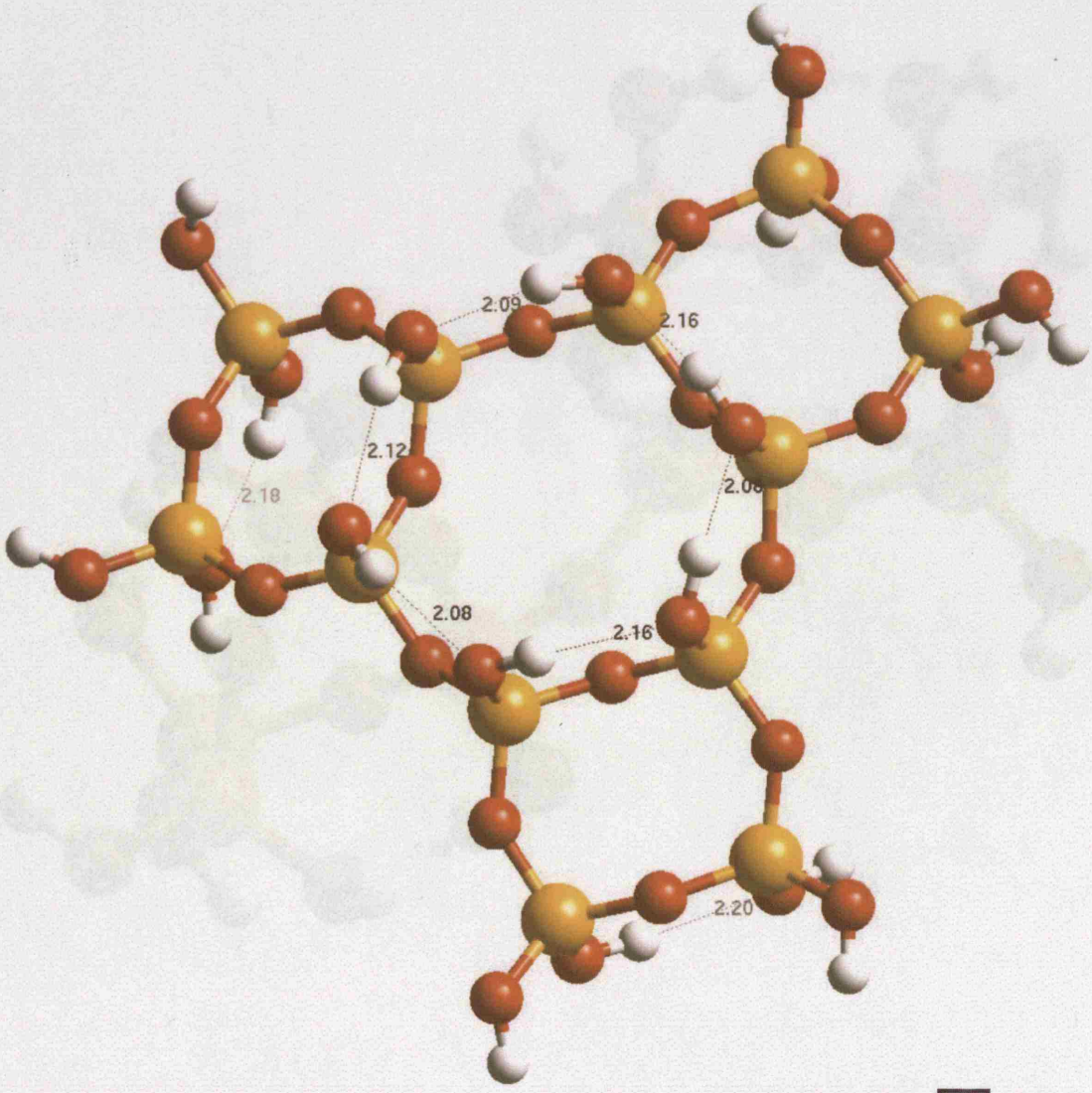

6-three4-ring $Si_{12}O_{15}(OH)_{18}$

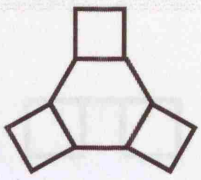

Figure 34 The 6-three4-ring.

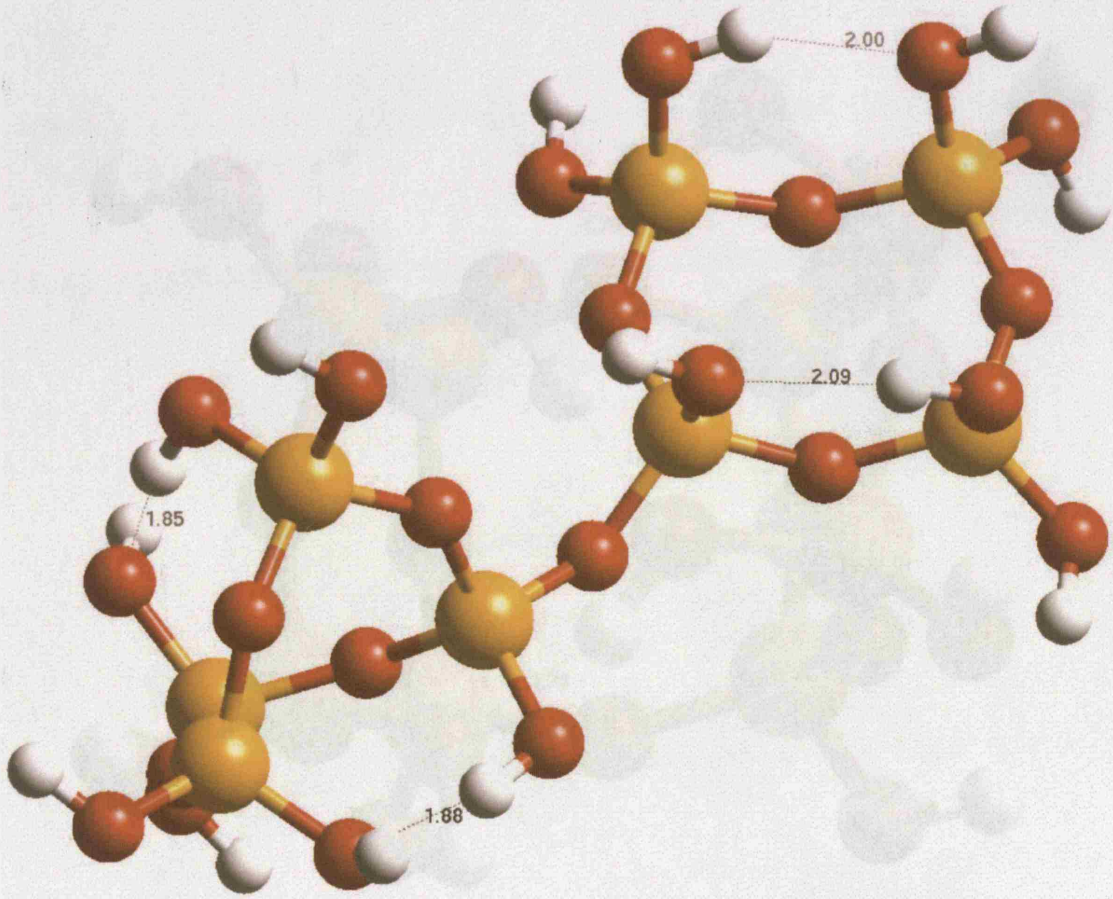

4-4-ring $Si_8O_9(OH)_{14}$

Figure 35 The 4-4-ring.

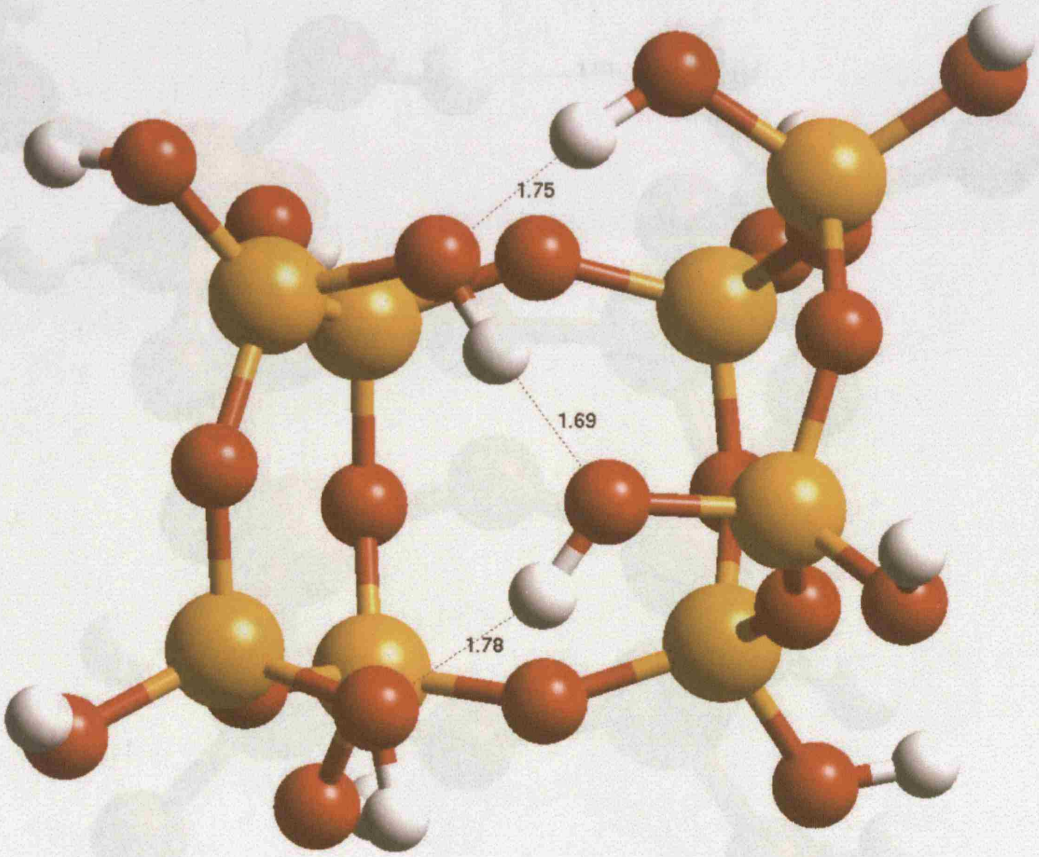

tri4-ring $Si_8O_{10}(OH)_{12}$

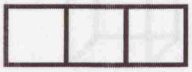

Figure 36 The tri4-ring.

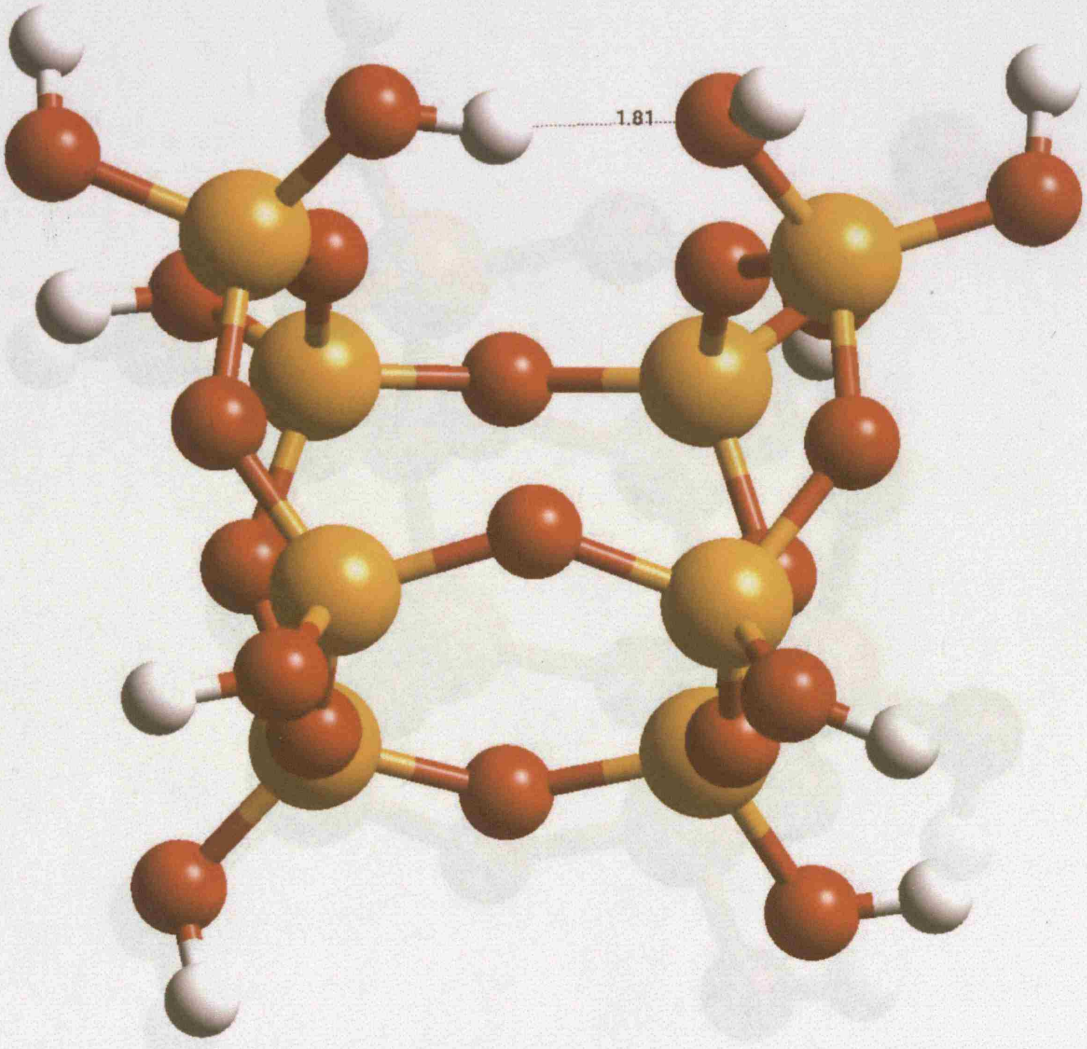

open-d4-ring $Si_8O_{11}(OH)_{10}$

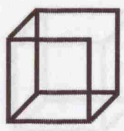

Figure 37 The open-d4-ring.

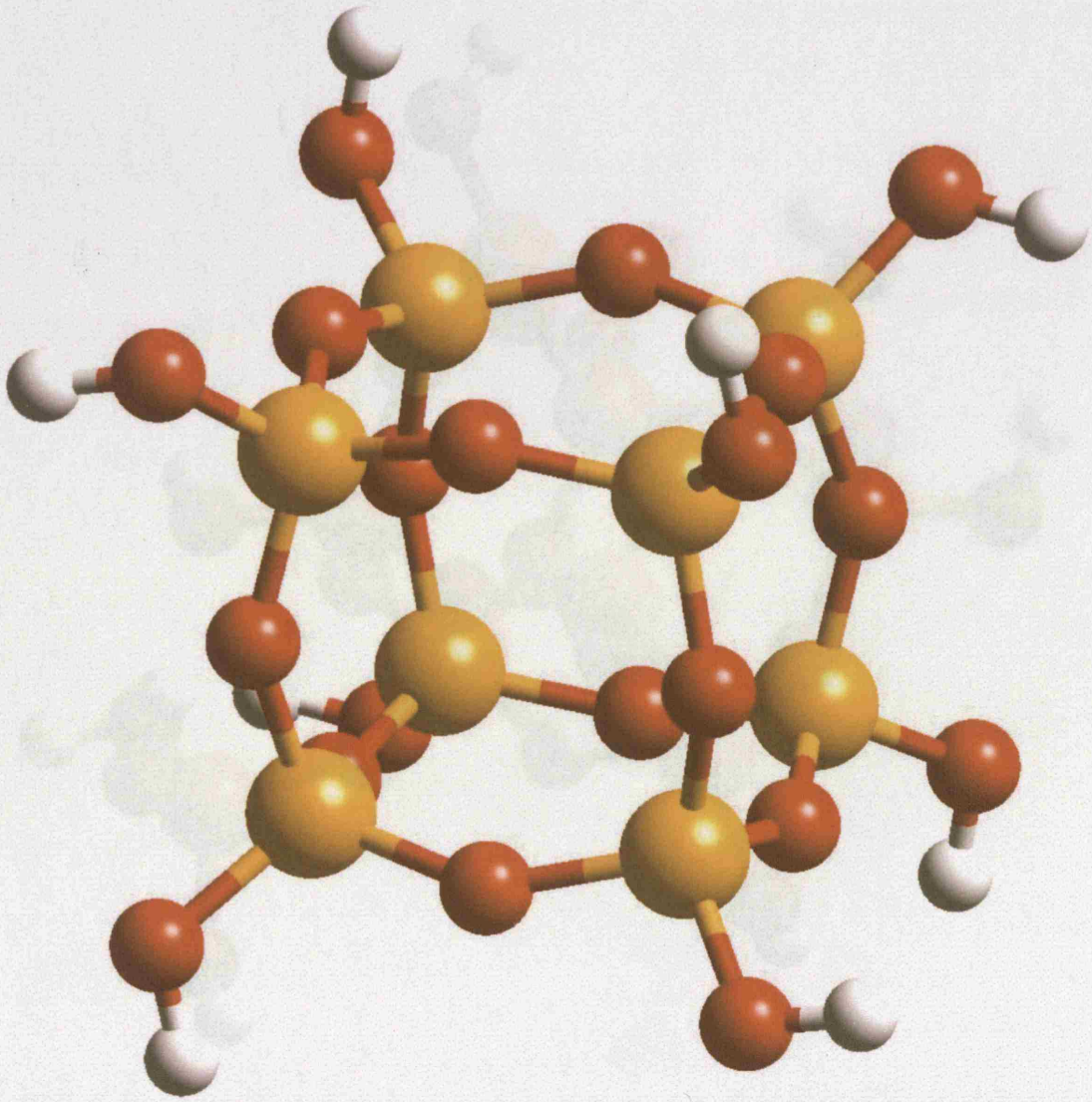

d4-ring $Si_8O_{12}(OH)_8$

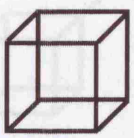

Figure 38 The d4-ring.

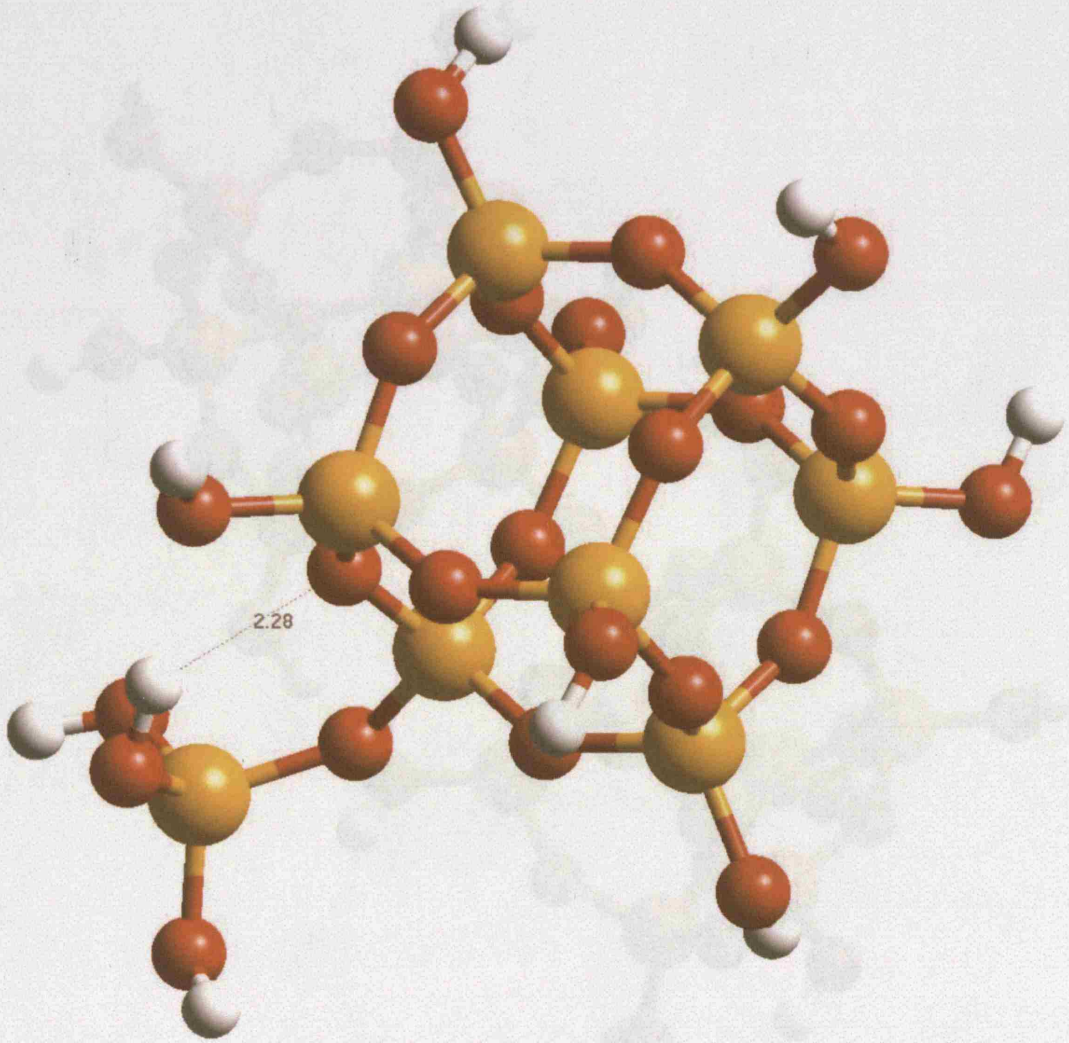

d4-1-ring $Si_9O_{13}(OH)_{10}$

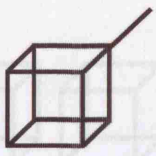

Figure 39 The d4-1-ring.

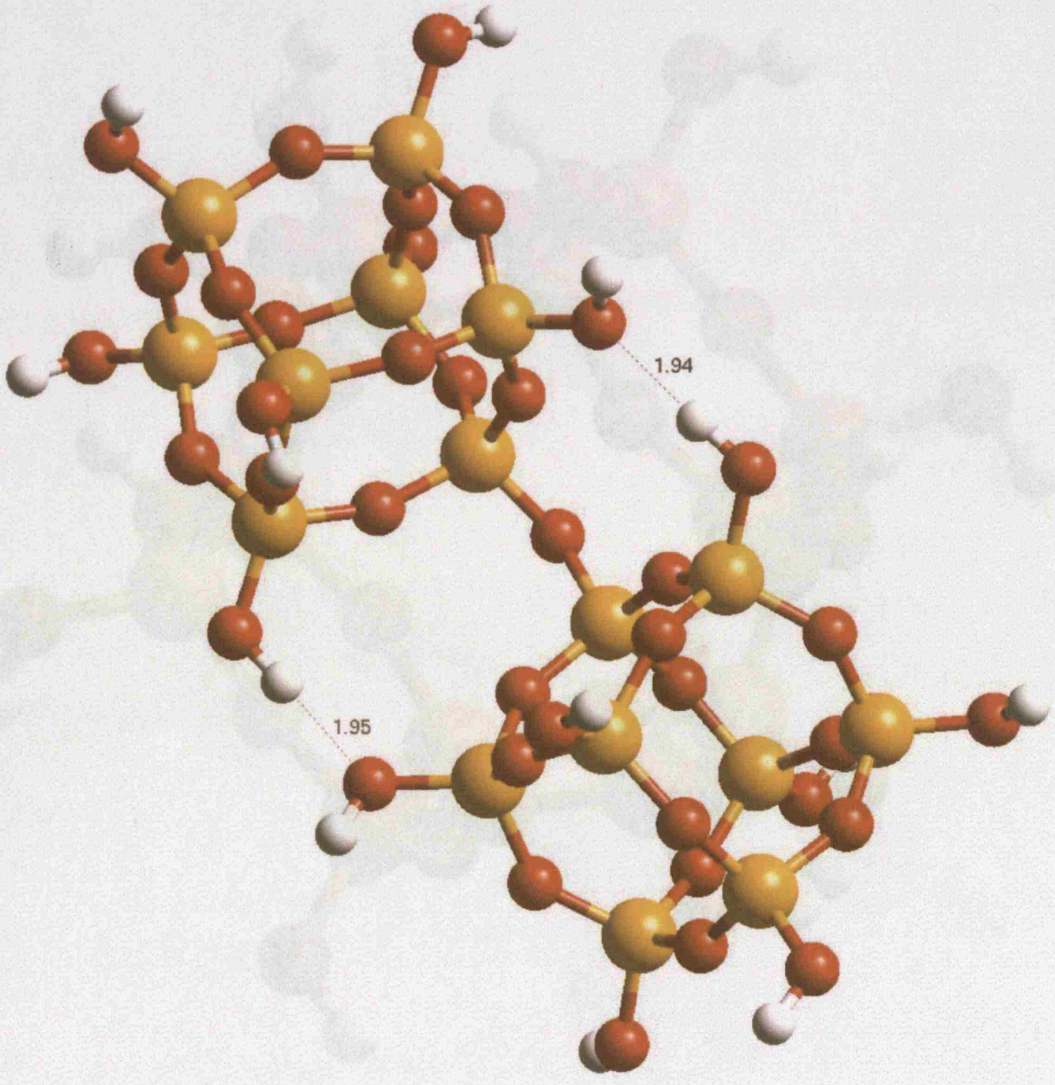

d4-d4-ring $Si_{16}O_{25}(OH)_{14}$

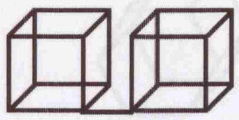

Figure 40 The d4-d4-ring.

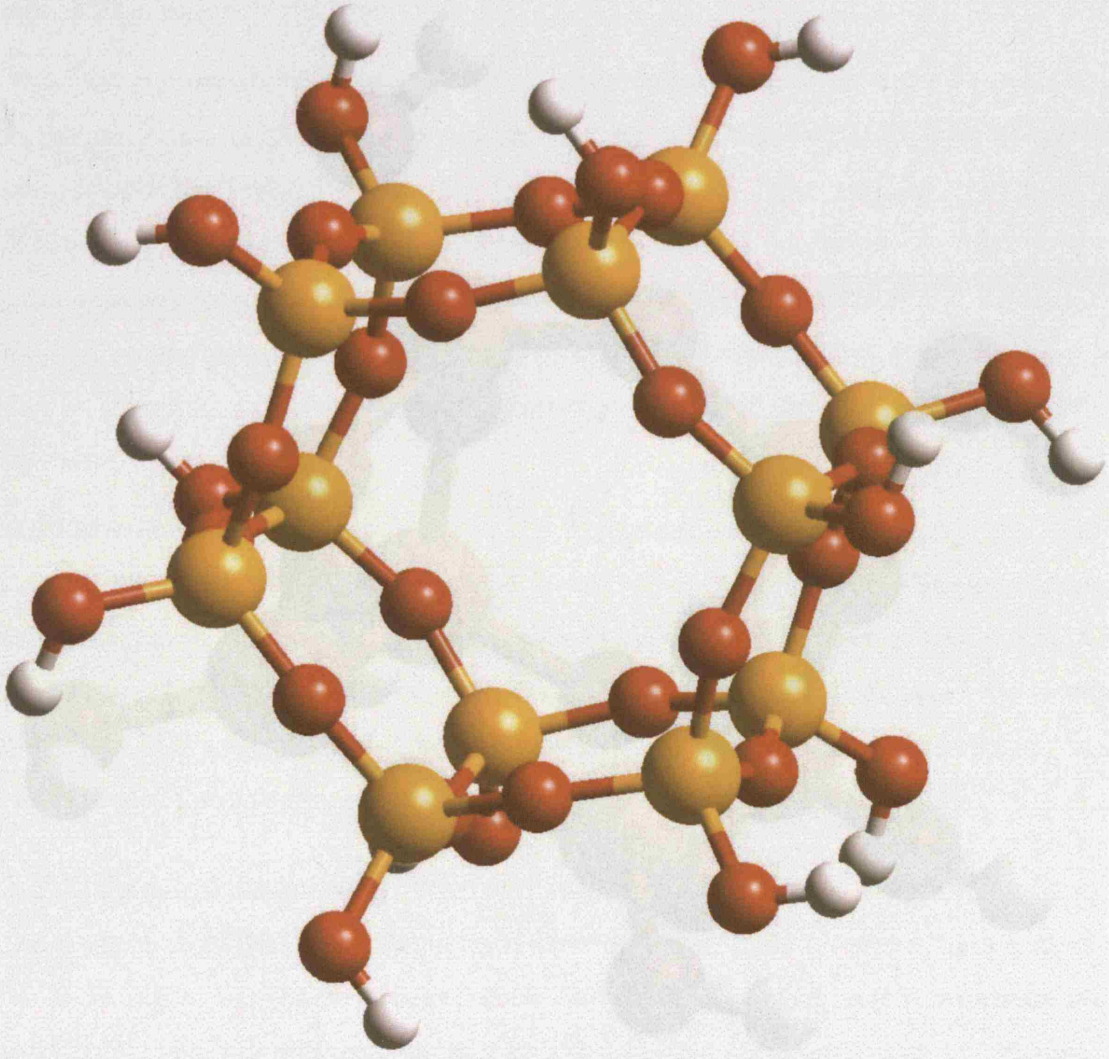

d6-ring $Si_{12}O_{18}(OH)_{12}$

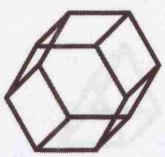

Figure 41 The d6-ring.

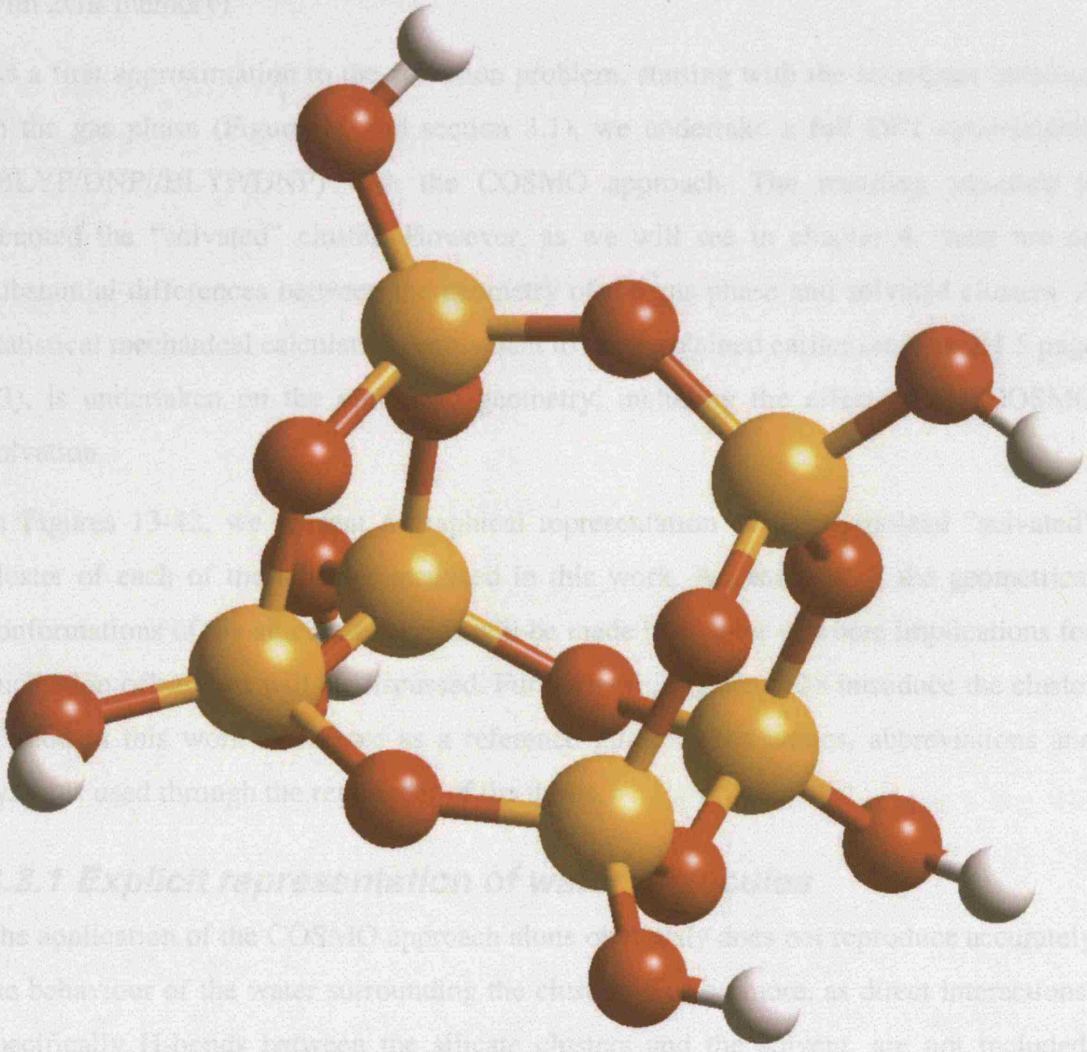

d3-ring $Si_6O_9(OH)_6$

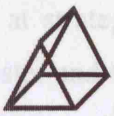

Figure 42 The d3-ring.

3.3 Modelling the solvent

Solvation is first modelled with a conductor like screening model (COSMO)[43, 44, 89]. This procedure has a clear advantage over a full explicit water treatment; it requires much less computational effort, because the solvent is treated as a dielectric in a self-consistent procedure during the DFT calculation. Silicate clusters containing 12 Si atoms can be optimized during a reasonable time (a week, on a 2.8GHz Xeon processor with 2GB memory).

As a first approximation to the solvation problem, starting with the structures obtained in the gas phase (Figure 11 and section 3.1), we undertake a full DFT optimization (BLYP/DNP//BLYP/DNP) with the COSMO approach. The resulting structure is denoted the "solvated" cluster. However, as we will see in chapter 4, there are no substantial differences between the geometry of the gas phase and solvated clusters. A statistical mechanical calculation, equivalent to that explained earlier (section 2.1.5 page 43), is undertaken on the optimized geometry, including the effect of the COSMO solvation.

In Figures 13-42, we present a graphical representation of the optimized "solvated" cluster of each of the silicates analysed in this work. An analysis of the geometrical conformations of the siliceous species will be made in chapter 4, where implications for nucleation of zeolites will be discussed. Furthermore, Figures 9-38 introduce the cluster studied in this work and serve as a reference guide to the names, abbreviations and symbols used through the remainder of the thesis.

3.3.1 Explicit representation of water molecules

The application of the COSMO approach alone obviously does not reproduce accurately the behaviour of the water surrounding the clusters. Furthermore, as direct interactions, specifically H-bonds between the silicate clusters and the solvent, are not included, intramolecular interactions may be exaggerated. Therefore, an improved description includes a limited number of explicit water molecules, which are located at strategic points, where an important chemical interaction takes place between the cluster and the solvent. The number of water molecules varies, but in every case, the smallest possible number is used, as the computational effort increases greatly with the number of atoms involved.

In general, neutral clusters are satisfactorily modelled with the COSMO approach explained previously. Thus, addition of explicit water molecules will only be considered where a strong interaction with the solvent is likely, for example when deprotonation is considered and ionic species are present. When such explicit water molecules are added to a cluster, a full DFT optimization (BLYP/DNP//BLYP/DNP) with the COSMO approach is undertaken. Similarly, as before, a statistical mechanical calculation is performed on the optimized geometry.

3.4 Modelling the effect of high pH

At high pH conditions during hydrothermal synthesis, the silicate clusters will undergo deprotonation. Due to the high concentration of hydroxyl anions (OH^-), an acid-base reaction will take place between the OH^- and the silicate clusters and the deprotonation of the silicate species will promote the formation of anionic silicate clusters. For example, the acid-base reactions for the first and second deprotonation of the monomer are represented by the following reactions:

$$SiOH_4 + OH^- \rightarrow (OH)_3SiO^- + H_2O, \quad (3.1)$$

$$(OH)_3SiO^- + OH^- \rightarrow (OH)_2SiO_2^{2-} + H_2O. \quad (3.2)$$

Further deprotonation reactions could be possible, although they are only likely at very high pH.

The degree of deprotonation in a cluster and the number of silicate clusters that will undergo a deprotonation depends principally on the pH, the ratio OH^-/Si ratio and the thermodynamics of the reactions. Whilst it is difficult to determine exactly the proportion of deprotonated clusters under synthesis conditions (pH ≈ 12.6 - 14[19] and 450K), we can assume that certainly some clusters, if not most, will be deprotonated. However, almost all of the previous theoretical studies on zeolite nucleation and crystallization consider only neutral silicate clusters. Therefore, a major new development in this study is the consideration of deprotonated clusters.

The solvated structures are taken as the starting configuration, to model further deprotonated species (optimized as described in the previous section). The site of the deprotonation is determined using symmetry and by building structures with different deprotonation sites. A full DFT optimization is performed to determine which of these

anionic silicates is the most stable and hence likely to be significant in the hydrothermal synthesis. Every anionic cluster is fully optimized first in the gas phase and then in "solution", as described above.

The anionic silicate clusters modelled in COSMO solution are to our knowledge the first models where the pH and the solution is taken into account in an atomistic modelling study. The results will show trends and correlations in reactions where these clusters have an important role. Furthermore, as in the section 3.3.1 we will also consider a further refinement where explicit water is placed surrounding the cluster. For example, by solvating explicitly the highly charge bare oxygen ($Si(OH)_3O^-$), the strong interactions between this charged oxygen and the (continuum) solvent is better described. Finally, the role of the cation present in the solution is considered by modelling the cation interacting with the anionic cluster. In this thesis, the only cation considered is sodium (Na^+). As before, the anionic clusters with explicit water and the cation are fully optimized in the gas phase and using COSMO.

Pure siliceous materials are the focus here. However, other interesting clusters containing aluminium and germanium can be analysed with the same method applied here. The calculations generate accurate geometries and thermodynamic properties, (primarily the Gibbs free energy) of the clusters, as we shall now demonstrate.

4 SILICATE CLUSTERS

As already discussed, the complexity of hydrothermal synthesis is clear. The work presented here cannot attempt to provide answers to all of the most demanding questions in zeolite synthesis: What is the decisive step that makes one zeolite nucleate rather than another? What is the actual mechanism through which a nucleus is formed? Once a successful nucleus has been formed, what is the mechanism to continue rapid growth? How does the nucleation-growth process occur in series or in parallel? In other words once the growth is established, does further nucleation occur? The intention is rather to provide a framework whereby some of these questions can begin to be answered, by giving an idea of how and why important steps take place during nucleation. By analyzing key clusters such as the monomer, dimer, four-ring, double-4-ring and by considering relevant aspects of the synthesis such as the solvation and high pH, important general principles can be obtained of what and how pieces are being assembled in the big jigsaw "puzzle" that is the nucleation of zeolites.

The results will be presented as follows. The first part of this chapter will present an analysis of the accuracy of the theoretical methods developed. Then an analysis of the geometric features of key structures will be presented and the implications of the conformations on the nucleation mechanism will be discussed. We consider the deprotonation of the clusters effected by high pH. The next topic is the polymerization and cyclization reactions for a range of oligomers containing up to twelve Si atoms. The specific cyclization that occurs for some clusters is highlighted. Finally, we focus in chapter 5 on: the relative strength of hydrogen bonds in water-water and water-silicate interactions.

4.1 Accuracy of the Method

We may begin to consider the precise mechanism of zeolite formation by evaluating the structure and the reactions of the key pre-nucleation species that have been identified experimentally[5, 33, 52]. As the aim of this work is to develop a better understanding of such clusters and their formation, a fundamental issue for progress is to establish whether the computational models and methods used are both accurate (preferably quantitatively *i.e.* "chemically accurate") and also reflect, as closely as possible, the conditions present during synthetic and natural zeolite formation.

Silicic acid ($Si(OH)_4$) – the monomeric silicate molecule – is the simplest but, perhaps, the most important species involved in the formation of zeolite nucleation centres. Little polymerization is noted at neutral conditions[vii] and zeolite syntheses are typified by high pH (12.6 - 14[19]). Two processes, in particular, are therefore vital in controlling the subsequent chemistry: the deprotonation of the monomer:

$$Si(OH)_4 + OH^- \rightarrow Si(OH)_3O^- + H_2O, \tag{4.1}$$

together with further deprotonations of the resulting anion; and the dimerization by condensation of both neutral and anionic species, *e.g.*:

$$2Si(OH)_4 \rightarrow (OH)_3\text{-}Si\text{-}O\text{-}Si(OH)_3 + H_2O, \tag{4.2}$$

$$Si(OH)_4 + Si(OH)_3O^- \rightarrow (OH)_3\text{-}Si\text{-}O\text{-}Si(OH)_2O^- + H_2O, \tag{4.3}$$

$$Si(OH)_3O^- + Si(OH)_3O^- \rightarrow (OH)_2O\text{-}Si\text{-}O\text{-}Si(OH)_2O^{2-} + H_2O. \tag{4.4}$$

Experimental measurements of monomer deprotonation and dimerization energies have been reported and summarised by Iler[15] and Brinker & Scherer[14], with Sefcik & McCormick[93] reviewing more recent measurements. Theoretical calculations have also been performed using a variety of different models.[60, 66, 90, 94] The complexity of silicate chemistry limits some of the experimental studies to only a few species – specifically the monomer and dimer – as many different reactions occur once polymerization is initiated, the individual speciation of which proves almost impossible. Similarly, computational methods have also been restricted by their relative high cost and lack, in most instances, of the incorporation of descriptions of solvent and pH effects.

[vii] When the concentration of the monomer is lower than 2×10^{-3} M at 298K[15].

In this section, we will describe how a dielectric solvent model combined with explicit hydration allows DFT methods to describe accurately the chemistry of small silicate oligomers, exemplified here by $Si(OH)_4$ and $(OH)_3$-Si-O-Si-$(OH)_3$, under conditions typical of zeolite formation. The energies and free energies of the deprotonation of both the monomer and the dimer, together with those of the dimerization reaction will be reported. As a further validation of the method, we investigate the well-characterised water-autoprotolysis reaction.

4.1.1 Solvation and degree of solvation

Before presenting the results for the deprotonation of the monomer and dimer, we will consider the interaction of the metallic cation and the anionic silicates. The geometric implications for these cation-anion interactions in the gas phase and in an explicit solvated environment will be analysed. Furthermore, in analysing the results we will consider the relative ratios for the main participants (Si/Al, H_2O, and OH^-) in the hydrothermal synthesis.

We consider first the relative components of the main participants in zeolite syntheses. Figure 43 shows a survey of Si (and/or Al), OH^- and H_2O concentrations, for several zeolite synthesis compositions. The data shown in Figure 43 is representative of 35 synthesis compositions for zeolites, with 26 different topologies. It is important to note that only high silica zeolite nucleation is considered in our calculations, whilst this analysis (Figure 43) also shows zeolites with important aluminium content. The aim of this chart is to provide a general overview of the relative populations of the species present at nucleation.

The most interesting result obtained from Figure 43 is the fact that the majority of synthesis solutions have an OH^-/T ratio between 0.1 and 0.5, so there are approximately between 2 and 10 tetrahedral sites for each OH^- anion. Thus, we would expect a double 6-ring (12 Si atoms) to have a charge, of between -2 and -6. This observation is useful in developing models, because it could be used to impose limits on the number of possible anions we need to consider as likely to be present in the solution. In the same way, the number of water molecules present for every tetrahedral site varies between 5

and 35[viii]. The concentration of OH^- increases with the water content, so the OH^-/H_2O ratio or pH is almost constant in all the synthetic conditions; but it remains very high.

The concentration of the metallic cation in most cases will be comparable with that of the OH^-, since typically the source of hydroxide is NaOH, KOH, etc. The role of the metallic cation has generally been considered to be only as a counterion for the anionic silicates[95]. However, it has also been suggested that it could act as a structure-direct agent.[1]

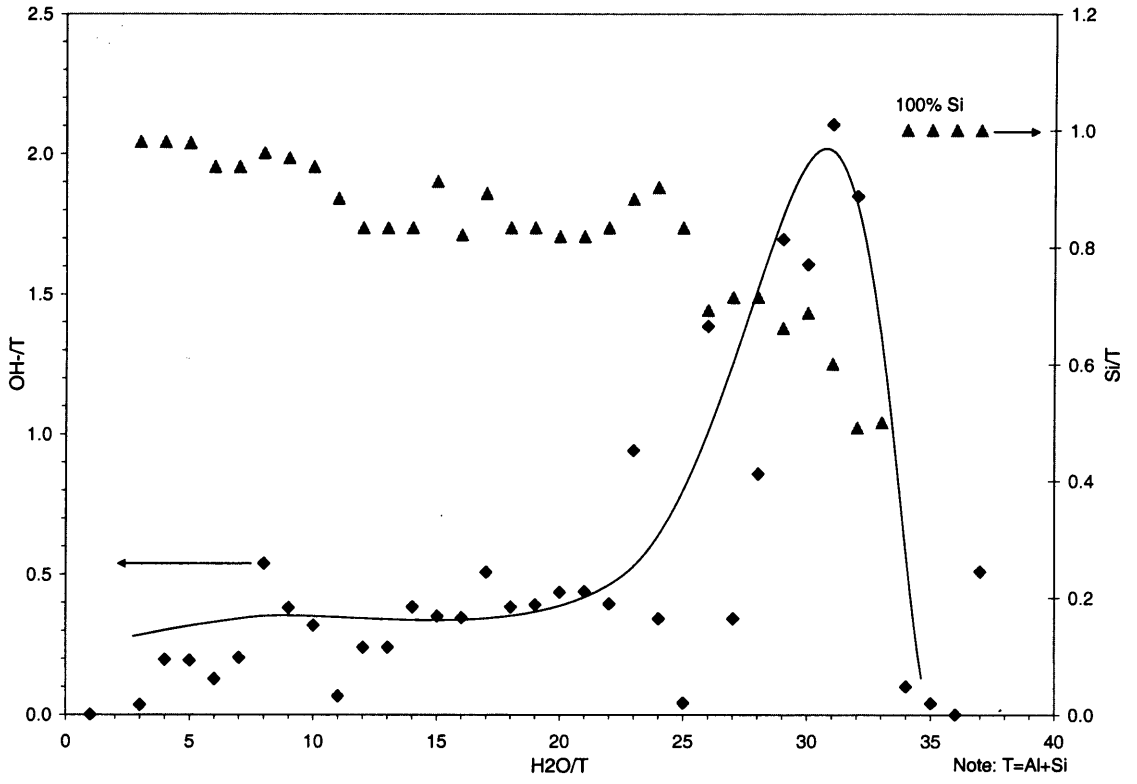

Figure 43 Starting composition for the synthesis of several zeolites, with information extracted from the International Zeolite Association compilation edited by Robson [19]. Each of the axes shows a molar ratio between the most important participants in the synthesis. Triangles are the Si/T ratio and diamonds the OH^-/T ratio. "T" is the sum of Al and Si content. The line is a guide to the eye for the OH^-/T ratio.

[viii] This experimental fact also validates our choice of few water molecules per Si. Furthermore the close interaction between silicates is assured, which will be studied in detail in section 5.3, page 228.

4.1.2 The metallic cation

The modelling of silicate clusters in the presence of the metallic cation and solvation, will, we expect, give a more complete and accurate model of the system under which zeolites are nucleated. However, it is clear that, as we might intuitively expect, the COSMO solvation model alone (see Figure 44 and the energy results of Table 1, page 92), describes poorly systems involving ionic bonds, given that water molecules are not explicitly considered. For example, in Figure 44 we show the optimized structures for NaOH and $H_3SiO_4^-Na^+$, two systems with strong ionic bonds: the gas phase is given in (a) and (c); the respective COSMO solvation optimizations are shown in (b) and (d).

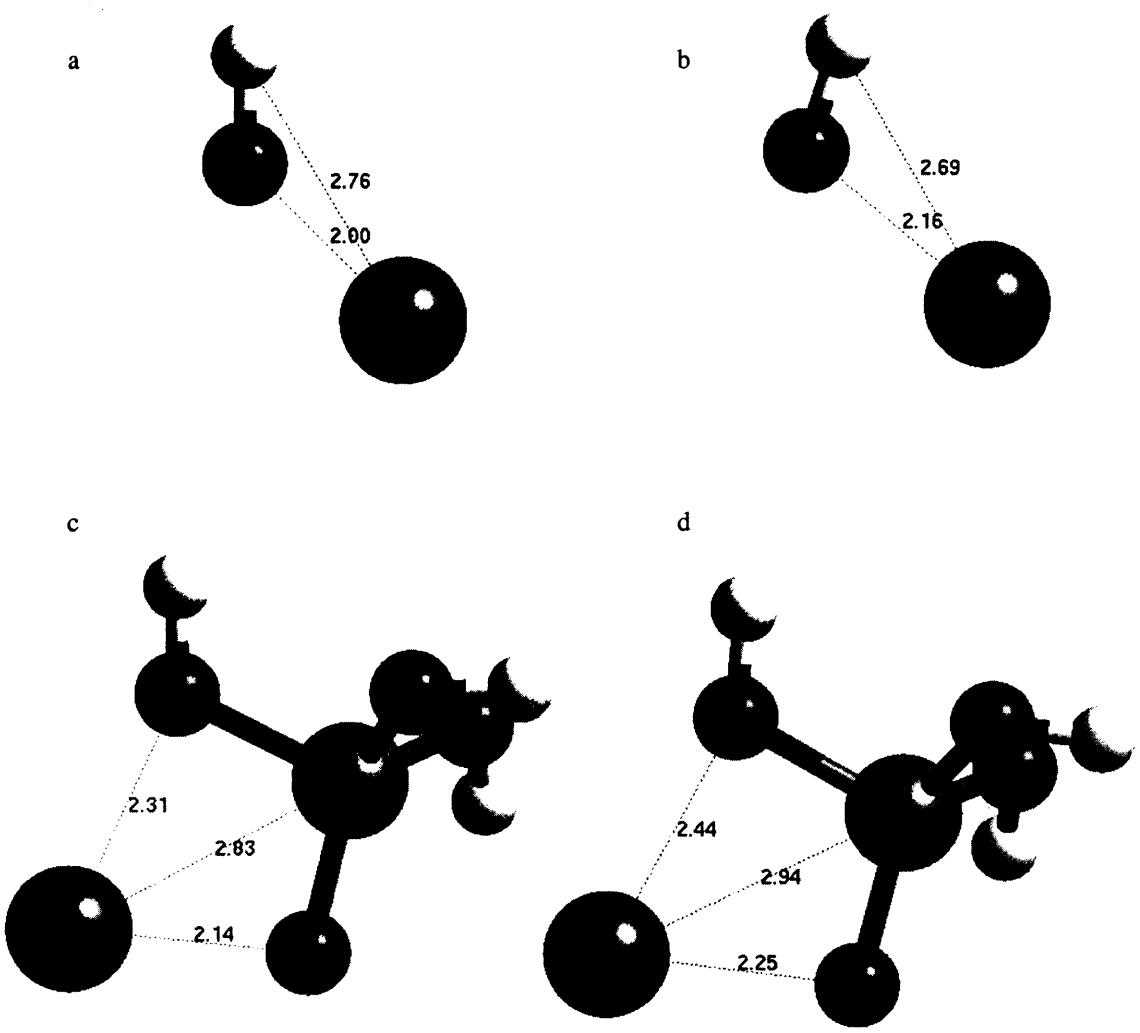

Figure 44 Optimized structures for NaOH in the gas phase (a), COSMO solvation (b) and $H_3SiO_4^-Na^+$ in the gas phase (c), COSMO solvation (d). The numbers indicate the internuclear distances between the sodium cation and their nearest neighbours, in angstroms.

The internuclear distances, show that the sodium cation is practically at the same position with respect to the nearest atoms, regardless of the presence of solvation. However, water should create a solvation shell around both anion and cation, as has been shown previously[96]. In the absence of such a full description of the solvation therefore, this close anion-cation distance will cause an overestimation of the calculated binding energies, since the cation-anion will interact as in the gas phase. Essentially, the COSMO model alone does not generate a proper treatment of solvation when ionized species are present.

A refinement of the solvation model, which includes the important intramolecular interactions between the O^-, Na^+ and the H_2O molecules, is presented in Figure 45. In

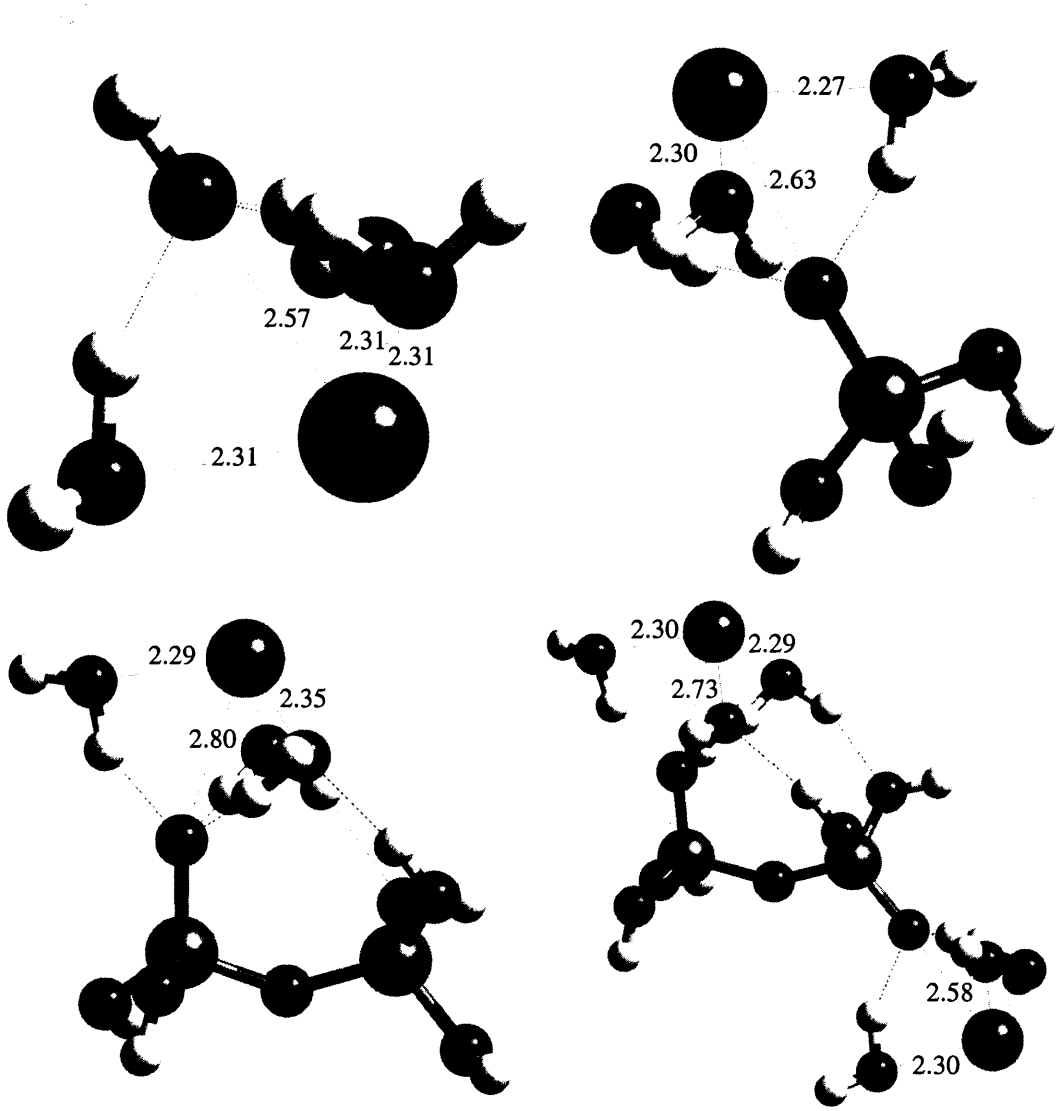

Figure 45 NaOH, singly deprotonated monomer and dimer, and the doubly deprotonated dimer models. Three explicit water molecules and a Na^+ ion coordinate to the deprotonated oxygen. Dotted lines indicate hydrogen bonds.

this figure, the "solvating" role of the water is clear, because it creates a shell of water molecules around the ionic species, resulting in a longer cation-anion distance compared with the COSMO solvation alone (Figure 44). Further consequences of the inclusion of explicit water and the reliability of the proposed solvation method are discussed in section 4.1.3.1 (page 91). However, as we shall see, the inclusion of full solvation shells may not be necessary to provide an accurate model and results for thermodynamic quantities that are comparable with experiment can be obtained with only three water molecules in the case of the monomer.

4.1.3 Monomer and dimer deprotonation

We present the calculated free energies of deprotonation when solvation is included, here solely with the COSMO approach, which are compared with the quantitative data from experimental deprotonation energetics of simple silicate species, to assess the reliability of the COSMO solvation calculations (Figure 46). The equilibrium constants[ix] for the successive deprotonation of both silicic acid (the silicate monomer) and disilicic

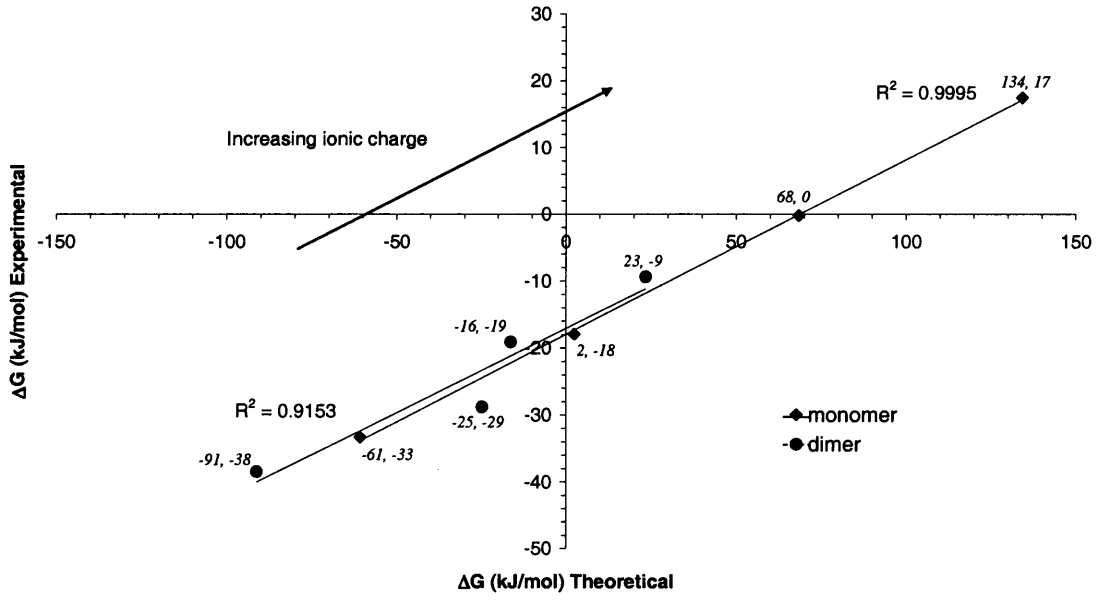

Figure 46 Experimental[97] and theoretical deprotonation energies at 298.15K. The most negative energy corresponds to the first deprotonation free energy.

[ix] The equilibrium constant (K) is related to the Gibbs free energy (G) by the equation: $\Delta G = -RT\ln K$. Where R is the ideal gas constant and T is the temperature.

acid (the silicate dimer) have been determined[15, 97] experimentally, and can be compared directly to the free energy changes determined here.

The first four deprotonation free energies for the monomer and dimer are plotted in Figure 46, from which it is clear that there is excellent linear correlation between the theoretical and experimental results. Previous studies of deprotonation reactions with the COSMO model, considering organic species[90], show a similar correlation between experiment and calculations. It is gratifying to find equally good results here, for what is arguably a more complex system given the high charge density (up to four, see Figure 46). It is important to stress that with the COSMO solvation alone, there is only a good correlation with the variation in experimental values (Figure 46). However, there are substantial discrepancies in the absolute values of the calculated free energy changes of deprotonation obtained. The first factor responsible for the difference in the absolute values of calculated and experimental data given in Figure 46 was discussed in section 4.1.2, where it was shown that the treatment of ionic species is not described accurately with COSMO alone. A second reason for the offset in Figure 46 is the implicit consideration of infinite dilution in the DFT/COSMO calculations. At this point, it is important to recall the low water content in the zeolite nucleation of only few water molecules per silicon atom ($H_2O/Si \approx 5$-35, Figure 43), in contrast to the dilute solution used to determine K (and the free energy).

In the next section (4.1.3.1), we shall see how the inclusion of an additional explicit solvation shell with water molecules on the species involved in the deprotonation reaction improves the results substantially. Nevertheless, the overall correlation is good and provides further evidence that the COSMO model used is robust, providing an acceptable correlation with the available experimental data, which will allow predictions to be made about the formation of larger silicate oligomers regarding trends in reaction parameters.

4.1.3.1 Model of deprotonation with "chemical accuracy"

The calculation of the monomer and dimer deprotonation reactions analyzed in the previous section is extended here, with a refined model, which includes explicit solvation and the use of counterions. The Gibbs free energy is calculated by combining the electronic energy (BLYP/DNP/COSMO), zero-point energy, together with the rotational, vibrational and translational contributions to the energy, using standard

statistical mechanics methods[x] at 298K (the temperature of the experimental measurements). Improvements to this initial solvated model are made by the inclusion of sodium counterions in the charged clusters, together with the addition of some explicit water molecules (rather than the purely continuum description of COSMO) in the first coordination sphere of all the species considered, to represent more completely the most important short-range interactions. Details of the number of explicit water molecules used for individual species are reported in Table 1, which gives the free energies calculated together with values derived from experimental pK_a or equilibrium constants reported in the cited literature. Examples of the models used are shown in Figure 45.

Table 1 Free energies of reaction at 298K ($kJmol^{-1}$). Monomer I and II are the first and second deprotonation reactions for the monomer respectively, with similar notation used for the dimer. ΔG_{gas} and ΔG_{COSMO} are the free energies for the reactions without the additional explicit water molecules (given in the reaction scheme) in the gas phase and the COSMO solvation model respectively. ΔG_{solv} is the free energy when both the explicit water molecules and the COSMO solvation model are included.

Reaction	ΔG_{gas}	ΔG_{COSMO}	ΔG_{solv}	ΔG_{expt}[a]	
Water autoprotolysis					
$H_3O^+(H_2O)_3 + OH^-(H_2O)_4 \rightarrow (H_2O)_4 + (H_2O)_5$	-1013	-258	-97	-101	Dewar[98] Pearson[99]
Monomer I					
$Si(OH)_4 + NaOH(H_2O)_3 \rightarrow SiO(OH)_3Na(H_2O)_3 + H_2O$	-226	-61	-29	-33	Iler[15]
				-36	Sefcik[93]
Monomer II				-18	Sefcik[93]
$SiO(OH)_3Na(H_2O)_3 + NaOH(H_2O)_3 \rightarrow SiO_2(OH)_2Na_2(H2O)_6 + H_2O$	285	2	-17	-17	Tossell[100]
				-23	Iler[15]
Dimer I					
$Si_2O(OH)_6 + NaOH(H_2O)_3 \rightarrow Si_2O_2(OH)_5Na(H_2O)_3 + H_2O$	-296	-91	-35	-38	Sefcik[93]
Dimer II					
$Si_2O_2(OH)_5Na(H_2O)_3 + NaOH(H_2O)_3 \rightarrow Si_2O_3(OH)_4Na_2(H_2O)_6 + H_2O$	119	-25	-25	-29	Sefcik[93]
Dimerization (neutral)					
$Si(OH)_4 + Si(OH)_4(H_2O) \rightarrow Si_2O_2(OH)_6(H_2O) + H_2O$	-13	-2	-4	-7	Sefcik[93]
Dimerization (basic)					
$Si(OH)_4 + SiO(OH)_3Na(H_2O)_3 \rightarrow Si_2O_2(OH)_5Na(H_2O)_3 + H_2O$	-83	-33	-7		

[a] The experimental free energy for the proton transfer between two water molecules in solution is calculated from a thermodynamic cycle. The experimental enthalpy of formation of the species in the gas phase is taken from Dewar et al[98], and the change in entropy for a proton transfer is considered zero, after Aue et al[101]. The free energies of hydration are taken from Pearson[99].

[x] See section 2.1.5 page 43.

The accuracy of the methodology is illustrated by considering the autoprotolysis of water. It is clear that consideration of this reaction (most simplistically) in the gas phase or even with the COSMO solvation model, drastically overestimates the free energy change. However, the inclusion of some explicit water molecules improves the description, giving a result within 4 $kJmol^{-1}$ of experiment. We note that the "experimental" value is derived using a thermodynamic cycle. The change in enthalpy in the gas phase is obtained from experiment[98], whilst the entropy change in the gas phase is considered to be zero for a proton transfer[101], which thus allows the free energy in the gas phase to be obtained. The free energies of hydration are also reported in the experimental literature[99]. Thus, the free energy for the autoprotolysis of water can be obtained.

Inclusion of a full, explicit hydration sphere does not appear necessary, as sufficient water is present to allow formation of the stabilized complexes, with three and four water molecules for the H^+ and OH^- ions respectively. These complexes, $OH^-(H_2O)_4$ and $H_3O^+(H_2O)_3$ have indeed been identified as the most prevalent species in such solution.[102, 103] Little change in the calculated energies is found if further explicit water is added.

The first deprotonation energy (as pK_a) of the monomer is possibly the most reliably determined thermodynamic property for the silicate oligomers. This value therefore serves as a key reference in evaluating the reliability and accuracy of any theoretical method whose aim is to investigate the self-assembly of silicate oligomers. From Table 1, it is evident that both the gas phase and the COSMO models are again inadequate in modelling accurately the monomer's first deprotonation energy, although as we saw above qualitative trends are well described. However, inclusion of water molecules and the counterion (Na^+) produces a free energy within 4 $kJmol^{-1}$ of the experimental value.

There is general agreement that deprotonation energies calculated with DFT/COSMO correlate well with experimental pK_a and as demonstrated in the previous section (4.1.3) it is possible to estimate pK_a values by linear extrapolation[90, 100, 104]. However, DFT/COSMO alone is not able to compute reliably absolute pK_a values.[90] Here, through the inclusion of some explicit solvation and counterions, quantitative agreement with experiment is achieved. Thus, such an approach, whereby some, but not necessarily all, of the inner solvation sphere of a deprotonated species is considered,

may be more generally applicable and "chemically accurate", as discussed further below.

The presence of multiple species in solution makes experimental determination of the pK_a of the dimer significantly more difficult and less accurate. Thus, values are extrapolated from a composite value following a fitting procedure to determine the relative populations of the monomer and dimer.[93] Again, there is good agreement (within 4 $kJmol^{-1}$) between the calculated deprotonation free energies and the available experimental results, once explicit hydration is considered. These results in both added confidence in the method and also in the robustness of the experimental fitting procedure.

Free energies for more highly deprotonated species have also been determined for the monomer.[105] However, these rely increasingly on fitting procedures, where the concentrations of the more deprotonated species are very small compared to the dominant singly and doubly deprotonated species. Hence, these values are likely to be less reliable. Indeed, DFT methods, regardless of the level of solvation are unable, to stabilise a fully deprotonated monomer; a nearby water molecule is always preferentially hydrolysed, transferring a proton back to the SiO_4^{4-} species. This result perhaps raises doubts as to whether such a strongly charged species may ever exist in the aqueous medium, typical of the hydrothermal synthesis.

The dimerization reaction is possibly the most important reaction in the whole of silica chemistry. Again, the range of conditions (acid, neutral, basic) and the difficulties in attempting to restrict further polymerization occurring makes it a challenging reaction to study experimentally. The experimental estimate of ΔG is $\approx$ -7 $kJmol^{-1}$.[93] In addition, there are a number of computed values: using DFT/TNP Catlow et al.[60] reported a gas phase dimerization free energy of -9.2 $kJmol^{-1}$, whilst Tossell[94], using MP2/6-311+G(2d,p) report a value of +24.7 $kJmol^{-1}$ in the gas phase but +8.8 $kJmol^{-1}$ when a G2/COSMO model is applied. Neither study considered explicit hydration.

The results of our calculations accurately reproduce the experimental data for the dimerization reaction (see Table 1), both under neutral and basic conditions. Note, that these calculations also correctly reflect how an increase in pH makes polymerization more favourable. Moreover, the reaction of two deprotonated monomers (with cations and explicit water) is slightly less favourable (ΔG = -3.4 $kJmol^{-1}$), again reflecting

experimental observation that very high pH does not necessarily result in increased reaction rates.

Thus, the combination of the DFT method used here, together with a suitable explicit representation of the inner solvation sphere of the key species and a continuum representation of the remainder of the solvent (with COSMO), allows the aqueous chemistry of silicate oligomers to be modelled accurately.

The effect of including explicit water molecules is twofold: first, they shield the highly charged regions from the continuum, allowing electrons to redistribute more "naturally"; secondly, they result in an improved description of the shape of the cavity in the dielectric continuum that is constructed by the COSMO methodology. COSMO uses atomic radii to construct the cavity[89] and the large difference in size between neutral atoms and these charged and ionic species is significant and results in a poorer description of the surface of the molecule. Thus, addition of explicit water near such atoms, particularly bare O^- and Na^+, effectively places these atoms "inside" the molecule and reduces the errors in the cavity shape and size.

Now that such a method, which allows us to consider conditions regarding zeolite synthesis that are chemically relevant, is demonstrated to perform well in modelling both the two key silicate reactions considered here, and that of the autoprotolysis of water, it can be applied with confidence to further aqueous silicate chemistry.

To summarise this section, gas phase modelling of silicates gives a poor description for the reactions in high pH hydrothermal synthesis. COSMO solvation provides results, which allow us to follow trends and compare reactions in relative terms. However, it is the use of explicit water molecules and the COSMO solvation, which provides accurate results comparable with experiments. Nevertheless, we remain confident that general trends reaction energies of similar species (differing essentially only in size) will be accurately described by the COSMO model alone. Only where added accuracy is needed, will further solvation be included.

4.2 Geometry analysis

Probably the most widely visited feature in theoretical studies of silicate oligomers is their geometry, both, because of the relatively fast calculation of geometry optimization, with a low level of theory and the reliability of the results, that are comparable with the

available experimental data. In the literature, there are detailed analyses of the bond lengths and angles for several of the clusters discussed in this work[39, 40, 60, 106], which are in good agreement with those obtained here. Therefore, the geometrical analysis presented in this section focuses on the geometrical implications on the condensation reactions and on the nucleation process, but not on the details of bond length and bond angles. However, the analysis of the optimized structures shows some interesting suggestions regarding the nucleation mechanism of zeolites. The most remarkable features in the clusters that we will show here are the prevalence of H-bonds in most of the clusters and the tendency to form very compact structures.

All the structures of the clusters shown in this section are the optimized clusters in the gas phase. However, the differences between the gas phase and solvated optimized structures are very small. As noted earlier, Figures 13-42 (pages 53-80) show a detailed description of the clusters analysed in this thesis, with their assigned name, chemical formula and line diagram representation, in the COSMO solvation.

4.2.1 Core silicates, linear and single ring structures

4.2.1.1 The monomer and dimer

The simplest silicates are the monomer ($Si(OH)_4$) and the two-silicon dimer: their calculated optimized structures are shown in Figure 47. Both the monomer and the dimer have been widely studied previously[41, 60, 62] and the structures are well established. The monomer and dimer are possibly the two most important structures in

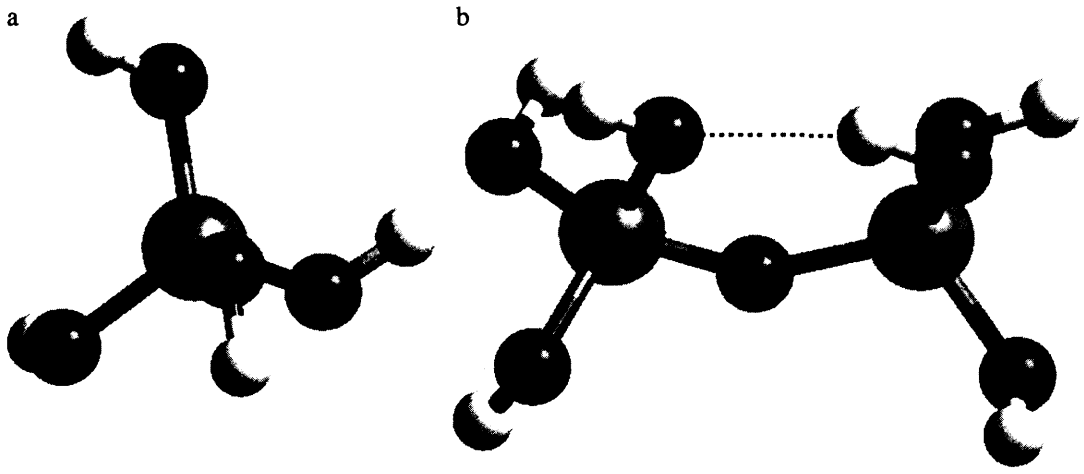

Figure 47 Optimized monomer (a) and dimer (b) structures in the gas phase; the larger spheres are Si; the H-bonds are denoted by a dashed line.

the chemistry of zeolite synthesis and perhaps in the whole of aqueous silica chemistry. Their importance and also their suitability for consideration using high level *ab initio* calculations (due to their very small size and low atomic number atoms) has made them the object of numerous theoretical studies[63, 106-109].

The two most significant characteristics are that the monomer has S_4 symmetry, whilst the dimer shows an intramolecular H-bond (denoted by the dashed line). In the gas phase, the Si-O and O-H length in the monomer are 1.65Å and 0.97Å respectively; while in the dimer the lengths for the $Si\text{-}O_{terminal}$, $Si\text{-}O_{bridging}$, and OH are 1.65-1.67Å, 1.64-1.65Å and 0.97Å respectively. The O-Si-O and Si-O-H angles in the monomer are 106.1° and 116°; for the dimer, the same angles are 104.1-112.8° and 114.2-116.7° and the angle formed after the condensation, the Si-O-Si, is 139.4°. Our calculations show that the H-bond in the dimer causes a slight distortion in the angles and lengths compared to the monomer.

The bond lengths and angles summarised above are similar to those reported in previous calculations[40, 60].

4.2.1.2 Three and four silicon clusters

The geometry optimized structures of the 3-silicon and 4-silicon structures are presented in Figure 48[xi]. The trimer (a) and the corresponding 3-ring (c), and the tetramer (b) with the 4-ring (d), with the same conformation shown here, were also considered by Pereira *et al.*[40] The almost "closed" structures for the linear silicates, trimer and tetramer, are the lowest energy conformations in both gas phase and solution, suggesting that a facile cyclization may be possible.

The tetramer structure is particularly prone to condense into a 4-ring, with the linear tetramer being 14 $kJmol^{-1}$ less stable than the "almost closed" conformation. The H-bonds present, linking the two terminal silicon atoms (where the cyclization will occur) are approximately 0.34Å closer than the other internal H-bonds, which may facilitate the closure. These arguments could also be used in the case of the trimer.

The *3-ring* is the smallest closed structure that is known to be formed in a silicate structure. Structures containing the strained 2-ring clusters have been proposed

[xi] The branched structures for oligomeric clusters is not investigated in this thesis, as it was shown previously[39] that such branched silicates will be less likely than their linear counterparts.

theoretically[110-113]; they have interesting properties, which could lead to a new range of tubular porous frameworks. However, they have not yet been synthesized. Other clusters including 2- and 3-rings[114] and only 3-rings[115] have also been proposed.

3-rings in zeolitic structures are rare in pure siliceous frameworks, being present only in the high-silica ZSM-18[116]. Some other zeotypes frameworks have 3-rings, however they have other elements in the tetrahedral positions like the beryllosilicate OSB-1[19], and other structures containing Zn[19]. However NMR and mass spectrometry studies of pure siliceous reaction gels find a considerable concentration of solution phase 3-rings[3] [34], a result that is supported by the reaction energetics presented later in section 4.5.3.1 (page 140). However, if the 3-ring species is apparently stable, why do we not find

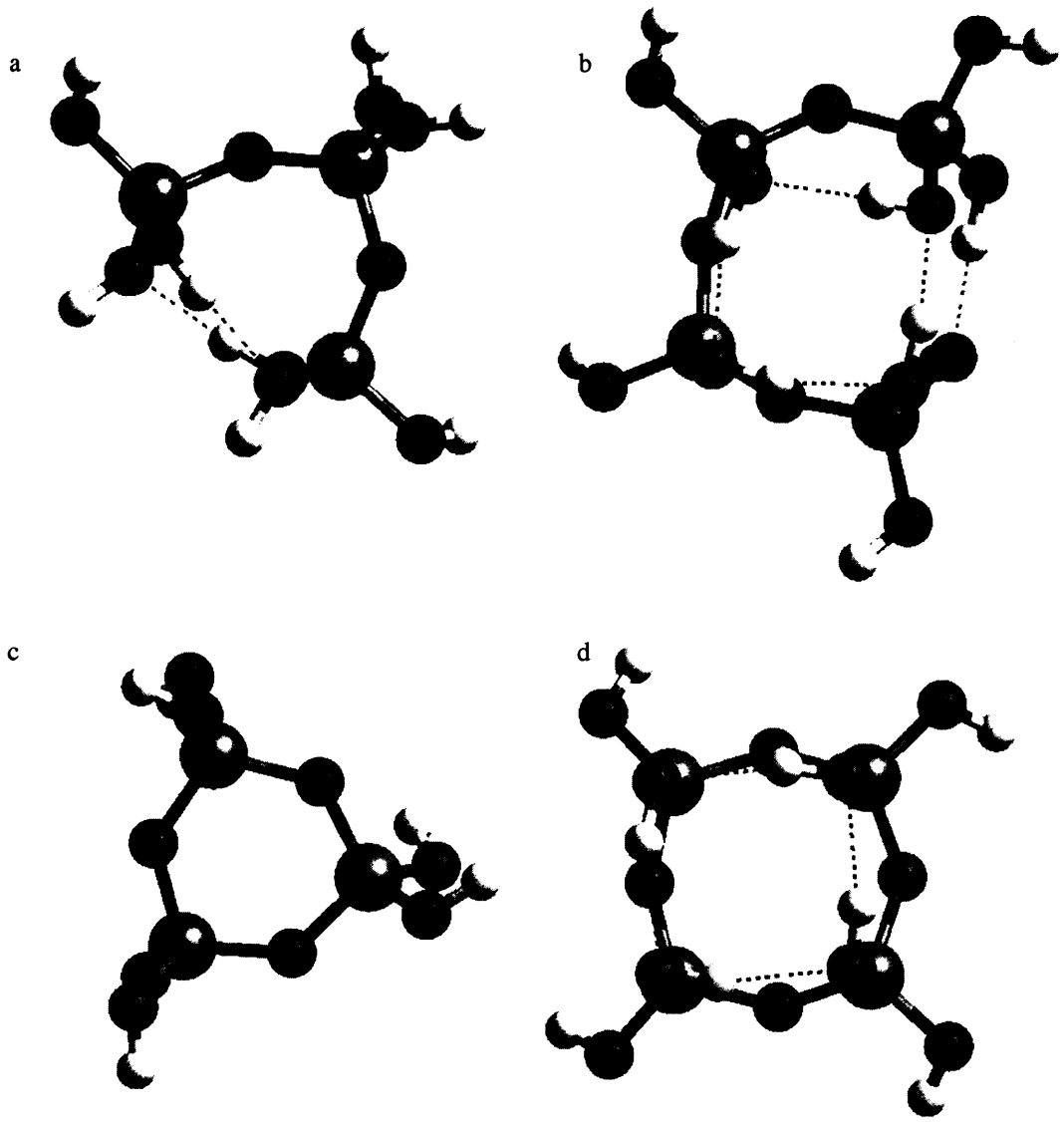

Figure 48 Optimized trimer (a), tetramer (b), 3-ring (c) and 4-ring (d) structures in the gas phase; the larger spheres are Si; the H-bonds are denoted by a dashed line.

more 3-ring containing structures? Perhaps, these rings (which are somewhat strained) can readily re-open? Thus, considering the reaction barriers for these internal condensations is important.

The *4-ring* is found in the majority of known zeolitic structures: indeed 61 zeolitic frameworks have the 4-ring as part of their structure[19]. Thus, the 4-ring is possibly the most important cyclic structure in zeolite chemistry. The wide spread presence of 4-rings in zeolite frameworks and their significant population in solution[3] (as found by NMR), suggest a special preference for their formation and therefore stability. Further analysis of this important cluster is addressed in section 4.5.3.2 (page 143).

Intramolecular hydrogen bonds in the trimer and tetramer appear to be a major factor in stabilising the cyclic conformation. In the 4-ring (C_4 symmetry), H-bonds form stable "circular" interactions in a plane above the ring formed by the silicon atoms. Thus, the "crown" of H-bonds in the optimized structure for the 4-ring definitely gives an extra stability to the structure. However, the contribution is not as large as we might expect for the formation of four H-bonds. A local minimum where the 4-ring does not have any H-bond is only 13 $kJmol^{-1}$ less stable than the H-bonded counterpart. Further consideration of the typical strength of an H-bond is given in section 5.3 (page 228).

The 3-ring does not exhibit intramolecular H-bonds, because of the small and restricted structure formed. Furthermore, we can consider the 3-ring to be slightly more strained compared to the 4-ring: the corresponding O-Si-O and Si-O-Si angles in the ring are 5° and 2° smaller respectively in the 3-ring, compared to the 4-ring. Consequently, we might initially conclude that the 3-ring would be difficult to form from the trimer. However, as we will discuss in section 4.5.3.1 (page 140) relating to cyclization energies, the direct 3-ring condensation from the trimer is highly favourable. Thus, we may conclude, that intramolecular H-bonds are important but in some cases, like the 3-ring, they are not necessarily essential for stabilizing ring clusters.

4.2.1.3 Five and six silicon clusters

The open and cyclic structures for the 5- and 6-silicon silicates are shown in Figure 49. The linear structures, pentamer (a) and hexamer (b), have an almost closed structure, similar to the trimer and tetramer. Again, the H-bonds formed in the linear structures are crucial to curve and stabilize these conformations.

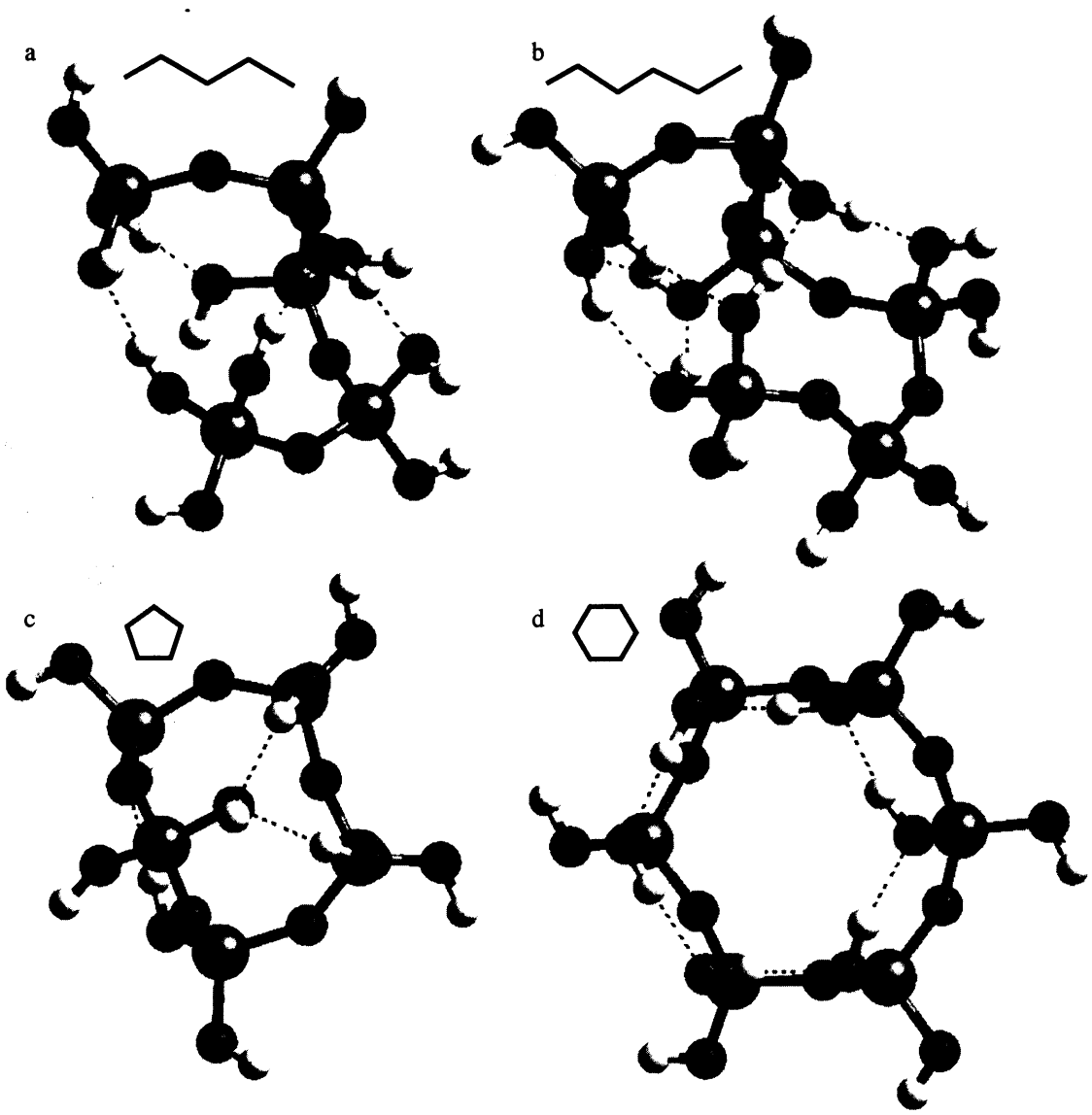

Figure 49 Optimized pentamer (a), hexamer (b), 5-ring (c) and 6-ring (d) structures in the gas phase.

The 6-membered ring has a planar structure with C_6 symmetry. The H-bonds for the 6-ring have a similar arrangement to those in the 4-ring: they are organized in a circular form above the plane formed by the silicon atoms. In contrast, the 5-membered ring has a non-planar structure, with two H-bonds fewer than the linear pentamer.

An initial geometrical analysis of the 5- and 6-silicon structures may lead to the conclusion that the cyclization of the 6-ring is more likely than the 5-ring cyclization, principally due to the stability given by the H-bonds. However, this is not the case, as

will be presented in section 4.5.3.3 (page 147), because, essentially, the 5-ring cyclization is more exergonic[xii] than the 6-ring.

Although the pentamer and hexamer are the largest linear polymeric units studied here, they can help explain some of the features of the amorphous silicate that serves as nutrient in many hydrothermal syntheses. In general, we expect, as for the pentamer and hexamer, that linear silicate chains will have a tendency to form a dense cluster, assisted by the formation of internal H-bonds, which can explain some of the hydrophobicity of silicate systems, where the intramolecular H-bonds are more favourable than the interaction between water and silica/silicate clusters (a more detailed study of this subject will be addressed in Chapter 5). In the "packed", more stable, conformation of the linear pentamer, the two ends are separated only by the distance of an H-bond, *i.e.* 1.9Å. The same is observed in the hexamer. However some other conformations could occur, where the two ends of the chain are further apart, which however, reduces the probability of an internal condensation occurring, in contrast to the trimer or tetramer. Finally, we should mention that a larger number of H-bonds in a conformation does not necessarily mean that the structure is a low lying energy minimum. For example for the hexamer, we find a conformation with 7 H-bonds that is 11 $kJmol^{-1}$ less stable than that with 6 H-bonds. Thus, it becomes clear that we cannot consider the number of H-bonds as an indicator of stability nor does it make an assignment of the strength of any individual H-bond.

The 5-ring structure (shown in Figure 49), is present in 18 zeolitic structures[16]. It is perhaps surprising therefore that there is little suggestion from NMR[3] of these species in solution. However, the structure of the 5-ring calculated here matches very well the structure of a 5-ring in a crystalline framework, as shown later (section 4.2.1.5, page 103). Indeed, the structure is very rigid, with few other conformations possible: in contrast to the 4- and 6-rings calculated here, which possess higher conformation flexibility. In fact, the 6-ring is more flexible despite having closer H-bond contacts (by 0.3Å) than the 4-ring.

The geometric evidence could suggest that the formation of solution phase 5-rings is therefore likely. However, the population of pentameric species (which cyclize to the

[xii] **Exergonic** refers to a reaction where the Gibbs free energy is negative, and **endergonic** when ΔG is positive[117]

5-ring) will be low as the favourable reaction of a tetramer (as we shall see in section 4.5.3.2 page 143) is to form a 4-ring. Therefore, we need to consider further, how and when 5-ring species form, allowing the crystallization of pentasil zeolites.

Six-membered rings are found in 39 of the zeolitic arrangements[19]. Since NMR[3] studies do not detect it in solution (as with the 5-ring), we need to consider how the 6-ring may result from either the condensation of smaller silicate species or the agglomeration of larger clusters; for example, three 4-rings could condense to form a 6-ring and subsequently a d6-ring[118].

4.2.1.4 Intramolecular H-bonds

A crucial feature exhibited by the structures shown in the previous section are the intramolecular H-bonds between the hydroxyl groups, in agreement with the analysis of Pereira *et al.*[40] The dominance of strong H-bond interactions in determining silicate cluster chemistry is also suggested by Lickiss[58]. As a result, these H-bonds are expected to dominate the conformations of silicate clusters.

The effects of H-bonds stabilizing different structures can be seen in Figure 50, which shows two different conformations of the tetramer. The first conformer (a) resembles

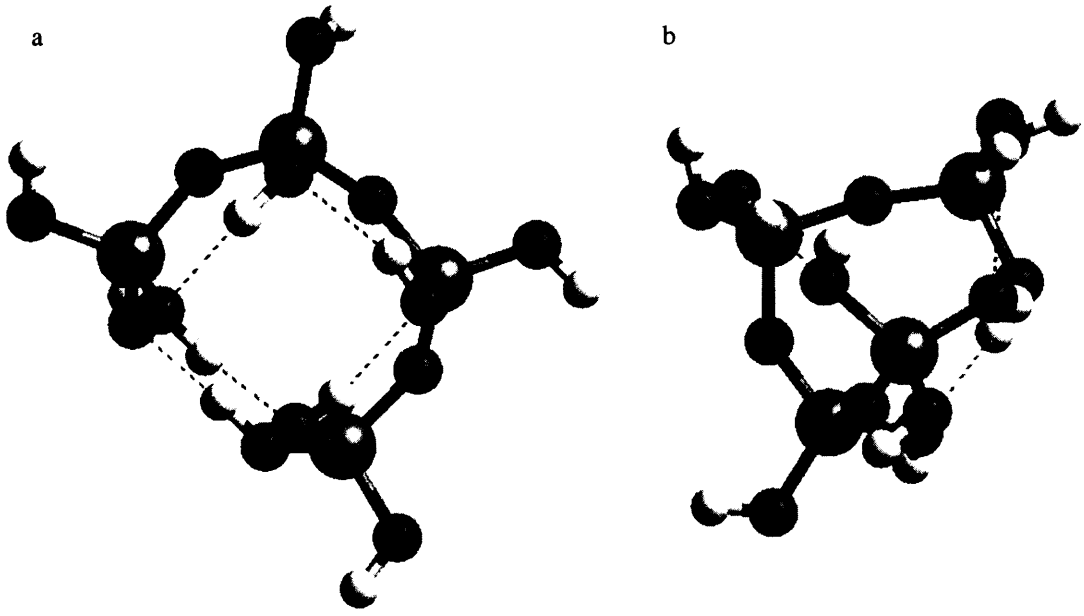

Figure 50 Optimized tetramer in two different conformations in the gas phase; the first (a) resembling a 4-ring, and the second (b) a tetrahedron; the larger spheres are Si; the H-bonds are denoted by a dashed line.

the 4-ring, and the second (b) a tetrahedron (which could form through three internal condensations, see Figure 60). The electronic energy of the former is only 2 $kJmol^{-1}$ lower than the latter, which has five H-bonds rather than four.

Clearly, another important class of H-bond interaction for these clusters are those with water molecules. However, these H-bond interactions are not described by the continuum dielectric (COSMO solvation) model, as there is no explicit water in the treatment. However, a detailed analysis of the interactions between water molecules and silicate clusters and between the clusters themselves will be described in the final sections of this thesis (section 5.2).

The linear clusters tetramer, pentamer and hexamer have a complex potential energy surface, with several local minima, because of the large number of degrees of freedom; (for example in the hexamer, there are 39 atoms). The degrees of freedom are reduced through the internal cyclization reaction, not only by the elimination of a water molecule, but also by the cyclization reaction. For the 4-, 5- and 6-silicon linear cluster, the simulated annealing procedure described in the methodology section (3.1) was found to be essential in avoiding local minima.

4.2.1.5 The 5-membered ring.

The 5-ring optimized cluster was found to have almost the same geometry as the 5-ring from the MFI[xiii] [16] zeolite crystal structure (Figure 51). There is almost an exact overlap for all the silicon atoms and a very close match for the oxygen atoms. This interesting feature could suggest a very early definition of the 5-ring structure, and the possible direct condensation of 5-rings in the nucleation-crystallisation process. The 5-ring-curved structure is facilitated by a double H-bond (Figure 49 (c)); so in order to keep this conformation, the 5-ring must maintain these H-bonds, suggesting that there are only a very limited number of ways a 5-ring can attach to a surface.

Figure 52 shows the geometric coincidence between the calculated and MFI crystalline 4- and 6-rings. The silicon atoms are largely superimposed, which is not the case for the oxygen atoms. In general, the overlap for the 5-ring (as seen in Figure 51) is significantly closer than that found for the 4- and 6-rings (Figure 52). However, this is

[xiii] MFI refers to the three letter code used by the Structure Commission of the International Zeolite Association to assign names to zeolitic structures. MFI is the structure code for the common zeolite ZSM-5 and its all-silica member silicalite.

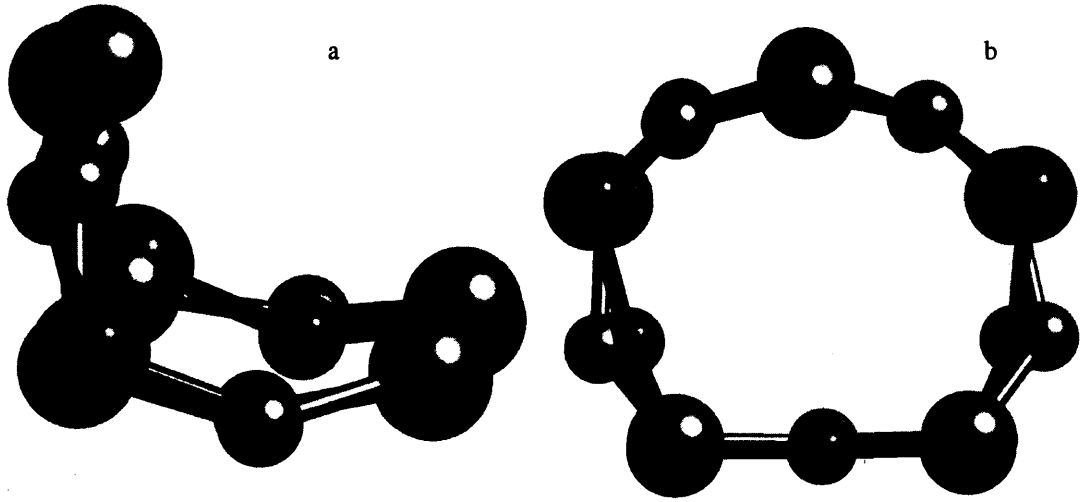

Figure 51 The overlapping of optimized 5-ring (grey structure) and the 5-ring extracted from the MFI zeolite structure. The hydrogens from the optimized cluster have been omitted for simplicity.

not, we should emphasize, necessarily a determining factor for synthesizing 5-ring containing zeolites, since the nucleation mechanism determines the framework assembly and not the availability of suitable clusters in solution. But, in the context of nucleation, this "locked" conformation may reveal why no 5-rings are seen in solution: they are possibly highly susceptible to further reaction and grow quickly.

The significant geometric similarity between the calculated ring structures and the rings found in actual crystals suggest that these clusters could be accommodated in larger

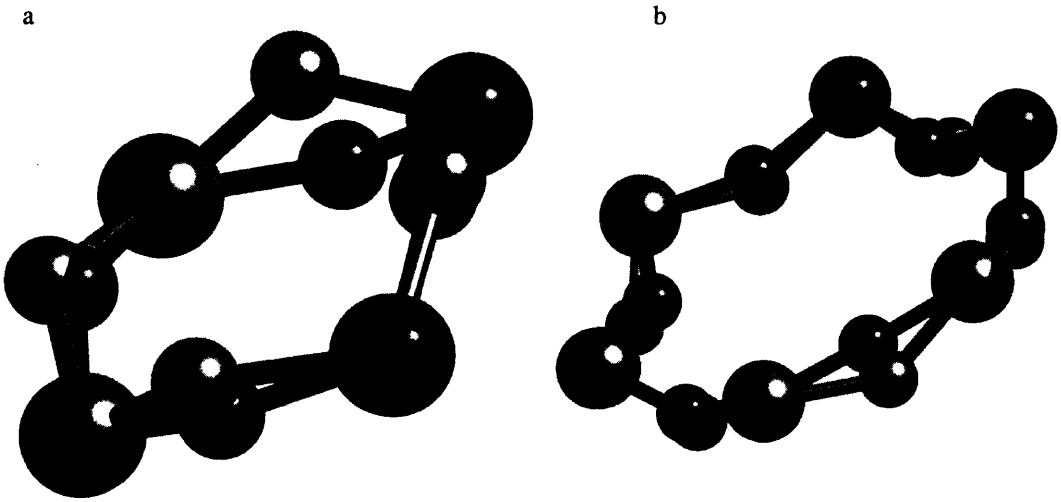

Figure 52 The overlapping of: (a) the optimized 4-ring (grey) and that from the MFI crystalline structure and (b) the optimized 6-ring (grey) and that from the CHA crystalline structure.

structures without important changes in the conformation of these rings. A consequence of the latter hypothesis is the possibility of forming these rings in the early stages of the nucleation, and not in the later growth.

Clearly, cluster geometries and energies are closely related. As discussed in this section, H-bonds play a major role controlling the cluster conformation. However, a more realistic description of the role of these clusters in zeolite nucleation will also include deprotonated silicates, a consequence of the high alkalinity. The structure of such anionic species will be analysed in the next section.

4.2.1.6 Anionic silicates

The structures analysed in the previous sections are neutral silicates. However, as emphasised earlier, the high pH present during hydrothermal synthesis results in the deprotonation of these silicates. Analysing the anionic silicate structures will therefore give a deeper insight into the actual structures present in the synthesis solution. This section will show some of the most significant anionic silicates and the important features found, particularly when compared with the neutral structures discussed above.

Even when only a single proton is removed, there are significant changes to the cluster geometry, which is clear in Figure 53, for the 4-ring. The 4-ring bends slightly so that there is closer contact between the remaining hydroxyls and the bare O^-. The O-Si-O angles next to the O^- are reduced from 134.7° in the neutral 4-ring to 122.1° and 123.8°

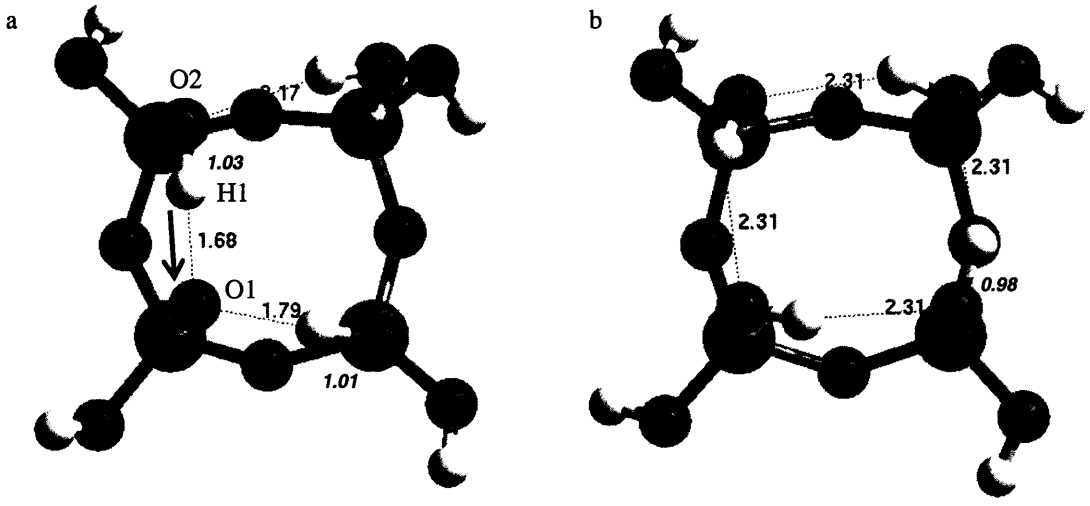

Figure 53 Comparison of H-bond distances between 4-ring$^-$ **(a)** and 4-ring (b), both in the gas phase. In italics are the bonded O-H distances. **Distances are in angstroms, as in all the models presented in this thesis.**

in the 4-ring$^-$. Furthermore, facile internal proton transfer is now possible, due to the short H-bond distances around the O^-. In the case of the 4-ring, for example, an H-bond distance is reduced from 2.3Å to 1.7Å. When further deprotonation occurs, the protons can be redistributed on the cluster more readily. Consequently, the minimum energy structure will be reached easily, having the oxygen bearing the charge in the most stable position. For example, consider the hydrogen and oxygen labelled as H1 and O1 in Figure 53. The short distance between H1 and O1 and the charge density on O1 facilitates a proton transfer, the new conformation will have the excess of charge over the oxygen O2 (the process is indicated by the arrow). Therefore, if the conformation with the proton on O1 has a lower energy conformation than in the O2, it can be easily reached and the charge will be on the oxygen, which has the most favourable position to bear the excess of charge.

Another important feature, observed in highly deprotonated clusters, is the complete opening of the compact linear silicates as seen in Figure 54, compared with Figure 48 and Figure 49. This effect is due to the electrostatic repulsion between the O^- atoms. However, in the synthesis solution, a counterion, for example, Na^+, K^+ or a large organic templating agent, will passivate the charge deficiency to some extent, depending on the distance from the counterions. However, even in the presence of counterions, it is likely that the highly charged clusters will not be as "dense" as those seen for the neutral clusters in solution. This simple opening effect could explain why very high pH solutions do not lead to zeolite nucleation, because to close such a high

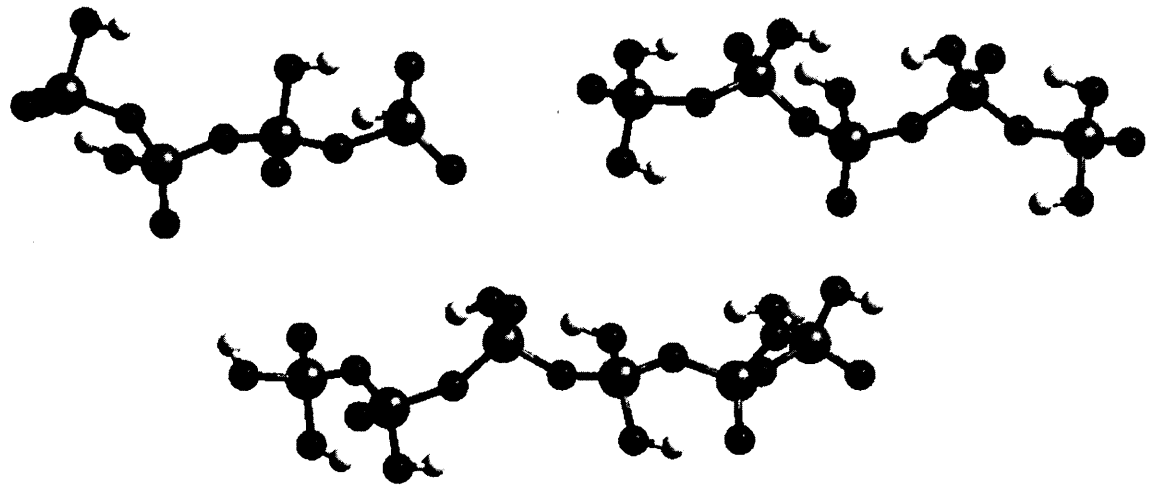

Figure 54 Structures for highly charged linear silicates. (a) Tetramer^{6-}, (b) pentamer^{5-} and (c) hexamer^{5-}.

charge species will need a high energy to overcome the electrostatic barrier. In Figure 54 the high charge implies an OH^-/Si ratio close to one, while in most of the zeolite synthesis a ratio of ≈ 0.1-0.5 is observed (see Figure 43). However, for the same clusters of Figure 54, an OH^-/Si ratio of ≈ 0.5 will imply a charge of -2 and -3 approximately and with these charges, clusters remain in their "closed" ring-like conformation, even when the counterion is not considered.

4.2.2 Ring structures with "hanging" monomers

We now consider the addition of a further monomer to these rings, which we shall refer to as a "hanging monomer"

Analysing ring clusters with hanging monomers is important, because the attachment of oligomers (especially the smaller species *i.e.* monomers and dimers), onto ring structures is very likely to occur in silica solution chemistry: such species are seen in solution. Furthermore, the addition of a small oligomer onto a ring can also be considered as a prototype for addition onto a growing nucleus or crystal surface.

The 3- and 4-rings with one and two hanging monomers are shown in Figure 55. These optimized clusters again exhibit the same patterns as the linear oligomers (see Figure 49): silicates are prone to form dense clusters, facilitated by internal H-bonds. At the same time, the addition of monomer units leads to some structural changes in the original ring clusters (as seen by comparing Figure 55 with Figure 48).

Of particular note here are the 3- and 4-rings with one monomer, because both are observed in silicate solutions[3]. Finding these silicates in solution implies that they are stable and relatively long-living species and thus studying their structure and thermodynamical properties help us to understand why they are preferentially stable. The 4-ring with one monomer (cluster (c) in Figure 55) is, in addition, considered as one of the Secondary Building Units (see Figure 5)[16], that is, a structural unit which can be periodically replicated to give a known zeolite crystal structure. In the past, these clusters have been suggested as possible growth units.

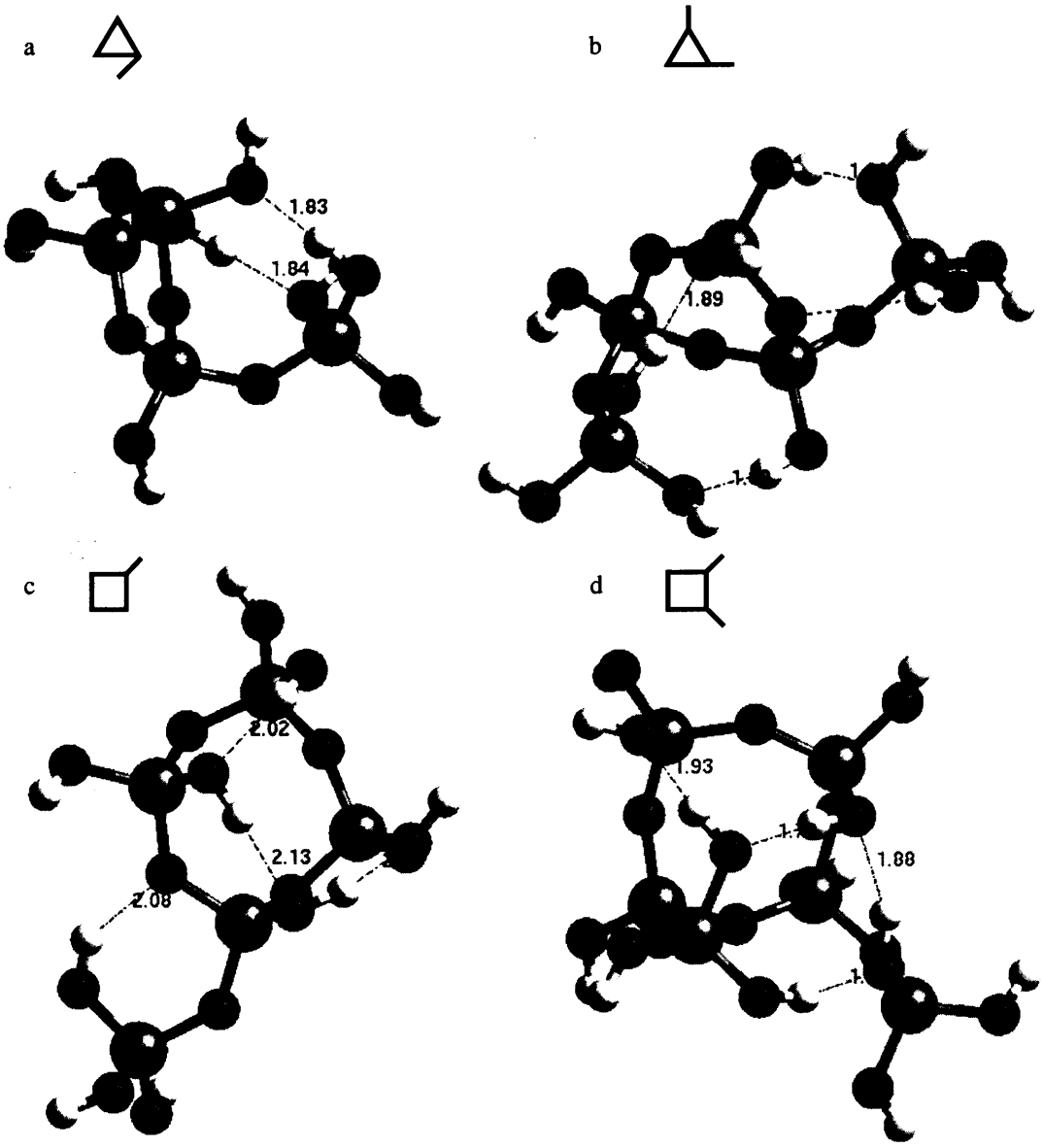

Figure 55 Structures representing ring clusters with hanging monomers. (a) 3-1-ring, (b) 3-2-ring, (c) 4-1-ring and (d) 4-2-ring. H-bond distances in angstroms.

4.2.3 Multiple ring structures

The occurrence of multiple linked rings is common in solutions containing silicates. In fact, zeolitic frameworks are made principally by multiple rings sharing sides, as can be observed in Figure 1 (page 18). In particular, certain clusters containing multiple ring structures, considered here, have been observed by NMR[3], specifically clusters (c) and (d) in Figure 56 and clusters (a) and (b) in Figure 57.

The small cluster with two 3-rings ((a) and (b) in Figure 56), analysed here, illustrates an important general characteristic, that even in these very early stages of polymerization, ring structures result in a "locking-in" of oligomeric geometry; that is, once rings are formed, we generate essentially rigid units.

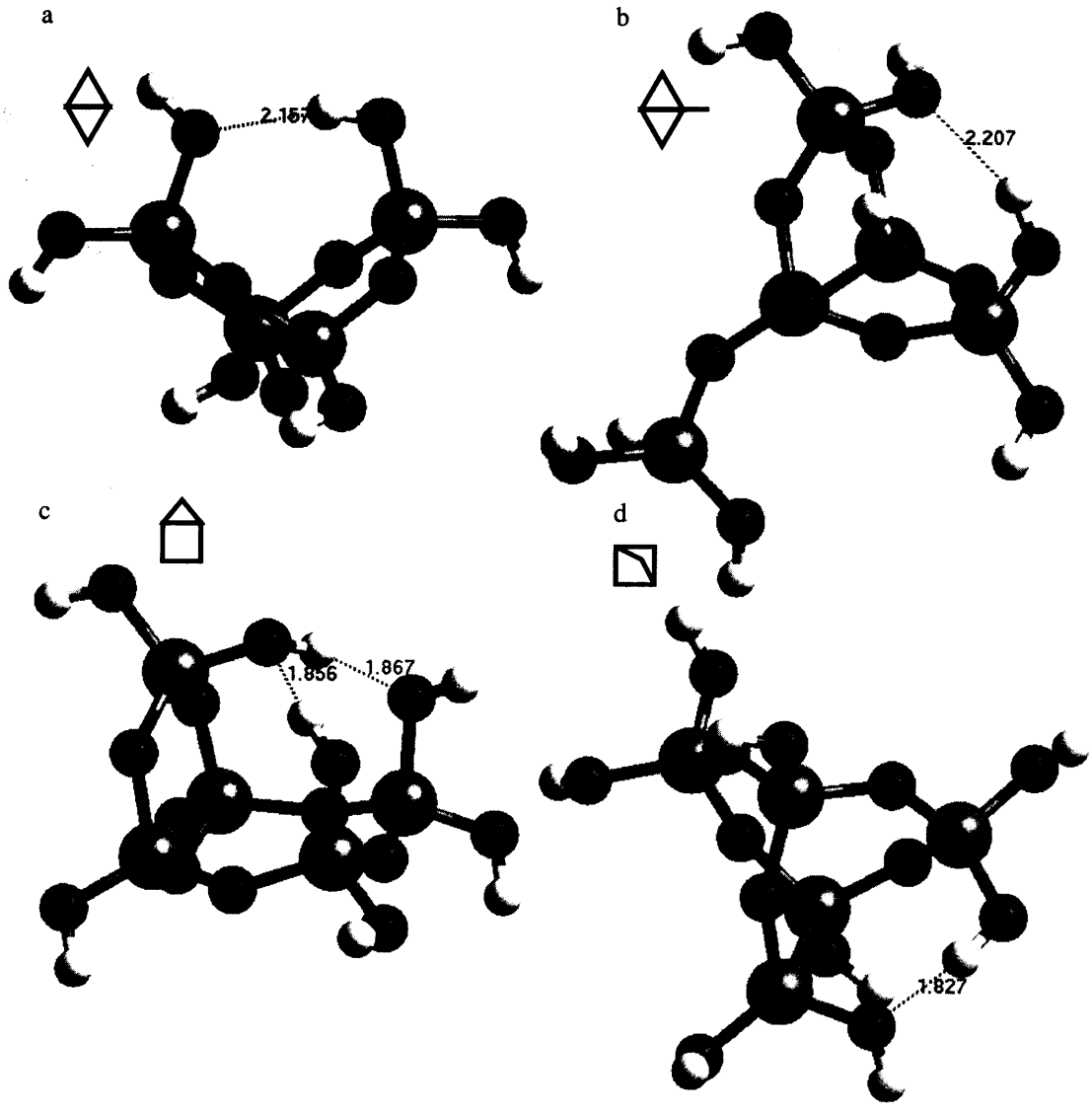

Figure 56 Structures representing clusters with multiple rings: (a) fused3-ring, (b) fused3-1-ring, (c) 4-three-ring and (d) 4-one-ring.

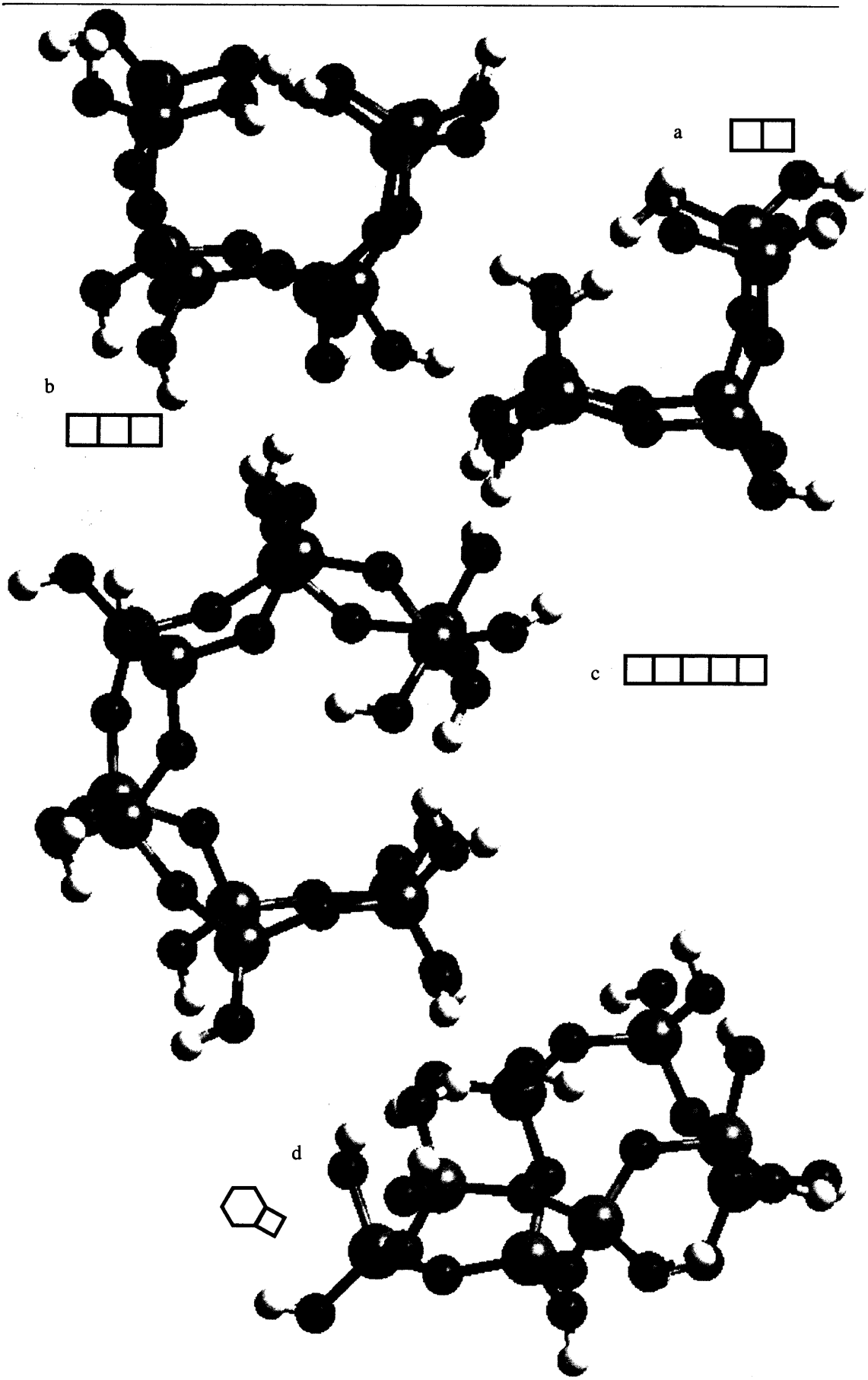

Figure 57 Structures representing clusters with multiple rings: (a) fused4-ring, (b) tri4-ring, (c) penta4-ring and (d) 6-one4-ring.

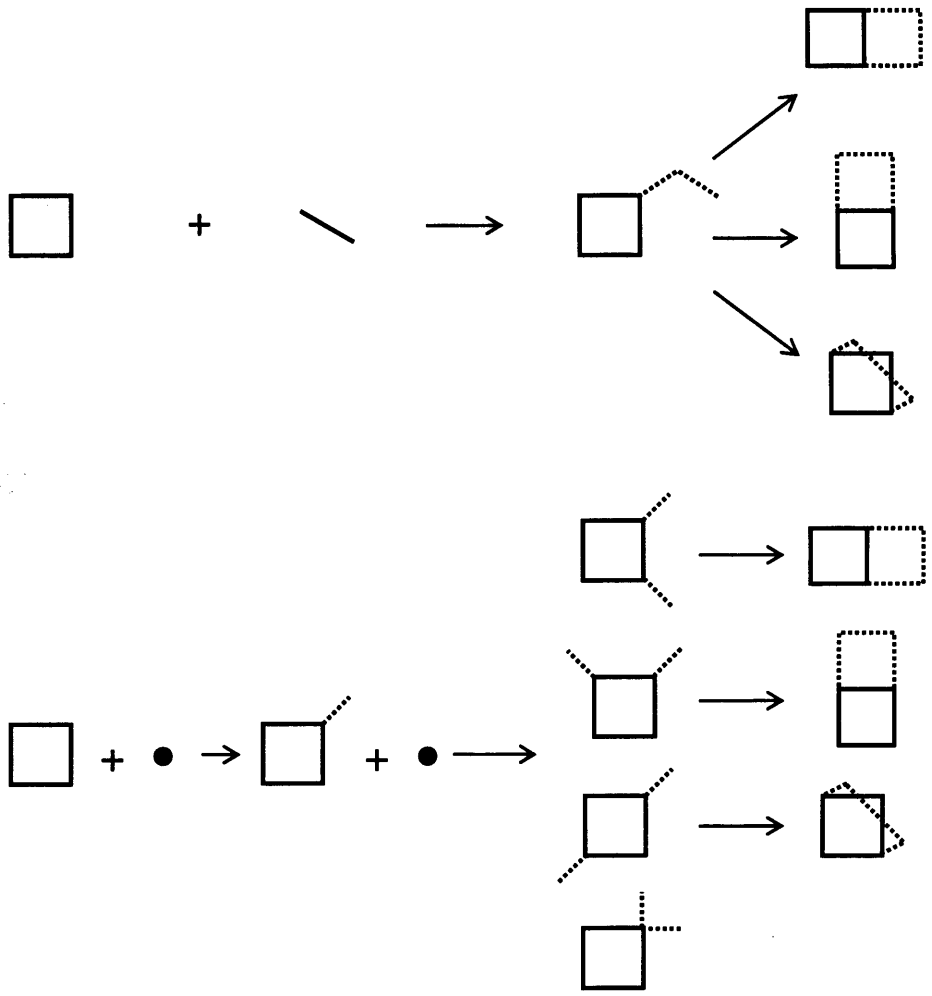

Figure 58 Two routes to obtain the fused 4-ring: from a dimer condensation over a 4-ring and the condensation of two monomers.

4-rings fused laterally (see Figure 57 (b)) have very interesting geometric features, with a direct impact on all the silicate cages studied here. Consider the possible formation of such an oligomer. The 4-ring, a species that is very common in solution[3], is taken as the starting point. The condensation of a dimer (again expected to be present in significant concentration) onto that 4-ring can occur in two ways (Figure 58), leading to the fused4-ring ((a) in Figure 57), whose formation has a high probability; in other words, this condensation has a high entropy. The second structure is a 4-ring with the dimer across (Figure 58), which has a lower geometric probability than the previous

structure. In contrast, consider now the formation of the fused4-ring by the addition of monomers. Two monomers condensing onto the 4-ring are less likely to form the fused4-ring structure as the condensation of a second monomer on a 4-ring (see Figure 55 (c) and (d)) can take place on any of the remaining (seven) hydroxyls, including the OH where the first monomer condensed (see lower part of Figure 58). Only addition on an adjacent Si can result in a fused4-ring. Therefore, addition of monomers does not favour any particular structure, and will favour the formation of many different oligomers, within the limits of exergonic condensations.

However, zeolites have very specific structural units, with prevalently 4-, 5-, 6-rings and cages involving these rings. Thus, statistically, addition of dimers (rather than monomers) results in the construction of larger structures more likely to lead to zeolite nucleation.

Extending further the reasoning in the latter paragraph, it can be found that dimer condensations are more likely to produce "planar" structures. However, a corollary of the latter argument suggests that the presence of dimers in solution will enhance the formation of clusters with similar geometric characteristics to the fused4-ring, which could lead to other specific clusters found in zeolites. The fused4-ring itself, is found in solution[3] and is a secondary building unit[16], however it has a structure suggesting that the next step is the condensation into a d3-ring cage (see Figure 60). Indeed the fused4-ring may be prone to condense internally into a d3-ring. However, no zeolitic structure contains a d3-ring as a structural unit.

Taking again the 4-ring as the starting oligomer, which we expect to be present in relative high concentrations, two 4-rings could condense (making two new Si-O-Si bonds only) in three different ways. Using an argument analogous to that above, the side condensation is more probable than the transverse mode. Thus, the most probable cluster after two 4-rings fuse is the tri4-ring ((b) in Figure 57), which has a conformation suggesting the subsequent formation of a cage: that is the d4-ring (see Figure 60), which is fully identified in solution [31, 119].

Further 4-ring condensation on the tri4-ring will produce a long chain composed of 4-rings, the penta-4-ring ((d) in Figure 57). The optimized structure is again "curved", suggesting that a direct condensation into the d6-ring cage structure is very likely. This route could be one way of generating the important d6-ring cage, which is observed

extensively in zeolitic frameworks[16]. The d6-ring is described sometimes as the triple-d4-ring, because it can be formed after the direct condensation of three 4-rings and has been proposed as a route to faujasite *i.e.* 4-rings → d6-rings → faujasite[118]. However, it should be noted that the NMR experiments on which these suggestions are based were conducted on zeolites containing aluminium.

4.2.4 Cages

The study of silicate cages is without doubt essential in gaining an understanding of the nucleation and growth of zeolites, as specific cages are found in most zeolitic frameworks.

In this section we analyse first the d4-ring cage, together with a number of related structures (see Figure 59). The d4-ring has been widely studied, because it is one of the characteristic clusters appearing in silica solutions[3, 31, 34, 119], and has also been identified in growing crystals[120]; additionally it also plays an important role in germanium containing zeolites[121-123]. However, perhaps intriguingly, only one example of a pure siliceous zeolitic framework containing d4-rings is known, zeolite A (LTA)[124], although we note preparation is only possible via a very specific fluoride mediated synthesis. This now leads to an interesting question, namely what happens to the large population of d4-ring oligomers observed in solution: are they dissolved to become a source material for the growing crystals? Alternatively, are they present in the solution at the end of the synthesis; and are then thrown down the sink? Regardless of whether we are able to answer to these specific questions, it is clear that the d4-ring has an important role in the nucleation-crystallization process of zeolites.

The optimized structure of the d4-ring (Figure 59 (a)) can be described as a symmetric 8-member silicate cube without internal H-bonds. The cage structure is rigid with little change possible to its geometry. In the anionic state, the d4-ring is likely to become a much more reactive species, in contrast to the tetramer and 4-ring (see above), as the charged oxygen cannot be passivated by internal H-bonds. However, water molecules have an important role in providing external H-bonding.

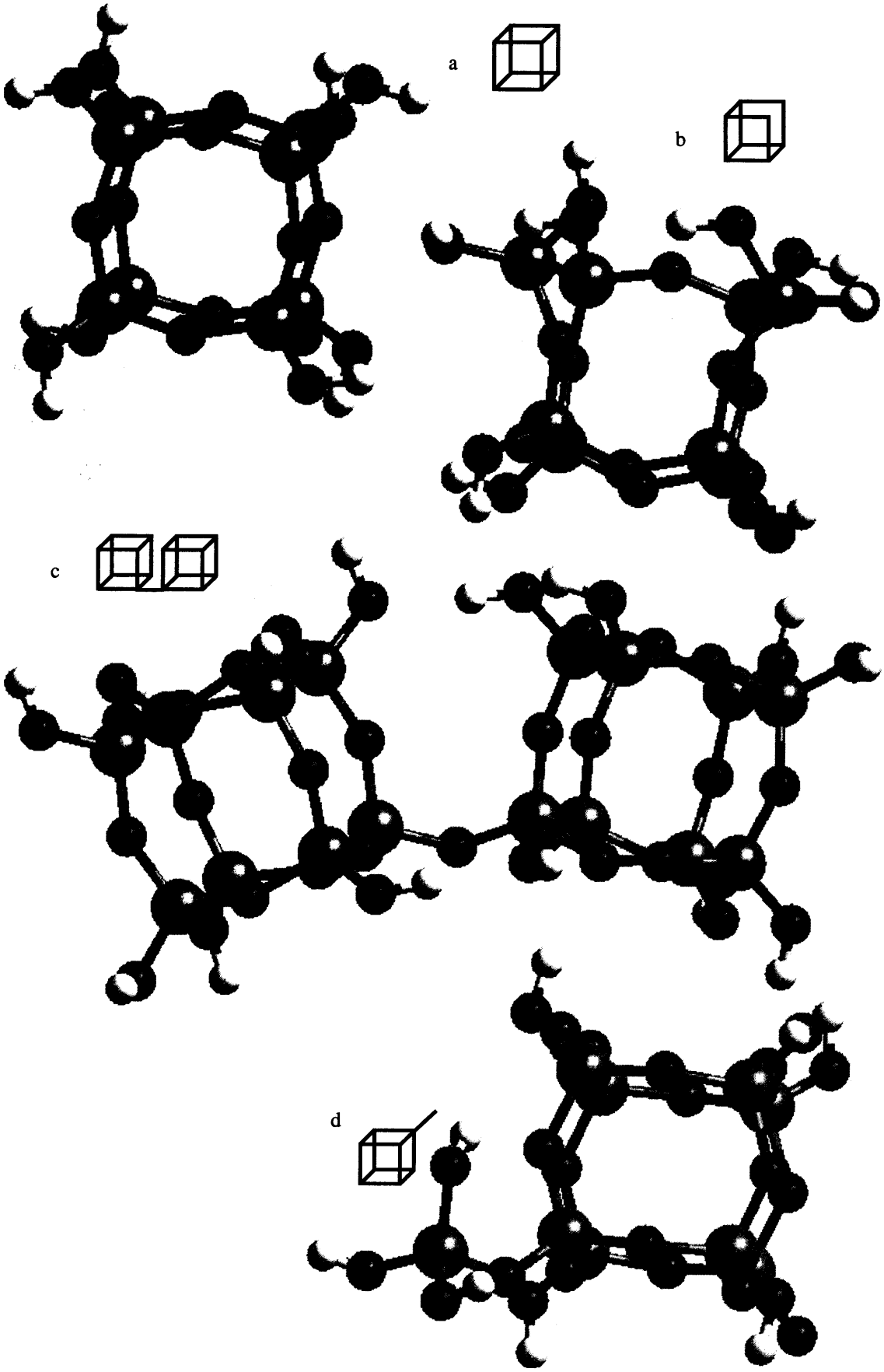

Figure 59 Structures representing clusters with cages: (a) d4-ring, (b) open-d4-ring, (c) d4-d4-ring and (d) d4-1-ring.

A d4-ring can be formed by the condensation of two 4-rings (Figure 61). In such a process, the tri4-ring structure (Figure 57 (b)) must first be formed and with a further condensation forming an open d4-ring structure, shown in Figure 59 (b). Once the latter is formed, it is unlikely that any other product will form, except for a d4-ring. This open d4-ring structure is important, because it both leads to d4-ring formation and it is the first step in a possible d4-ring dissolution.

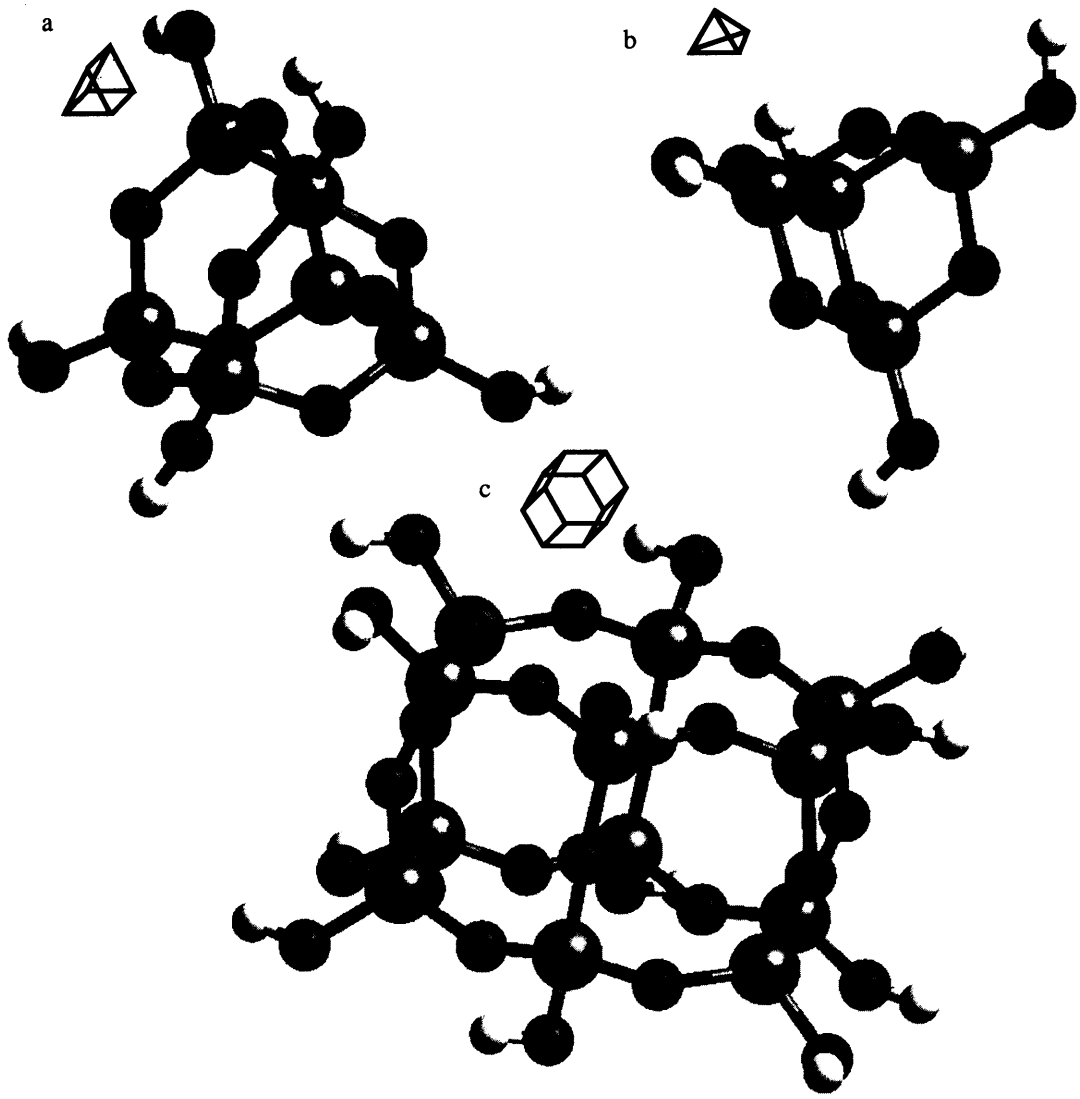

Figure 60 Clusters representing clusters with cages: (a) d3-ring, (b) tetrahedron and (c) d6-ring. H-bond distances in angstroms.

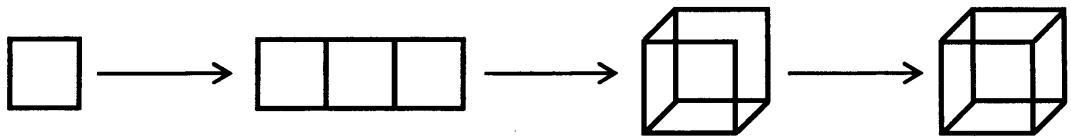

Figure 61 A proposed mechanism for the formation of a double 4-ring.

A most significant question in the nucleation and growth of zeolites is whether larger species form by the condensation of small silicates, such as the monomer or via the condensation of larger units such as d4-rings. Some investigations have interpreted experimental results as showing predefined clusters assembling into the final crystal[3, 9]. Other authors consider it more feasible that condensation occurs by clusters such as monomers[12]. It is of particular note, however, that d4-rings have been observed in the growing surface of zeolite A (LTA framework) which include Al[120, 125], and that the d4-rings have been suggested as the "building units" in this particular zeolite. So, in order to make clearer which mechanism is favoured, it is of vital importance to study the condensation either of a monomer on a d4-ring or of two d4-ring, as illustrated in Figure 59 (c) and (d).

The d4-ring symmetry makes for an easy analysis of the structures in Figure 59, as, in particular, structures (c) and (d) (Figure 59) can only have the conformations shown. Also we note the interesting fact that both of these structures have been observed in NMR experiment[31].

We now turn to the smallest cage-like silicate structure possible which is the tetrahedron shown in Figure 60 (b), although there is, of course, almost no free space inside the cage. The tetrahedron is a very strained symmetric structure but one that has been identified by NMR in silica solutions[3]. The cage with five silicon atoms is presented in Figure 56 (d), and the next cage, containing six silicon is the d3-ring (Figure 60 (a)). Finally the large d6-ring cluster which occurs in ten zeolite frameworks[16] is presented in Figure 60 (c).

Most of the cages studied here are found in silica solutions. Indeed, with the exception of the d6-ring, the cages shown with 4, 5, 6 and 8 silicon atoms have been detected by NMR[3]. However, not all the cages we consider are present in zeolite structures. Furthermore, the question arises of how cages that are larger than the d4-ring, like the

d6-ring, form in the zeolitic framework? A possible answer is that they are built by the successive condensations of 4-rings or other smaller clusters and so are never observed in solution. Nevertheless, this argument does not yet answer the question of how the zeolitic nucleus will be formed, because at some point this d6-rings (along with other clusters) should appear in the primitive nucleus.

In concluding this section, we note that silica/silicate cages are less flexible than the linear silicates, and thus fewer conformations are possible. None of the cages exhibit internal H-bonds, with the sole exception of the 5 silicon cage (which has a single H-bond), compared with the linear or ring silicates that can have as many H-bonds as silicon atoms. We may speculate therefore that once such structures are formed, interaction with other clusters and solvent is more favoured.

Our aim has been to give a detailed account of the geometrical aspects of the clusters studied in order to provide a basis on which to build a mechanism of self-assembly. We have seen how by simply considering the clusters as building blocks (neglecting other thermodynamic properties for now) leads us to expect some structures to be more prevalent than others on statistical grounds. For example, growth of small clusters from dimers is more likely to lead to zeolite-like structures, monomer growth is more likely, statistically, to lead to open glass-like clusters, as shown in Figure 58. The rest of the chapter will deal with the thermodynamic properties involved in the typical reactions that can take place in hydrothermal solutions, containing the silicate clusters addressed and illustrated above.

4.3 Deprotonation reactions

At the high pH levels (12.6 - 14[19]), normally present in the synthesis conditions of zeolites, we expect deprotonation of the silicate clusters. Thus, as argued earlier the silicates will be present in the solution as anionic species[6].

By calculating the structure and energetics of the different anionic species that may be present in the synthesis solution, it is possible to analyse the energies involved in the process of deprotonation. In Table 2 and Table 3, the deprotonation energies of the neutral clusters considered above are shown. A maximum anion charge of -4 was investigated. The tables show first the change in electronic energy (including the correction for the zero point energy (ZPE)) and next the change in enthalpy, entropy and

Gibbs free energy, for the clusters in the gas phase, COSMO solvation and with explicit water molecules. Note that the solution treatment with COSMO reproduces trends well (Figure 46) but not absolute values (section 4.1.3.1). However, the last part of Table 2 and Table 3 includes both explicit water and the COSMO solvation, for selected species which can be considered quantitative.

Table 2 The free energy change and other thermodynamical properties at 298K, associated with the anionic oligomer formation. The reaction for the first row is $M + OH^- \rightarrow M^- + H_2O$.

	Gas				COSMO Solvation				Explicit water			
Product	ΔE_0	ΔH	$T\Delta S$	ΔG	ΔE_0	ΔH	$T\Delta S$	ΔG	ΔE_0	ΔH	$T\Delta S$	ΔG
monomer$^-$	-220	-219	7	-226	-55	-54	6	-61	-34	-29	0	-29
monomer^{2-}	287	286	1	285	6	5	2	2	-27	-23	-6	-17
monomer^{3-}	821	821	5	816	73	73	4	68				
monomer^{4-}	1380	1380	4	1376	138	137	3	134				
dimer$^-$	-297	-299	-3	-296	-90	-89	2	-91	-49	-45	-10	-35
dimer^{2-}	121	120	2	119	-25	-27	-2	-25	-32	-27	-2	-25
dimer^{3-}	531	531	4	527	-7	-6	10	-16				
dimer^{4-}	942	942	6	936	22	19	-4	23				
trimer$^-$	-347	-349	-4	-345	-104	-107	-5	-103	-57	-52	-8	-44
trimer^{2-}	58	58	3	55	-56	-55	6	-60	-29	-24	1	-25
trimer^{3-}	409	408	3	405	4	4	5	-2				
trimer^{4-}	718	720	12	708	-7	-7	5	-12				
3ring$^-$	-307	-310	-7	-303	-71	-75	-10	-65	-51	-50	-16	-34
3ring^{2-}	62	62	3	58	-57	-57	5	-62	-39	-39	-16	-23
3ring^{3-}	399	399	5	394	-40	-41	4	-44				
3ring^{4-}	793	791	-2	793	-3	-5	0	-4				
tetramer$^-$	-375	-377	-1	-376	-119	-120	5	-124	-69	-63	-3	-60
tetramer^{2-}	-6	-8	1	-8	-76	-78	-2	-77	-52	-52	-15	-37
tetramer^{3-}	326	327	8	319	-27	-27	4	-31				
tetramer^{4-}	613	612	6	606	-9	-10	3	-13				
4ring$^-$	-361	-364	-15	-349	-115	-112	7	-119	-57	-48	0	-48
4ring^{2-}	14	14	5	9	-65	-66	3	-68	-48	-46	-13	-32
4ring^{3-}	356	358	9	349	-27	-27	4	-31				
4ring^{4-}	654	653	0	653	-13	-13	4	-17				
pentamer$^-$	-415	-420	-7	-413	-131	-130	8	-138				
pentamer^{2-}	-45	-43	11	-54	-78	-79	-1	-78				
pentamer^{3-}	256	256	5	251	-78	-77	6	-83				
pentamer^{4-}	574	573	7	566	19	16	-3	19				
5ring$^-$	-398	-403	-12	-391	-131	-133	-2	-131				
5ring^{2-}	-53	-55	1	-55	-76	-87	-16	-71				
5ring^{3-}	324	326	7	319	-40	-31	19	-51				
5ring^{4-}	579	579	4	575	-22	-22	4	-26				

The first row of Table 2 has the results for a very simple reaction involving the silicate monomer discussed in section (4.1.3.1.), *i.e.*:

$$Si(OH)_4 + OH^- \rightarrow H_3SiO_4^- + H_2O. \quad (4.5)$$

Table 3 The free energy change and other thermodynamical properties at 450K, associated with the anionic oligomer formation. The reaction for the first row is $M + OH^- \rightarrow M^- + H_2O$.

	Gas			COSMO Solvation			Explicit water		
Product	ΔH	TΔS	ΔG	ΔH	TΔS	ΔG	ΔH	TΔS	ΔG
monomer$^-$	-220	10	-229	-55	9	-64	-28	1	-30
monomer^{2-}	285	1	284	4	2	2	-23	-9	-14
monomer^{3-}	820	6	814	72	6	66			
monomer^{4-}	1379	5	1375	136	3	133			
dimer$^-$	-300	-6	-294	-90	2	-92	-44	-14	-30
dimer^{2-}	119	1	118	-28	-5	-23	-27	-3	-24
dimer^{3-}	530	6	525	-7	15	-21			
dimer^{4-}	941	8	934	17	-9	26			
trimer$^-$	-351	-9	-342	-110	-10	-100	-52	-12	-40
trimer^{2-}	57	3	53	-55	8	-63	-25	1	-26
trimer^{3-}	407	3	404	3	7	-4			
trimer^{4-}	720	18	702	-8	7	-15			
3ring$^-$	-313	-14	-299	-77	-18	-60	-51	-25	-26
3ring^{2-}	61	4	57	-58	6	-64	-41	-27	-14
3ring^{3-}	399	8	391	-41	4	-46			
3ring^{4-}	790	-4	794	-6	-2	-4			
tetramer$^-$	-379	-4	-375	-121	6	-127	-61	-3	-58
tetramer^{2-}	-9	-1	-8	-80	-4	-76	-54	-24	-29
tetramer^{3-}	327	12	315	-29	4	-33			
tetramer^{4-}	611	8	603	-10	5	-15			
4ring$^-$	-365	-24	-341	-110	12	-123	-43	6	-49
4ring^{2-}	13	6	7	-66	3	-69	-46	-20	-26
4ring^{3-}	357	13	344	-28	5	-33			
4ring^{4-}	653	-1	654	-13	5	-19			
pentamer$^-$	-424	-16	-408	-131	10	-141			
pentamer^{2-}	-43	17	-59	-81	-3	-77			
pentamer^{3-}	255	7	249	-78	8	-86			
pentamer^{4-}	573	10	563	14	-8	21			
5ring$^-$	-406	-22	-384	-135	-5	-130			
5ring^{2-}	-57	-2	-55	-96	-35	-61			
5ring^{3-}	327	11	316	-24	38	-62			
5ring^{4-}	579	6	573	-23	6	-29			

Despite its simplicity, this reaction is critical because the monomer and its monoanion will be the dominant species at the start of any synthesis. Details of thermochemistry of the monomer deprotonation were already given previously in section 4.1.3.1, and we recall that a very good agreement was achieved between calculations and experiments for this reaction. In this section, deprotonation of larger clusters is considered (some of them without taking into account explicit water molecules) so the values for that reaction (Table 2 and Table 3) will be overestimated. The aim of these tables is to show the trends for the deprotonation reactions for a series of silicates with different charges.

In the gas phase, monomer deprotonation by OH^- releases a large quantity of enthalpy and the change in the entropy is small as would be expected. Therefore, the enthalpy change dominates the calculated change in free energy. On the introduction of solvation, we find significant energetic differences for the monomer deprotonation. First of all the energy released is much lower, showing the stabilizing effect of the solvation on ionic species. The change in entropy however is almost the same as in the gas phase. We recall, however, that the agreement with experiment is poor until explicit water molecules and the counterion are included (section 4.1.3.1), when quantitative agreement is achieved.

Solvation has an important effect on the deprotonation of the monomer, lowering significantly the energy change. It provides a stabilization shell for the anionic species reducing the energy difference between reactants and products.

Further deprotonation of the $monomer^-$ in the gas phase is energetically unfavourable. The second and third deprotonation free energies are highly positive while the entropy contribution is almost negligible. Solvation has a very significant effect on the second and third deprotonation energy of the monomer – even greater than those for the first (compare the solvated and gas phase free energies for the monomer in Table 2). Thus, the role of solvation is more important with higher charges, and under zeolite synthesis conditions of high pH, high charges for silicate clusters are expected.

The deprotonation energies for the dimer show similar trends to the monomer: the reactions are dominated by the change in electronic energy. In the gas phase, formation of species other than the monocharged anion is energetically prohibitive. However, on solution, the dimer also has a much lower deprotonation energy compared with the gas

phase and it appears that species with higher charges will form. For the trimer, the deprotonation energies exhibit similar behaviour to the dimer.

For larger silicates, higher charges seem to be stable in the gas phase. The formation of the tetramer^{2-} may be thermodynamically favourable in the gas phase, as are those of the doubly charged 5- and 6-silicon clusters. An explanation for this observation is the higher number of H-bonds in the larger silicates, which could help to stabilize these anions sharing the negative charge. Indeed these stable anionic structures in gas phase could help us understand how some "dry" syntheses[1] (with a very low water content) take place, because as will be shown later (section 4.4), charged species are necessary for successful condensations.

It is clear that in solution, many anionic species could be present as oligomer size increases; for example, the 4-ring could be present with several charges as well as the neutral state, because the free energy change makes several deprotonations feasible. However, it is important to note the limit to deprotonation imposed by the relative concentration of silicon and the hydroxyl anion, the OH^-/Si ratio. There is, as well, a general tendency for a decrease in the change in energy, entropy and free energy with the growing of the cluster, for the formation of a given charge state. For example to form a single deprotonated species (Table 3), the energy change decreases following the trend trimer$^-$ < dimer$^-$ < monomer$^-$. Similarly, for any silicate cluster, the higher the charge the less favourable are the changes in energy, entropy and free energy, *i.e.* very high deprotonations are less likely.

Thus, clusters larger than the monomer could be present in solution in a variety of charges states. These results again stress how important it is to consider pH to explore the different possible anions present in the nucleation solution, and the necessity of the solvation as a stabilization medium for these anionic structures.

4.3.1 Relative anionic concentrations

The extensive results in Table 3 could be used to chart approximate relative anionic concentrations, because all the reactions are with OH^-, and the conjugate acid is the H_2O. In other words, Table 3 can be interpreted in a similar way to acidity tables. Consequently, we can expect that the monomer will be less acidic than the dimer, whilst the 4-ring will be more acidic than the smaller species. Because the acidity of the

neutral monomer is relatively high, it is readily deprotonated and will be a minor species in nucleation, *i.e.* monomer species are predominantly present as monomer$^-$. However, because the dimer is a stronger acid than the monomer, it can transfer a proton to the monomer$^-$; following with the same analysis to larger clusters, we can conclude that the larger clusters will be more likely charged than the smaller ones.

A much better description of the relative populations of the different neutral and charged species is obtained when Figure 43 and Table 3 are used in conjunction. For example, whilst from simple thermodynamic consideration the monomer$^-$ will be expected as a more favourable species (over the neutral monomer), the synthesis conditions for zeolites only provide, at most, with one OH^- anion for two Si atoms. Thus, in this limit case (see Figure 43 where $OH^-/Si=0.5$) at the beginning of the nucleation, at most, only half of the monomer population will be anionic.

The thermodynamics, the initial OH^-/Si ratio and the kinetics will dictate the distribution of the neutral and charged silicates found in solution. Thus, a simple conclusion can now be drawn: for an OH^-/Si ratio less than one (as is the case in the hydrothermal synthesis), there is always a mixture of neutral and anionic silicates. The kinetics, not considered so far, will probably not have a significant impact, because it is expected that the deprotonation reactions will be fast (given the magnitude of the free energy changes). Thus, when considering the condensation key reactions in the early stage of nucleation, we must clearly consider both neutral and anionic oligomers.

4.4 Condensation reactions, an overview

In the past decade, there have been a number of studies of model structures and reactions involved in the nucleation process of silicates, including the structures of small clusters containing up to 5 silicon atoms of Pereira *et al*[39, 40]. One conclusion that could be drawn from these results was that linear silicate species were favoured over cyclic structures a situation which is not conducive to the formation of zeolitic structures, favouring instead the formation of amorphous silicates[39]. However, these early calculations were performed using a local DFT method and considered only neutral species, although solvation effects were included using the COSMO method[43]. The role of water and organic templates in pre-nucleation gels were studied by Lewis *et al*[41] and Catlow *et al*[60], using more approximate molecular mechanics methods. They identified a key role for template molecules – preventing the collapse of large

hydrophobic silicate clusters to more dense structures – and for charge interactions between anionic silicates and templating cations – necessary to maintain intimate cluster-template interactions.

The formation of small cyclic species is a key step in the nucleation and growth of silicates and zeolites, since 4-, 5- and 6-membered rings dominate zeolite structures. However, earlier *ab initio* calculations suggested that linear silicate oligomers are favoured[39]. This section therefore uses the results of the calculated clusters discussed earlier to address the key question of how the cyclization process occurs and of the role of pH and solvation in forming such pre-nucleation species.

4.4.1 Polymerization and cyclization reactions, a diagrammatic representation

In order to clarify the discussion that follows in the rest of this work, a complete schematic representation of the relations between the clusters analyzed here is presented in Figure 62. This diagram does not aim to provide an actual illustration of the mechanistic assembly for the silicates analysed, but to make, in first instance, a "navigation chart" of the silicate clusters, considered in this thesis.

4.4.2 The first linear condensations and cyclizations

The linear oligomer condensations shown in Figure 62 and their first internal cyclizations are the most important. The species observed in solution[3, 5, 31], are shown in this diagram. The rings, in particular, are important because they are directly related to those observed in the final crystal framework of the zeolite (Figure 62 shows the Secondary Building Units[16]). A summary of the results is presented in the Figure 63 and Table 4; before going into a detailed analysis of each reaction, some important but general remarks need to be made on the subject.

Initially, the species and reactions in the gas phase are considered; and in most previous studies, only these neutral and gas phase clusters were investigated. The condensation reactions for the formation of silicate oligomers (with an emphasis on cyclic structures) with up to six silicon atoms are shown in Figure 63, together with all the results for the solvated structures, which are discussed below. The condensation reactions of neutral species are considered first and are presented in the first row of each table of Figure 63. From the free energy of these neutral reactions, in the gas phase, there is a clear

tendency for cyclic species to form rather than the linear oligomers. This tendency is observed as well in Table 4, where the energies are calculated for direct condensations from the monomer. Since cyclic species are found experimentally in the pre-nucleation gel, these initial calculations suggest that it is essential to consider the free energy of formation, rather the simpler case of the enthalpy, if a reliable description of the reactions present is to be achieved.

Whilst zeolite formation is clearly not a gas phase process, it is important to note that zeolites have been formed in media that are very different from water, for example in ionic liquids or in eutectic mixtures[126]. Similarly, a dry gel conversion method has also been fruitful[127]. Thus, such gas phase results may help us understand what the important characteristics are during such non-aqueous syntheses. However, the typical aqueous case must, of course, be considered.

Table 4 Condensation energies from the neutral monomer at 298.15 and 450K. For example, $3M \rightarrow 3ring + 3H_2O$.

	298.15K						450K					
	Gas phase			COSMO			Gas phase			COSMO		
	ΔH	TΔS	ΔG	ΔH	TΔS	ΔG	ΔH	TΔS	ΔG	ΔH	TΔS	ΔG
dimer	-11	1	-13	-7	-5	-2	-11	3	-14	-7	-8	0
trimer	-28	-13	-15	-21	-18	-3	-28	-19	-8	-21	-27	6
tetramer	-51	-26	-25	-29	-32	2	-51	-39	-11	-30	-48	18
pentamer	-72	-38	-35	-46	-44	-1	-72	-57	-16	-47	-68	21
hexamer	-105	-47	-58	-54	-46	-7	-105	-71	-34	-54	-70	16
3ring	4	32	-29	-5	33	-38	3	48	-45	-6	50	-55
4ring	-25	30	-55	-18	8	-26	-27	43	-70	-22	7	-29
5ring	-43	15	-59	-34	6	-40	-43	23	-66	-34	9	-43
6ring	-70	1	-72	-43	-12	-31	-71	1	-72	-46	-22	-24

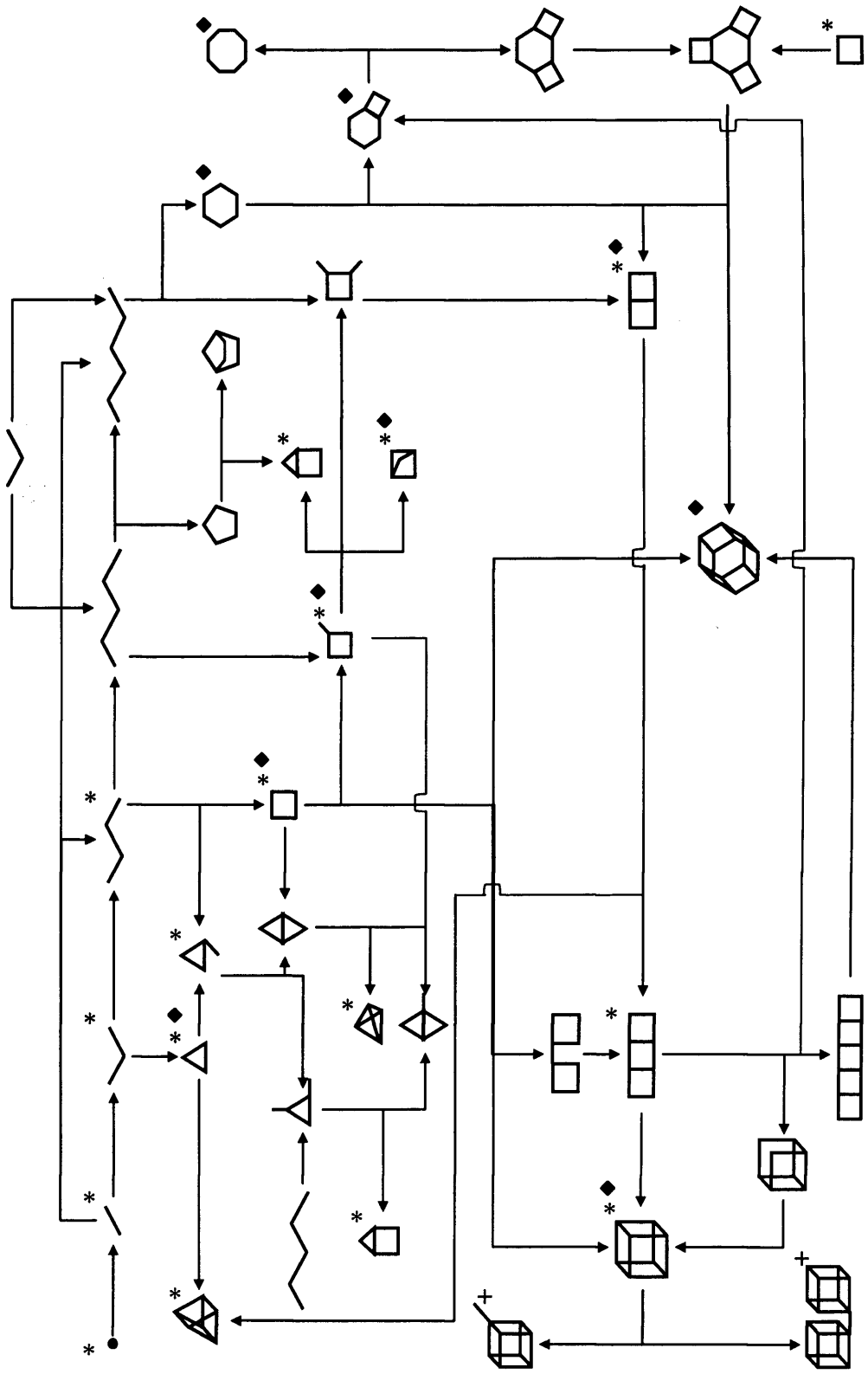

Figure 62 A diagram showing the different pure siliceous clusters analysed in this work. The species identified experimentally are shown here: (*)[3], (+)[31] as well the Secondary Building Units (♦)[16].

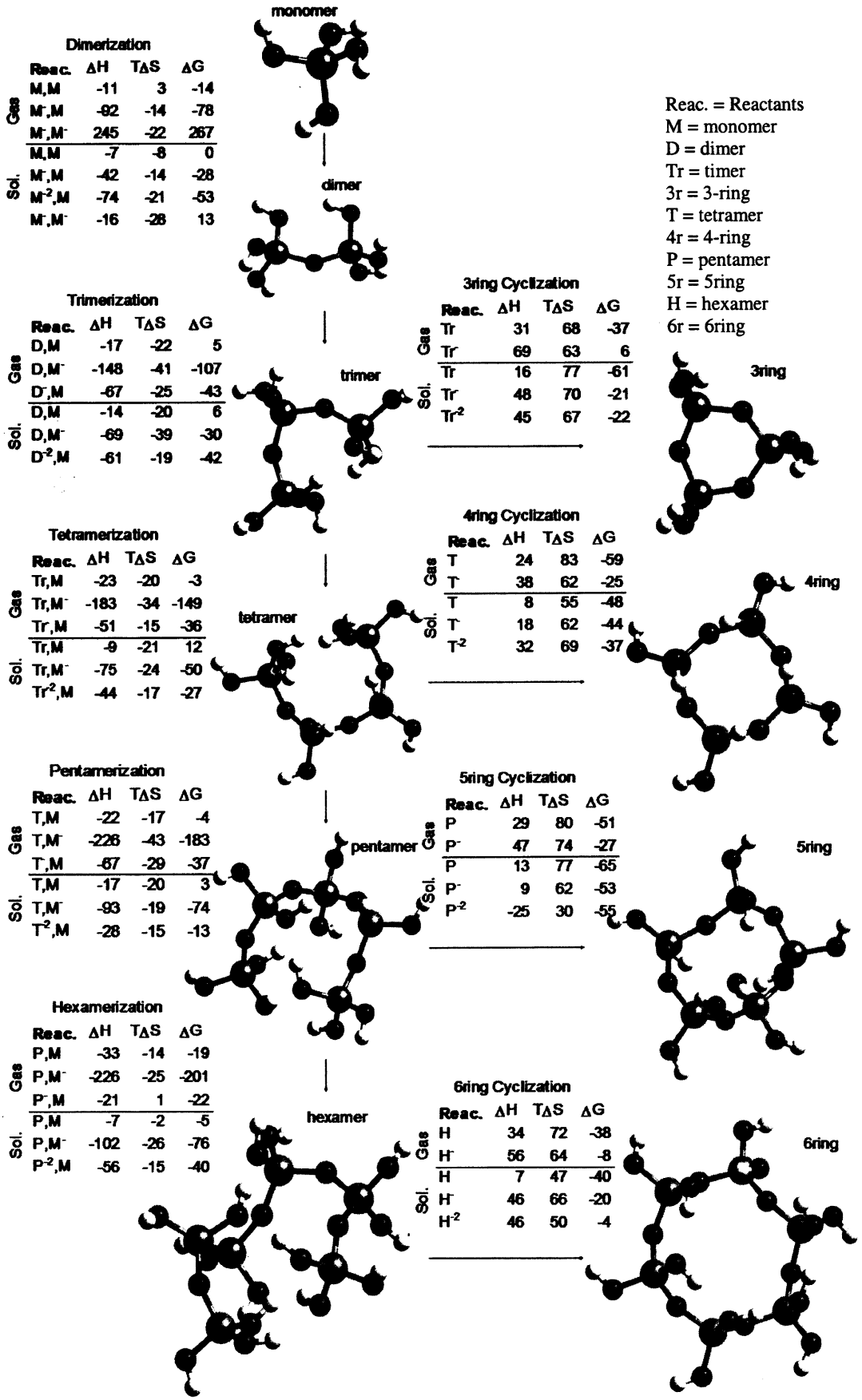

Figure 63 Condensation enthalpies, entropies and free energies at 450K.

The treatment of solvation is made in an approximate way with the dielectric screening method embodied in the COSMO[43, 89] model, as described in the section 3.3. The condensation reaction energetics obtained using this particular model (again with neutral species) is given in the second row of the two sections of the tables in Figure 63. The inclusion of the solvation via this model, results in a significant (and general) decrease in the free energy released during the linear condensation reactions (*i.e.* neutral reactions become less favourable when solvation is included). Similarly, in solution, it would be expected that condensation of neutral species would become less favourable as species increase in size. Experimentally of course, polymerization (and specifically zeolite crystallisation) typically occurs at extremes of pH (alkaline in the case of zeolites[19]). Thus, again our results are consistent with experimental observation: neutral conditions overall do not lead to zeolite nucleation and crystallization.

Further improvements are now considered to the model, to include a description of the necessary high pH. At the highly alkaline conditions typical of zeolite crystallisation (pH ≈ 12.6 - 14[19]), the principal effect of the OH^- present is to deprotonate the silicate species. Thus, the condensation reactions of the dominant anionic silicate species at such conditions are presented, both in the gas phase and in the solvent model (Figure 63). In the gas phase, we observe a general increase in the free energy released during condensation when this model of high pH is considered, with the notable exception of the formation of the 3-ring species. Additional inclusion of solvation results in a reduction in the free energy change of these anionic condensations compared to the gas phase (as was the case for neutral reactions). However, it is clear that the condensation reactions of the anionic species are considerably more favourable than those of condensations of neutral species in solution, again in agreement with experimental observations.

The net result is therefore, that solvation and high pH promote the polymerization of cyclic silicate clusters. Furthermore, since cyclization reactions are more favourable than linear growth (*e.g.,* formation of 4-ring compared to formation of a linear pentamer, both from the linear tetramer) larger solution phase cyclic species (certainly from 6-ring upward) are unlikely to form. It should also be noted that the principal contributor to the favourable free energy of the polymerization reactions is the change

in enthalpy (mostly electronic energy). However, it is entropic factors that favour the formation of the cyclic species, as presented here[128].

4.5 Polymerization vs. Cyclization

The polymerization and cyclization reactions involved in zeolite nucleation, with formation of clusters of up to six silicon atoms will now be discussed in more detail, considering successive condensation of monomers, or any other reaction involving the creation of a new Si-O-Si bond. The key features to be highlighted will be the role of pH, water, the species present in a clear silica solution and the competing reactions of polymerization and cyclization.

Our analysis will start with the ideal situation where synthesis is initiated from only monomeric species. These monomeric species will react to produce dimers and so on. In each stage of this early nucleation, we will identify the most probable species to be produced. The aim is therefore to identify the paths allowed and the species most likely to be important during these processes. This deterministic approach is a good starting point to clarify the mechanisms involved in zeolite nucleation. A summary of the different reactions, presented in the following sections, can be obtained from Figure 62.

4.5.1 Experimental Environments

As discussed earlier, synthesis starts with the mixing of the raw materials in a "clear solution" at room temperature. After a short time a gel or a sol (clear solution) is obtained[12]. The reaction mixture is taken to the synthesis conditions at high temperature and hydrothermal pressure. During the room temperature mixing, important reactions are taking place in a solvated state and are part of the pre-nucleation process. But at high temperature there are two phases: the solution itself, where reactions are occurring in a solvated environment and the gel or sol phase, where the environment is different and the water inside the amorphous material is limited to those solvating the silicates.

The results presented from here onwards will attempt to explain the pre-nucleation and nucleation states under different experimental conditions (see Table 5). Thus at room temperature (298K), the reactions modelled with the explicit water representation will be the most meaningful for a clear solution. Inclusion of explicit water is necessary, as discussed before (section 4.1.3.1), to obtain reliable data, which reproduce the

Table 5 The modelling approach for the different environments in the nucleation of zeolites.

Experimental Environment	Modelling approach
Dry synthesis	Gas phase
Clear solution	COSMO solvation and explicit water
Sol or gel	COSMO solvation

thermodynamical experimental data available under clear solutions. At higher temperatures (450K), our approach to model the environment inside the gel or sol particles will be based on the anionic species with COSMO solvation, without the explicit water molecules. In these clusters inside a gel or sol, the sodium cation is very important and because of the limited number of water molecules, the distance to the anionic silicate should be closer than in the full solvated state. The reactions taking place in full solution at high temperature are modelled with the anionic species with explicit water in COSMO solvation (Table 5), as the cation will have its own, possibly full, solvation shell. In a sol or gel, in contrast, the cation is more likely to coordinate directly to the silicate. For some of the larger clusters a further approximation is made and the solvated state is represented solely with the COSMO solvation, due to computational limitations.

4.5.2 Polymerization

4.5.2.1 The monomer and dimer

The first reaction analyzed is dimerization (Table 6), where two monomers condense. Previously, in section 4.1.3.1, a description of this reaction was made, showing what elements in the modelling are necessary to obtain a realistic energy profile. Here, a more detailed analysis of the dimerization will be made and a comparison with other reactions (which will be shown later) will help us understand in relative terms the importance of this reaction.

The energies associated with several forms of the reaction, for both the gas and solvated cases are presented in Table 6. The first row concerns one of the most modelled reaction involving silicates, the neutral dimerization in the gas phase. The change of electronic energy at zero kelvin is -12.7 $kJmol^{-1}$ and -15 $kJmol^{-1}$ (including the zero point energy correction, ZPE), and the entropy change is almost negligible. As a comparison we calculated this energy reaction with the B3LYP/6-311++G(3df,3pd) method, resulting

Table 6 Free energy ($kJmol^{-1}$) change in the gas phase and in solution and other thermodynamical properties at 0, 298 and 450K, in the dimerization reaction. The first row reaction is M + M → D + H_2O. MNa and MNa_2 are the clusters M^-Na^+ and $M^{2-}Na_2^{2+}$, see Figure 44 and Figure 45. **Note "Sol." refers to COSMO solvation and "Exp. H_2O" is the cluster with explicit water molecules in COSMO solvation. These labels are used in all the tables of this chapter.**

		Dimerization						
		0K	298K			450K		
	Reactants	ΔE_0	ΔH	$T\Delta S$	ΔG	ΔH	$T\Delta S$	ΔG
Gas	M,M	-15	-11	1	-13	-11	3	-14
	MNa,M	-32	-29	-7	-23	-30	-10	-20
	MNa_2,M	-39	-36	-4	-32	-36	-7	-29
	MNa,MNa	-14	-11	-5	-6	-11	-8	-3
	M^-,M	-93	-91	-8	-83	-92	-14	-78
	M^{-2},M	-259	-257	-8	-249	-258	-13	-244
	M^-,M^-	248	248	-14	262	247	-22	270
Sol.	M,M	-9	-7	-5	-2	-7	-8	0
	MNa,M	-42	-36	-3	-32	-33	-1	-31
	MNa_2,M	-43	-41	-8	-33	-41	-13	-28
	MNa,MNa	-36	-27	-1	-26	-21	6	-27
	M^-,M	-43	-42	-9	-33	-42	-14	-28
	M^{-2},M	-74	-73	-14	-60	-74	-21	-53
	M^-,M^-	-13	-15	-18	3	-16	-28	13
Exp. H_2O	MNa,M	-24	-23	-15	-7	-23	-23	0
	MNa_2,M	-29	-27	-11	-16	-27	-17	-10
	MNa,MNa	-22	-21	-18	-3	-22	-27	6

in -17.8 $kJmol^{-1}$. These energies are comparable with that obtained by Catlow *et al.*[60], -11.7 $kJmol^{-1}$ (without ZPE). However, with a HF/6-31G** level of theory, Sauer[62] obtained -32.6 $kJmol^{-1}$, and Tossell[94] with the compound method G2[68] obtained -27.6 $kJmol^{-1}$ a significant difference. The free energy calculated here for this reaction is -14 $kJmol^{-1}$, so this suggests that it is feasible to form a dimer in the gas phase. This viability also increases five-fold with the presence of monomer$^-$ as a reactant, which confirms the role of OH^- (high pH) acting as a facilitator, as suggested before[58].

However, it should be noted that when solvation is included, the free energy of the reaction is slightly unfavourable (-2 $kJmol^{-1}$ at 298K and +0.4 $kJmol^{-1}$ at 450K) for neutral species, in contrast to reactions where charged species are considered. Similar trends are also observed for the condensation of larger oligomers. Our results, therefore,

highlight the role of pH in driving the initial polymerization processes to give these small oligomers. However, the reaction of two $Si(OH)_3O^-$ species is unfavourable, suggesting that stabilization of such species by cationic species (as confirmed in Table 6) or mechanisms for re-arrangement via proton transfer are also important. But it should also be noted that very high pH is not conducive to zeolite nucleation[12, 13, 129].

The two different dimerization reactions considered in the gas phase involving two charges give completely different results; if the charge is only in one of the reactants, (M^{2-} + M) the free energy is -247 $kJmol^{-1}$, but if the charge is shared among the reactants (M^- + M^-), it is +267 $kJmol^{-1}$. The contribution to the free energy in these reactions is mainly due to the change in electronic energy. The exothermicity of the first reaction is principally due to the higher acidity of the monomer than the dimer as an isolated species (see Table 3): the $dimer^{2-}$ is comparatively much more stable. Thus, two $monomer^-$ ions will not condense in the gas phase. However, the passivation effect of the counterion can reverse the effect as suggested by the slightly favourable free energy to form the dimer/Na_2 from two monomer/Na[xiv], as shown in Table 6.

The same reactions, analyzed above, but now including solvation are also shown in Table 6. Solvation has the same effect of reducing the change in the electronic energy substantially, as observed in the deprotonation energies (see Table 3). The most notable result is the slightly positive free energy for the neutral condensation at 450K compared to the slightly negative free energy change found at room temperature. This tendency is also observed for the more accurate model involving explicit water molecules and charged species (Table 6). In this case, the reaction of a monomer/Na and a monomer has a calculated free energy of -7 $kJmol^{-1}$ at 298K and 0 $kJmol^{-1}$ at 450K. Only when the double deprotonated species monomer/Na_2 is considered, does the reaction proceed at 450K. However, at very high pH (higher than the synthesis conditions) where most of the monomers will be deprotonated, then the most likely reaction to take place is the last shown in Table 6; the condensation of two monomer/Na clusters. This reaction is only marginally favourable at 298K (-3 $kJmol^{-1}$), but less favoured at 450K (+6 $kJmol^{-1}$). Thus, the dimerization results confirm the observation that at very high pH nucleation is unlikely to happen[12, 13, 129].

[xiv] In the text the monomer/Na refers to the cluster where the anionic monomer has the counterion Na^+, the same notation is used for the other clusters.

The more accurate results with explicit water molecules offer two interesting suggestions. First, dimerization in solution is favoured at 298K, but possibly not at 450K (bottom of Table 6), indicating the significance of the low temperature mixing step, *i.e.* important reactions take place only at low temperatures. We note that an "ageing" step at room temperature is often included in most synthesis, deliberately or not! Thus, an interesting (although difficult) experiment that our result suggests is as follows: pre-heat all the raw material and mix them at high temperatures, then different species should be present than the species resulting after mixing at room temperature, as our results show that some reactions will be prohibitive at high temperature. The second conclusion drawn from the explicit water results in the last section of Table 6 is that it is unfavourable for a dimer to form at high pH, unless the very reactive monomer/Na_2 species is stable and no other proton transfer between the silicates takes place first, which will form mostly monocharged species.

Thus, these results would suggest that neutral condensation at 298K would be energetically restricted. On the other hand, the dimerization will occur when one charge is involved in the reaction, again emphasizing the role of pH as a promoter of condensation reactions. The doubly charged monomer as a free species is highly prone to condense, and under all circumstances, gas phase, fully solvated, restricted solvation (as inside a gel phase), low or high temperature, will react with a monomer to produce a dimer. The monomer with double charge could be a key species in the condensation mechanism of clusters, as it will lead to a successful condensation. However, it is the single charged monomer that is more interesting, because it can be "tuned", depending on the conditions, to proceed into a successful condensation, *i.e.* the monomer$^-$ reacts easily at 298K but possibly not at 450K. Therefore, changing the temperature allows us to alter the result of a reaction.

Finally, if both monomers are charged, condensation will be limited. This situation could happen in a synthesis solution with an OH^-/Si ratio higher than 0.5 (i.e. high pH). If equilibrium conditions are reached, where most of the monomers are singly charged, dimerization is inhibited. This, could help to explain why very high pH solutions do not lead to zeolite formation[12, 13, 129].

The enthalpy change in the dimerization is exothermic under all conditions (with the single exception of the gas phase). This change is more exothermic when charged

species are considered than when neutral species react. The high pH contribution to the condensation is reflected directly in the higher exothermicity when the anionic silicates react. The final conclusion from the enthalpy results is: exothermicity in the dimerization shows a favourable tendency to form the Si-O-Si bond.

In addition to dimerization being thermodynamically favoured when the charged monomers are considered, there is a further mechanistic aspect favouring the reaction. In particular, the bare oxygen in the anionic monomer will certainly lead to a more direct attack on the silicon of a second (neutral) monomer, due to the favourable electrostatic attraction and possibly a more favourable geometric approach. Thus, we may expect, a lower reaction barrier for the dimerization involving charged species.

The entropy contribution to the free energy is almost negligible in the gas phase, but is more important in the COSMO solvation models. When explicit water molecules are used to model the solvation, the change in entropy is a significant contribution to the overall free energy change. These results show how important the environment is for the entropy: in a fully solvated state (clear solution) the entropy contribution to the free energy will be more significant than inside a gel or sol particle. However, as can be appreciated from Table 6, the entropic contribution to the free energy is always unfavourable, regardless of the conditions. The negative entropic contribution to the dimerization will be more important at high temperatures and as explained before, under certain conditions, could even inhibit the formation of the dimer. The reduction in the entropy of the system, with the reaction, could be due to the presence of the intramolecular H-bond of the dimer.

Dimer formation is critical not just in zeolite synthesis, but in the whole chemistry of silicates, simply because it is the first reaction in all condensations starting from the monomer. However, in this work, another key role of dimer formation is suggested. As discussed in the geometry analysis section (4.2.3). The dimer (as the 4-ring) leads to a more restricted number of possible clusters compared to those possible from monomers. In other words, condensing one monomer each time, almost every silicate structure is reachable and will probably lead to an amorphous material. However, every time a dimer condenses via both its ends, a 4-ring structure is the most likely structure to be formed. Thus, the dimer can lead to specific ring structures, whereas the monomer could form more oligomer-like structures. As a consequence, dimer formation is clearly a

necessary step in forming nucleation centres, which are more likely to give crystalline products.

4.5.2.2 The trimer and tetramer

We now consider the reaction of a dimer and a monomer to give the trimer. The main results for the different conditions are presented in Table 7. The condensation of two

Table 7 Free energy ($kJmol^{-1}$) change in the gas phase and in solution and other thermodynamical properties at 0, 298 and 450K, in the trimerization reaction. The first row reaction is $D + M \rightarrow Tr + H_2O$.

		Trimerization						
		0K	298K			450K		
	Reactants	ΔE_0	ΔH	$T\Delta S$	ΔG	ΔH	$T\Delta S$	ΔG
Gas	D,M	-19	-17	-15	-2	-17	-22	5
	D,MNa	-75	-72	-20	-52	-73	-31	-42
	DNa, M	-58	-54	-12	-42	-54	-18	-36
	D, MNa_2	-153	-150	-16	-134	-150	-25	-125
	DNa_2, M	-129	-125	-11	-115	-125	-15	-109
	DNa, MNa	-110	-106	-9	-97	-106	-13	-93
	D,M^-	-146	-147	-26	-121	-148	-41	-107
	D^-,M	-68	-67	-16	-51	-67	-25	-43
	D,M^{-2}	-375	-375	-24	-351	-377	-39	-338
	D^{-2},M	-132	-130	-15	-115	-130	-23	-108
	D^-,M^-	209	209	-20	230	209	-31	240
Sol.	D,M	-18	-15	-14	-1	-14	-20	6
	D,MNa	-66	-60	-14	-46	-57	-17	-40
	DNa, M	-33	-31	-15	-16	-31	-23	-8
	D,M^-	-67	-68	-25	-43	-69	-39	-30
	D^-,M	-32	-33	-20	-13	-34	-32	-2
	D,M^{-2}	-128	-127	-21	-106	-127	-33	-95
	D^{-2},M	-63	-60	-12	-48	-61	-19	-42
	D^-,M^-	-33	-33	-21	-12	-34	-33	-1
Exp. H_2O	D,MNa	-41	-38	-22	-16	-37	-33	-4
	DNa, M	-25	-22	-12	-10	-22	-17	-4
	D, MNa_2	-43	-39	-15	-24	-39	-23	-16
	DNa_2, M	-23	-19	-8	-10	-20	-14	-6
	DNa, MNa	-21	-17	-11	-6	-18	-18	-1

dimers will be analysed subsequently. The viability of trimerization in the gas phase increases with the charge involved in the reactions. Formation of a neutral trimer seems to be unlikely, but when one charge is involved, it is clearly feasible in the gas phase. With two charges, the free energy is largely negative, and the most exergonic reaction is when the monomer is carrying both charges. The dimer$^-$ and monomer$^-$ will not condense, not only because of the change in the free energy (ΔG = +240 kJmol^{-1}), but also there is a large electrostatic repulsion between the reactants; they are unlikely to approach in the gas phase.

The electrostatic repulsion will certainly be reduced by the presence of the counterions, *e.g.* Na^+, K^+, TPA^+, or whatever cationic species are present in the nucleation solution. The presence of cations will change the energy involved in the condensation completely, as illustrated in Table 7. In the gas phase, reaction of a monomer/Na and a dimer/Na is highly exothermic. In the same situation condensation of two monomer/Na has a small negative change in the energy (see Table 6) which shows the ability of the trimer/Na_2 to distribute the negative charge: a general and expected feature for larger silicate oligomers.

In solution, the trimerization follows the same behaviour as in the gas phase: the higher the charge the more feasible the reaction. However, the change in enthalpy (the principal component of the free energy), is reduced by almost a half, compared to the dimerization. Under nucleation conditions (high pH), the dimer is most likely to exist in solution as the dimer$^-$. As indicated in the Table 7 the only two reactions involving this cluster have a free energy of -2 and -1 kJmol^{-1} at 450K, indicating a low tendency to form a trimer. Even when Na^+ is present, this condensation shows a small change in free energy (-8 kJmol^{-1}). Only when the clusters dimer^{2-}, monomer^{2-}, or monomer/Na are reacting will the condensation become thermodynamically favoured in solution, which is a direct consequence of the high reactivity of double charged clusters.

The above analysis only considers the results at 450K. At the start of zeolite synthesis (298K) the reactions involving the dimer$^-$, with and without the cation are more feasible than at the elevated high temperature. However, the neutral conditions for the trimer condensation are less favourable, independently of the temperature or the solvation. This stresses once more, the key role played by the high pH, in producing the most reactive species for the nucleation of zeolites.

Trimerization in the gas phase and in solution has a negative change in entropy: double that of the dimerization reaction, which could be explained by the two strong H-bonds present in the trimer (see Figure 48), whereas in the dimer there is only one. The H-bonds impose restrictions on the geometry of the trimer, limiting the vibrational entropy and conformational change.

The formation of the trimer modelled with explicit water molecules confirms the tendency shown by the results of the COSMO solvation model (Table 7). The reaction proceeds more readily at 298K than at 450K, and the most favoured reaction is that involving the highly reactive monomer/Na_2. The results with explicit water molecules are the best representation of what happens in the fully solvated clusters. However, previous results with the COSMO solvation alone can be interpreted as an approximation to the processes taking place inside sol particles or in gel structures.

Thus, the condensation to form trimers is a reaction limited at high temperature unless high charges are involved and the cations do not have an important direct influence in the changes of energy. Thus, as a preliminary conclusion it could be considered that the formation of a trimer could be a limiting reaction (or certainly a slow process) in the nucleation process. Thus, we need to consider how large oligomers may form, if as suggested trimerization is unfavourable.

The next larger cluster that will form by polymerization is the tetramer, which could be formed either by the condensation of trimer and a monomer (see Table 8) or from two dimers (Table 9)[xv]. In the gas phase and in COSMO solvation, tetramerization energies follow a similar pattern to those of trimerization: when charged species are present, the reaction is much more likely to take place and the neutral condensation is the least favoured. Similarly, increasing the temperature decreases the free energy released in the condensations. However, there are some differences that should be mentioned.

The reactions producing a tetramer (Table 8) are in general more exothermic and exergonic, compared with the formation of trimer. The entropy change is also less pronounced. The formation of a tetramer is clearly very important, as it can lead directly to the formation of a 4-ring – the most prevalent cyclic structure in zeolite structures.

[xv] For some clusters like 4-, 5- and 6-Si linear clusters, we will show all the different ways in which they can be obtained, but always in a single condensation reaction, *i.e.* for example, the direct condensation of hexamer from monomer clusters is not analysed in this section, because is quite unlikely that five condensations will occur simultaneously.

Table 8 Free energy ($kJmol^{-1}$) change in the gas phase and in solution and other thermodynamical properties at 0, 298 and 450K, in the tetramerization reaction. The first row reaction is $Tr + M \rightarrow T + H_2O$.

		Tetramerization						
		0K	298K			450K		
	Reactants	ΔE_0	ΔH	$T\Delta S$	ΔG	ΔH	$T\Delta S$	ΔG
Gas	Tr,M	-25	-23	-13	-10	-23	-20	-3
	Tr,MNa	-82	-80	-14	-66	-80	-22	-59
	TrNa, M	-26	-24	-8	-16	-24	-13	-11
	Tr, MNa_2	-151	-150	-22	-128	-151	-35	-116
	$TrNa_2$, M	-17	-16	-20	4	-18	-32	15
	TrNa, MNa	-70	-69	-17	-51	-70	-27	-42
	Tr,M^-	-181	-181	-21	-160	-183	-34	-149
	Tr^-,M	-54	-51	-9	-41	-51	-15	-36
	Tr,M^{-2}	-474	-475	-21	-453	-477	-35	-442
	Tr^{-2},M	-118	-116	-12	-104	-117	-19	-98
	Tr^-,M^-	160	160	-16	176	159	-25	185
Sol. H_2O	Tr,M	-10	-8	-14	5	-9	-21	12
	Tr,MNa	-55	-50	-14	-36	-48	-19	-30
	TrNa, M	-7	-5	-14	9	-5	-21	16
	Tr,M^-	-74	-73	-15	-58	-75	-24	-50
	Tr^-,M	-25	-20	-4	-16	-19	-5	-15
	Tr,M^{-2}	-156	-156	-19	-137	-158	-30	-128
	Tr^{-2},M	-46	-44	-11	-33	-44	-17	-27
	Tr^-,M^-	-47	-44	-12	-32	-44	-18	-26
	Tr,MNa	-45	-42	-17	-25	-42	-26	-16
	TrNa, M	-23	-19	-8	-10	-18	-12	-6

Although a 4-ring can form from larger oligomers, the tetramer is the simplest structure, which would directly form this building unit.

The tetramer is expected to be a much more stable structure than the trimer, because the former has five H-bonds, compared with two in the latter. However, the increase in the energy released to form a tetramer is not in accordance with the expected increase from a simple count of H-bonds (see Table 8). However, the condensation of a tetramer from a monomer and trimer is always exothermic under all the conditions studied (Table 8). Solvation stabilizes the anionic species, which decreases the energy released during the

condensation. However, for the reactants where both are anionic, it is the inclusion of solvation that results in favourable condensation energetics.

Again, the negative change in the entropy can be attributed to the higher number of H-bonds in the tetramer, "locking" in some way, the structure. The change in entropy is not significant at 298K, but is more significant at 450K. Indeed, under some circumstances the reaction is unfavourable at the higher temperature; for example, the condensation of trimer/Na and monomer.

Recall that for trimer formation at 450K, it was found that, unless high charges are present, the reaction is unfavourable. However, in the formation of a tetramer this is not always true: when explicit water is included, a reasonable negative free energy is calculated for the formation of the tetramer from trimer/Na (with neutral monomer) or monomer/Na (with neutral trimer).

These latter results allow us to speculate on the role of "aging". Low temperatures favour the formation of the dimer and consequently enable the formation of higher oligomers. Then, at high temperatures, the formation of tetramers and possibly larger clusters is more probable than the condensation of very small clusters, which were previously formed at lower temperatures.

Another important observation in the case of trimer and monomer condensation (Table 8), is that the electronic energy (and consequently the free energy) released is greater when the carrier of the charge is the monomer, rather than the trimer. The latter statement applies to gas and solution results (including with explicit water) and for all the temperatures analysed. The same conclusion can be obtained from the condensation of a monomer and dimer (Table 7). Another way to interpret the observation is that the charged monomer in both cases is the most reactive of the species. Of course, we recall how easily the monomer may be deprotonated.

However, there are serious implications of the latter finding. As the condensation reactions take place in the pre-nucleation, the majority of the cluster will be charged, because from the beginning condensations of neutral species are much less favourable (or perhaps completely inhibited). Thus, the larger charged clusters will condense with the monomer (possibly neutral, because of the limited amount of OH^- per Si, Figure 43), although, this reaction is in fact the least favoured. We can conclude: that the high pH makes the condensation reactions possible (through anionic silicates), but that these

reactions take place via a route which is not the lowest energy pathway. Nevertheless, a general conclusion is that more exothermic reactions will be those where the charge is principally on the smaller oligomers.

The tetramer can also be formed from two dimers (Table 9). Indeed, given the above discussion of the difficulty in forming trimers (and the ease of dimerization), this is perhaps the more likely route, and it is important to verify our hypothesis that the dimer provides a more direct route to ring structures (see section 4.2.3). We find that under all the conditions studied, the formation of a tetramer from two dimers is exothermic, and moreover, have very similar free energies to the reaction of the trimer and monomer.

However, a significant difference is the entropic contribution, which has a more important negative contribution to the free energy when two dimers condense (compared with trimer + monomer). At 450K, the entropy change is so significant, that the condensation of neutral species is probably completely inhibited. The larger negative change in entropy from the condensation of two dimers is attributed to the less

Table 9 Free energy ($kJmol^{-1}$) change in the gas phase and in solution and other thermodynamical properties at 0, 298 and 450K, in the tetramerization reaction (via dimer). The first row reaction is $D + D \rightarrow T + H_2O$.

		Tetramerization (via dimer)						
		0K	298K			450K		
	Reactants	ΔE_0	ΔH	$T\Delta S$	ΔG	ΔH	$T\Delta S$	ΔG
Gas	D,D	-29	-28	-29	1	-29	-45	16
	DNa,D	-69	-67	-22	-45	-67	-33	-34
	DNa_2,D	-131	-130	-32	-98	-131	-50	-81
	DNa,DNa	-95	-93	-23	-70	-94	-35	-59
	D^-,D	-107	-107	-27	-80	-108	-42	-66
	D^{-2},D	-235	-234	-28	-207	-236	-44	-192
	D^-,D^-	184	184	-23	208	183	-37	220
H_2O Sol.	D,D	-19	-16	-23	6	-15	-33	18
	DNa,D	-31	-29	-24	-5	-29	-37	8
	D^-,D	-49	-46	-19	-27	-46	-29	-17
	D^{-2},D	-100	-97	-19	-79	-98	-29	-69
	D^-,D^-	-35	-35	-23	-12	-36	-36	0
	DNa,D	-39	-34	-16	-19	-33	-22	-11

rigid structure of the dimer compared with the trimer, due to the presence of H-bonds.

The results with explicit water for tetramer formation from two dimers show a favourable free energy for condensation at 298K and 450K. Thus, as an extension we would expect the condensation of a dimer onto other larger oligomers. Therefore, the hypothesis formulated above (see section 4.2.3) is supported: dimer addition is thermodynamically as well as statistically favoured.

Thus, the calculated condensation energies show how dimers, trimers and larger oligomers can be readily formed from monomeric species. Again, it is emphasised, that pH has a critical role. Note that condensation of neutral species is not favoured beyond the formation of the dimer. Thus, at low pH, where anionic species are less prevalent, polymerization is inhibited. Indeed, it is also noted that, for the trimerization reaction (and for the formation of higher oligomers) it is the favourable change in energy that drives the reaction, overcoming the adverse negative change in the entropy, which is more significant at higher temperatures.

4.5.3 Cyclization

We now consider the formation of cyclic species that are the principal constituents of zeolitic frameworks. In the different zeolite topologies there will be present one or more silicates rings, 4-, 5-, 6-, 8-, 10- and 12- rings being the most predominant. A silicate ring could be formed either by the direct condensation of a linear chain or by a condensation of larger clusters. At first glance, if the latter is more likely due to the entropy argument, it is important to know how and when the rings (observed in the final crystalline structure) are formed.

An analysis of internal condensation reactions giving a single ring structure is now presented. At the same time a comparison of the possible routes from a given cluster is given. For example, from the tetramer we consider the formation of the pentamer or its internal condensation to produce a 4-ring.

4.5.3.1 Three-membered ring

Once a trimer forms, it can of course grow further. However, it can also condense internally to form the 3 membered-ring. Since the lowest energy conformation for the trimer is almost cyclic (Figure 16 page 54), it is suggestive that an internal condensation may be possible (Table 10). Indeed, with the exception of the condensation of the

Table 10 Free energy ($kJmol^{-1}$) change in the gas phase and in solution and other thermodynamical properties at 0, 298 and 450K, in the 3-ring cyclization reaction. The first row reaction is $Tr \rightarrow 3r + H_2O$

		3ring Cyclization						
		0K	298K			450K		
	Reactants	ΔE_0	ΔH	$T\Delta S$	ΔG	ΔH	$T\Delta S$	ΔG
Gas	Tr	27	31	45	-14	31	68	-37
	TrNa	52	56	43	13	55	64	-9
	$TrNa_2$	71	73	37	36	73	56	17
	Tr^-	67	70	43	27	69	63	6
	Tr^{-2}	71	74	43	31	73	64	9
	Tr^{-3}	61	66	45	20	65	68	-3
	Tr^{-4}	136	137	32	105	135	46	89
Sol. H_2O	Tr	10	16	51	-35	15	77	-61
	TrNa	28	32	44	-12	31	66	-34
	Tr^-	43	48	46	2	48	70	-21
	Tr^{-2}	42	45	45	0	45	67	-22
	Tr^{-3}	-3	1	43	-42	0	64	-64
	Tr^{-4}	1	3	37	-34	2	55	-53
	TrNa	15	18	43	-25	17	64	-47
	$TrNa_2$	5	3	26	-23	0	36	-36

charged trimer in the gas phase, all conditions considered show a favourable formation of a 3-ring, wholly consistent with NMR experiments where this cluster is observed[9]. However, the seeming ease of formation of the 3-ring raises the question of the role of this species in nucleation and subsequent growth processes, since these rings are not found (with the sole exception of ZSM-18 – and here only as an aluminosilicate[116]) in crystalline zeolites.

The energetics of direct condensation of the 3-ring from the trimer in the gas phase and in solvation is shown in Table 10. The change in electronic energy is, in almost all the cases endothermic, which is not favourable to the reaction. The endothermicity of the 3-ring cyclization could be explained by the geometry: the 3-ring being strained. It is important to note that the 3-ring is a structure with six atoms forming its ring: three silicon and three oxygen. Whilst the optimized trimer has a conformation that suggests ring formation (see Figure 16), the closed ring cluster is more strained (Figure 15) and has no intramolecular H-bonds in contrast to the open trimer, which has two H-bonds. The endothermicity of the formation of the 3-ring is more evident in the gas phase; solvation reduces the positive change in the enthalpy.

The changes in enthalpy for most of the reactions become less favourable as the charge (pH) decreases, except for the trimer^{3-} and trimer^{4-}, where it decreases drastically. This result contrasts to those for linear polymerization, where the feasibility of the reaction increases with higher charges. One reason for this behaviour is the loss of H-bonds on cyclization, since in the trimer the H-bonds could stabilize the charge in the anionic form. The cation has some effect in stabilizing the 3-ring effectively, as shown by the case where the Na^+ cation is present in solution, where the condensation energy is lower than when it is not included. Furthermore, such a change in the overall enthalpy is also observed when the same reactions are considered in the gas phase.

The entropy change for the 3-ring cyclization is largely positive, which drives the condensation in solution. The entropy contribution ($T\Delta S$) is fairly constant, ranging roughly from 30 to 40 kJmol^{-1} at 298K and 60 to 70 kJmol^{-1} at 450K, for both the gas phase and the solution reactions. This trend in the entropy change is again in contrast to that observed for the linear polymerizations. At high temperature, the entropy change is more negative for the linear condensations, while for ring cyclizations the entropy is more positive. Certainly, changes in temperature could lead to significant changes in the relative distribution of ring and oligomer structures. For example, at 298K, 3-ring formation is unfavoured in solution when single and double charges are considered, but at high temperature, these reactions are feasible. Thus, at low temperature, the formation of small oligomers is favoured, while at high temperature the 3-ring condensation will be comparatively more feasible. The entropy changes positively with the reaction principally because the internal condensation reduces the number of particles.

The free energy indicates that the formation of the 3-ring is most favoured in the gas phase when neutral species react. However, formation of the neutral trimer is not favoured in the gas phase (see Table 7); hence, the reaction is unlikely to occur regardless of the thermodynamics. In solution, the free energy is negative in all the reactions; however, the trimer$^-$ and trimer^{2-} are the dominant solution trimeric species, so, the 3-ring$^-$ and 3-ring^{2-} will be the expected species in solution, but again mainly favoured at higher temperatures.

3-ring cyclization is evidently favoured (Table 10) in the models involving explicit water molecules, both, at 298 and 450K. Indeed, with the exception of the neutral condensation, which is very unlikely to happen (as discussed above); the condensations

with explicit water are more exergonic. This result can be tentatively interpreted as suggesting that 3-ring formation is more likely under conditions of high hydration (*i.e.* in the solution phase) than in the sol or gel, where the water content is limited.

From the trimer, two competitive reactions can occur: 3-ring cyclization and tetramerization. Under COSMO solvation, tetramerization seems more favourable, while the models with explicit water show a preferential 3-ring cyclization. Furthermore, the cyclization involves only one reactant, while the polymerization requires the meeting of two particles with the correct orientation, so the kinetics will have a very important role here. This, could explain why the 3-ring species are observed in solution, although the fate of this cluster is not clear, as it is not observed in final complete structures. However, our model suggests that in highly concentrated gels will again form tetramers and we note again that the experiments where 3-rings are observed, are typically with clear solutions *i.e.* high dilution.

To conclude, in the 3-ring condensation, there are cooperative effects, which drive the cyclization, the entropy contributing positively to the free energy and the solvation lowering the enthalpy from the gas phase sufficiently for the cyclization to happen.

4.5.3.2 The pentamer and 4-ring

While both 3- and 4-ring clusters are found in solution[3], the 4-ring is the only species in zeolitic frameworks[19]. How can this fact be interpreted in the light of the above calculations, which suggest that 3-ring may well be formed, certainly in dilute systems, but it is not in a zeolite structure? One option is that the trimer is bypassed by the direct condensation of tetramer from two dimers (which we have already suggested will be formed rapidly). However, the answer is not so simple and involves the analysis of the relative energetics of all these reactions. Thus, we must first consider the further polymerization of tetramers, giving pentamers; a reaction competing with the 4-ring closure.

The pentamer (5-member silicon linear oligomer) may be produced via two main routes: by condensation of a tetramer and monomer (Table 11) and by the condensation of a dimer and a trimer (Table 12). For both routes, in the gas phase, the change in enthalpy exhibits the same characteristics as previous linear polymerizations studied so far: the energy released is larger with increasing charge.

However, in solution an interesting trend can be seen for the two pentamer condensations (Table 11 and Table 12). The most exothermic reaction is that where the monomer has the charge, with the enthalpy decreasing according to the following trend: monomer > dimer > trimer > tetramer; *i.e.* the highest enthalpy released is for the reaction tetramer + monomer^{2-}, while the lowest is for the reaction tetramer^{2-} + monomer. As a conclusion from these results, we suggest a higher reactivity for a reaction when the charge is on the smaller cluster.

The change of enthalpy in both routes, forming the pentamer, contributes favourably to the free energy, with the polymerization from the dimer being slightly less favoured. Clearly, the entropy change is unfavourable, because during the condensation reactions, there is an increase in order. For example in the case of the reaction of neutral trimer and dimer, two additional H-bonds are found. As discussed earlier, the change in entropy (in this case negative) has a more significant contribution to the free energy at higher temperatures.

Table 11 Free energy (kJmol^{-1}) change in the gas phase and in solution and other thermodynamical properties at 0, 298 and 450K, in the pentamerization reaction. The first row reaction is T + M → P + H_2O.

		Pentamerization						
		0K	298K			450K		
	Reactants	ΔE_0	ΔH	$T\Delta S$	ΔG	ΔH	$T\Delta S$	ΔG
Gas	T,M	-25	-22	-12	-10	-22	-17	-4
	T,MNa	-78	-78	-20	-57	-80	-33	-47
	TNa, M	-21	-21	-19	-2	-23	-31	9
	T,M$^-$	-220	-223	-26	-197	-226	-43	-183
	T$^-$,M	-65	-65	-18	-47	-67	-29	-37
	T,M^{-2}	-552	-552	-16	-535	-554	-27	-527
	T^{-2},M	-103	-100	-8	-92	-100	-12	-88
	T$^-$,M$^-$	110	111	-14	126	110	-23	133
Sol.	T,M	-18	-16	-12	-4	-17	-20	3
	T,MNa	-80	-73	-8	-65	-71	-9	-61
	TNa, M	-35	-31	-8	-23	-31	-12	-19
	T,M$^-$	-94	-92	-11	-81	-93	-19	-74
	T$^-$,M	-30	-27	-10	-17	-27	-15	-12
	T,M^{-2}	-177	-176	-15	-161	-177	-24	-153
	T^{-2},M	-31	-28	-10	-18	-28	-15	-13
	T$^-$,M$^-$	-52	-52	-18	-34	-53	-28	-25

The expected reactant species in solution leading to pentamer are tetramer^{-}, tetramer^{2-} and for the other route, the dimer^{-} is most likely, results that are given in Table 12. Thus, with three possible reaction pathways (one of them ΔG = -25 kJmol^{-1} at 450K), pentamer formation is more likely from a tetramer and a monomer. Thus, as before, the growth of oligomers is more feasible by monomeric addition, again emphasizing the high reactivity of the monomer.

Previously, we noted that the condensation of two small charged clusters is unfavourable. However, the delocalisation of the charge over larger structures, such as the pentamer^{2-}, makes such reactions more likely. The H-bonds present in the pentamer also stabilize this excess charge.

Table 12 Free energy (kJmol^{-1}) change in the gas phase and in solution and other thermodynamical properties at 0, 298 and 450K, in the pentamerization reaction (via dimer). The first row reaction is Tr + D → P + H_2O.

		Pentamerization (via dimer)						
		0K	298K			450K		
	Reactants	ΔE_0	ΔH	$T\Delta S$	ΔG	ΔH	$T\Delta S$	ΔG
Gas	Tr,D	-35	-33	-26	-7	-34	-40	6
	Tr,DNa	-71	-71	-27	-44	-73	-43	-30
	TrNa, D	-33	-33	-29	-5	-36	-46	11
	Tr,D^{-}	-153	-155	-30	-124	-158	-49	-108
	Tr^{-},D	-103	-104	-29	-75	-107	-47	-60
	Tr,D^{-2}	-319	-318	-21	-297	-319	-34	-285
	Tr^{-2},D	-206	-205	-21	-184	-206	-33	-173
	Tr^{-},D^{-}	149	152	-15	167	151	-24	175
Sol.	Tr,D	-20	-18	-21	4	-18	-33	15
	Tr,DNa	-48	-46	-19	-27	-46	-29	-18
	TrNa, D	-33	-29	-17	-13	-29	-25	-4
	Tr,D^{-}	-61	-58	-16	-43	-59	-25	-34
	Tr^{-},D	-46	-40	-9	-31	-39	-12	-27
	Tr,D^{-2}	-113	-111	-15	-96	-112	-24	-88
	Tr^{-2},D	-69	-65	-16	-49	-65	-24	-41
	Tr^{-},D^{-}	-34	-30	-13	-18	-30	-18	-12

4.5.3.2.1 The 4-ring

As mentioned above, although 3-rings are present in solution and their stability is confirmed here, their role in zeolite formation is unclear. Perhaps less in doubt is the role of the 4-ring, which is found in solution but is also present in many zeolites (in 61 zeolite frameworks). We now consider the formation of the 4-ring and Table 13 summarizes the self-condensation of the tetramer to give 4-ring species. This internal condensation shares some characteristics with the 3-ring cyclization. The change in enthalpy is positive in all the reactions that produce the 4-ring, and becomes even less favoured with increasing anionic charge, both in solution and in the gas phase. However, the change of entropy shows largely positive values, and is therefore (as in the case of 3-ring formation) the driving force in producing the 4-ring.

In the gas phase, the more stable (and hence prevalent) reactant is the tetramer$^-$ species (see above) and in solution tetramer$^-$ and tetramer^{2-}. We find that the free energy released when these oligomeric tetramers internally condense is indeed, strongly

Table 13 Free energy (kJmol^{-1}) change in the gas phase and in solution and other thermodynamical properties at 0, 298 and 450K, in the 4-ring cyclization reaction. The first row reaction is T → 4r + H_2O.

		4ring Cyclization						
		0K	298K			450K		
	Reactants	ΔE_0	ΔH	$T\Delta S$	ΔG	ΔH	$T\Delta S$	ΔG
Gas	T	22	26	56	-31	24	83	-59
	TNa	31	34	37	-3	33	55	-22
	TNa_2	3	6	40	-34	5	60	-55
	T^-	36	39	42	-3	38	62	-25
	T^{-2}	56	60	46	14	60	69	-10
	T^{-3}	86	90	47	44	90	70	20
	T^{-4}	127	132	40	91	132	61	71
Sol.	T	12	12	40	-28	8	55	-48
	TNa	14	16	38	-22	14	55	-41
	T^-	16	19	42	-23	18	62	-44
	T^{-2}	28	32	46	-14	32	69	-37
	T^{-3}	27	32	46	-14	33	70	-37
	T^{-4}	24	29	47	-17	29	70	-41
H_2O	TNa	24	27	43	-17	26	64	-38
	TNa_2	29	33	45	-12	33	69	-35

favoured when solvation is included. Whilst 4-ring formation in the gas phase is thermodynamically feasible, the cyclization is made more favourable by solvation.

In Table 13, the 4-ring cyclization for the monocharged tetramer in COSMO solvation (TNa and T^-) and with explicit water, have the same energetics. The same is observed for the double charged tetramer in solvation (T^{2-}) and with explicit water. This result suggests that the 4-ring may cyclize independently of the cation present or that the cation will have little effect on this process. A possible reason for this behaviour is that the internal network of H-bonds effectively stabilizes the excess negative charge in the cluster.

Comparing the free energies for the pentamerization (-12 and -25 $kJmol^{-1}$) with those for the 4-ring cyclization (around -40 $kJmol^{-1}$), the formation of a ring appears to be considerably more favoured than further polymerization. This tendency, to form a ring rather than continue with the polymerization, is a fundamental step which favours zeolite nucleation. We can consider this favourable formation of the 4-ring as key in understanding zeolite nucleation, simply because the 4-ring is one of the commonest rings found in their structure.

The thermodynamics of formation of the 4-ring is to some extent more favourable than that for the 3-ring (Table 10). Tetramer formation is also a favoured process. Therefore, even though the 3-ring is present, the 4-ring could dominate. However, we must also considerate the fate of the 3-ring formed (see section 4.5.4).

The small ring structures studied so far can also be formed from larger oligomers that internally condense to form these rings. For example, a pentamer can condense internally to produce either a 3-ring with a dangling dimer, or can condense to produce a 4-ring with a dangling monomer. However, before analysing these other routes, larger oligomers and ring clusters will be considered.

4.5.3.3 The hexamer and 5-ring

The pentamer can condense with a further monomer, to produce the hexamer. However, the pentamer may also internally condense leading to the formation of a 5-ring that is present in some zeolite frameworks. Similarly, the hexamer can be formed by a direct condensation from smaller clusters such as the trimer and tetramer.

In this thesis the hexamer is the largest linear silicate studied, because under zeolite synthesis conditions there is no evidence of very large isolated oligomeric structures[3]. Moreover, the theoretical results shown so far reveals a strong tendency to condense from linear oligomers to ring structures. There are also technical difficulties with calculations on larger linear oligomers: as the size of the linear cluster increases, the number of local minima increases hugely. The great flexibility exhibited by these structures make it difficult to analyse them (with confidence) with the approach followed in this thesis.

The energies associated with hexamerization from the pentamer are given in Table 14, from the tetramer in Table 15 and from the trimer in Table 16. In each of the different paths to form the hexamer, we again find similar trends to those found in the previous polymerizations considered, namely: the increase of charge (pH) increases the enthalpy released in the reaction; the entropy change does not favour the reaction and in the gas phase the free energy changes are larger than in solution.

Charged pentamers, tetramers and trimers are more likely to occur in solution as shown earlier. With these clusters, hexamer formation through the pentamer is associated with

Table 14 Free energy ($kJmol^{-1}$) change in the gas phase and in solution and other thermodynamical properties at 450K, in the hexamerization reaction. The reaction in the first row is $P + M \rightarrow H + H_2O$.

		Hexamerization						
		0K	298K			450K		
	Reactants	ΔE_0	ΔH	$T\Delta S$	ΔG	ΔH	$T\Delta S$	ΔG
Gas	P,M	-36	-33	-9	-23	-33	-14	-19
	P,M^-	-225	-224	-15	-209	-226	-25	-201
	P^-,M	-29	-23	-1	-22	-21	1	-22
	P,M^{-2}	-634	-634	-18	-616	-637	-30	-607
	P^{-2},M	-106	-104	-13	-91	-105	-20	-84
	P^-,M^-	68	72	-9	81	72	-14	86
Sol.	P,M	-14	-8	-2	-6	-7	-2	-5
	P,M^-	-103	-102	-17	-85	-102	-26	-76
	P^-,M	-27	-26	-18	-8	-26	-27	1
	P,M^{-2}	-217	-215	-12	-203	-216	-20	-196
	P^{-2},M	-58	-55	-10	-45	-56	-15	-40
	P^-,M^-	-81	-80	-18	-63	-81	-28	-53

a free energy change of -40 kJmol^{-1} and -53 kJmol^{-1}, where from the tetramer ΔG changes by -37 kJmol^{-1} and from the trimer; by -50 kJmol^{-1}, respectively, when the reactions are at 450K.

Table 15 Free energy (kJmol^{-1}) change in the gas phase and in solution and other thermodynamical properties at 450K, in the hexamerization reaction (via tetramer). The first row reaction is T + D → H + H_2O.

		Hexamerization (via tetramer)						
		0K	298K			450K		
	Reactants	ΔE_0	ΔH	TΔS	ΔG	ΔH	TΔS	ΔG
Gas	T,D	-46	-43	-22	-21	-44	-34	-9
	T,D^-	-157	-155	-18	-137	-156	-29	-127
	T^-,D	-79	-76	-20	-56	-77	-31	-46
	T,D^{-2}	-400	-399	-21	-378	-401	-34	-367
	T^{-2},D	-195	-192	-22	-170	-193	-35	-159
	T^-,D^-	96	98	-19	117	98	-29	127
Sol.	T,D	-24	-18	-10	-8	-16	-14	-3
	T,D^-	-78	-76	-20	-56	-77	-31	-46
	T^-,D	-48	-46	-23	-23	-46	-35	-11
	T,D^{-2}	-162	-158	-11	-146	-159	-18	-140
	T^{-2},D	-81	-76	-15	-61	-76	-22	-54
	T^-,D^-	-67	-65	-18	-47	-66	-29	-37

Table 16 Free energy (kJmol^{-1}) change in the gas phase and in solution and other thermodynamical properties at 450K, in the hexamerization reaction (via trimer). The first row reaction is Tr + Tr → H + H_2O.

		Hexamerization (via trimer)						
		0K	298K			450K		
	Reactants	ΔE_0	ΔH	TΔS	ΔG	ΔH	TΔS	ΔG
Gas	Tr,Tr	-52	-50	-21	-29	-50	-32	-18
	Tr^-,Tr	-114	-111	-15	-96	-111	-24	-88
	Tr^{-2},Tr	-294	-292	-19	-272	-294	-31	-262
	Tr^-,Tr^-	111	115	-12	127	114	-19	133
Sol.	Tr,Tr	-16	-11	-10	-1	-11	-15	4
	Tr^-,Tr	-56	-52	-14	-38	-51	-20	-31
	Tr^{-2},Tr	-109	-106	-13	-93	-106	-20	-86
	Tr^-,Tr^-	-61	-53	-3	-51	-51	-1	-50

These condensations producing the hexamer show a similar behaviour to those of smaller oligomers considered above. However, an important characteristic exhibited by large oligomeric cluster is the possibility of the multiple pathways leading to the same product. For example, in the case of the hexamer, there are three different routes (analysed here) and larger linear clusters will exhibit even more routes. Most of the reactions that produce a hexamer from smaller clusters seem feasible. As a result, the hexamer should be one of the species present during nucleation. However, they are not detected in NMR experiments[3]. One possible reason is that they are short-lived species, which react easily to form other species. Indeed, the hexamer can condense internally in a single step to produce ring structures including the 6-ring and smaller 3-, 4-, and 5-ring structures with dangling monomers or dimers. Some of these ring structures are indeed observed in solution. Consequently, the hexamer may form easily but only be present in low concentrations due to rapid internal condensations of further reactions. Furthermore, as smaller rings are favoured, the population of oligomers which will form the hexamer may be relatively low.

The internal cyclization of the pentamer leading to the 5-ring is summarized in Table 17. The enthalpy change in solution is lower than those calculated for the 3- and 4-ring

Table 17 Free energy ($kJmol^{-1}$) change in the gas phase and in solution and other thermodynamical properties at 450K, in the 5-ring cyclization reaction. The first row reaction is $P \rightarrow 5r + H_2O$.

		5ring Cyclization						
		0K	298K			450K		
	Reactants	ΔE_0	ΔH	$T\Delta S$	ΔG	ΔH	$T\Delta S$	ΔG
Gas	P	23	29	53	-24	29	80	-51
	P^-	40	46	48	-2	47	74	-27
	P^{-2}	32	34	38	-4	32	55	-23
	P^{-3}	101	104	39	64	103	59	44
	P^{-4}	106	110	36	73	109	55	55
Sol.	P	5	12	51	-39	13	77	-65
	P^-	6	9	41	-32	9	62	-53
	P^{-2}	7	2	27	-25	-7	30	-37
	P^{-3}	45	48	40	7	47	60	-13
	P^{-4}	4	10	48	-38	11	73	-63

condensation, whereas the entropy change is roughly the same. The rings more likely to be present in solution, as a result of the availability of the reactants, are the 5-ring^{-} and 5-ring^{2-} (Table 17).

The favourable formation free energy of the 5-ring in solution again raise the question of its role in the nucleation, because some NMR experiments do not show the presence of this cluster[3], despite the fact that an important number of zeolitic frameworks (18) contain 5-rings. So, for the zeolites containing 5-rings, when and where are the 5-rings being formed? Possibly, the 5-ring is not detected in solution because it is in another phase as gel or sol. Another possibility is that the 5-ring could be a short-lived species in solution, which will condense rapidly to other clusters, for example after an internal condensation the 5-ring can produce a 4-ring joined with a 3-ring (4-three-ring, see Figure 56 "c"), which is observed in solution[3]. In a later stage of the nucleation, the 4-three-ring cluster could open to re-form the 5-ring. Furthermore, it is important to point out the high similarity found in the 5-ring optimized structure with the 5-ring found in the MFI zeolite structure (see Figure 51 and section 4.2.1.5). This shows that the 5-ring reaches its final conformation in the early stages of the nucleation.

The hexamer produced from the pentamer competes with the cyclization reaction to form a 5-ring. The two likely reactions forming the 5-ring, have free energy changes of -53 and -55 kJmol^{-1}, which are comparable with the -40 and -53 kJmol^{-1} found for the hexamerization from the pentamer. Therefore, 5-ring cyclization is almost as favoured as the hexamerization.

A full analysis of the 5-ring will be continued later (section 4.5.6), together with its internal condensation. We now concentrate on the analysis of the 6-ring structure.

4.5.3.4 The 6-ring

The 6-ring can result from the internal condensation of the linear hexamer; the energies related with this condensation are shown in the Table 18. The enthalpy does not favour this cyclization either in the gas phase or in solution (except for the hexamer^{4-}). This is a surprising result both because the 6-ring has six strong internal H-bonds in a ring above the plane formed by the silicon atoms (see Figure 49) and because of the size (12 atoms) this ring should be more flexible than the smaller cyclic clusters. Nevertheless, our results show that in all but one case the change in enthalpy on 6-ring closure will be negative. However, the topology of zeolites implies that the formation of this ring

Table 18 Free energy ($kJmol^{-1}$) change in the gas phase and in solution and other thermodynamical properties at 450K, of the 6-ring cyclization reaction. The first row reaction is linear hexamer (H) → 6r + H_2O.

		6ring Cyclization						
		0K	298K			450K		
	Reactants	ΔE_0	ΔH	$T\Delta S$	ΔG	ΔH	$T\Delta S$	ΔG
Gas	H	32	35	48	-13	34	72	-38
	H^-	55	57	43	14	56	64	-8
	H^{-2}	68	71	42	29	70	63	8
	H^{-3}	43	45	42	3	44	62	-18
	H^{-4}	38	42	44	-2	41	65	-25
Sol.	H	11	11	34	-23	7	47	-40
	H^-	45	48	45	3	46	66	-20
	H^{-2}	50	49	36	14	46	50	-4
	H^{-3}	22	26	48	-22	27	74	-47
	H^{-4}	-6	-6	39	-45	-10	54	-63

should be very widespread. Then, alternative routes for the formation of this important cluster should be analysed.

The change in entropy has similar values to those calculated in the previous cyclization and is again the favourable driving force to form this ring. The hexamerization reactions suggest that the main species in solvation will be the hexamer^{2-}. However, cyclization of this species is only marginally exergonic (Table 18). This result suggests that the formation of the 6-ring, is in some conditions unfavourable from the hexamer, and possibly the 6-ring will form by other routes, resulting in a low solution phase population of this species. Other routes to form the 6-ring could be, for example, the condensation of smaller rings such as the 4-ring, producing a bigger cluster that includes the 6-ring (see section 4.5.6). We also note that NMR measurements do not detect the 6-ring in solution[3].

The hexamer, as discussed previously, could condense internally into different ring structures, smaller than the 6-ring. Therefore, the direct formation of a 6-ring from a hexamer has several competing reactions, which could result in a low probability for 6-ring formation. In contrast, when 4-rings, condense in three steps to produce the double 6-ring (Figure 64), the rigid (compared with linear oligomers) nature of the 4-ring, reduces enormously the possible competing reactions, and provides a possible

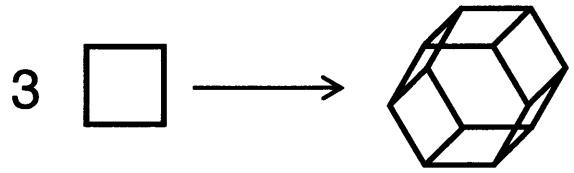

Figure 64 The formation of a double-6-ring from 4-rings through eight condensations.

route to 6-ring containing units. This reasoning is similar to that used earlier to postulate how 4-ring-like structures are most readily formed from the dimer (see section 4.2.3).

4.5.3.5 The role of pH

From these initial calculations, we can draw a number of conclusions and inferences. Firstly, there is a good agreement between the overall energetics of the processes considered and the experimental observations of small oligomers in solution. There is also a pH dependence for polymerization and the formation of small rings. Thus, it can be concluded, tentatively, that the methods selected, whereby solvation is included (albeit as a continuum) and pH is treated by considering anionic silicate species, gives a reasonable description of the system. However, the inclusion of explicit water to describe the mechanism of condensation and the solvation of counter ions such as Na^+, had proved to be necessary for the accurate reproduction of the chemistry of silicates in solution (see section 4.1.3.1). Furthermore, the formation of cyclic fragments is clearly favoured (at "high pH"), in agreement with experiment and with the expectation of the formation of zeolite-like nucleation species. It is therefore, unlikely that larger (non-cyclic) oligomers play a significant role in either nucleation or crystal growth. Hence, growth is much more likely to occur via condensation of relatively small units, particularly those that lead to "closed" rings, in either nucleation species or in subsequent surface growth. Our analysis suggests that units formed by dimer addition will be most strongly favoured. It is noted that there is clear evidence that surfaces with complete (small) rings are prevalent from both HRTEM studies and computational models[65]. Large rings are less likely to be formed from free solution species – although bridged species remain to be considered – and will thus be produced from the condensation of smaller units.

If such cyclic units grow further and form credible nucleation centres, we must now consider the further addition of small silicates (such as the monomer), as well as their

internal cyclization to form fused ring clusters. We must also consider the formation of small cages.

4.5.4 Monomer addition to ring structures

An important aspect, in the nucleation of zeolites, is the addition of oligomers to ring structures (see Figure 65), as it is very probable that the formation of small nuclei will involve this step. Ring and linear oligomer condensation will now be studied with the addition of one and two monomers to the 3- and 4-ring, as exemplar cases.

3- and 4-rings with a dangling monomer are both observed in solution[3] and the routes proposed in the present section are thus very likely to occur in solution. Furthermore, these ring clusters with dangling monomers can easily be formed from larger oligomers; condensations that will be analysed in section 4.5.5. The formation of the clusters studied in this section are also likely to be intermediates for the formation of multiple ring structures which is a key step in the formation of a viable nucleus.

The knowledge gained from the analysis of small oligomers condensing onto ring clusters, can also provide an initial insight into the crystal growth process. A ring cluster can be a first (yet crude) approximate representation of an edge in a growing crystal. If the growth mechanism takes place with the addition of very small particles such as the monomer, then the elemental processes of the condensation at such crystal faces can be

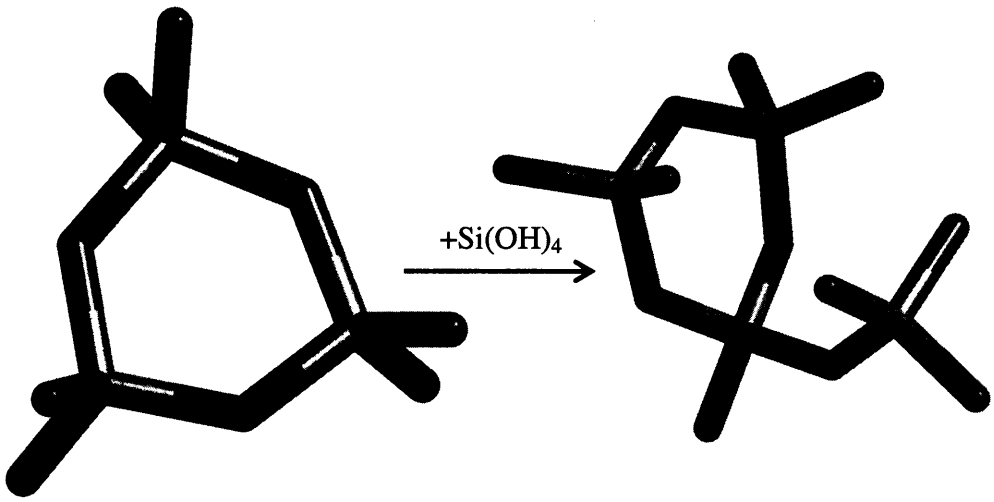

Figure 65 The monomer and 3-ring condensation; the other product is water. See Table 19. The hydrogen atoms are not shown for simplicity. **Note, this convention is used in all the molecular graphics of this section.**

deduced. The condensation of a monomer into a d4-ring will be considered later (section 4.5.7.4), in such a context.

We note that the addition of a monomer to a 3-ring (summarized in Table 19) show similar trends to the oligomer and monomer condensation shown before (section 4.5.2, page 129): as the charges increase, we see an increase in exothermicity of the reaction. However, in the gas phase, none of the condensations are exothermic if both reactants are charged; a situation that is radically reversed when COSMO solvation is employed.

Table 19 Free energy ($kJmol^{-1}$) change in the gas phase and in solution and other thermodynamical properties at 0, 298 and 450K, in the 3-ring condensation with a monomer. The first row reaction is 3-ring + M → 3-1r + H_2O, see Figure 65.

		0K	298K			450K		
	Reactants	ΔE_0	ΔH	$T\Delta S$	ΔG	ΔH	$T\Delta S$	ΔG
Gas	3r + M	-38	-37	-16	-21	-37	-25	-12
	$3r^-$ + M	-76	-74	-13	-61	-74	-19	-55
	$3r^{-2}$ + M	-147	-144	-12	-132	-145	-19	-126
	$3r^{-3}$ + M	-187	-184	-11	-173	-185	-17	-168
	$3r^{-4}$ + M	-425	-421	-2	-419	-420	-2	-418
	3r + M^-	-163	-165	-27	-138	-167	-43	-124
	$3r^-$ + M^-	135	136	-16	152	136	-25	161
	$3r^{-2}$ + M^-	431	434	-13	446	434	-19	453
	$3r^{-3}$ + M^-	587	589	-11	600	589	-17	605
	3r + M^{-2}	-459	-460	-25	-436	-462	-40	-423
	$3r^-$ + M^{-2}	206	209	-11	220	209	-16	225
	$3r^{-2}$ + M^{-2}	700	703	-7	709	703	-10	712
Sol.	3r + M	-24	-24	-20	-4	-24	-31	7
	$3r^-$ + M	-49	-48	-15	-33	-50	-25	-25
	$3r^{-2}$ + M	-83	-80	-6	-73	-80	-10	-70
	$3r^{-3}$ + M	-1	2	-9	11	2	-13	16
	$3r^{-4}$ + M	-58	-54	-5	-49	-53	-6	-47
	3r + M^-	-65	-69	-32	-37	-72	-52	-20
	$3r^-$ + M^-	-86	-83	-8	-74	-83	-13	-70
	$3r^{-2}$ + M^-	14	16	-12	28	16	-18	34
	$3r^{-3}$ + M^-	-6	-4	-12	7	-5	-18	13
	3r + M^{-2}	-163	-163	-20	-142	-164	-33	-131
	$3r^-$ + M^{-2}	-49	-46	-9	-37	-46	-14	-32
	$3r^{-2}$ + M^{-2}	-52	-50	-10	-40	-50	-16	-34

In the latter, the change in entropy is always negative and is similar to that found for the trimerization reaction, a result of the more restrained internal movement of the product, where two H-bonds lock the geometry (see Figure 23 page 61). In the condensations analysed so far, building up the 3-ring from the monomer require the condensation of charged species to produce finally the 3-ring. Furthermore, if present in solution, a neutral 3-ring will be easily deprotonated because of the high pH. Thus, from the reactions presented in Table 19, those where the neutral 3-ring is a reactant are very unlikely to occur, even if the free energy is favourable.

There are two especially interesting results when solvation is included. The condensation of both the 3-ring^{3-} + monomer and 3-ring^{2-} + monomer^{-} have a positive free energy, because the change in enthalpy is positive; the high charges involved in the condensation can be used to explain this behaviour. However, the last row in Table 19 shows a favourable free energy for the 3-ring^{2-} + monomer^{2-} condensation, where the charges are even higher. A selective, pH dependent, condensation is therefore suggested from these results.

A comparison of the equivalent reactions of the monomer condensing to form a dimer, trimer and a 3-ring is very useful, as it gives us an idea of where it is energetically more probable that monomer condensations onto rings or oligomers will occur. In the gas phase, there is a clear indication of a more exothermic and more exergonic monomer condensation onto a 3-ring rather than on the monomer, dimer or trimer, which applies for both neutral and charged species. In solution the behaviour is similar, with the monomer condensation on the 3-ring releasing more enthalpy and free energy than when it condenses with a monomer, dimer or trimer; again both for neutral and charged clusters. The reaction of a neutral monomer condensing with a neutral ring or oligomer, always shows a positive change in free energy under all conditions. However, there are exceptions in the gas phase, where the monomer condenses exergonically with another monomer and with a 3-ring. In effect, there is no neutral monomer addition to either the neutral 3-ring or other small oligomers, in COSMO solvation (in addition the neutral clusters are minority species). Thus overall, we conclude that monomer addition to the 3-ring is favoured over that to small linear oligomers.

The latter conclusion is of importance, since the preference for monomer condensation on a ring rather than to an oligomer will create structures where the ring has dangling

oligomers (which to some extent could be considered as a pre-nucleus species) and not long chains. This result again suggests that long chains will not be present in synthesis solution; previously we found how the oligomeric chains will cyclize towards ring structures rather than continue growing (see section 4.2.1.2 page 97).

We now consider the adducts of a monomer and a 4-ring. The reactant and product are shown in Figure 66 and the change in energy under different conditions is shown in Table 20. We find a similar trend to other monomer condensations, with a higher energy release when, for the reactants, higher charges are involved (the pH effect). The entropy change is always negative and is relatively unimportant at low temperatures, which is similar to the results for the polymerization reactions (section 4.5.2). In the gas phase, condensation is not favoured when both reactants are charged; also these reactions are not favoured due to the Coulombic repulsion between the species. However, there are a number of individual comparisons which are worthy of comment.

The gas phase addition of a monomer to a 3-ring releases more energy than the same addition to a 4-ring (see Table 19 and Table 20). The differences between the 3- and 4-rings are further enhanced when the ring structure is charged. This result possibly echoes the influence of the H-bonds on the stability of the 4-ring, as when the 4-ring is charged the H-bonds help to distribute the excess of charge. This stability is in some way lessened when a monomer is added because the coordination of H-bonds is broken and the H-bond lengths are slightly larger (see Figure 20 and Figure 25). An important question now emerges: does the 4-ring continue to grow by further addition of

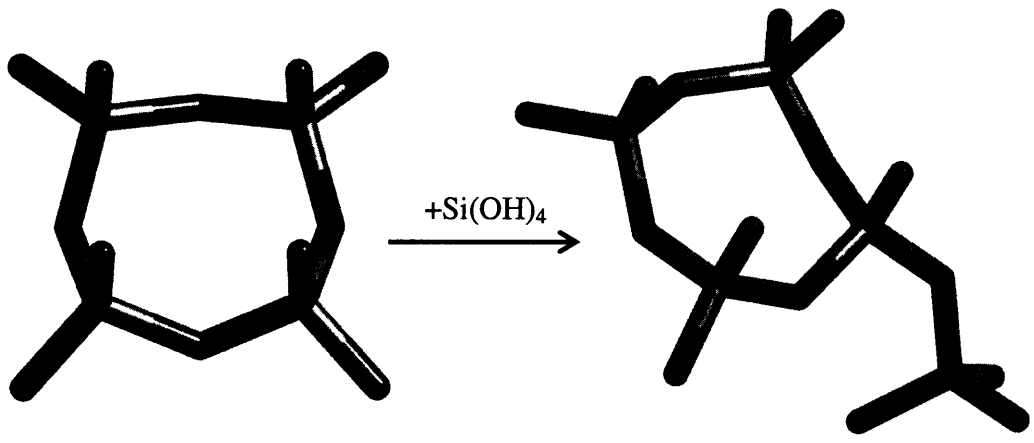

Figure 66 The monomer and 4-ring condensation. See Table 20.

Table 20 Free energy ($kJmol^{-1}$) change in the gas phase and in solution and other thermodynamical properties at 0, 298 and 450K, in the 4-ring condensation with a monomer. See Figure 66.

		0K	298K			450K		
	Reactants	ΔE_0	ΔH	$T\Delta S$	ΔG	ΔH	$T\Delta S$	ΔG
Gas	$4r + M$	-16	-12	-14	3	-10	-20	9
	$4r^- + M$	-37	-35	-10	-25	-35	-16	-20
	$4r^{-2} + M$	-80	-78	-14	-64	-79	-22	-57
	$4r^{-3} + M$	-147	-148	-23	-125	-149	-36	-113
	$4r^{-4} + M$	-313	-311	-9	-302	-312	-14	-298
	$4r + M^-$	-179	-180	-32	-148	-181	-50	-131
	$4r^- + M^-$	154	154	-17	171	154	-26	179
	$4r^{-2} + M^-$	429	429	-21	449	428	-33	460
	$4r^{-3} + M^-$	560	561	-16	577	561	-24	585
	$4r + M^{-2}$	-495	-496	-33	-463	-497	-50	-446
	$4r^- + M^{-2}$	156	156	-17	174	155	-27	183
	$4r^{-2} + M^{-2}$	630	633	-8	641	633	-12	645
Sol.	$4r + M$	-10	-2	1	-3	2	7	-4
	$4r^- + M$	-8	-5	-11	6	-5	-16	11
	$4r^{-2} + M$	-15	-13	-10	-3	-13	-15	2
	$4r^{-3} + M$	-26	-28	-23	-5	-30	-38	8
	$4r^{-4} + M$	-45	-43	-9	-34	-43	-14	-30
	$4r + M^-$	-67	-63	-11	-52	-60	-13	-48
	$4r^- + M^-$	-25	-24	-14	-11	-25	-21	-4
	$4r^{-2} + M^-$	1	-1	-26	25	-4	-42	38
	$4r^{-3} + M^-$	-3	-1	-11	10	-2	-17	15
	$4r + M^{-2}$	-145	-141	-9	-132	-138	-11	-128
	$4r^- + M^{-2}$	-69	-71	-26	-46	-73	-41	-32
	$4r^{-2} + M^{-2}$	-35	-33	-9	-24	-34	-14	-19

monomers, or by the addition of larger species, such as dimers or even another 4-ring? In solution, there are even more significant differences, but with the same trend: monomer + 3-ring condensation is more exothermic and exergonic than the adduct to a 4-ring.

Another important comparison to make is that between a monomer condensation onto a 4-ring and onto a small linear oligomer. When the monomer is neutral, it reacts more favourably with a small oligomer than with a ring. Nevertheless, when the monomer is

charged, the more favourable reaction is in general, the condensation with a 4-ring. It is important to recall at this point that both the neutral 4-ring and neutral oligomers, are unlikely to be present in high pH solution. Therefore, the preference of the addition of monomer either to an oligomer or to a ring will depend on the pH.

The 4-ring does not condense with a neutral monomer in solution, unless it is highly charged (4-ring^{4-}). Addition of the monomer seems more favoured in solution when the 4-ring is neutral and the monomer has a -1 or -2 charge. However, the neutral 4-ring, as explained before, is very unlikely to occur under zeolite synthesis conditions. Thus, a low probability for monomer addition to the 4-ring is postulated from these observations. However, the 4-ring with a dangling monomer is observed in silicate solutions[3]; so are there alternative routes to this species? One possible route is through the internal cyclization of a pentamer to produce the 4-ring with a dangling monomer; in the next section (4.5.5), this reaction will be studied. Furthermore, if the 4-ring + monomer condensation seems not very likely, it leaves the 4-ring available to condense with other clusters like the dimer or even another 4-ring.

To conclude this subsection, we consider a second monomer condensation onto a 3-ring which releases less energy than for the first one, under neutral gas and solvated conditions (see Table 21 and Figure 67), and at 450K in solution is not thermodynamically favoured. However, in contrast, the addition of a second monomer to the 4-ring has the opposite result (see Table 22 and Figure 68).

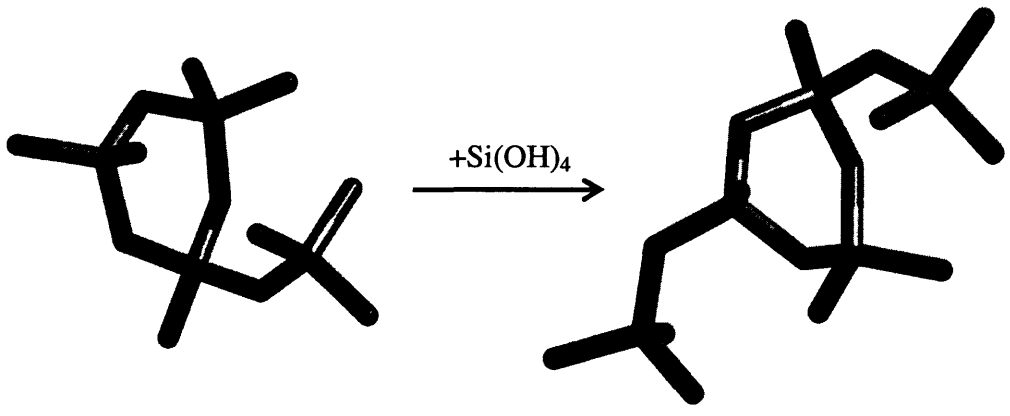

Figure 67 The second monomer condensation on a 3-ring. See Table 21.

Table 21 Free energy ($kJmol^{-1}$) change in the gas phase and in solution and other thermodynamical properties at 0, 298 and 450K, in the second monomer condensation on a 3-ring. See Figure 67.

		0K	298K			450K		
	Reactants	ΔE_0	ΔH	$T\Delta S$	ΔG	ΔH	$T\Delta S$	ΔG
Gas	3-1r + M	-17	-14	-7	-8	-14	-10	-4
	$3\text{-}1r^{-}$ + M	-32	-27	-1	-26	-27	-1	-26
	$3\text{-}1r^{-2}$ + M	-96	-91	-1	-90	-90	-1	-89
	3-1r + M^{-}	-157	-156	-12	-144	-157	-19	-138
	$3\text{-}1r^{-}$ + M^{-}	115	119	-5	124	119	-7	126
	3-1r + M^{-2}	-516	-514	-10	-505	-515	-16	-500
Sol.	3-1r + M	-4	-1	-11	10	-1	-17	15
	$3\text{-}1r^{-}$ + M	-25	-18	0	-18	-17	2	-19
	$3\text{-}1r^{-2}$ + M	-20	-19	-16	-3	-19	-24	5
	3-1r + M^{-}	-66	-64	-12	-52	-64	-18	-46
	$3\text{-}1r^{-}$ + M^{-}	-57	-53	-9	-45	-52	-12	-40
	3-1r + M^{-2}	-159	-158	-16	-142	-159	-25	-133

The results presented here give rise to some interesting possibilities. First, we find that the addition of a monomer to a 3-ring is generally preferred to the addition to linear oligomers. Conversely, for the more probable reactants, the monomer does not seem to condense on the 4-ring. What is the crucial difference between these similar ring structures? Geometrically, the largest differences between the 3-ring and 4-ring are the

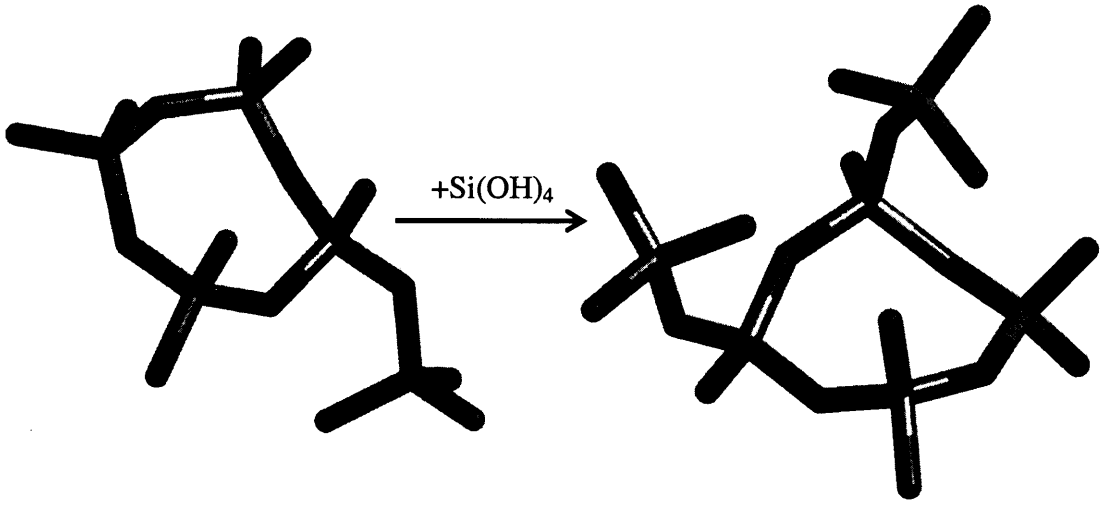

Figure 68 The second monomer condensation on a 4-ring. See Table 22.

Table 22 Free energy ($kJmol^{-1}$) change in the gas phase and in solution and other thermodynamical properties at 0, 298 and 450K, in the second monomer condensation on a 4-ring. See Figure 68.

		0K	298K			450K		
	Reactants	ΔE_0	ΔH	$T\Delta S$	ΔG	ΔH	$T\Delta S$	ΔG
Gas	4-1r + M	-52	-50	-21	-29	-50	-32	-18
	$4\text{-}1r^{-}$ + M	-80	-76	-5	-72	-77	-8	-69
	$4\text{-}1r^{-2}$ + M	-95	-90	-5	-85	-89	-7	-83
	$4\text{-}1r + M^{-}$	-244	-245	-23	-222	-248	-38	-210
	$4\text{-}1r^{-} + M^{-}$	96	100	-11	110	100	-16	116
	$4\text{-}1r + M^{-2}$	-574	-574	-23	-551	-576	-37	-539
Sol.	$4\text{-}1r^{-}$ + M	-59	-55	-10	-45	-55	-15	-40
	$4\text{-}1r^{-2}$ + M	-69	-66	-15	-51	-66	-22	-44
	$4\text{-}1r + M^{-}$	-116	-116	-22	-94	-117	-35	-83
	$4\text{-}1r^{-} + M^{-}$	-87	-85	-18	-67	-86	-27	-58
	$4\text{-}1r + M^{-2}$	-204	-205	-25	-180	-207	-40	-167

internal H-bonds; the 3-ring has none while the 4-ring has a ring system with four H-bonds (Figure 15, page 54 and Figure 20, page 58).

Thus, in isolated cyclic clusters with H-bonds, as in the 4-ring (and possibly larger rings), monomer condensation will be less favourable. However, in a growing crystal, adducts of a monomer will be more similar to the 3-ring case, as surface structures will possess fewer H-bonds. Hence, we may speculate further, that crystal growth from monomeric species is favoured over further (amorphous) oligomeric growth, under zeolite synthesis conditions.

4.5.5 Internal condensation from oligomer to ring with dangling monomer

Both the 3- and 4-ring with a dangling monomer are observed in silicate solutions[3], and we now consider a possible route to their formation via the internal condensation of larger oligomers. All the condensations presented here are an alternative to the monomer addition reactions shown before. These internal condensation reactions are straightforward as the oligomer is the only reactant, while in the monomer addition, the encounter of monomer and ring is necessary.

The internal cyclization of a tetramer forming a 3-ring with a dangling monomer is shown in Figure 69 and the associated changes in energies shown in Table 23. The reactant tetramer has a conformation that is quite stable with five H-bonds (Figure 17 page 55). There is also a second tetramer conformation with a tetrahedral shape (Figure 50 page 96) which has almost the same energy. This latter conformation seems to be more suitable for internal condensation to the 3-1ring and thus knowledge of the energy barrier for interconversion between these two tetramers conformers could be useful.

Nearly all the enthalpy changes for this internal condensation are positive (see Table 23) with a general increase in endothermicity as higher charged tetramers are considered: a trend also noted for the single ring condensations, presented previously (section 4.5.3 page 140). A high positive change in the entropy is also found; therefore, in general the temperature will have an important role here. Again, this result is similar to that found for the formation of the single rings.

The free energy is therefore negative for reactions under the neutral conditions, and is found to become more favourable when charged clusters are considered. The latter result again is comparable to the simple ring closures. As the positive energy change is higher for the charged clusters, there is a suggestion that the excess of negative charge is better distributed when the cluster is linear than when it is cyclic.

When the tetramer internal condensation (to a 3-1ring) is compared with the trimer to 3-ring closure, we find the enthalpy change is more positive and the respective free

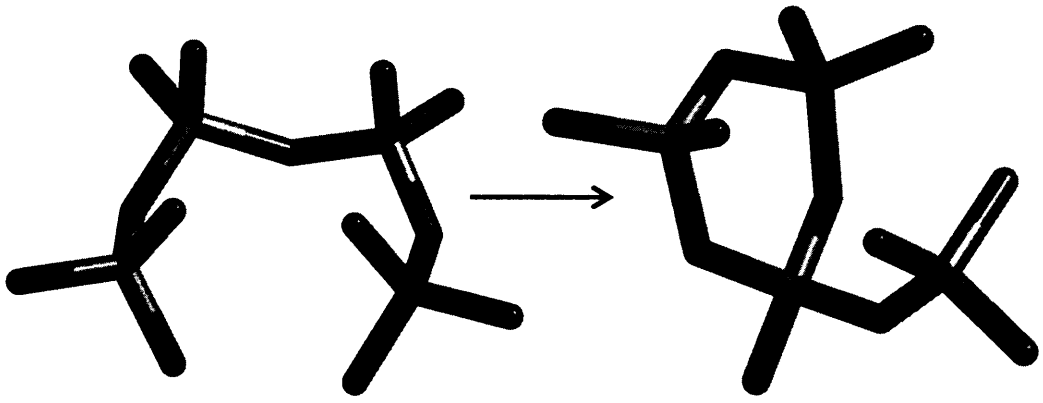

Figure 69 The internal condensation of tetramer into a 3-ring with a dangling monomer. See Table 23.

Table 23 Free energy ($kJmol^{-1}$) change in the gas phase and in solution and other thermodynamical properties at 0, 298 and 450K, for the internal condensation of tetramer into a 3-ring with a dangling monomer. See Figure 69.

		0K	298K			450K		
	Reactants	ΔE_0	ΔH	$T\Delta S$	ΔG	ΔH	$T\Delta S$	ΔG
Gas	T	14	18	42	-25	17	63	-46
	T^-	45	47	40	8	46	58	-12
	T^{-2}	42	46	42	3	45	63	-18
	T^{-3}	75	78	41	37	78	61	16
	T^{-4}	17	21	42	-21	21	63	-43
Sol.	T	-4	0	45	-44	0	67	-67
	T^-	20	20	35	-14	18	49	-31
	T^{-2}	4	9	50	-40	9	75	-65
	T^{-3}	73	78	47	31	79	71	7
	T^{-4}	22	27	47	-20	27	71	-44

energy less negative for the 3-ring single condensation. Thus, this result suggests that 3-ring containing species are more likely formed from oligomers larger than the trimer.

Tetramers can condense internally in two ways, to produce the 4-ring or to produce a 3-ring. Given the relative abundance of zeolites with 3- and 4-rings, it is clearly important to analyse these competing reactions. The change in energy is similar for both reactions although, there are significant differences with the tetramer^{2-} and tetramer^{3-} in solvation. At 298K, both routes have a comparable entropy change, but they are slightly different at 450K, mainly for the neutral tetramer. The free energy changes are also similar for both routes; however the tetramer^{2-} and more especially the tetramer^{3-} show important differences when they condense either to a 3-1ring or to a 4-ring. The tetramer^{2-} will condense more favourably to a 3-1ring and the tetramer^{3-} will cycle into a 4-ring. Certainly the tetramer$^-$ in gas and solution is more likely to condense into a 4-ring (rather than a 3-1ring), as well as the neutral tetramer in the gas phase. The tetramer^{3-} cluster in solution and in the gas phase shows an interesting behaviour, because when it condenses internally into a 3-1ring there is a large positive change in the electronic energy with a consequent positive free energy change. As a consequence, the 4-ring cyclization is largely favoured from a tetramer^{3-} in solution, rather than the cyclization to the 3-1ring.

What is of general note here is the selectivity of certain condensations to the reaction conditions, which will result in significant changes in the relative population of various species during nucleation. For example, from the results for the tetramer, the product will depend on the charge; if it bears a charge of -2 the 3-1ring will be formed; otherwise with a charge of -3, the 4-ring is more likely to be formed. From these results, there is a suggestion that the pH could be used to "tune" the selectivity to one or other species: a suggestion that concurs with experimental observations. Moreover, local variation in pH will have a significant influence.

The internal condensation of a pentamer can also lead to the formation of a 3-ring, this time with two dangling monomers. In this case, the condensation is slightly different from the tetramer presented before, because two internal silicon atoms are linked (see Figure 70), while the tetramer condenses one of its ends to an internal silicon. However, this difference does not appear to have a large influence on the free energy released (Table 24), but note the enthalpy change is more positive for the condensation of the pentamer.

The pentamer could also form a 4-ring with a dangling monomer. This direct reaction is shown in Figure 71 and the associated energies are in Table 25. As can be seen, all the energies are positive and a higher charge results in a larger energy change. This endothermicity is a characteristic shared with single ring condensations. However, a large positive change in the entropy is also observed, which, as with the other cyclic

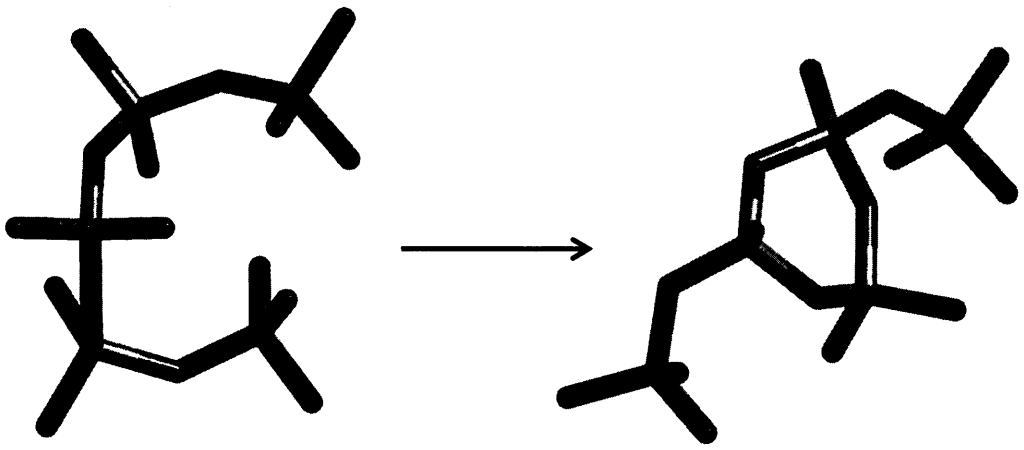

Figure 70 The internal condensation of pentamer into a 3-ring with two dangling monomers. See Table 24.

Table 24 Free energy ($kJmol^{-1}$) change in the gas phase and in solution and other thermodynamical properties at 0, 298 and 450K, for the internal condensation of pentamer into a 3-ring with two dangling monomers. See Figure 70.

		0K	298K			450K		
	Reactants	ΔE_0	ΔH	$T\Delta S$	ΔG	ΔH	$T\Delta S$	ΔG
Gas	P	21	25	47	-22	24	70	-46
	P^-	77	85	57	28	86	87	-1
	P^{-2}	50	55	49	6	55	74	-19
Sol.	P	11	15	46	-31	15	70	-54
	P^-	25	28	44	-16	28	67	-38
	P^{-2}	15	19	43	-25	18	65	-47

structures, makes the reaction feasible in some cases. The internal condensation of the neutral pentamer has a negative free energy (see Table 25) even at room temperature. However, the charged pentamers will only cyclize in this way at higher temperatures.

The pentamer^{3-} deserves a special mention, as it has a large positive change in energy, resulting always in a positive free energy change, when condensing into a 4-1ring. This particular behaviour, we believe, is due to a very favourable conformation for the pentamer^{3-}, which successfully distributes the negative charge. Furthermore, this conformation of the charged pentamer strongly resembles the 5-ring cluster. Perhaps, further studies of this particular cluster are necessary to confirm the relative low probability to produce a 4-1ring.

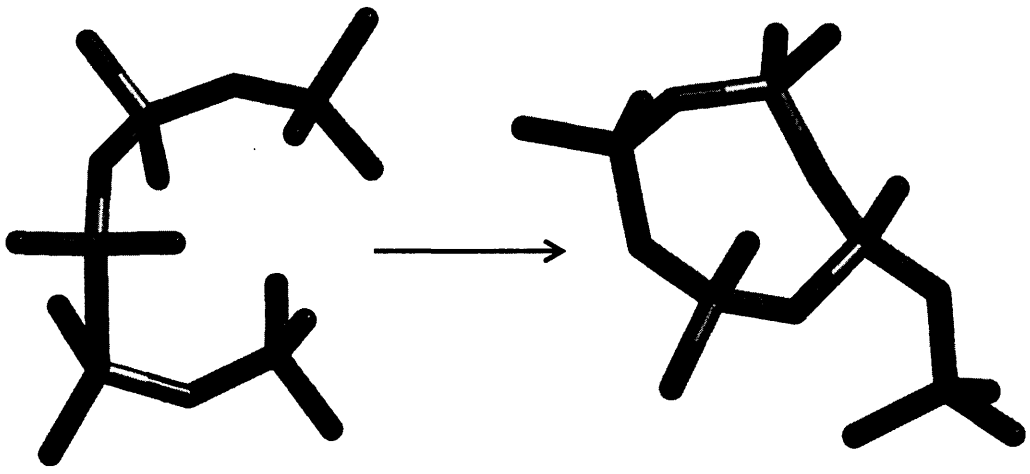

Figure 71 The internal condensation of pentamer into a 4-ring with a dangling monomer. See Table 25.

Table 25 Free energy ($kJmol^{-1}$) change in the gas phase and in solution and other thermodynamical properties at 0, 298 and 450K, for the internal condensation of pentamer into a 4-ring with a dangling monomer. See Figure 71.

		0K	298K			450K		
	Reactants	ΔE_0	ΔH	$T\Delta S$	ΔG	ΔH	$T\Delta S$	ΔG
Gas	P	31	36	53	-18	35	80	-45
	P^-	63	68	50	18	69	76	-7
	P^{-2}	79	81	40	42	81	59	21
	P^{-3}	113	113	35	78	112	52	60
	P^{-4}	27	30	42	-12	30	63	-33
Sol.	P	20	26	54	-28	27	82	-55
	P^-	38	41	41	0	40	61	-21
	P^{-2}	44	47	46	1	46	69	-22
	P^{-3}	83	82	31	51	79	43	36
	P^{-4}	33	38	52	-14	39	80	-41

The internal condensations of the pentamer to 4-1ring (Figure 71) and tetramer to 3-1ring (Figure 69) are very similar and a comparison between these reactions will show the conditions under which one reaction is favoured over the other.

A larger endothermic change is found for the pentamer condensation, but the entropy change is similar for both cyclizations. However, the difference in free energy shows that it is more thermodynamically favourable to form the 3-ring rather than the 4-ring (both with a dangling monomer) from their respective linear oligomers.

In the condensation of the tetramer to 3-1ring, we found a behaviour that was out of the ordinary for the charge -3, and here for the pentamer^{3-} the same is found. The pentamer^{3-} and the tetramer^{3-} have a large positive enthalpy change with a consequent positive change in free energy. Why do we see such behaviour for these -3 species, which result in cyclization to a ring with dangling monomer being unfavourable? Particularly since the linear tetramer^{-3} and pentamer^{-3} will readily form the 4-ring^{-3} and 5-ring^{-3} respectively.

The pentamer can self-condense to form a 5-ring and a 4-ring with a dangling monomer. These two reactions are competing and their relative feasibility is important because both, 4- and 5-rings are present in zeolite frameworks.

The pentamer has a lower positive enthalpy change when it condenses to a 5-ring, but it has a similar change in entropy compared with the 4-1-ring cyclization. The free energy makes the formation of a 5-ring from the pentamer more favourable than 4-1-ring especially when it is charged and in solution. The latter result prompts an interesting question: why if the most favourable product from the pentamer is a 5-ring, no evidence of the latter is found, but the 4-ring with a dangling monomer is observed? Clearly, alternative routes are important as well as consecutive reactions, and the analysis here only differentiates some of the possible reactions.

The final linear oligomer internal condensation studied here is the hexamer condensing to a 4-ring (Figure 72). The hexamer is a large chain where several internal condensations could take place: 3-, 4-, 5- and 6-rings can be formed from this species. However, the analysis is restricted here to one internal condensation, towards a 4-ring with two dangling monomers. Under the conditions analysed, the hexamer condenses successfully to a tetramer with two dangling monomers (see Table 26), with the exception of when the species is double charged. As a result, the 4-ring is a species, which could be formed from several linear oligomers: tetramer, pentamer and hexamer.

Considering the results of this section more generally, we found that nearly all the internal neutral condensations studied here have almost the same free energy at 298 and

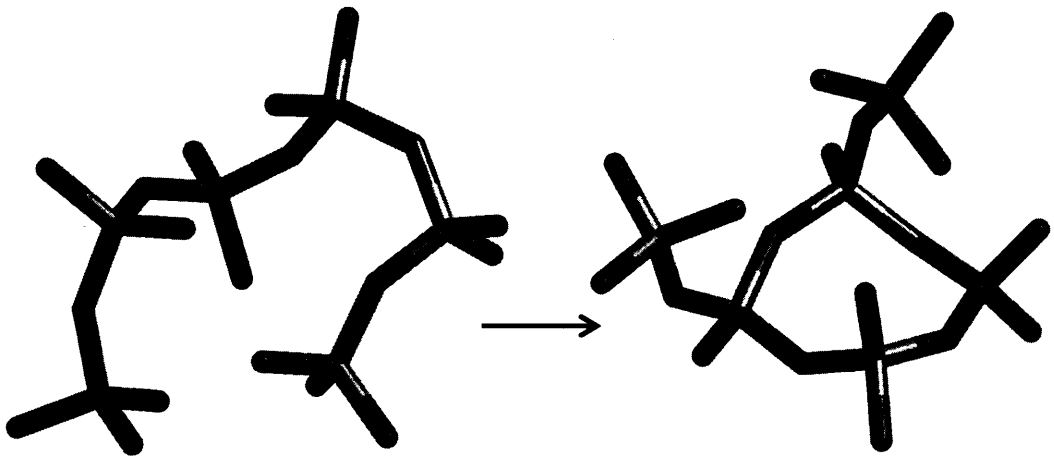

Figure 72 The internal condensation of hexamer into a 4-ring with two dangling monomers. See Table 26.

Table 26 Free energy ($kJmol^{-1}$) change in the gas phase and in solution and other thermodynamical properties at 0, 298 and 450K, for the internal condensation of hexamer into a 4-ring with two dangling monomers. See Figure 72.

		0K	298K			450K		
	Reactants	ΔE_0	ΔH	$T\Delta S$	ΔG	ΔH	$T\Delta S$	ΔG
Gas	H	15	19	42	-23	18	63	-45
	H^-	12	15	46	-31	13	67	-54
	H^{-2}	90	96	48	48	96	73	23
Sol.	H^-	7	12	48	-37	12	73	-61
	H^{-2}	33	36	41	-5	36	62	-26

450K for both gas and solution conditions. This is a very interesting result, because all the starting oligomers are different (tetramer, pentamer and hexamer) and the products as well (3-, 4-rings with dangling monomers), although they share important characteristics; but the free energy found is similar in all cases. On the other hand, the series of cyclizations producing single 3-, 4- and 5- rings discussed earlier (see section 4.4.2 page 123) do not show such similarity: under neutral conditions the free energy released is quite different.

Thus, a preliminary general conclusion drawn from the results in this section is that there is a broad similarity in the thermodynamics of internal neutral condensation for all small oligomers. Additionally, we have found that the selectivity towards the formation of certain clusters depends strongly on the synthesis conditions.

4.5.6 Internal condensation in cyclic structures

The ring structures, already studied, could further react internally to produce double rings (Figure 73). These are important species in the context of zeolite nucleation, as they will lead to denser structures.

We may expect such a process to be more difficult to occur than the internal condensations from linear oligomers studied earlier, because of the flexibility exhibited by a linear species compared with rings. Furthermore, we have seen how single ring structures are stable due to internal H-bonding.

The internal condensations studied in this section are most likely to occur in isolated species (i.e. in the early stages of the nucleation), since when a ring forms part of a larger structure (for example a 4-ring in a double 4-ring condensing in the way shown in

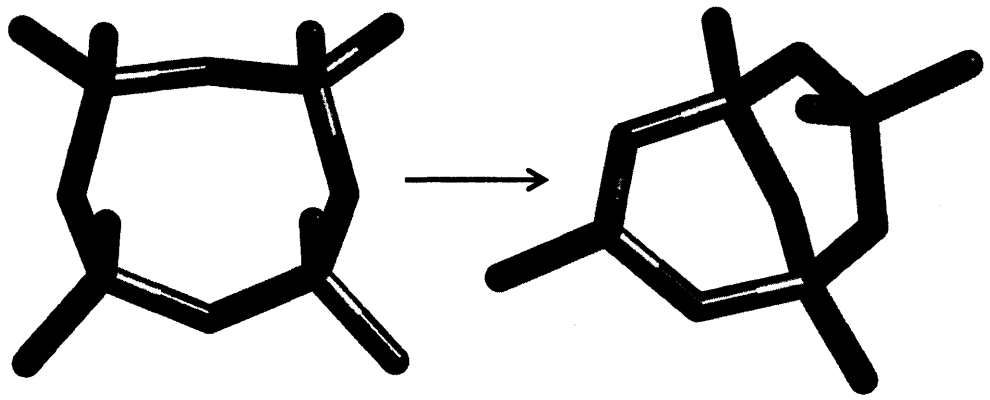

Figure 73 The internal condensation of a 4-ring into a fused 3-ring. See Table 27.

the Figure 73), internal condensation will be much less feasible because of the resulting high internal stress. Thus, the following analysis may provide clues of why open microporous structures are formed rather than dense amorphous structures.

Taking first the 4-ring, which could internally condense when one of the oxygen atoms in the ring attacks a silicon atom in the other extreme of the ring (Figure 73); however, the distortion of the ring is large and furthermore the oxygen atoms are to an extent locked in the H-bonding system of the 4-ring. There is a considerable decrease in the

Table 27 Free energy ($kJmol^{-1}$) change in the gas phase and in solution and other thermodynamical properties at 0, 298 and 450K, for the internal condensation of a 4-ring into a fused 3-ring. See Figure 73.

		0K	298K			450K		
	Reactants	ΔE_0	ΔH	$T\Delta S$	ΔG	ΔH	$T\Delta S$	ΔG
Gas	4r	54	56	27	30	56	40	16
	$4r^-$	74	78	41	36	77	62	15
	$4r^{-2}$	110	113	41	72	113	62	51
	$4r^{-3}$	65	68	39	29	67	58	10
	$4r^{-4}$	60	63	43	20	62	64	-2
Sol.	4r	15	22	45	-24	24	72	-47
	$4r^-$	26	29	40	-12	28	60	-32
	$4r^{-2}$	39	42	41	0	41	62	-20
	$4r^{-3}$	42	46	45	1	46	68	-22
	$4r^{-4}$	24	29	56	-27	29	84	-55

number of H-bonds, for such a reaction, from four to only one.

The results in Table 27 show that the reaction is endothermic under all the conditions considered and the change in entropy is positive: mainly because there is only one reactant but two products. These results are again analogous to the other ring condensations studied here.

In the gas phase, at 298 and 450K, none of the free energies suggests this reaction to be favourable, which could be interpreted as suggesting that under drier conditions, as in the inner parts of a gel or sol system, the reaction could be inhibited.

In solution at 298K, the internal condensation of 4-ring^{2-} and 4-ring^{3-} is unfavourable. However, at 450K, both neutral and charged species display a tendency to form the fused 3-ring. Under synthesis conditions, the 4-ring is most likely to be charged, so only the temperature will decide if the internal condensation of the 4-ring will take place. This possibly explains partly why the fused 3-ring is not observed in silicate solutions, which are identified at room temperature[3].

The 5-ring could also undergo an internal condensation producing a fused 3- and 4-ring (Figure 74). This reaction seems to be the only probable internal condensation, and the energies associated are presented in Table 28. Again, all the enthalpy changes for this reaction are endothermic and the entropy change is largely positive, both characteristics are typical of the cyclization process, as shown in this thesis (see section 4.5.3).

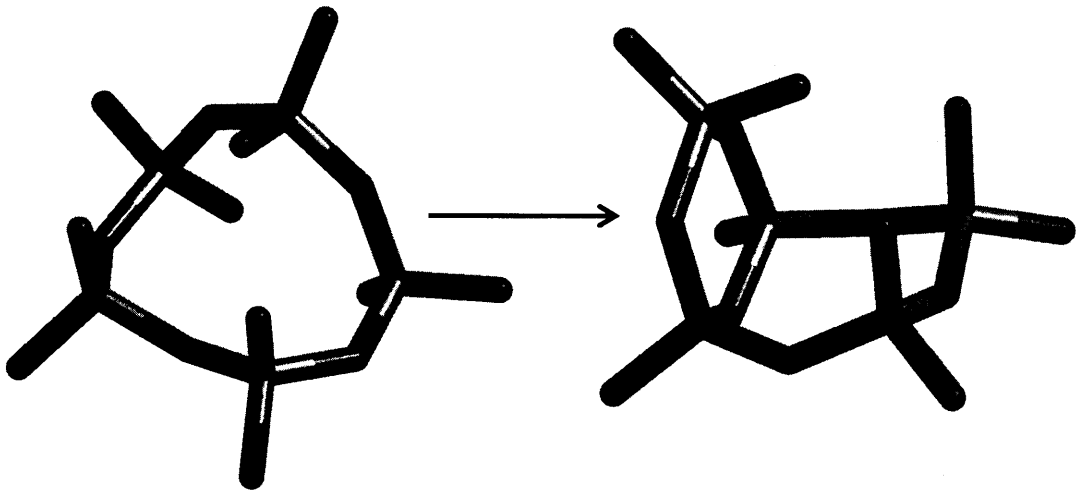

Figure 74 The internal condensation of a 5-ring into a fused 3-4-ring. See Table 28.

Table 28 Free energy ($kJmol^{-1}$) change in the gas phase and in solution and other thermodynamical properties at 0, 298 and 450K, for the internal condensation of a 5-ring into a 4-three-ring. See Figure 74.

		0K	298K			450K		
	Reactants	ΔE_0	ΔH	$T\Delta S$	ΔG	ΔH	$T\Delta S$	ΔG
Gas	5r	16	16	32	-16	14	47	-33
	$5r^-$	30	33	43	-10	32	63	-31
	$5r^{-2}$	118	121	41	81	121	61	60
	$5r^{-3}$	80	83	42	41	82	63	19
	$5r^{-4}$	57	60	42	18	60	63	-3
Sol.	5r	6	7	36	-29	5	52	-47
	$5r^-$	8	10	38	-28	8	56	-47
	$5r^{-2}$	43	54	57	-2	61	94	-33
	$5r^{-3}$	43	47	45	2	47	68	-21
	$5r^{-4}$	23	26	44	-18	26	66	-41

In the gas phase, the favoured reactions are for the less deprotonated species, so the neutral and single charged 5-ring could condense in nearly anhydrous conditions. In solution, the reaction is more favoured, but the internal condensation for the 5-ring^{2-} and 5-ring^{3-} at room temperature are not favoured. However, at 450K neutral and all the charged 5-rings internal condensation reactions are exergonic. The same behaviour is observed for the 4-ring (Table 27) in solution, only at room temperature the double and triple charged ring do not condense, as discussed above.

Comparatively the internal condensation of a 4-ring and of a 5-ring (Table 27 and Table 28 respectively) are quite similar, and with the exception of the reaction of the neutral and singly negatively changed species under gas phase conditions, there are no significant differences in the thermodynamic properties calculated for such internal cyclizations.

We again emphasize that the product of the 5-ring internal condensation (see Figure 74) is found experimentally in silicate solutions[3], but not the 5-ring itself. However, the 5-ring is an important cyclic unit in zeolite frameworks. The results on Table 28 show that both ring structures may be interchangeable, depending on the synthesis conditions, *i.e.* at 298K some charges may favour the 5-ring presence, but not at 450K.

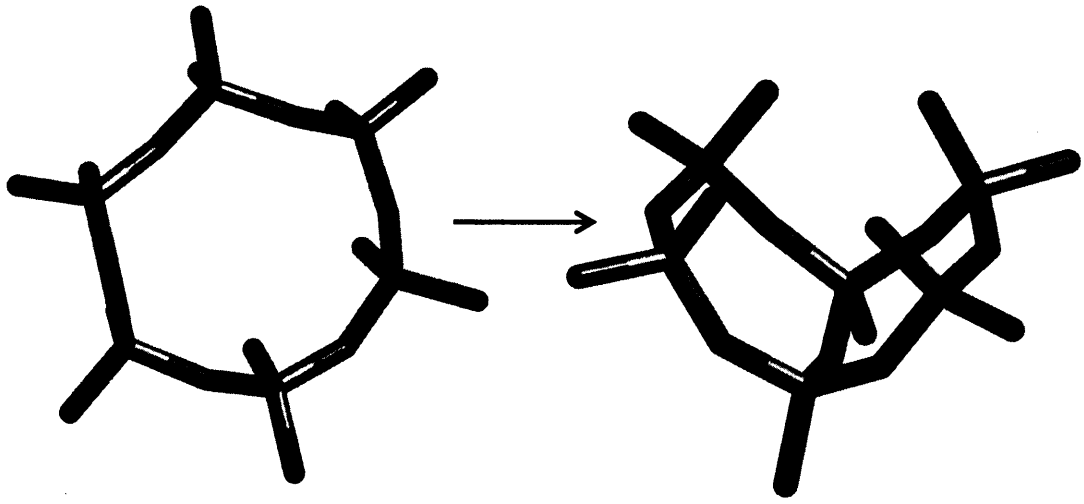

Figure 75 The internal condensation of a 6-ring into a fused 4-ring. See Table 29.

The final internal condensation of a cyclic structure studied here is the 6-ring producing a fused 4-ring (Figure 75). Other internal condensations for the 6-ring are possible, but that analysed here links to important species in zeolite synthesis, many zeolite structures contain both units.

In comparison with the 4-ring and 5-ring internal condensations, the 6-ring appears to condense more readily (Table 29). Whilst, in the gas phase either the 6-ring or the fused 4-ring could be present depending on the charge and temperature, but in solution our

Table 29 Free energy ($kJmol^{-1}$) change in the gas phase and in solution and other thermodynamical properties at 0, 298 and 450K, for the internal condensation of a 6-ring into a fused 4-ring. See Figure 75.

		6ring Cyclization						
		0K	298K			450K		
	Reactants	ΔE_0	ΔH	$T\Delta S$	ΔG	ΔH	$T\Delta S$	ΔG
Gas	H	32	35	48	-13	34	72	-38
	H^-	55	57	43	14	56	64	-8
	H^{-2}	68	71	42	29	70	63	8
	H^{-3}	43	45	42	3	44	62	-18
	H^{-4}	38	42	44	-2	41	65	-25
Sol.	H	11	11	34	-23	7	47	-40
	H^-	45	48	45	3	46	66	-20
	H^{-2}	50	49	36	14	46	50	-4
	H^{-3}	22	26	48	-22	27	74	-47
	H^{-4}	-6	-6	39	-45	-10	54	-63

calculations suggest that any free 6-ring would react to form the fused 4-ring, which agrees with the experimental observation of the fused 4-ring in silicate solutions[3] and the lack of 6-ring.

4.5.6.1 Fused rings in solution and zeolite frameworks

Table 30 summarizes the experimental findings for the structures in the reactions considered in this section, where in each row the clusters are related with an internal cyclization reaction. The fact that only one of the clusters from these reactions is present in the work of Knight and Kinrade[3] (left column in Table 30) and the other is present in zeolite frameworks, suggests that the idea of a direct link between the clusters studied, *i.e.* the reactions analysed are very likely to take place. As observed, the charge, temperature and solvation determines the prevalence of one structure over the other. Thus, if one structure is formed the other can be obtained by changing the conditions.

Why are the 5- and 6-ring not observed in silicate solutions, when they are clearly present in numerous zeolite frameworks? The answer to this important question can be inferred from the results of this section. The degree of solvation (somewhere between the gas and solvated models), the temperature and the pH will dictate which of the clusters will prevail. So, while no 5-ring or 6-ring are detected in the studies of Knight and Kinrade[3], they may be accessible from the clusters that they reported, *i.e.* the fused 3- and 4-rings. Thus, whilst in solution the more dense fused rings are clearly favoured, in less hydrated environments (such as a nanoparticle or growing surface) more open structures could be formed from the denser units.

Table 30 Clusters detected in the silicate solution by NMR[3], observed in zeolitic frameworks and their relation with the reactions analysed in this section.

Solution		In zeolite frameworks	
Detected	Not detected		
4-ring	fused 3-ring	4-ring	Figure 73
fused 3-4-ring	5-ring	5-ring	Figure 74
fused 4-ring	6-ring	fused 4-ring and 6-ring	Figure 75

4.5.7 The formation of cages

After ring structures, cages are possibly the most important feature of zeolite frameworks. They are an important part in the tiling of several zeolite structures, because they can retain metallic cations or even bigger cations/molecules. Moreover, cage units can be considered as prototypical nuclei. The size of the cage will depend on the size of the rings forming them. The cages analysed in this thesis are limited to the tetrahedron and double rings, in particular three, four and six double rings, partly as they can be considered the least "zeolitic". Consequently, these cages may provide more evidence on the formation mechanisms of larger units (e.g. a cancrinite cage), where the influence of extra-framework species will be more important. Some of the cages analysed are found in silicate solutions and others in zeolite frameworks. However, no cages are known to be present both in solution and in a zeolite structure. This observation opens up the interesting question of how and when these important cages are formed in zeolite synthesis and what is the fate of the cages, which are observed in silicate solutions but not in any zeolite framework.

4.5.7.1 The tetrahedron

The tetrahedron is a very compact cage reported to exist in solution; however it is not observed in any zeolite framework. A question similar to that raised for the 3-ring is prompted: what is the role of the tetrahedron in the nucleation of a zeolite? How is it consumed?

A possible reaction pathway to form a tetrahedron directly is from the fused 3-ring: reactant and product are shown in Figure 76. This reaction is always endothermic, as seen in Table 31, and the entropy is largely positive. In solvation, the reaction is more likely than in the gas phase, and the high charge and high temperature makes it even more favourable.

A comparison between the formation of the tetrahedron (Table 31) and the 3-ring (Table 10) gives insight into the relative probability of their formation as judged by the free energy. These reactions share an important characteristic: they produce, from a relatively open structure, a strained cyclic cluster which both contain a 3-ring. Thus, analysing these reactions may help us to understand the presence of the 3-ring like structures in silicate solutions[3]. The enthalpy for the 3-ring formation is more favourable than that to form a tetrahedron, with larger differences (up to 50 $kJmol^{-1}$)

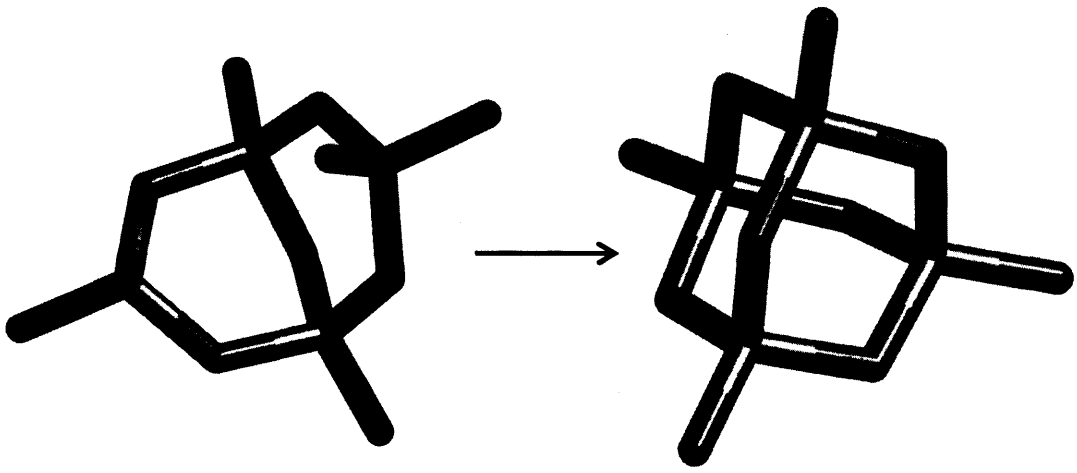

Figure 76 The internal condensation of a fused 3-ring into tetrahedron. See Table 31

under neutral conditions. The entropy for these two reactions is essentially the same, because the processes are similar (3-ring-like structures are being formed). The free energy change is more exergonic for the 3-ring, again with the most significant differences being for neutral conditions. Thus, we can conclude that, the 3-ring is more readily formed than the tetrahedron, presumably as the tetrahedron is more strained.

Although, at this moment we cannot explain the lack of 3-rings in the zeolite structures, this latest result confirms again how the conditions favour the formation of the more open structures than denser units, which will more likely form dense glassy materials, rather than zeolites.

Table 31 Free energy ($kJmol^{-1}$) change in the gas phase and in solution and other thermodynamical properties at 0, 298 and 450K, for the internal condensation of a fused 3-ring into tetrahedron. See Figure 76.

		0K	298K			450K		
	Reactants	ΔE_0	ΔH	$T\Delta S$	ΔG	ΔH	$T\Delta S$	ΔG
Gas	f3r	84	86	44	43	85	64	21
	$f3r^-$	111	113	40	73	111	58	53
	$f3r^{-2}$	67	69	41	28	68	60	8
	$f3r^{-3}$	92	93	37	57	92	53	39
	$f3r^{-4}$	114	115	35	81	114	50	63
Sol.	f3r	63	66	42	24	65	63	2
	$f3r^-$	70	73	43	31	73	64	9
	$f3r^{-2}$	46	50	47	4	50	70	-20
	$f3r^{-3}$	11	13	41	-28	12	60	-48
	$f3r^{-4}$	1	1	27	-26	-1	39	-39

4.5.7.2 The formation of a double 3-ring.

The d3-ring (see bottom of Figure 77) is again a species found in silicate solutions[3, 34], but not in any pure siliceous nor any aluminosilicate zeolite. As with the 3-ring however, it provides a benchmark species: larger double rings, the double 4-ring and double 6-ring are key structural units in zeolite frameworks. We propose two alternative routes for the double 3-ring to be formed. First by the fusion of two 3-rings, which requires three condensations and secondly by an internal condensation of the fused 4-ring (see Figure 77). Both mechanisms produce a d3-ring, but the number of bonds formed is different. We shall now make a comparison of the two routes.

The reaction of a fused 4-ring to form a double 3-ring is endothermic and there is a positive change in entropy, under all the conditions studied (see Table 32). The resulting free energy change is negative in solution but positive in the gas phase (with the exception of the neutral condensation). The reaction is more favourable in solution at low charges and high temperatures.

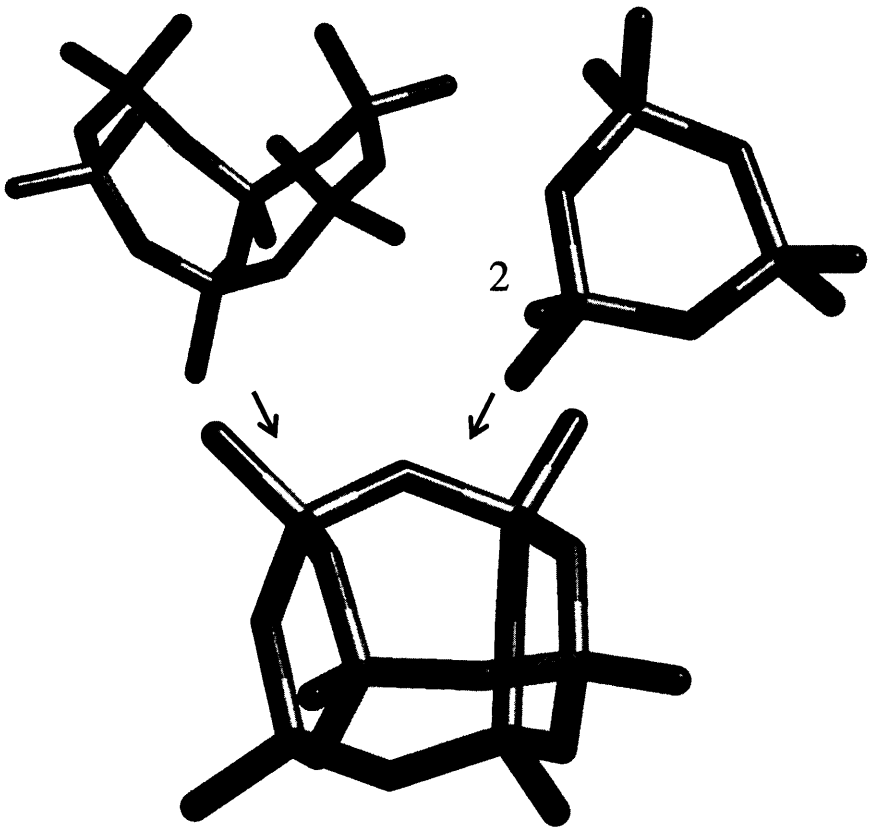

Figure 77 The internal condensation of a fused 4-ring into a double 3-ring, and the fusion of two 3-rings into a double 3-ring. See Table 33 and Table 32.

Table 32 Free energy ($kJmol^{-1}$) change in the gas phase and in solution and other thermodynamical properties at 0, 298 and 450K, for the internal condensation of a fused 4-ring into a double 3-ring. This reaction involves two condensations; the results are per condensation. See Figure 77.

		0K	298K			450K		
	Reactants	ΔE_0	ΔH	$T\Delta S$	ΔG	ΔH	$T\Delta S$	ΔG
Gas	f4r	18	25	53	-28	25	80	-55
	$f4r^-$	71	75	43	32	75	65	11
	$f4r^{-2}$	71	74	37	37	73	55	18
	$f4r^{-3}$	87	91	43	48	90	64	26
	$f4r^{-4}$	92	96	44	52	95	66	29
Sol.	f4r	9	12	39	-27	11	58	-47
	$f4r^-$	32	36	46	-10	35	68	-33
	$f4r^{-2}$	32	36	43	-7	36	64	-28
	$f4r^{-3}$	31	36	45	-10	35	68	-33
	$f4r^{-4}$	27	30	41	-11	28	60	-32

The condensation of two 3-rings (Table 33) however, is somewhat different. It is always exothermic with the exception, when both 3-rings are charged in the gas phase; however, the entropy is always favourable for the reaction, as was the case for the condensation of a fused 4-ring. The resulting free energies of fusion of two 3-rings are always favourable in the gas phase and solution, except under neutral conditions.

Comparing the free energies of the two pathways, the double 3-ring will be formed preferentially from two 3-rings (see Table 32 and Table 33), which leaves the fused 4-ring available for further condensations. Perhaps this is the fate of the relatively large concentration of 3-rings in synthesis solutions that lead to zeolites? However, clearly this does not explain the fate of a double 3-ring.

The energetics of the internal condensation of a trimer into a 3-ring (Table 10) are in fact similar to those for the formation of a double 3-ring from the fused 4-ring, presumably as the same 3-rings are formed. This latter observation opens an interesting possibility: can we consider even such a small cluster as prototypical of all the larger species; that is we expect all further condensations where a 3-ring is formed to be similar in energetics (and structurally) to that of the simple cyclization of the trimer? If so, then further self-assembly can be treated in more approximate ways.

Table 33 Free energy ($kJmol^{-1}$) change in the gas phase and in solution and other thermodynamical properties at 0, 298 and 450K, in the fusion of two 3-rings into a double 3-ring. This reaction involves three condensations; the results are per condensation. See Figure 77.

		0K	298K			450K		
	Reactants	ΔE_0	ΔH	$T\Delta S$	ΔG	ΔH	$T\Delta S$	ΔG
Gas	$3r + 3r$	-1	1	19	-19	-1	28	-28
	$3r + 3r^-$	-6	-3	21	-24	-4	32	-35
	$3r + 3r^{-2}$	-39	-36	21	-57	-37	32	-68
	$3r + 3r^{-3}$	-76	-73	21	-94	-74	31	-104
	$3r + 3r^{-4}$	-152	-149	23	-172	-149	34	-183
	$3r^- + 3r^-$	84	88	25	63	88	37	51
	$3r^- + 3r^{-2}$	160	164	25	139	164	38	126
	$3r^- + 3r^{-3}$	215	219	25	194	218	37	181
	$3r^{-2} + 3r^{-2}$	327	331	26	306	331	39	292
Sol.	$3r + 3r$	-4	-2	17	-20	-3	25	-28
	$3r + 3r^-$	-9	-5	23	-28	-6	34	-40
	$3r + 3r^{-2}$	-13	-10	22	-32	-10	32	-43
	$3r + 3r^{-3}$	-15	-11	23	-34	-11	35	-46
	$3r + 3r^{-4}$	-25	-22	22	-44	-22	32	-55
	$3r^- + 3r^-$	-8	-4	27	-30	-4	40	-44
	$3r^- + 3r^{-2}$	-4	1	28	-27	1	42	-42
	$3r^- + 3r^{-3}$	-2	2	25	-23	1	38	-36
	$3r^{-2} + 3r^{-2}$	4	8	25	-17	7	37	-30

4.5.7.3 The formation of a double 6-ring

The double 6-ring is a key feature found in numerous zeolitic frameworks, but is not detected in silicate solutions. If not present as a solution species, then perhaps is it formed as the further condensation of 4-ring containing species? This postulate can be probed by considering two alternative routes: by the condensation of two 6-rings (Table 34) and from three 4-rings (Table 35). The reactants and the double 6-ring are shown in Figure 78.

The overall enthalpy changes of the d6-ring to be formed by both routes are similar: the reactions are endothermic when the charge is distributed in the reactants, while when one of the reactants is neutral, the reactions are exothermic. Although the entropy change for both routes is positive, it is higher when 6-rings condense.

A comparison of the free energies for both routes shows that in the gas phase it is more feasible to form a d6-ring from the 4-rings. However, in solution the free energies are almost the same. As explained, before the 6-ring is not observed in silicate solutions. The results of this section, however, suggest that if 6-rings were present, (which have previously shown to be unlikely) they are as likely to form a d6-ring as it would be from the experimentally observed 4-ring (which we already have seen are a major solution species). This observation is important because the 6-ring is a more specific species to certain zeolites (for example the ones containing d6-rings) than the 4-ring, *i.e.* 4-rings can form a d6-ring or a d4-ring. Nevertheless, d6-ring formation is statistically more likely from 4-rings, and as result these show that such a structure could form.

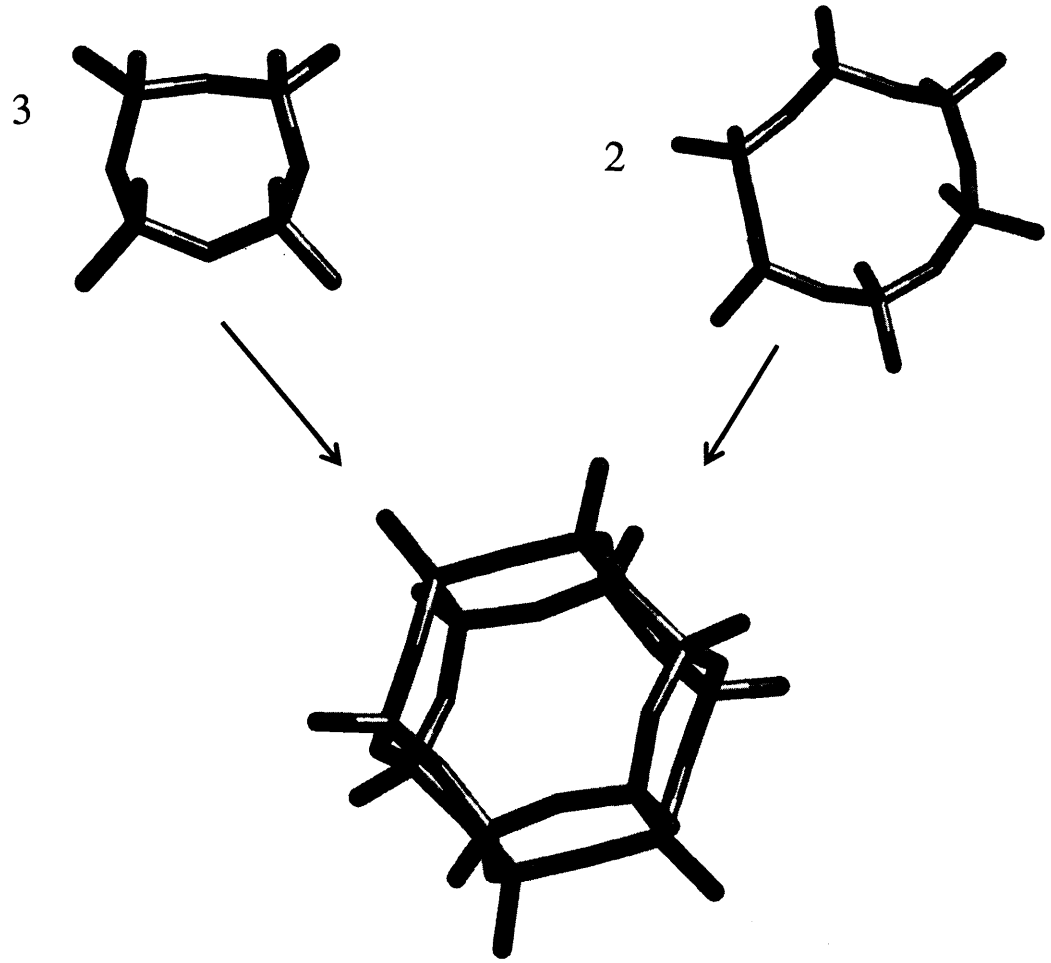

Figure 78 The condensation of three 4-rings into a double 6-ring, and the fusion of two six rings into a double 6-ring. See Table 35 and Table 34.

Table 34 Free energy ($kJmol^{-1}$) change in the gas phase and in solution and other thermodynamical properties at 0, 298 and 450K, in the fusion of two six rings into a double 6-ring. This reaction involves six condensations; the results are per condensation. See Figure 78.

		0K	298K			450K		
	Reactants	ΔE_0	ΔH	$T\Delta S$	ΔG	ΔH	$T\Delta S$	ΔG
Gas	6r + 6r	0	2	26	-24	0	37	-37
	6r + $6r^-$	5	8	33	-24	8	49	-41
	6r + $6r^{-2}$	-3	1	31	-30	0	46	-46
	6r + $6r^{-3}$	-21	-18	30	-48	-19	45	-64
	6r + $6r^{-4}$	-41	-38	29	-68	-39	43	-83
	$6r^-$ + $6r^-$	43	47	31	16	47	47	0
	$6r^-$ + $6r^{-2}$	78	82	31	51	81	46	35
	$6r^-$ + $6r^{-3}$	98	102	30	72	101	44	57
	$6r^{-2}$ + $6r^{-2}$	152	155	30	125	155	45	109
Sol.	6r + 6r	-1	3	31	-29	2	47	-45
	6r + $6r^-$	0	5	36	-31	5	54	-49
	6r + $6r^{-2}$	1	6	34	-28	6	52	-46
	$6r^-$ + $6r^-$	2	7	33	-27	6	50	-44

Table 35 Free energy ($kJmol^{-1}$) change in the gas phase and in solution and other thermodynamical properties at 0, 298 and 450K, in the condensation of three 4-rings into a double 6-ring. This reaction involves six condensations; the results are per condensation. See Figure 78.

		0K	298K			450K		
	Reactants	ΔE_0	ΔH	$T\Delta S$	ΔG	ΔH	$T\Delta S$	ΔG
Gas	4r + 4r + 4r	-10	-9	11	-20	-10	16	-26
	4r + $4r^-$ + 4r	-10	-6	20	-26	-7	30	-37
	4r + $4r^{-2}$ + 4r	-38	-35	17	-52	-35	26	-61
	4r + $4r^{-3}$ + 4r	-80	-78	15	-93	-79	22	-101
	4r + $4r^{-4}$ + 4r	-134	-132	14	-146	-133	20	-153
	$4r^-$ + $4r^-$ + 4r	25	28	21	8	28	31	-3
	$4r^-$ + $4r^{-2}$ + 4r	39	42	19	23	42	28	14
	$4r^-$ + $4r^{-3}$ + 4r	36	38	16	21	37	24	13
	$4r^{-2}$ + $4r^{-2}$ + 4r	93	95	17	78	94	25	69
	$4r^-$ + $4r^-$ + $4r^-$	102	105	22	83	105	33	72
	$4r^-$ + $4r^-$ + $4r^{-2}$	155	158	20	138	157	30	127
Sol.	4r + 4r + 4r	-7	-3	23	-26	-2	36	-38
	4r + $4r^-$ + 4r	-6	-1	27	-27	0	41	-41
	4r + $4r^{-2}$ + 4r	-11	-6	24	-31	-6	38	-43
	$4r^-$ + $4r^-$ + 4r	-3	1	24	-22	2	36	-34

4.5.7.4 The d4-ring

The d4-ring is an interesting cluster, since, in contrast to the d6-ring, it is widely observed in silicate solutions[3, 34] but only forms part of one pure siliceous zeolite framework (LTA, zeolite A)[xvi]. This opens the question of the role of d4-rings in zeolite nucleation, and as with the 3-rings, of their fate during synthesis.

We analyse in detail the formation of this important cage, surveying all the structures, which condense gradually from the 4-ring to the d4-ring (see Figure 79).

We will start by analysing the formation of the d4-ring with the addition of a dimer to the fused 4-ring (Table 36). This reaction forms a new 4-ring after adding a dimer. The reaction is exothermic for most of the conditions studied here; and the free energy is favourable to the formation both in the gas phase and in solution, and is more likely at high temperatures. However, we note that the reaction is less favourable when high charged species are involved.

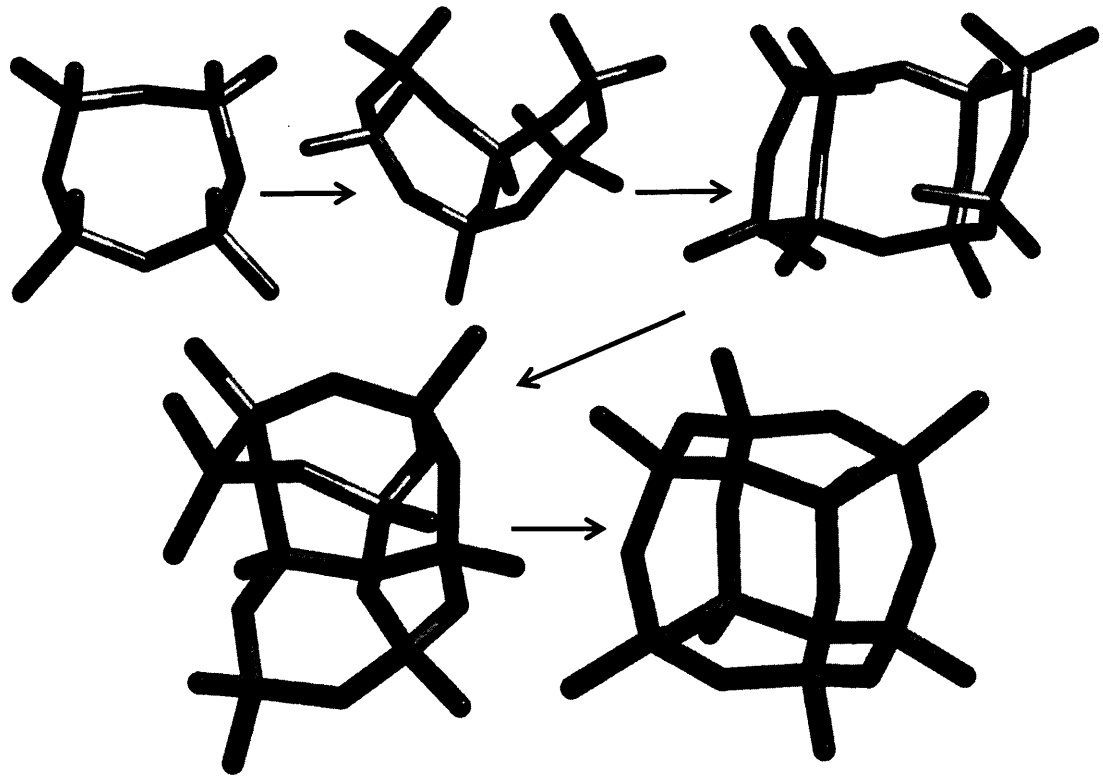

Figure 79 The formation of a double 4-ring starting from a 4-ring. The steps analysed are: addition of a dimer to a fused 4-ring, then an internal condensation to produce the open double 4-ring and finally the condensation to produce the double 4-ring. See Table 36 to Table 39.

[xvi] The d4-ring is found in aluminosilicates zeolites. Furthermore siliceous zeolite A can only be formed in a fluoride media and not in the traditional hydroxide mediated synthesis.

Table 36 Free energy ($kJmol^{-1}$) change in the gas phase and in solution and other thermodynamical properties at 0, 298 and 450K, in the condensation of a fused 4-ring and a dimer. This reaction has two condensations and there is a new ring. See Figure 79.

		0K	298K			450K		
	Reactants	ΔE_0	ΔH	$T\Delta S$	ΔG	ΔH	$T\Delta S$	ΔG
Gas	f4r + D	-33	-26	23	-49	-25	36	-61
	$f4r^-$ + D	-311	-167	-42	-231	-297	-93	-157
	$f4r^{-2}$ + D	-56	-55	2	-57	-57	1	-57
	$f4r^{-3}$ + D	-335	-211	-42	-257	-335	-92	-184
	$f4r^{-4}$ + D	-371	-256	-41	-294	-378	-91	-223
	$f4r^-$ + D^-	74	77	10	66	77	16	61
	$f4r^{-2}$ + D^-	-58	66	-44	22	-59	-96	96
	$f4r^{-3}$ + D^-	54	170	-39	129	49	-86	200
	$f4r^{-2}$ + D^{-2}	123	237	-43	201	116	-93	274
Sol.	f4r + D	-11	-7	11	-18	-7	17	-24
	$f4r^-$ + D	-15	-11	16	-27	-11	24	-35
	$f4r^{-2}$ + D	-22	-19	9	-28	-19	14	-33
	$f4r^{-3}$ + D	-16	-14	9	-23	-14	13	-27
	$f4r^-$ + D^-	-12	-10	12	-21	-10	17	-27
	$f4r^{-2}$ + D^-	7	10	10	0	9	14	-5

Table 37 Free energy ($kJmol^{-1}$) change in the gas phase and in solution and other thermodynamical properties at 0, 298 and 450K, for the internal condensation of a 3-4-ring into an open double 4-ring. See Figure 79.

		0K	298K			450K		
	Reactants	ΔE_0	ΔH	$T\Delta S$	ΔG	ΔH	$T\Delta S$	ΔG
Gas	3-4r	24	29	47	-18	28	70	-42
	$3\text{-}4r^-$	634	356	156	413	616	295	227
	$3\text{-}4r^{-2}$	103	111	61	50	112	94	18
	$3\text{-}4r^{-3}$	583	343	148	372	591	280	193
	$3\text{-}4r^{-4}$	564	344	146	356	584	276	180
Sol.	3-4r	5	9	45	-36	9	67	-58
	$3\text{-}4r^-$	38	43	45	-2	43	67	-24
	$3\text{-}4r^{-2}$	62	69	55	14	69	83	-14
	$3\text{-}4r^{-3}$	30	32	52	-19	29	74	-45

Table 38 Free energy ($kJmol^{-1}$) change in the gas phase and in solution and other thermodynamical properties at 0, 298 and 450K, for the internal condensation to produce a double 4-ring. See Figure 79.

		0K	298K			450K		
	Reactants	ΔE_0	ΔH	$T\Delta S$	ΔG	ΔH	$T\Delta S$	ΔG
Gas	open-d4r	18	19	37	-17	18	53	-35
	open-d4r$^-$	70	69	26	43	67	37	30
	open-d4r^{-2}	66	65	24	41	63	34	29
	open-d4r^{-3}	106	107	33	74	106	49	57
	open-d4r^{-4}	119	119	32	87	118	47	71
Sol.	open-d4r	17	18	42	-23	16	60	-44
	open-d4r$^-$	47	47	35	13	46	50	-5
	open-d4r^{-2}	41	42	32	9	41	48	-7
	open-d4r^{-3}	59	65	38	27	67	61	7
	open-d4r^{-4}	63	67	41	26	67	62	6

Table 39 Free energy ($kJmol^{-1}$) change in the gas phase and in solution and other thermodynamical properties (divided by the number of condensations, 4) at 0, 298 and 450K, in the fusion of two 4-rings into a double 4-ring. See Figure 79.

		0K	298K			450K		
	Reactants	ΔE_0	ΔH	$T\Delta S$	ΔG	ΔH	$T\Delta S$	ΔG
Gas	4r + 4r	-5	-1	22	-23	-2	33	-35
	4r + 4r$^-$	5	8	23	-15	7	34	-26
	4r + 4r^{-2}	-14	-11	23	-33	-11	34	-45
	4r + 4r^{-3}	-48	-45	21	-66	-46	31	-77
	4r + 4r^{-4}	-93	-90	21	-111	-91	31	-122
	4r$^-$ + 4r$^-$	80	84	28	56	83	41	42
	4r$^-$ + 4r^{-2}	131	135	27	108	135	40	94
	4r$^-$ + 4r^{-3}	161	164	25	139	164	37	127
	4r^{-2} + 4r^{-2}	247	250	26	224	250	39	211
Sol.	4r + 4r	-6	0	32	-32	1	49	-48
	4r + 4r$^-$	4	9	29	-20	9	45	-35
	4r + 4r^{-2}	4	9	29	-20	9	44	-35
	4r + 4r^{-3}	-1	4	29	-25	4	45	-40
	4r + 4r^{-4}	-5	-1	29	-30	-1	44	-45
	4r$^-$ + 4r$^-$	17	20	28	-8	20	42	-22
	4r$^-$ + 4r^{-2}	21	25	29	-3	25	43	-18
	4r$^-$ + 4r^{-3}	20	24	28	-5	23	42	-19
	4r^{-2} + 4r^{-2}	30	33	29	5	33	43	-10

The fused 4-ring can also form the double 3-ring, as discussed in section 4.5.7.2, so the addition of a dimer to the fused 4-ring is a reaction, which competes with this internal condensation. In the gas phase under most conditions, the addition of a dimer to the fused 4-ring is much more favoured than its internal condensation. In solution at room temperature, the addition of a dimer again is more favourable, but at 450K, both reactions have almost the same free energy change. Thus, at low temperatures, the formation of a precursor for the d4-ring is more likely than the formation of a d3-ring. Perhaps, here we see why the siliceous d4-rings are observed under typical hydrothermal conditions?

The first internal condensation of the previous cluster (a three 4-ring fused by the side, see Figure 79) produces an open double 4-ring (Table 37). This reaction in the gas phase shows a surprising high positive change in enthalpy; the entropy change is as well positive and the free energy is largely positive. However, in solution, the enthalpy of the reaction is slightly positive and the entropy is similar to that for small ring condensations. This reaction seems more likely to occur at high temperature and low charge (lower pH).

The final step for the formation of a d4-ring is the condensation of an open d4-ring into a d4-ring (Table 38); the reverse reaction is of course also the first step in the dissolution of a d4-ring.

As with previous cyclization reactions, this reaction has positive changes in the enthalpy, but it is less endothermic than the last stage of internal condensation of the 3-sided cube. The entropy is similar to that for single cyclizations presented before in section 4.5.3 (page 140). As in the previously considered condensations, the reaction is again more favoured at low charge and higher temperature.

In conclusion, d4-ring formation will be more favourable when the charge is low and the temperature is high. Consequently, increasing the charge (high pH) at low temperatures could lead to the opening of the d4-ring.

Alternatively, the d4-ring can be formed from the assembly of two 4-rings. In this condensation, the enthalpy change is strongly endothermic when high charges are involved, and the highest values are found when the charge is distributed into the reactants. The entropy change is almost constant and positive at 298K and 450K for the gas phase and in solution, having twice the value at 450K than at 298K. In the gas phase

and in solution, the reaction is feasible when the charge is only on one of the 4-rings. In solution, the reaction is more likely at high temperature. Therefore, two 4-rings are less favoured to condense, if both have a charge and the temperature is 298K, this restricts the formation of a d4-ring under these conditions. However, other routes could be available, for example, the addition of dimers.

4.5.7.5 Reactions involving cages

The reactions of small cages (including the d4-ring and d6-ring) can be considered as models for the formation of zeolite nuclei (and to the crystal growth). If the cages are indeed formed as isolated species then to grow further they have to condense with either a small oligomer or with another cage or ring. Both possibilities are studied here. The results obtained in this section could be used as an initial approximation for the modelling of a growing surface, because a cage could be interpreted as a limiting case of a surface *i.e.* the smallest surface possible.

The first case is the addition of a monomer to a d4-ring cage: the reactant and product are shown in Figure 80[xvii]. In this reaction, the enthalpy is exothermic when at least one

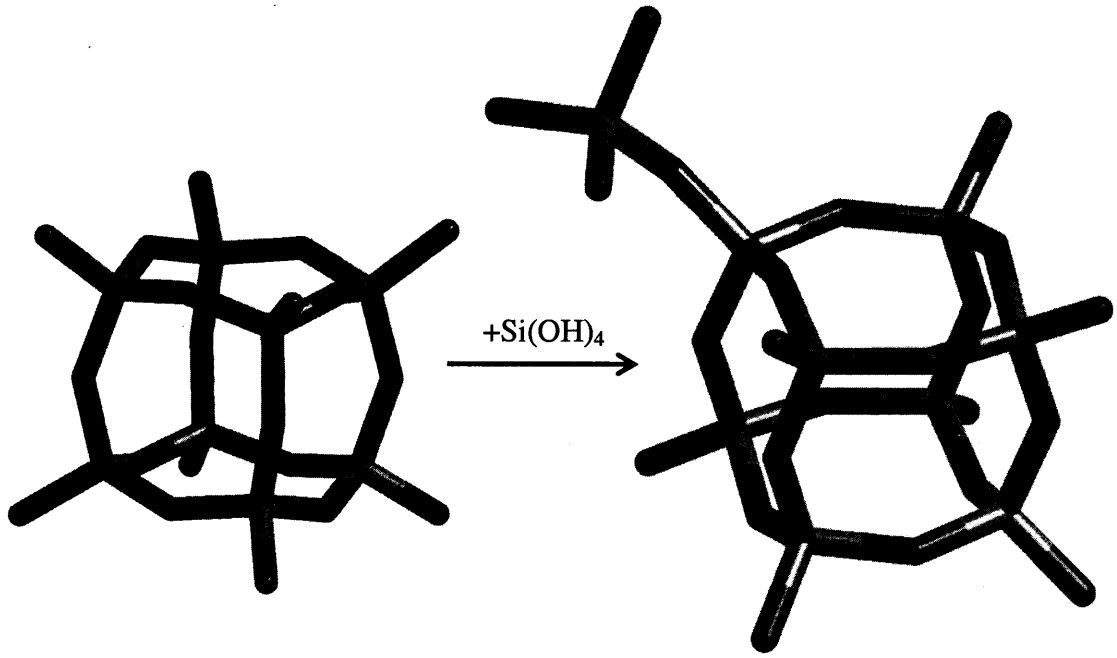

Figure 80 The condensation of a d4-ring and a monomer. See Table 40.

[xvii] The d4-ring with a dangling monomer is observed in silicate solutions[31].

Table 40 Free energy ($kJmol^{-1}$) change in the gas phase and in solution and other thermodynamical properties at 0, 298 and 450K, in the condensation of a d4-ring and a monomer. See Figure 80.

		0K	298K			450K		
	Reactants	ΔE_0	ΔH	$T\Delta S$	ΔG	ΔH	$T\Delta S$	ΔG
Gas	d4r + M	-19	-13	3	-15	-12	5	-17
	$d4r^-$ + M	-70	-63	6	-69	-61	11	-72
	$d4r^{-2}$ + M	-98	-92	3	-95	-92	4	-96
	d4r + M^-	-172	-169	-12	-157	-170	-19	-151
	$d4r^-$ + M^-	59	65	0	66	67	1	66
	d4r + M^{-2}	-549	-546	-13	-533	-547	-20	-527
Sol.	d4r + M	-12	-6	-1	-5	-4	1	-5

of the reactants is neutral (Table 40), while the entropy change is almost negligible, as in the small linear condensations. Hence, the enthalpy change determines the feasibility of the reaction. Therefore, the addition of small deprotonated oligomers seems the most favoured route for this reaction: in particular, we note that the high enthalpy is released when a deprotonated monomer reacts with a d4-ring.

This behaviour is readily rationalized in the context of the synthesis mixture: we have found previously how monomer (and dimer) species will be spontaneously deprotonated. Furthermore, we have also seen how the neutral d4-ring is the most likely product in the proposed route (see section 4.5.7.4); however the deprotonation of the d4-ring is also feasible.

We now consider how larger cage structures may react with each other. The condensation of two d4-rings[xviii] is presented in Figure 81 and in Table 41. The modelling of the dimer of d4-rings requires a considerable computational effort, and hence only the neutral gas phase model was considered.

Comparing with the previous result, the addition of two d4-rings is more likely than a monomer. This result is important because it shows how cages might condense. However, the conclusion is preliminary, because investigation of the charged (high pH) and solvated species is necessary to corroborate this trend.

[xviii] d4-d4-ring, the product shown in Figure 81 in silicate solutions[31].

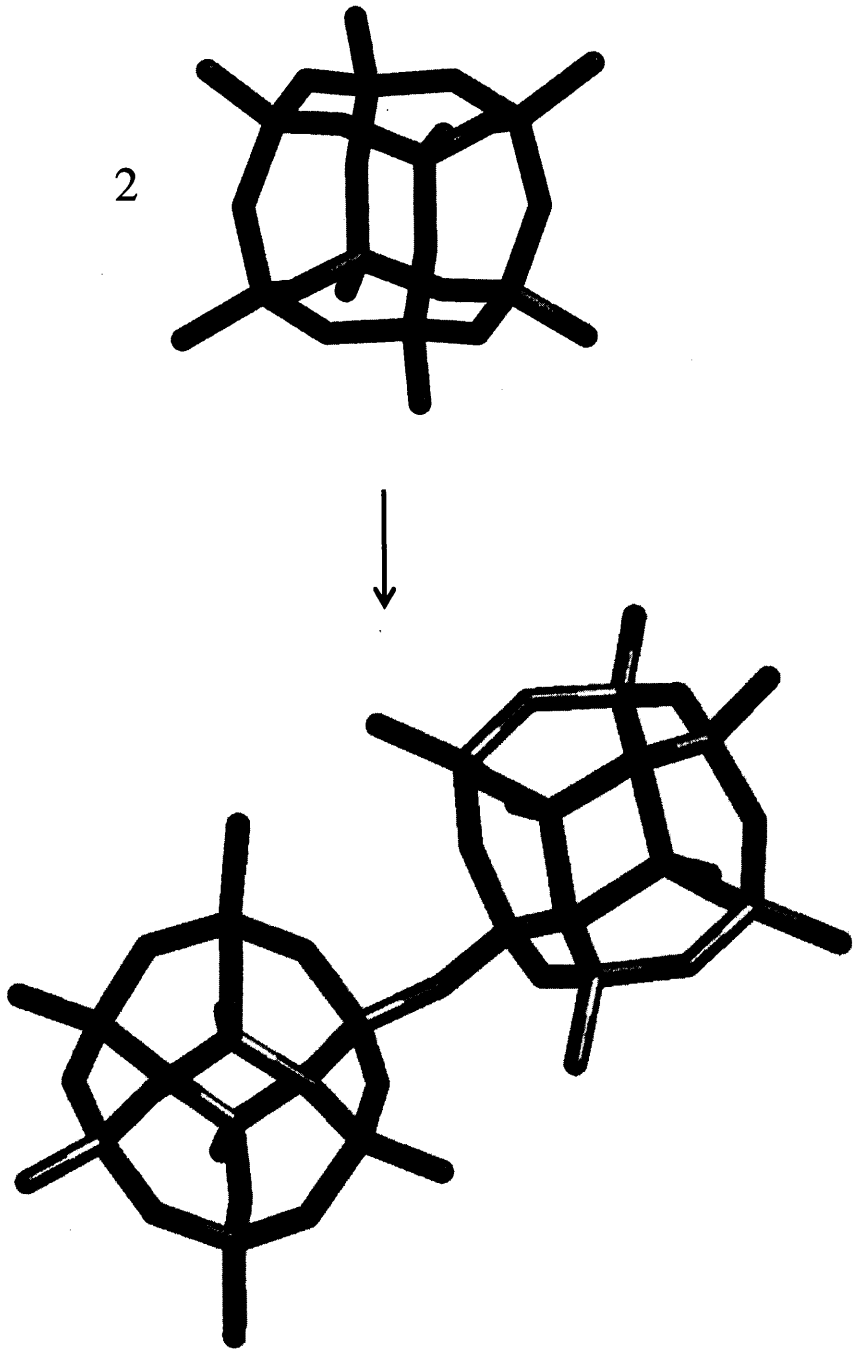

Figure 81 The condensation of two d4-rings. See Table 41.

Table 41 Free energy ($kJmol^{-1}$) change in the gas phase and other thermodynamical properties at 0, 298 and 450K, in the fusion of two d4-rings. See Figure 81.

	0K	298K			450K		
Reactants	ΔE_0	ΔH	$T\Delta S$	ΔG	ΔH	$T\Delta S$	ΔG
d4r + d4r	-45	-43	-22	-22	-45	-35	-10

4.6 General nucleation analysis

The general approach followed to analyse the reactions taking place in zeolite nucleation was to study reactions sharing some similarities; for example the oligomerization, cyclization, monomer addition to a ring, etc. We now consider a more global view of these reactions and how they are inter-linked, with the aim of establishing more general ideas of the relative population of the different species during nucleation.

In this section a series of diagrams (Figure 82 to Figure 101), showing reactions for the different clusters studied in this thesis, are presented. The aim of the section is to show some important trends and to offer another view of the complex series of reactions studied here. The analysis here is limited to neutral species and monocharged species (the charge always being on the larger cluster), because studying all the possible reactions for the different charged species expands the number of results considerably.

Each of the reactions presented here has already been considered in detail. This section rather then provides a reference resource for all the processes considered. Of particular note for future work are the free energies at 450K in COSMO solvation (Figure 91 and Figure 101).

The analysis of the data in this section (Figure 82 to Figure 101) is presented in the following order: Figure 82 to Figure 91 show results for the neutral condensations in the gas phase and COSMO solvation; Figure 92 to Figure 101 then show the same, but for the condensation of a monocharged species (the charge always being on the larger cluster).

In the gas phase (Figure 82) the neutral condensations show a general trend: oligomerization is favoured over cyclization. The more exothermic reactions are found for the larger oligomers and the most endothermic when a second ring forms. However, temperature has little effect on the enthalpy change, and the contribution of the ZPE is more significant (Figure 84 and Figure 85).

Free energy changes suggest that in the gas phase most of the reactions presented are feasible, with few exceptions such as internal cyclization forming rings like the 4-ring and the 6-ring (Figure 86). However, cyclizations are more exergonic than oligomerizations. Increasing the temperature (from 298 to 450K) promotes cyclization

with even more exergonic reactions, while the oligomerizations become less exergonic (Figure 87). This highlights again our proposal that, at room temperature, certain reactions are favoured, while at higher temperatures other reactions are more feasible, *i.e.* temperature controls which species are likely to being form.

Solvation stabilizes neutral structures (Figure 93) and as a result, reactions in general are not as endothermic or exothermic as in the gas phase (there is a general tendency to go to near zero free energy). However, in solvation, the same trends are evident as in gas phase, with cyclization being unfavourable compared to oligomerization.

When solvation is included, the free energy for oligomerization indicates that these reactions are less likely than in gas phase. However, cyclization reactions become more favourable relative to the gas phase (Figure 90).

We now summarize the results in alkali media (high pH). For charged clusters in the gas phase, only oligomerization (or monomer addition) reactions are exothermic, while all cyclizations are endothermic (Figure 92). Again, as with the neutral species, the temperature has only a small effect on the enthalpy change (Figure 94 and Figure 95).

The free energy results for the charged clusters in the gas phase show that all the oligomerizations are feasible, while most of the cyclizations are still endergonic (Figure 96). Furthermore, as the temperature is raised (to 450K), cyclization becomes relatively more favourable; although they do not become dominant (Figure 97).

Solvation generally makes species more stable. Oligomerization reactions are certainly exothermic and cyclizations endothermic (Figure 98). Finally, the free energy for the charged clusters in solvation indicates that most of the reactions are feasible (almost all the reactions are exergonic, see Figure 100). But at higher temperature the cyclizations are favoured, whilst oligomerizations are not (Figure 101).

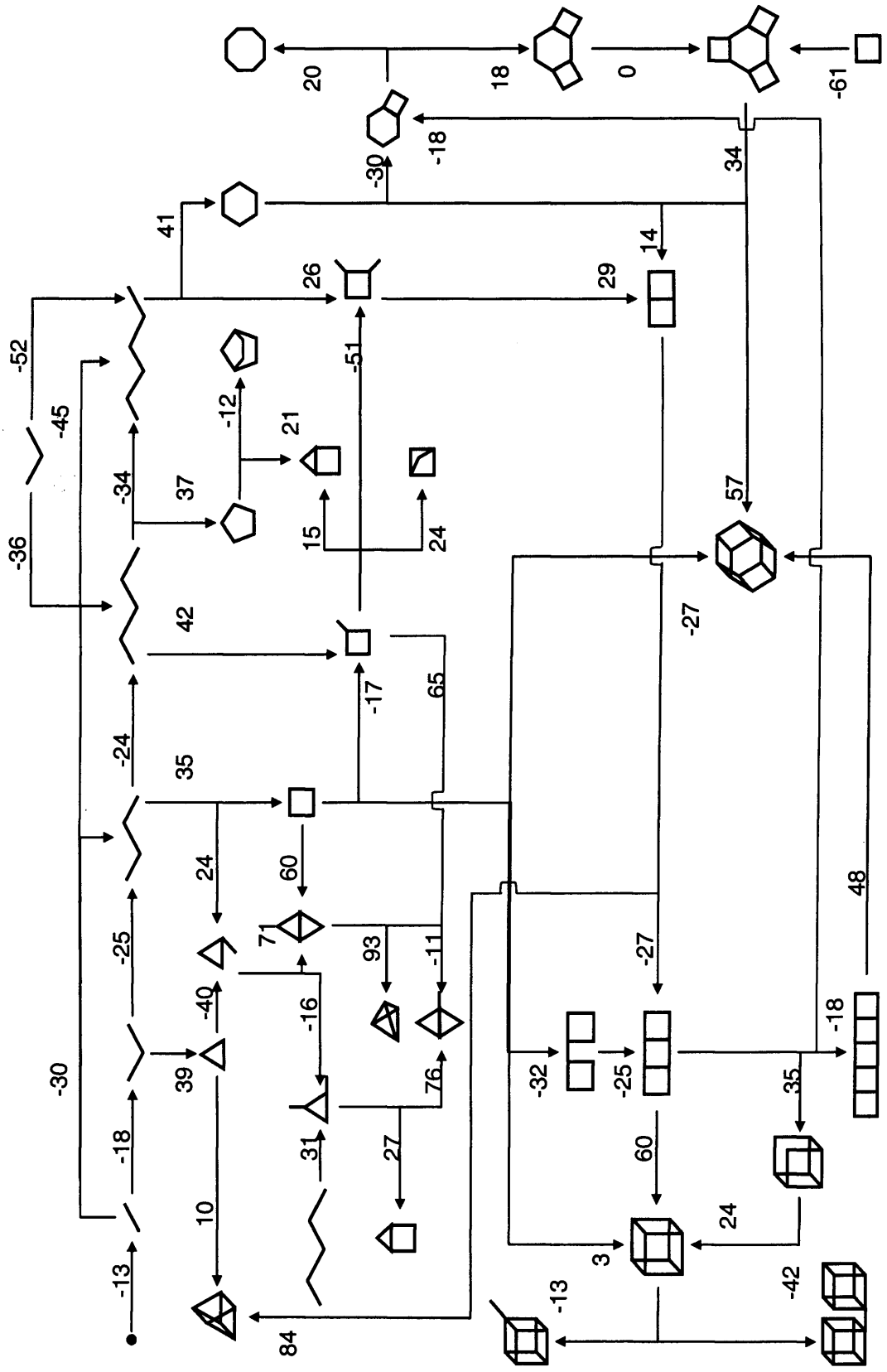

Figure 82 Reaction energies ($kJmol^{-1}$) at 0K in the gas phase.

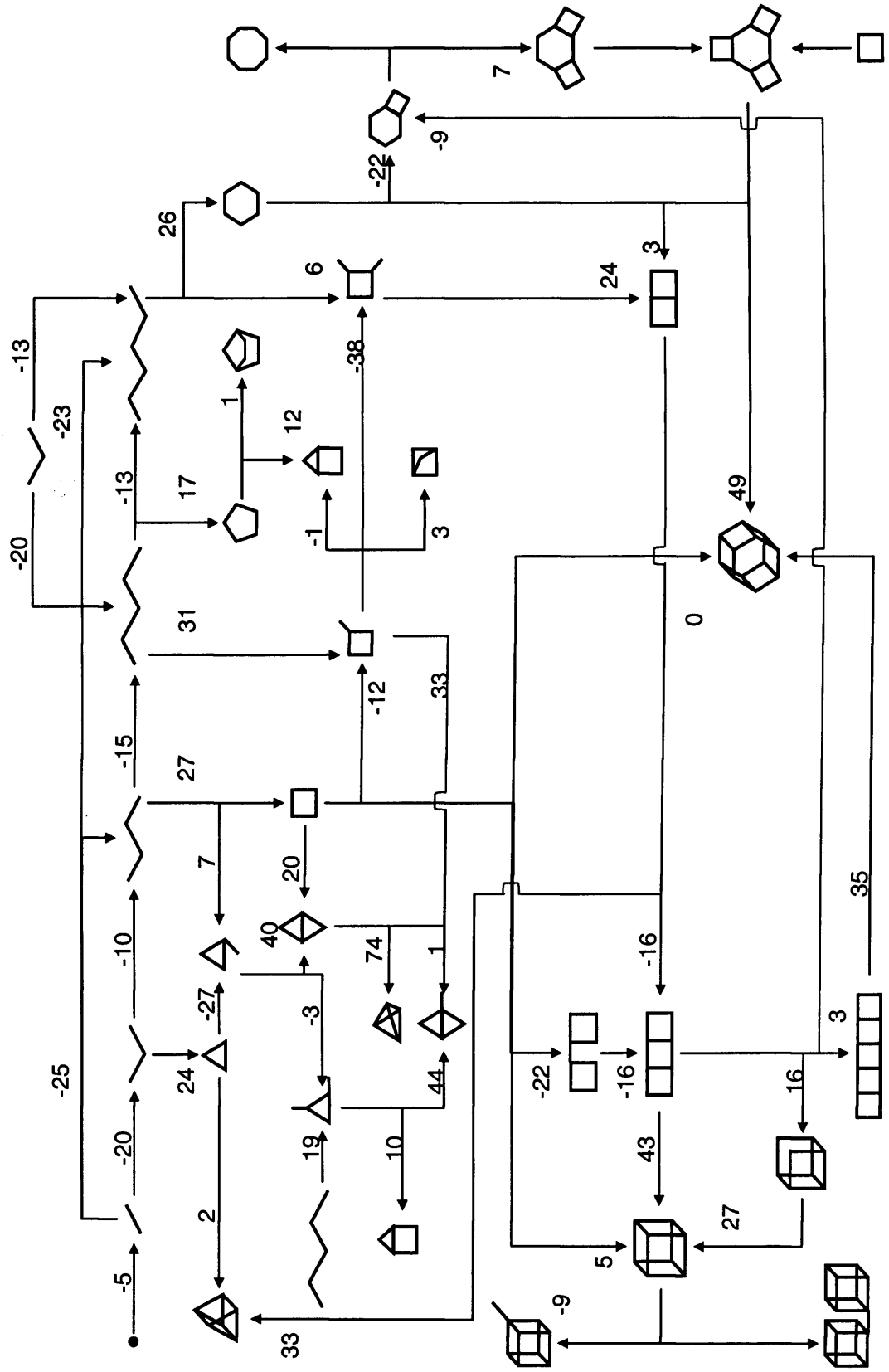

Figure 83 Reaction energies ($kJmol^{-1}$) at 0K in the COSMO solvation.

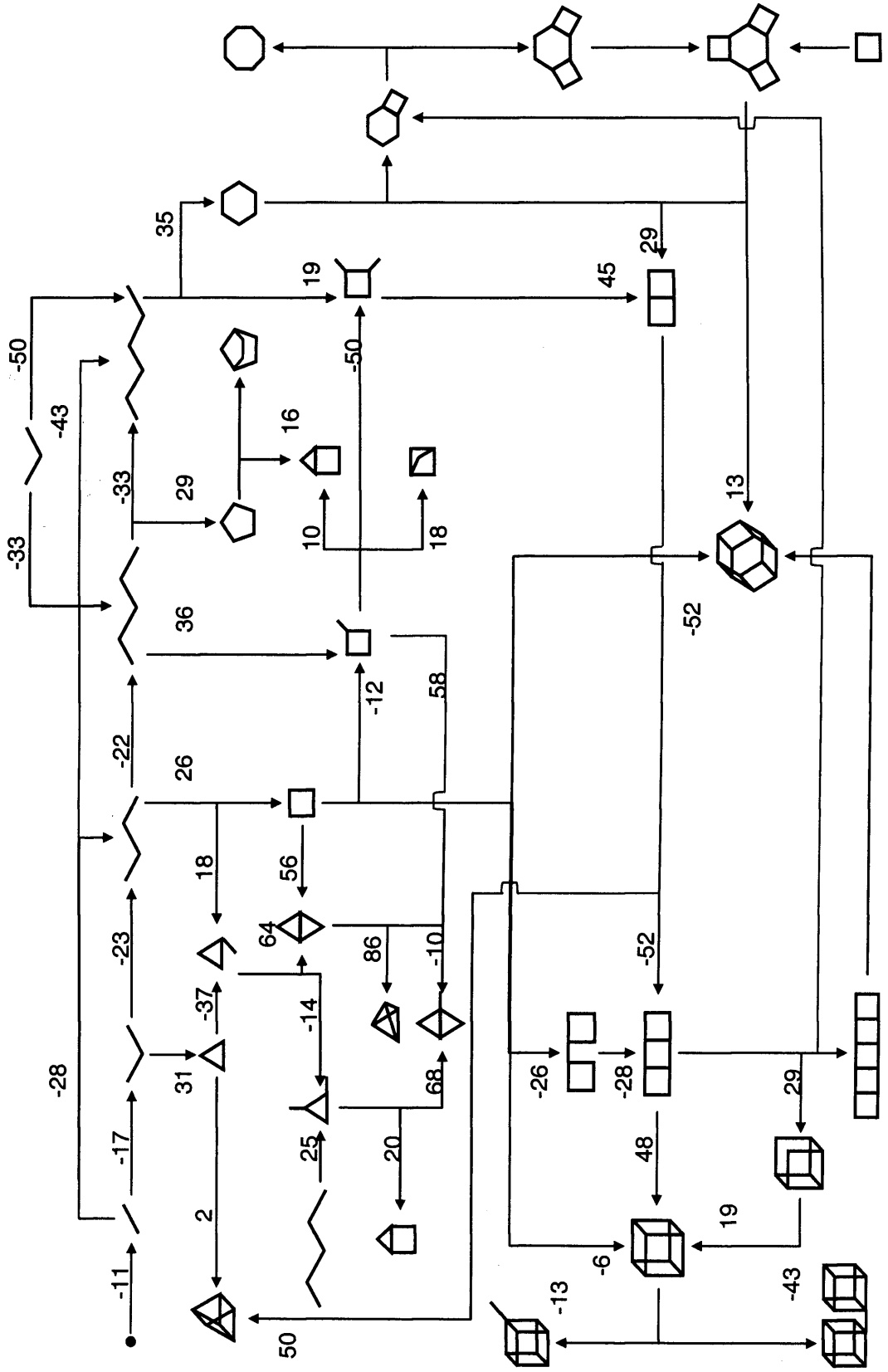

Figure 84 Reaction enthalpies ($kJmol^{-1}$) at 298K in the gas phase.

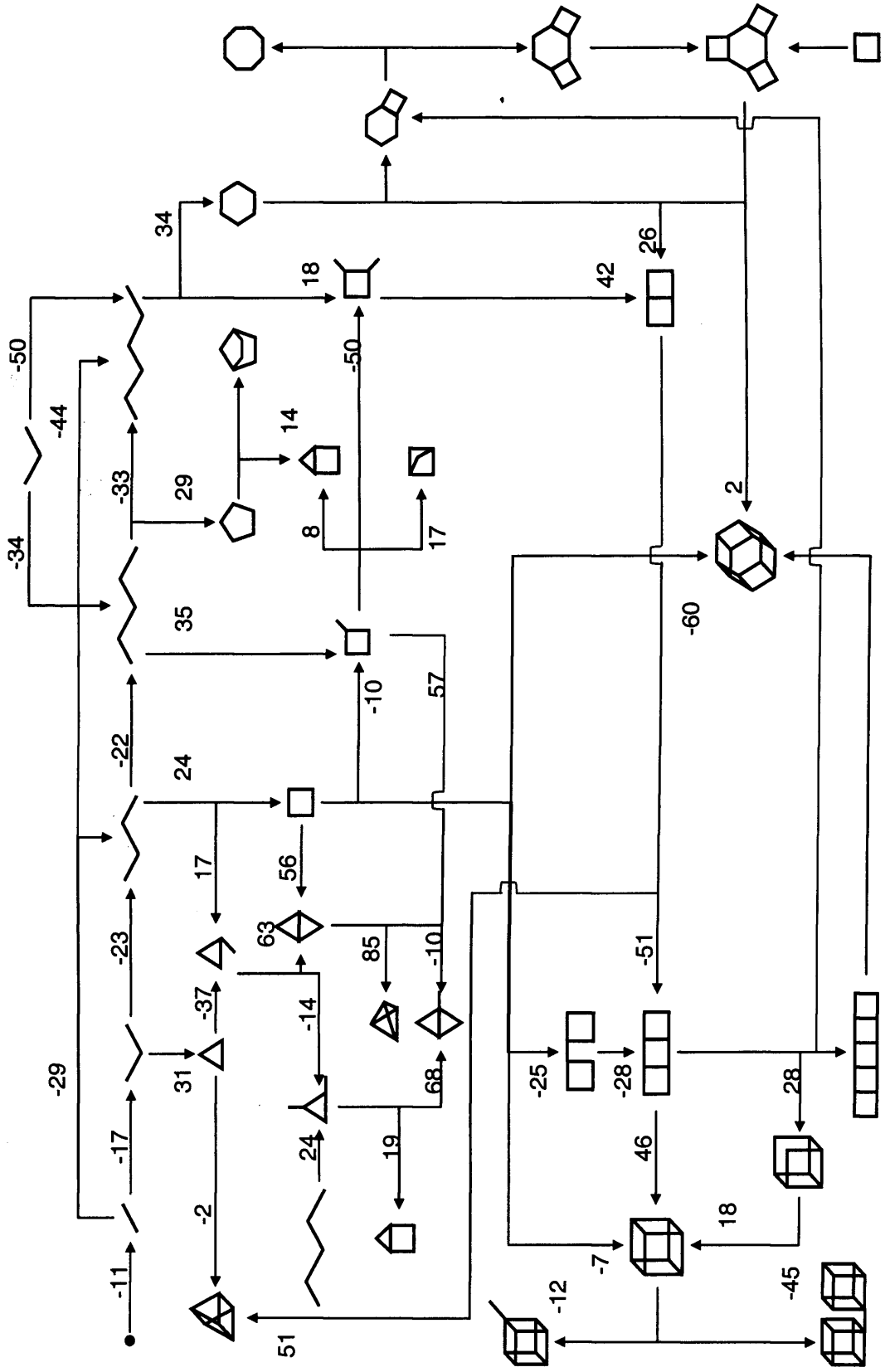

Figure 85 Reaction enthalpies (kJmol^{-1}) at 450K in the gas phase.

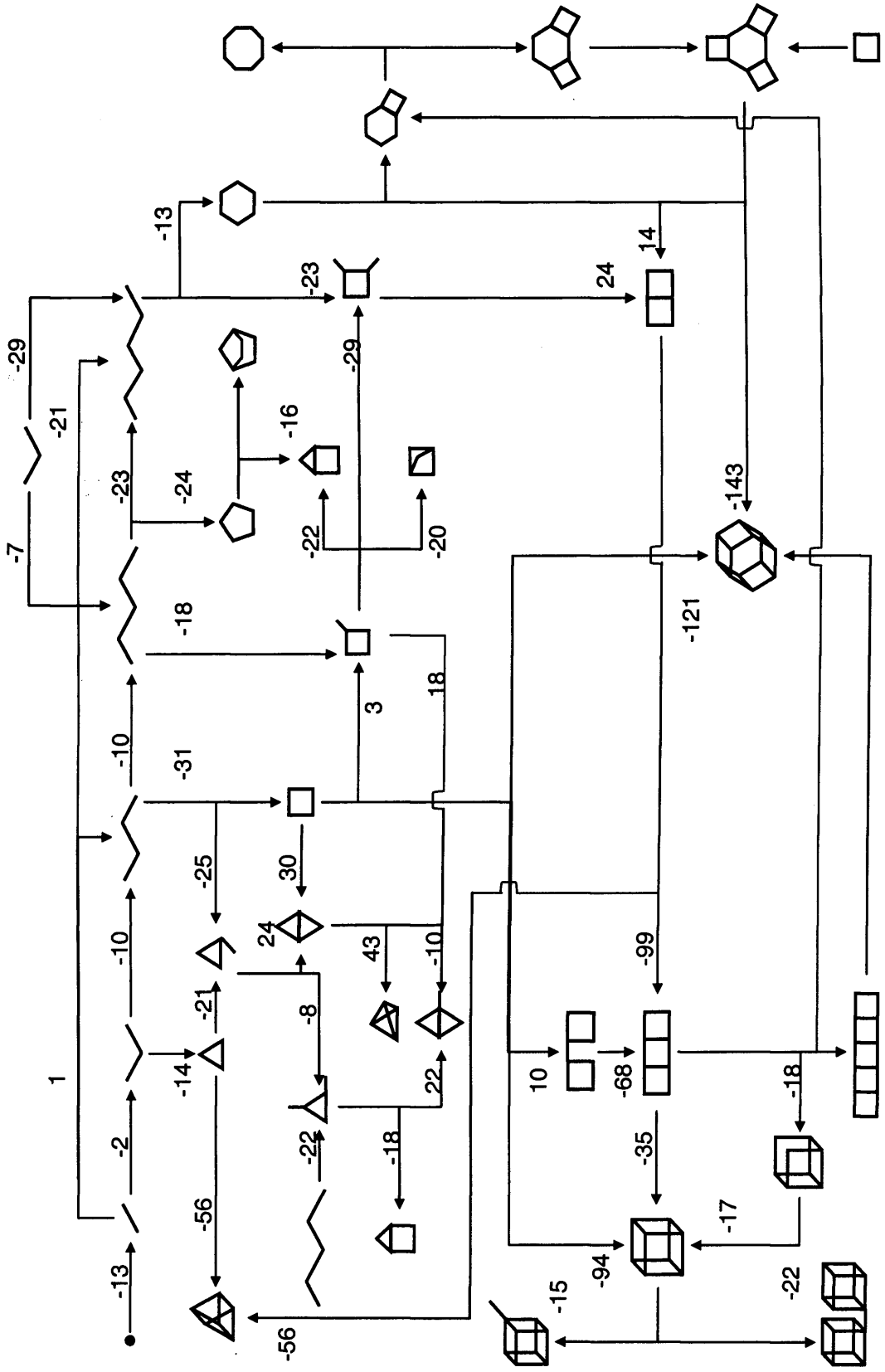

Figure 86 Reaction free energies ($kJmol^{-1}$) at 298K in the gas phase.

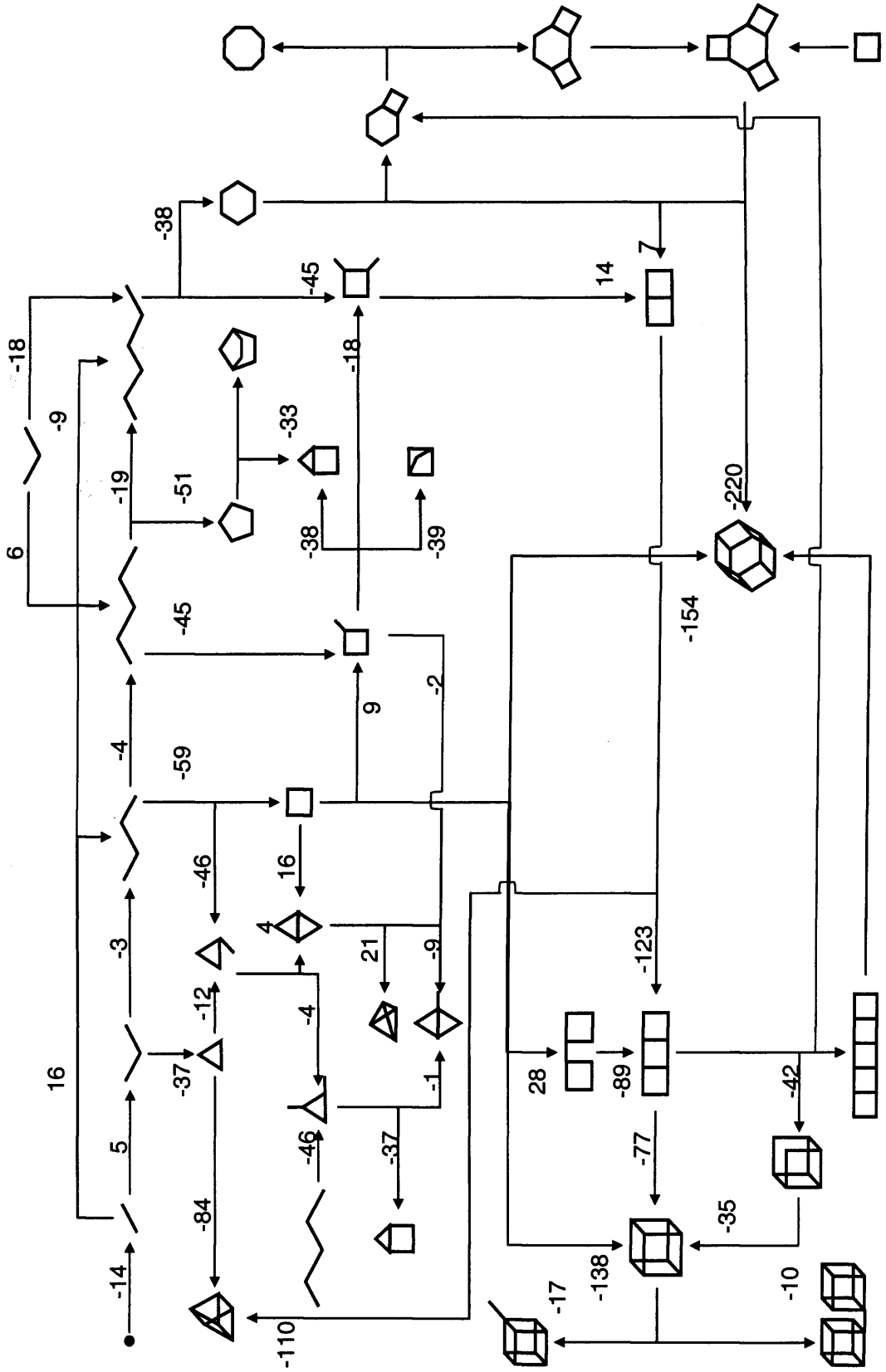

Figure 87 Reaction free energies ($kJmol^{-1}$) at 450 in the gas phase.

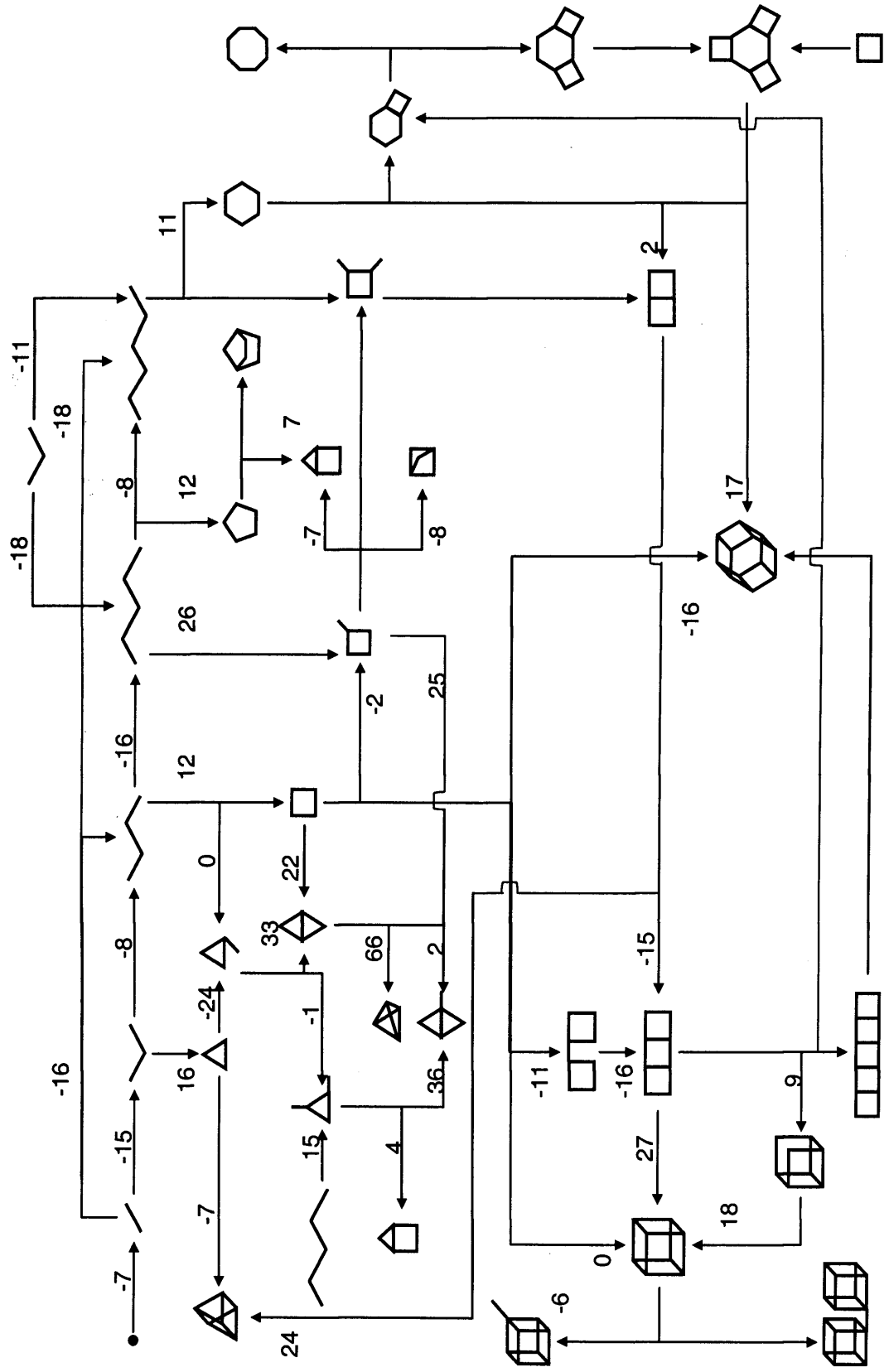

Figure 88 Reaction enthalpies ($kJmol^{-1}$) at 298K in the COSMO solvation.

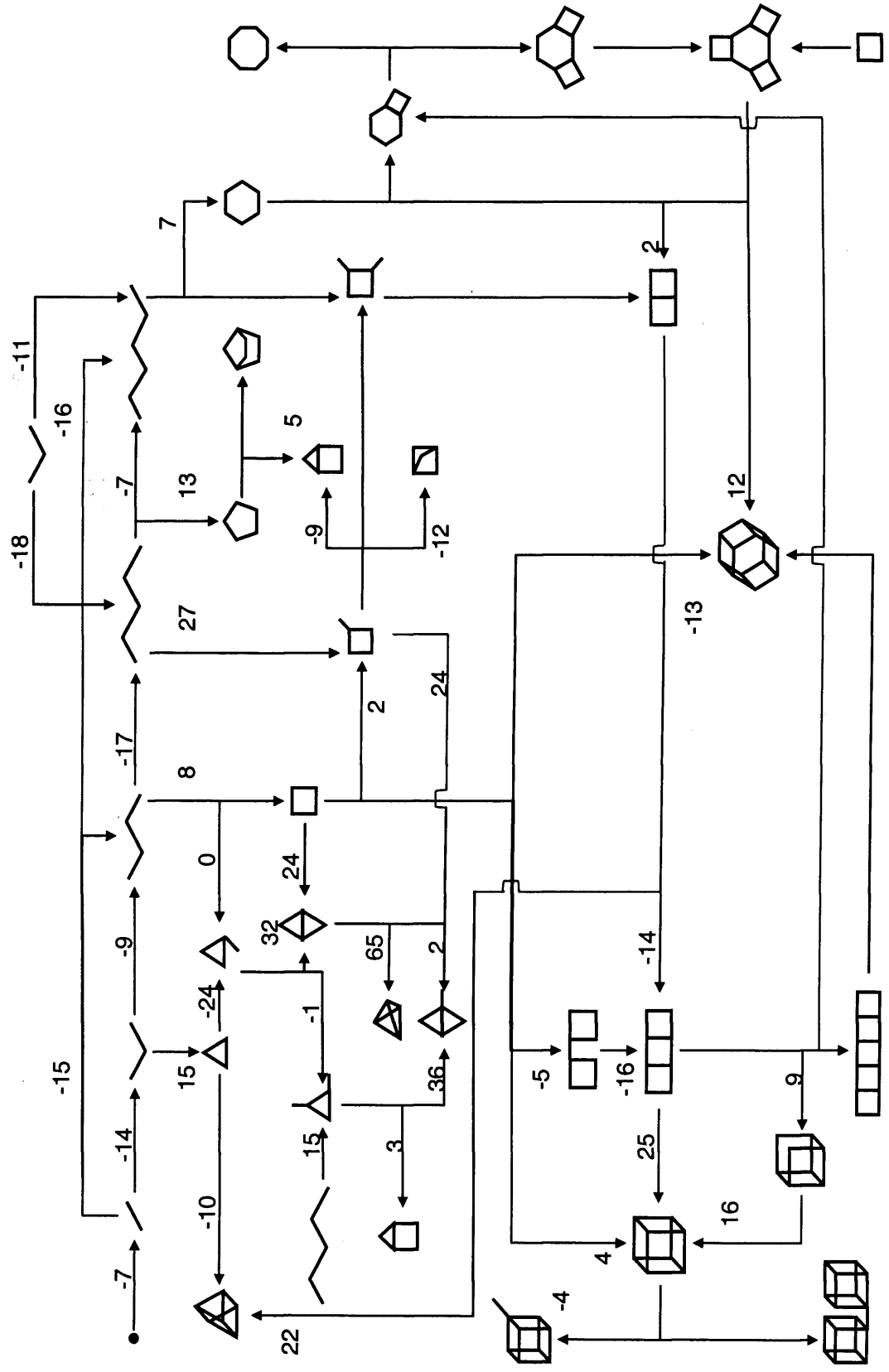

Figure 89 Reaction enthalpies ($kJmol^{-1}$) at 450K in the COSMO solvation.

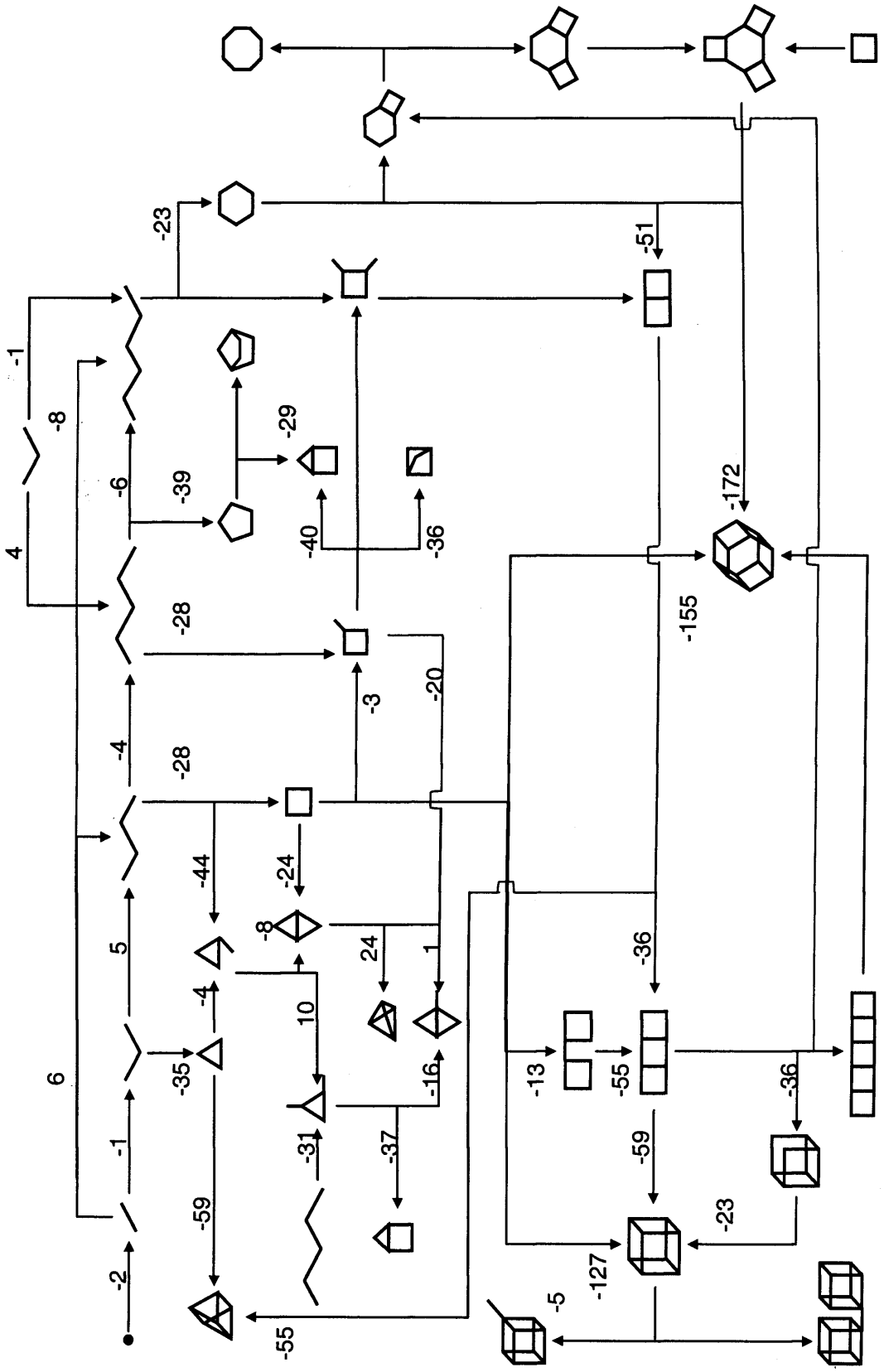

Figure 90 Reaction free energies ($kJmol^{-1}$) at 298K in the COSMO solvation.

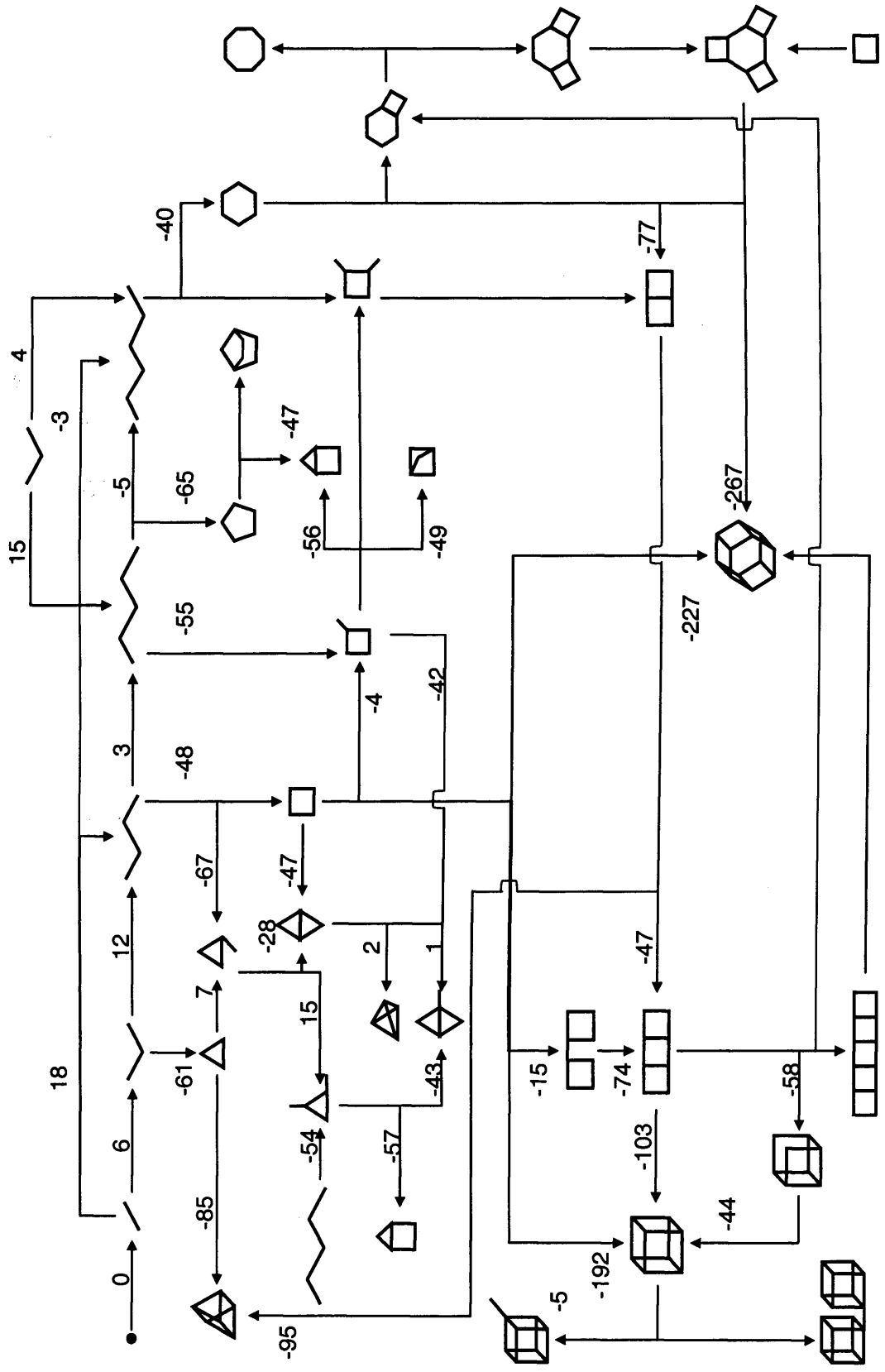

Figure 91 Reaction free energies ($kJmol^{-1}$) at 450K in the COSMO solvation.

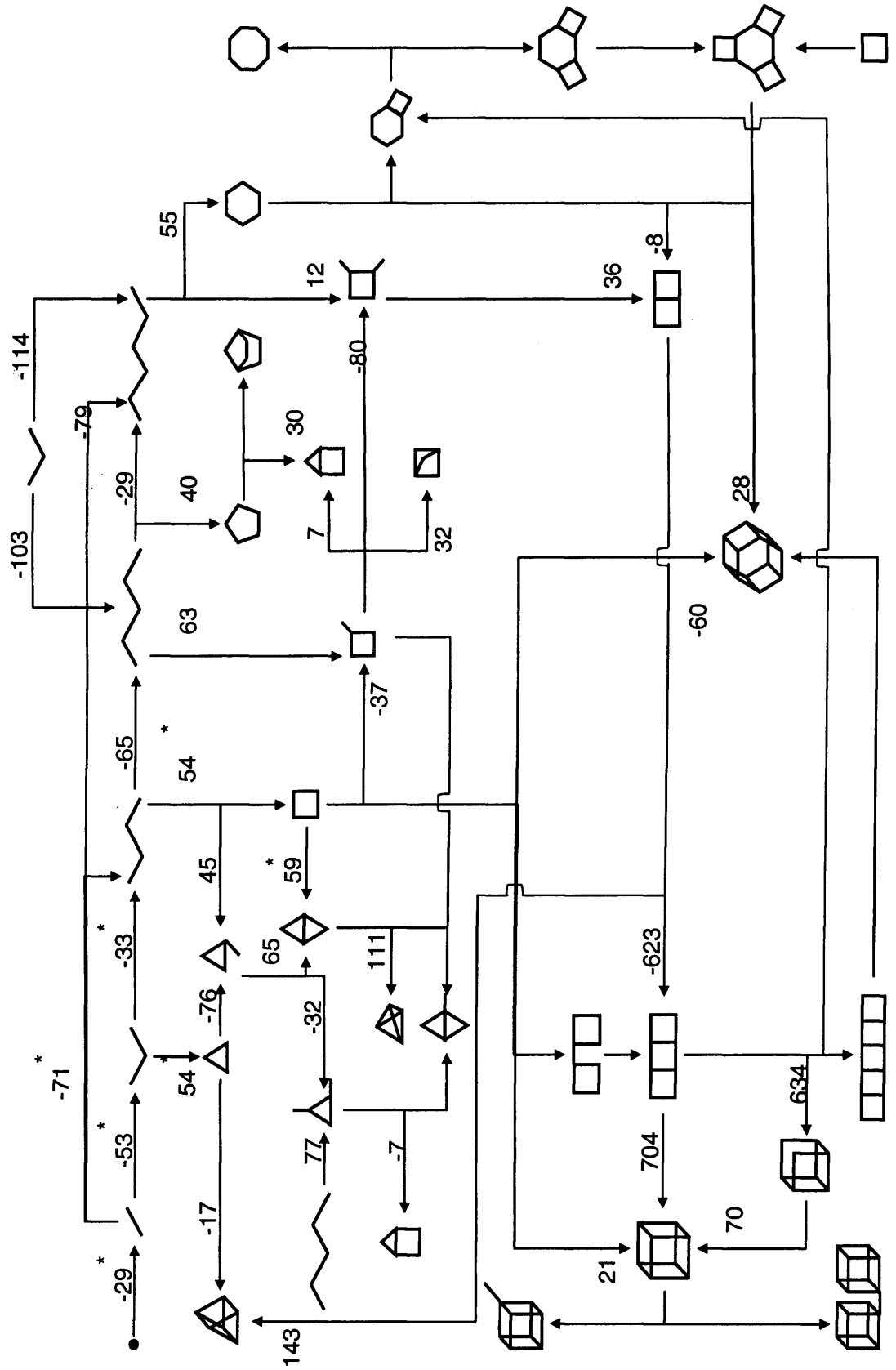

Figure 92 Reaction energies (kJmol^{-1}) at 0K in the gas phase. **Note, in this and the following diagrams there is a charge (-1) on the largest cluster condensing. (*) refers to the clusters modelled with explicit water.**

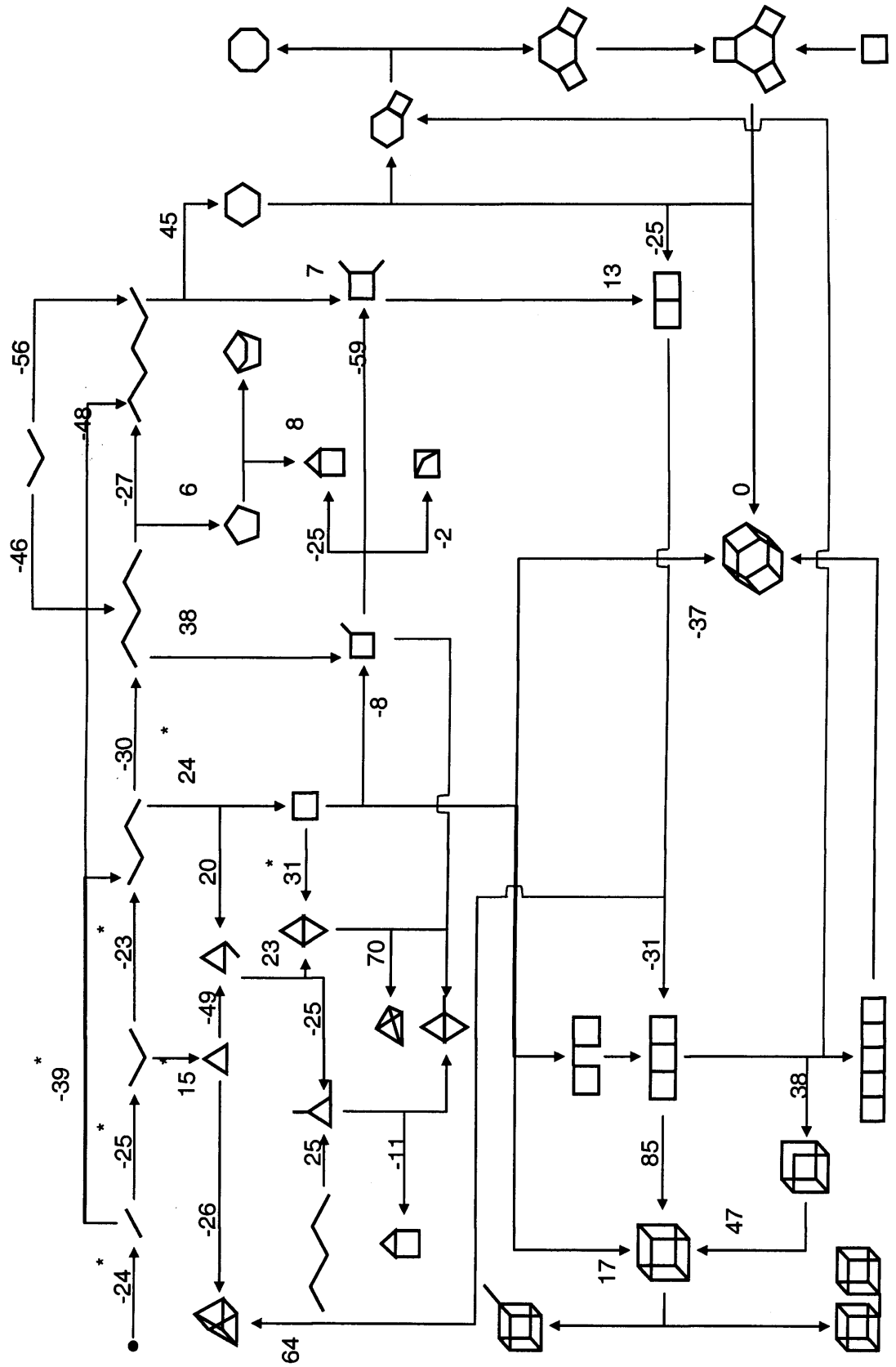

Figure 93 Reaction energies ($kJmol^{-1}$) at 0K in the COSMO solvation.

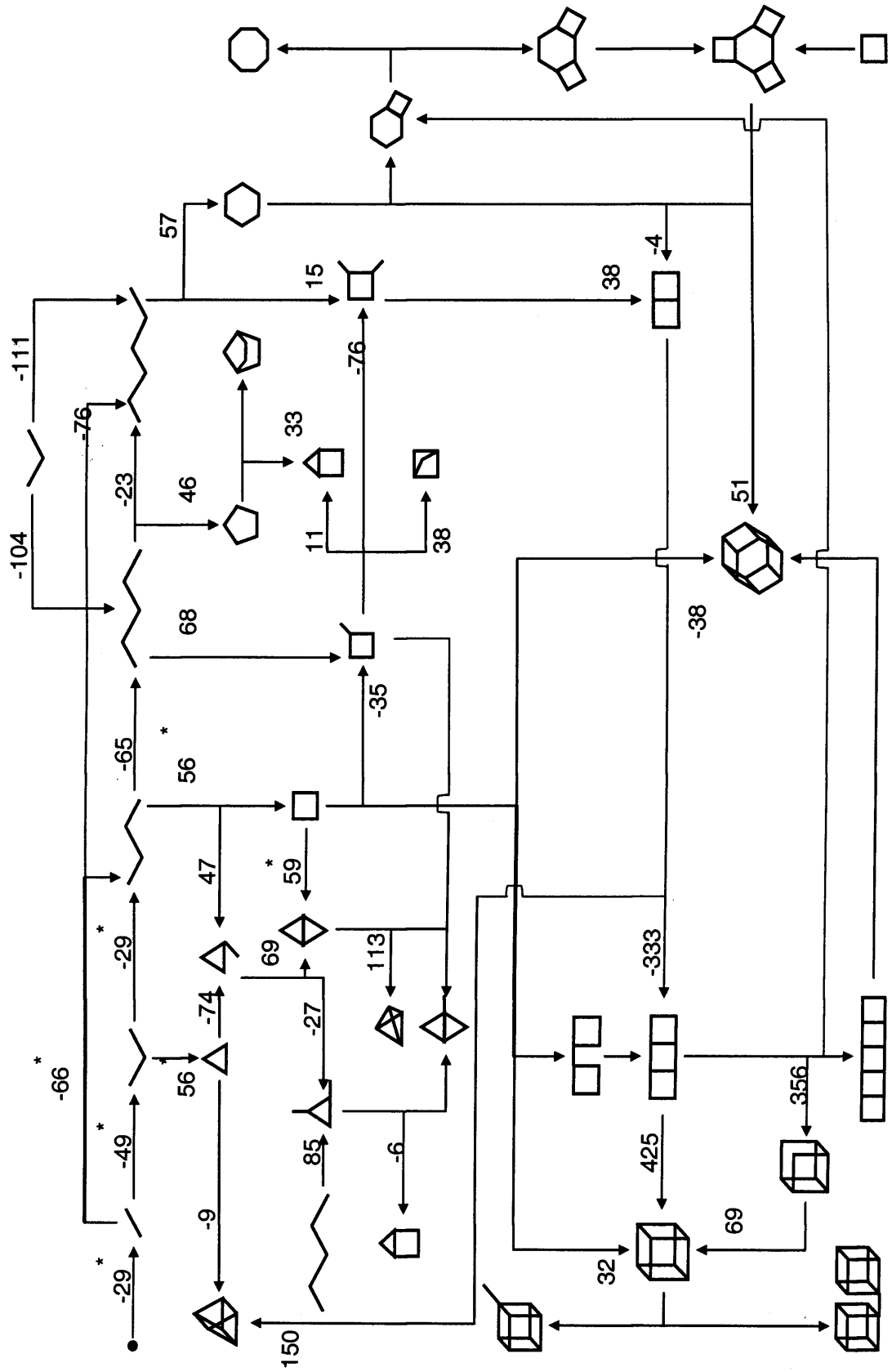

Figure 94 Reaction enthalpies ($kJmol^{-1}$) at 298K in the gas phase.

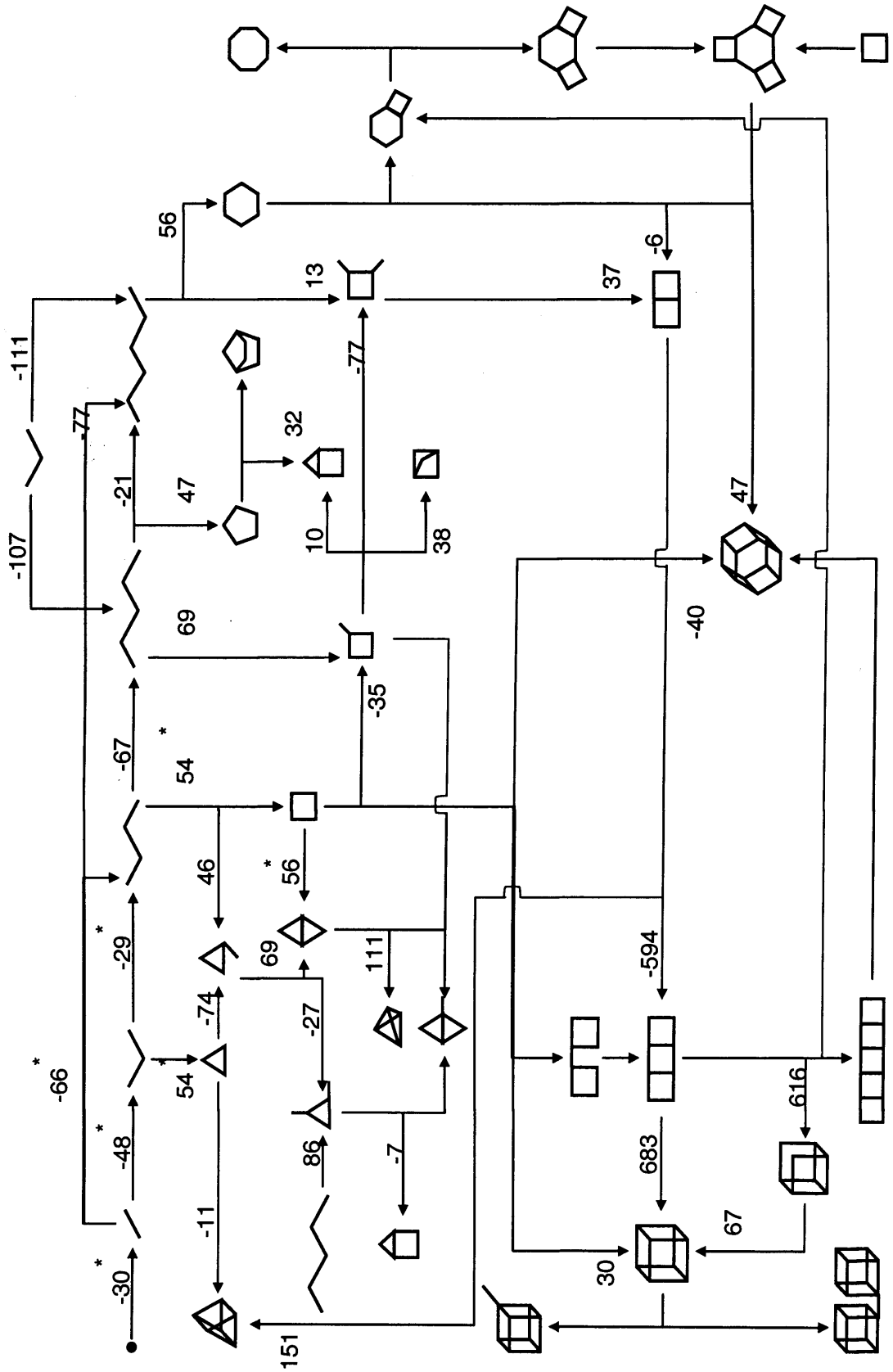

Figure 95 Reaction enthalpies (kJmol^{-1}) at 450K in the gas phase.

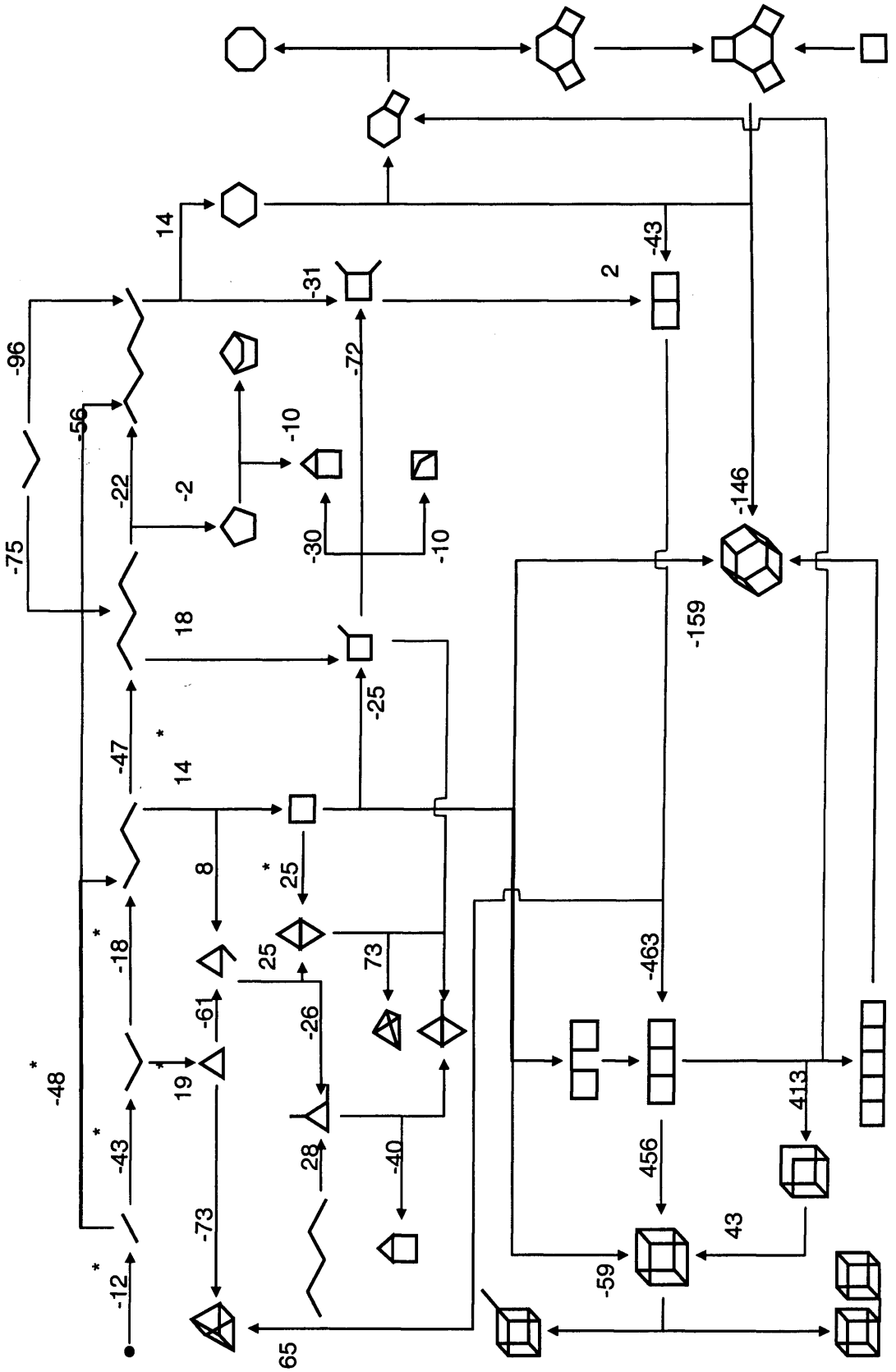

Figure 96 Reaction free energies ($kJmol^{-1}$) at 298K in the gas phase.

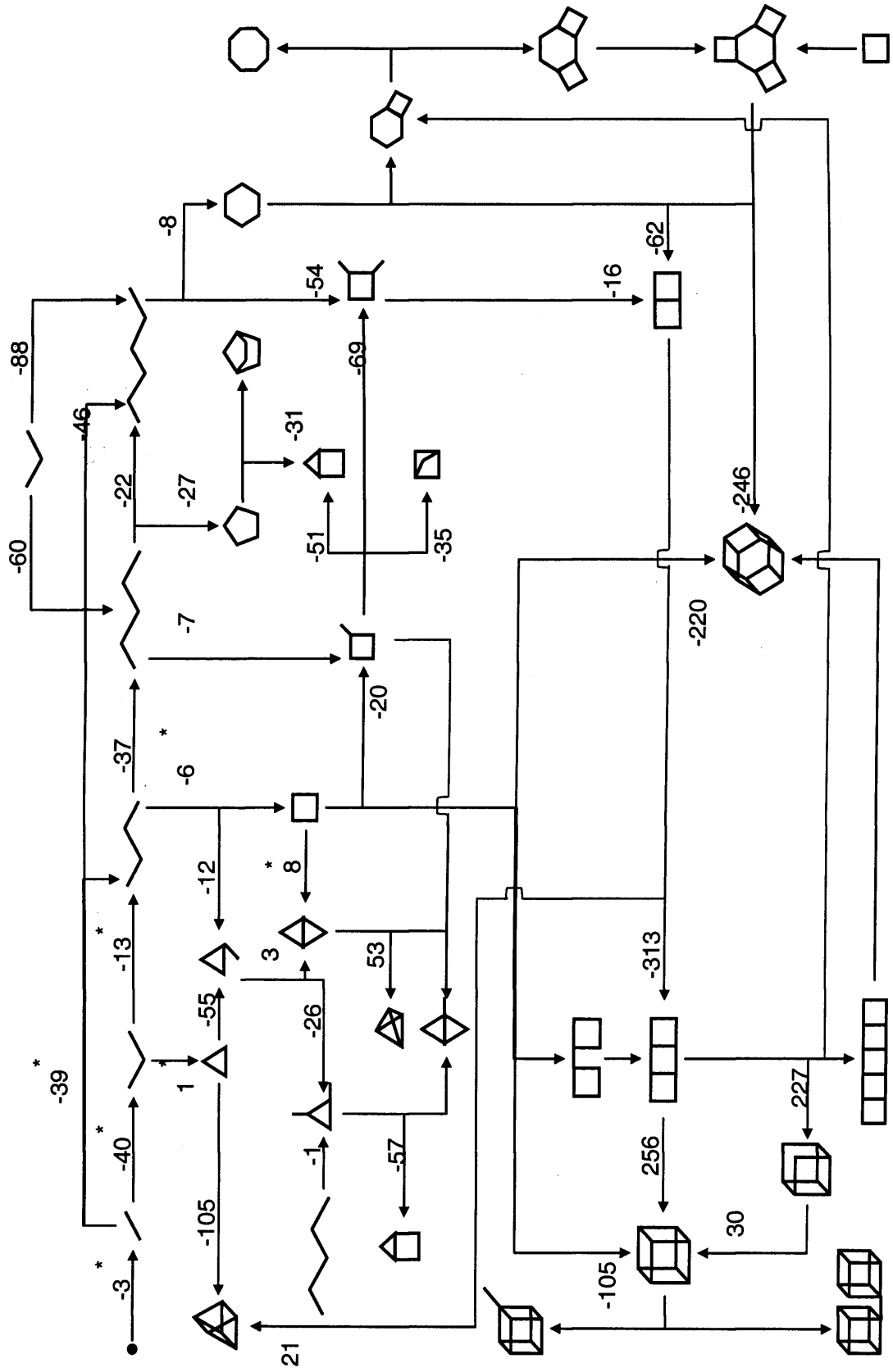

Figure 97 Reaction free energies ($kJmol^{-1}$) at 450K in the gas phase.

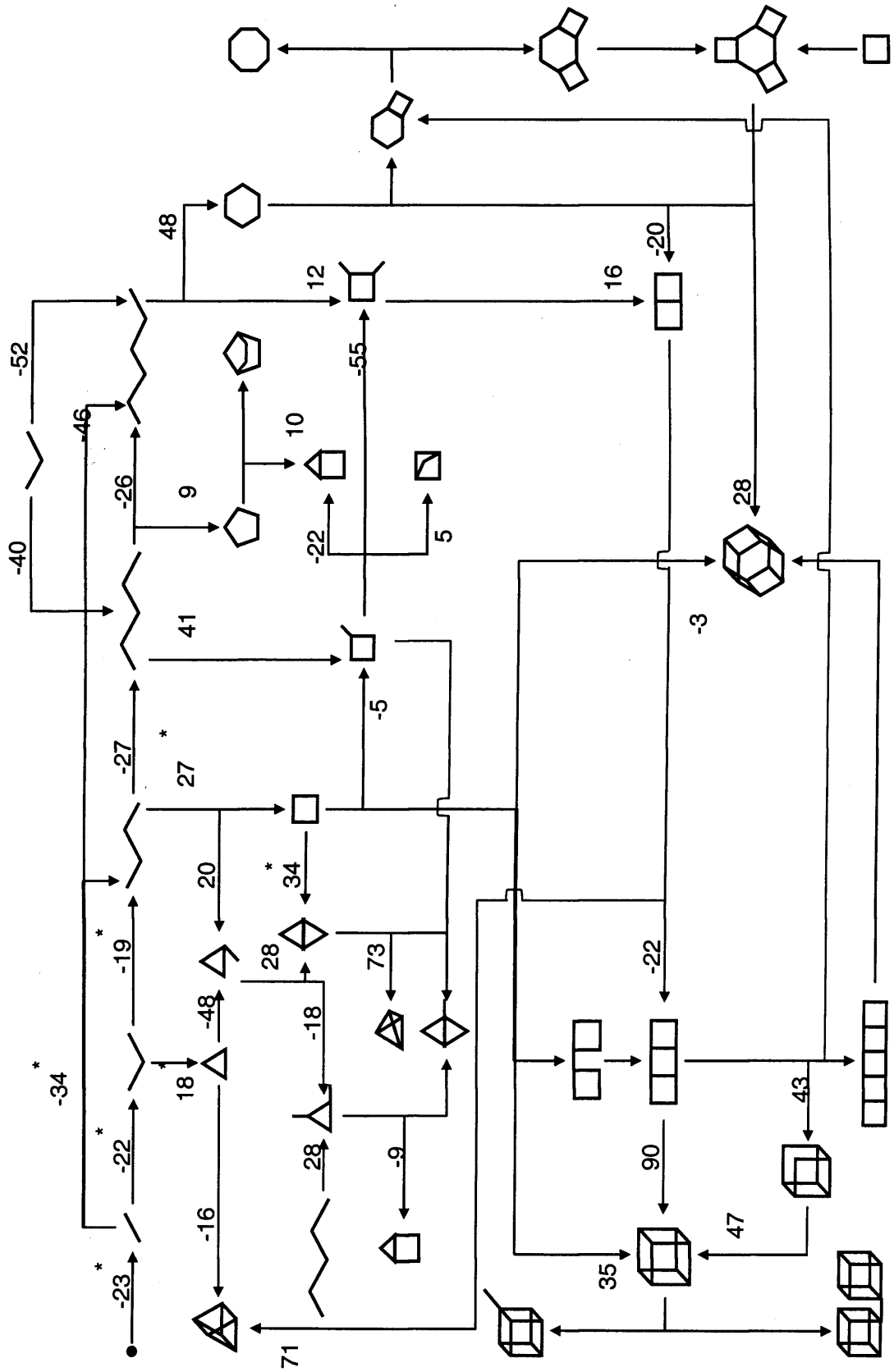

Figure 98 Reaction enthalpies ($kJmol^{-1}$) at 298K in the COSMO solvation.

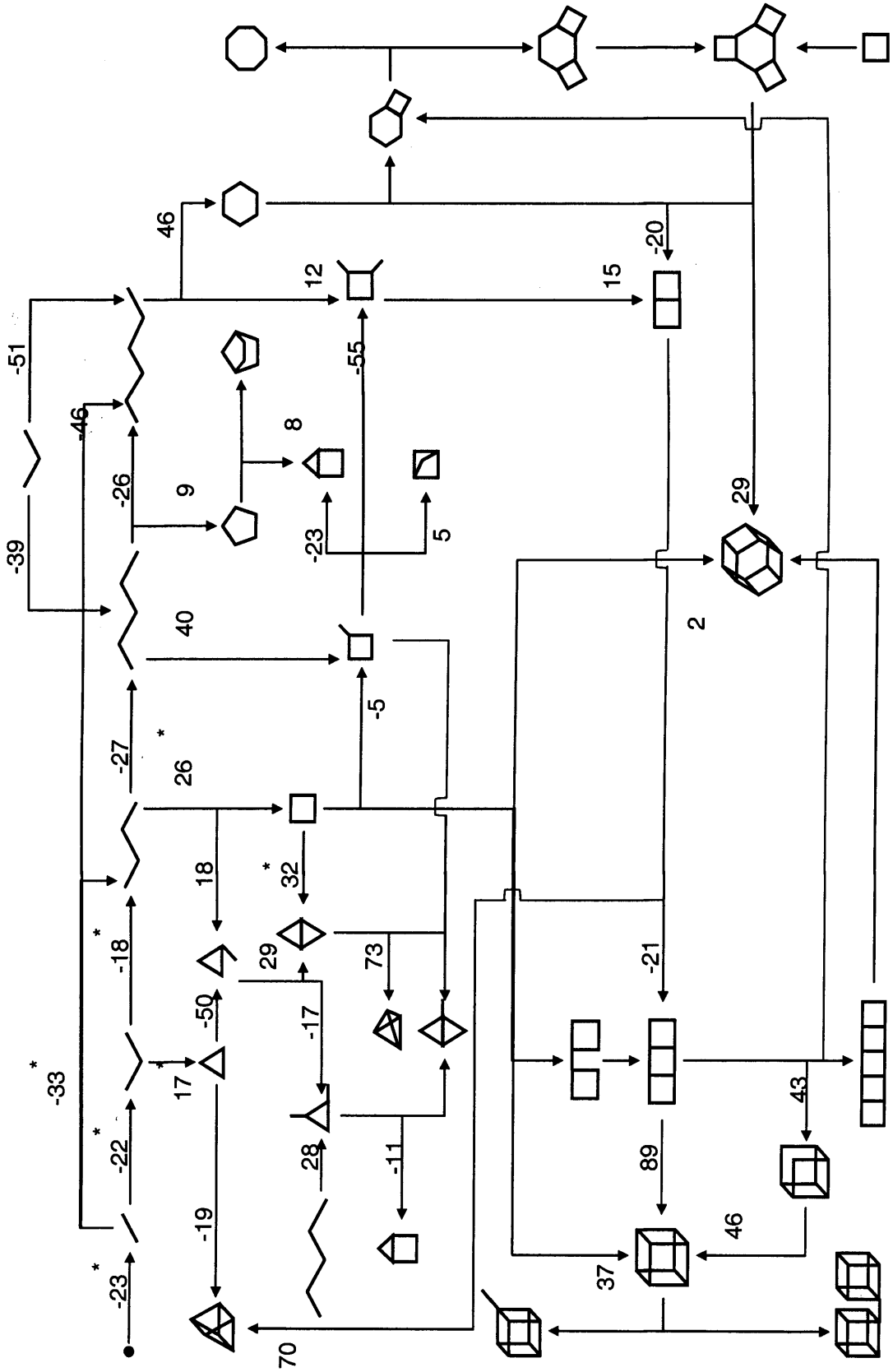

Figure 99 Reaction enthalpies ($kJmol^{-1}$) at 450K in the COSMO solvation.

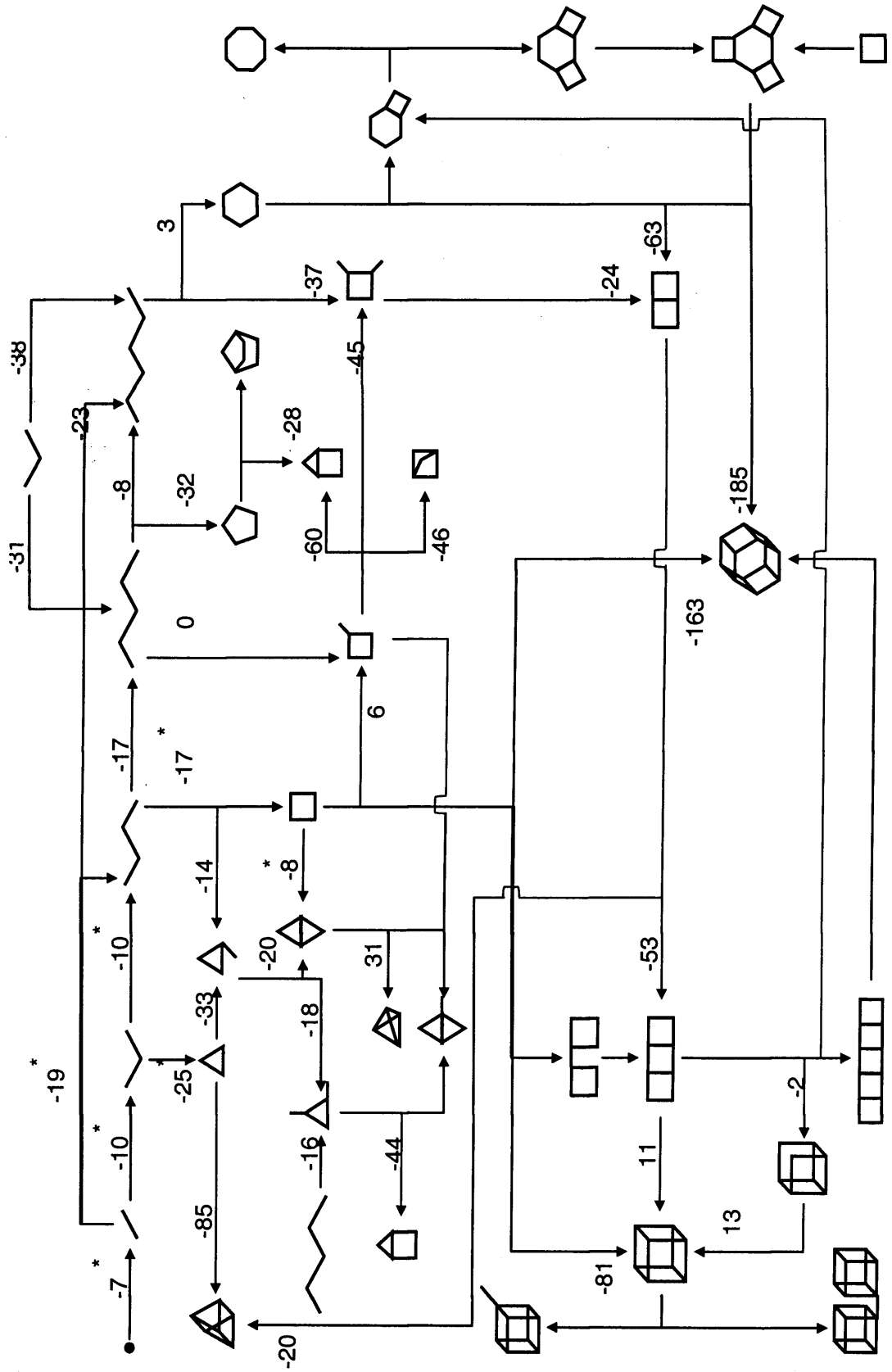

Figure 100 Reaction free energies ($kJmol^{-1}$) at 298K in the COSMO solvation.

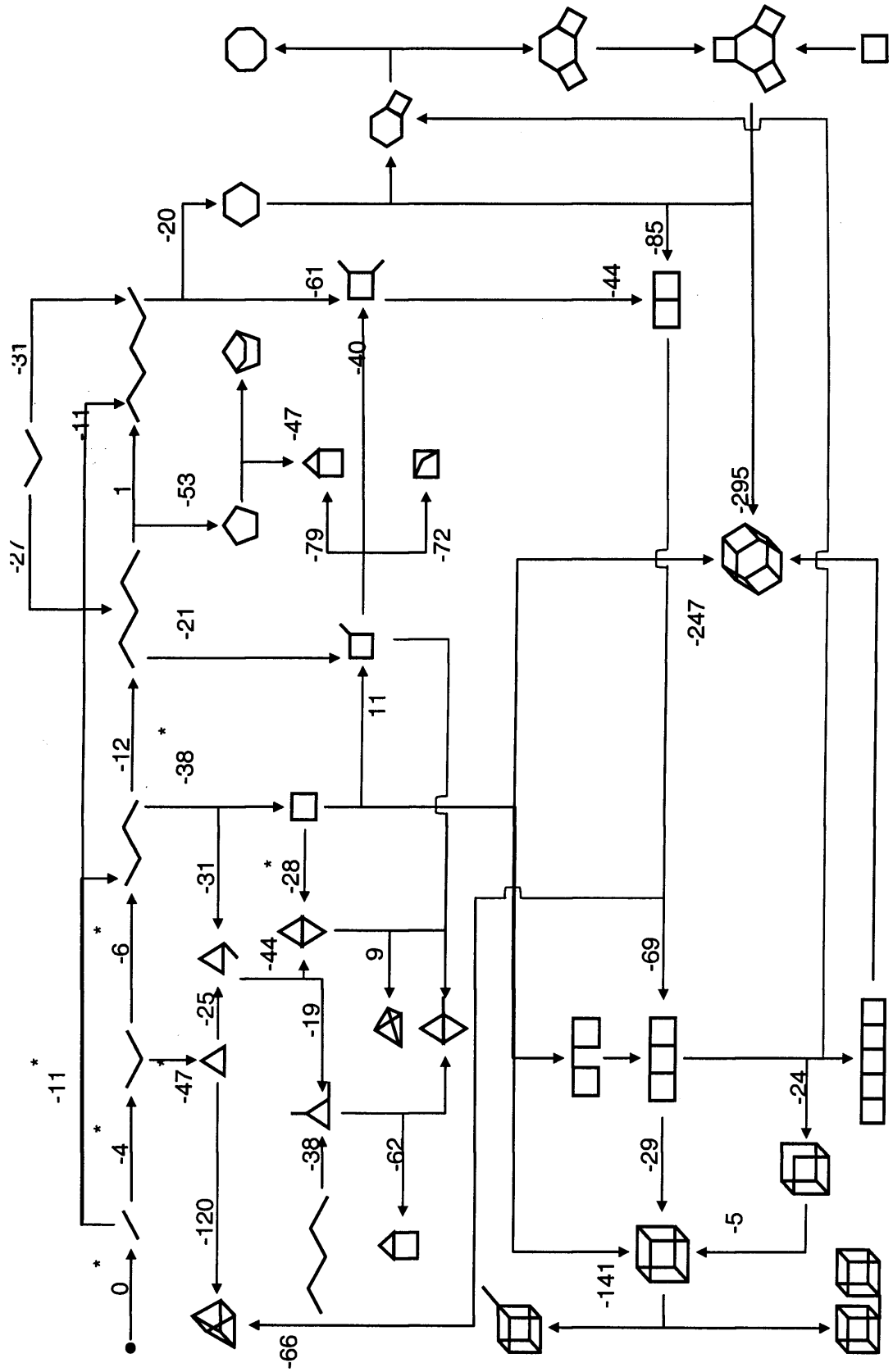

Figure 101 Reaction free energies ($kJmol^{-1}$) at 450K in the COSMO solvation.

4.7 Concluding remarks on silicate clusters.

Throughout this thesis, we have modelled a large variety of silicate clusters, some of them observed in silicate solutions and others proposed in this work; but most of them presumably implicated in the pre-nucleation stage of zeolite synthesis. The general approach followed for modelling such silicates has been to model the most probable silicates within the physical limits imposed by the synthesis conditions (high pH, temperature from 298 to 450K), under the most realistic manner (explicit solvation) and permitted by the present computational chemistry methods. For example, the approach to model the clusters embedded into a sol particle is with COSMO solvation alone, whilst to consider a fully solvated cluster (as in a clear solution) explicit water molecules are also included. Finally, rather than predicting novel clusters, our aim has been to understand the pre-nucleation stage for the known zeolites. After obtaining a reliable method, the way is open to model the possible synthesis of theoretical zeolites.

Our geometry analysis of the optimized silicates provides us with significant conclusions about their state during synthesis. The silicate clusters are very compact through multiple internal H-bonds, with the ring and ring-like structures being the most stable. We found that addition of dimers (and structures similar to it like the 4-ring) will more favourably lead to ring-like structures, while monomer addition could form virtually any silicate. Moreover, it is expected that condensation of quite large clusters could form frameworks with defects. Also of note is the 5-ring, which whilst not being observed in experimental solutions, our calculations reveals its geometry to be almost identical to that of the 5-ring in the MFI framework. Furthermore, the free energy of forming the 5-ring is favourable.

The effect of the pH is modelled by considering anionic (deprotonated) silicates. We find that solvation stabilizes these anionic clusters. However, highly charged ($OH^-/Si > 1$) linear oligomers are more linear in structure (unlike the almost ring-like structures at lower charge) and will possibly therefore not cyclize due to electrostatic repulsion.

When high pH is considered (with deprotonated silicate clusters) the number of feasible reactions increases dramatically (as shown in this chapter). However, some general trends are worthy of note. Firstly, in all reactions with two reactants, the most exothermic reactions are those in which the greater negative charge is borne by the smaller cluster. However, which of these two routes occurs during nucleation of course

depends on the availability of the reactants. Two further factors will determine this: the stability of the deprotonated species – and we find that larger anionic clusters are more stable – and the propensity for proton transfer between oligomers – and here we found that proton transfer to small clusters is favoured. Hence, on balance it is more likely that the reaction where the charge is in the larger species will be the dominant reaction to consider.

Another aspect important in zeolite nucleation is selective condensation. We found that high pH is not only a driving force for multiple oligomerization reactions, but also in some cases, that the degree of deprotonation (a function of the pH) will determine whether certain reactions are feasible. For example, we observed that the internal cyclization of a pentamer^{3-} to a 4-ring with dangling monomer is not favoured, while for all the other charged pentamers this reaction is feasible. Similarly, the single and double charged 4-ring and 5-ring will not undergo internal cyclization at room temperature, whilst these reactions are favoured for other charge states.

Temperature also plays a role in selecting some reactions which pathway is favoured. This is observed mainly in the oligomerization reactions, which are more favourable at lower temperatures (298K). Finally, geometric stability appears to be important. We observed how the addition of a monomer is more likely in a 3-ring rather than to a linear oligomer, whilst addition of such a monomer is less favourable for the 4-ring compared to an open tetramer. This result is a direct consequence of the geometric differences between 3- and 4-ring: the presence in the latter of strong intramolecular H-bonds.

The final conclusions above, confirm the possibility of "tuning" the species in solution through changes in the pH and temperature. Indeed, it is well known how different aging conditions can alter the final product. Thus, whilst we cannot at present suggest specific methods for controlling the final product, the level of detail gave here provides valuable insight into the actual chemistry occurring in the pre-nucleation.

It is clear from our calculations that ring formation is a consequence of a positive change in entropy. Thus, cyclization processes, in general, will be favourable at higher temperatures. However, some ring structures like the 5- and 6-ring pose interesting questions. Both structures are part of several zeolite frameworks, but are not observed in silicate solutions. However, our calculations show a favourable energy of formation when they condense from oligomers. One possible reason for the "absence" of the 5-

and 6-ring is that they are in fact present in low concentrations due to the more favourable formation of the smaller ring structures. However, this does not explain their presence in zeolite frameworks. Another possibility is that the 5- and 6-ring undergo rapid internal condensation to produce double rings – which *are* observed in solution – and in a later stage these double rings could reopen to produce back the 5- and 6-ring.

But special mention should be made of the 5-ring. The geometry in solution for this ring is almost identical to that in the final MFI structure. Moreover, this geometry is "locked" by internal H-bonds. We, therefore, suggest that such a species is highly susceptible to further rapid growth. Hence, in media which result in MFI formation their population is negligible as they quickly become larger, even possibly forming nucleation centres.

A final issue is that related to the internal H-bonds present in most of the silicate structures analysed in this thesis. A preliminary conclusion from the results presented until now, is that while they are very important in the geometry and energy of the silicates, they are not wholly responsible for determining the feasibility of forming a particular cluster. For example, the 3-ring, which does not have H-bonds, is thermodynamically favoured, over the open trimer which has two H-bonds. Furthermore, our results suggest that the H-bonds have dramatically different strengths, depending on the particular silicate. In the next chapter, we will present a further analysis of this important subject.

4.7.1 About the uncertainties in the models

The results presented in this thesis have different degrees of uncertainties, depending on how the model approximates the reaction in particular. At one end are the approximate results for the reactions in gas phase, for which there are considerable differences compared to experimental results. For example, in Table 1, the results in gas phase show differences of up to 200 $kJmol^{-1}$ for reactions involving ionic species, but less for reactions with neutral species. This highlight how important is to take into consideration the role of the solvent, as has been done in this work. Nevertheless, the results with the COSMO solvation approach, but without explicit water molecules, are much closer to the experimental results. Although with COSMO solvation alone the uncertainty of the model can not be precisely established, we note that a good linear correlation with experimental results is observed in Figure 46. The more realistic model presented in this

work, which includes explicit water molecules and the counterion (Na^+), give the smallest discrepancies with respect to the experimental results. As can be seen in Table 1 the values obtained with this model are on average within 3.6 $kJmol^{-1}$ of the experimental measurements. The limited experimental data available in the literature for the energy involving reactions with silicates makes it difficult to provide a detailed analysis of the accuracy of the models presented here, but at the same time encourages further research in these important reactions, key in the synthesis of zeolites.

5 H-BOND RELATIVE STRENGTH

In addition to analysing the chemical reactions of the participants in the nucleation of zeolites, we must also consider their physical interactions. These interactions will dictate the conformations adopted by silicate clusters, their solubility and possibly give insight into the physical behaviour of the silicates inside the sol or gels, which can be present in zeolite nucleation. For this purpose, the participants in the nucleation of a pure siliceous zeolite can be classified as: silicates, solvent (water) and cation (both metal cation and organic template). There is obviously an interaction between the water molecules solvating the silicates. But, it may be that a key process in nucleation involves silicate clusters interacting in an intramolecular manner; in particular, due to the hydroxyl groups that can form H-bonds.

Water, indisputably and obviously, plays a key role in hydrothermal synthesis. However, we have seen already (Figure 43) how the amount of water present is restricted to between 5 to 40 water molecules per silicon. An important consequence of the low amount of water in the synthesis solutions will be a higher probability of silicate-silicate interactions, and perhaps a lower frequency of water-water interactions (as few water molecules will be available for solvating the silicate clusters). There have been some claims of dry zeolites synthesis[127, 130]. However most can be considered as having a very limited water content and not 100% anhydrous[12]. Hence, although there is no visible solution phase, a (local) gel phase probably exists in most cases[127].

A main objective of this section is to consider in more detail the relative strength of the water-water, water-silicate and silicate-silicate interactions. An understanding of these interactions may help to explain the low solubility of monosilicic acid ($Si(OH)_4$), and assist in describing better the features of the optimized clusters presented in section 4.2,

and possibly, give an insight into the structures immediately after a condensation, where a water molecule is produced.

Silicic acid, $Si(OH)_4$, (the monomer), has a very low solubility and at 25°C only remains as the monomer in solution below a concentration of $2x10^{-3}$ M[15]. This result may at first glance be surprising, as other molecules such as methanol (CH_3OH), which has a hydroxyl group, dissolves easily in water. However, zeolite synthesis does not proceed in such dilute systems; hydrothermal synthesis occurs under a very different hydration regime, as noted above. A concentration of $2x10^{-3}$ M implies an H_2O/T ratio of $27.8x10^3$, whilst synthesis ratios are between 5-40. Therefore, it is clear that silicate-silicate interactions will be expected and will have a significant impact on the chemistry of zeolite synthesis.

A large proportion of the silicates discussed in section 4.2 have internal hydrogen bonds (H-bonds). All the optimized linear oligomers (Figure 48), from the dimer to hexamer, exhibit H-bonds and, with the exception of the 3-ring, all the optimized ring structures possess at least two internal H-bonds (Figure 49). Therefore, changes in conformation will be strongly connected to the strength of these H-bonds. Indeed, in some cases the strength of these may be such that certain conformations may be "locked-in", that is, certain oligomers may not be able to change conformation easily. Furthermore, a conclusion drawn from the optimized oligomer cluster geometries is that the densely packed ("ring-like") structures prevail over the more open structures. However, we recall that these calculations considered solvation through the COSMO model. Therefore, a more detailed study with explicit water (as given in this section) is necessary to confirm that this observation is not a consequence of the neglect of explicit water; that is, these H-bonds could in fact be weakened or even break if water is also available for the formation of intramolecular H-bonds.

The reactions that occur inside sol and gel particles all have a common characteristic: diffusion of the reactants and products is slow, compared with that for fully solvated isolated clusters. The clusters analysed in this section can therefore give insight into the short-range interactions between the participants in those condensations occurring in a sol or gel. For example, if two monomers approach without sufficient energy to overcome the energy barrier for a dimerization and remain in the proximity of each other, then we must understand how these two silicate species interact (section 5.3) and

how they are modified by the presence of the solvent. Similarly, as a product of a condensation is a water molecule we need to study the water-water (section 5.1) and silicate-water interactions (section 5.2.2), to understand how the formed water molecule influences the local environment.

The interactions analysed in this section are very difficult to study experimentally, with the exception of the water clusters, where in particular the dimer has been studied extensively[131, 132]. In the gas phase, DFT methods have been shown to model successfully the weak van der Waals interactions found in the H-bonds for the clusters in this section[133]. Comparisons with experiments are made in the next section.

We do not claim that those approximated methods have high accuracy. However, they provide a robust description, which gives a good correlation to experiments.

5.1 H_2O-H_2O Interactions

Water clusters have been studied extensively[131-138] using a range of experimental techniques, and much of computational work is also reported[135-137, 139], because of the importance and simplicity of the clusters, but also the complex nature of these interactions are crucial in demonstrating the effectiveness of new quantum methods. The water dimer is used as a benchmark, because there is reliable experimental data for comparison[131]. The calculated association energies for the water dimer and for further water clusters, up to six molecules, are given in Table 42. The gas phase DFT (BLYP/DNP) calculations here, for the water dimer are within 2-3 $kJmol^{-1}$ of the experimental results for H_2O vapours obtained using thermal-conductivity by Curtiss *et al*[131]. Compared with the composite, high level of theory method G3B3MP2[140], the BLYP/DNP method produces results within 1 $kJmol^{-1}$ of the former. Good agreement between DFT methods and experimental results is also found by Jursic[133] for the water dimer. For the purposes of this section, therefore our computed values of 20 $kJmol^{-1}$ at 0K and 13 $kJmol^{-1}$ at 373K (close to synthesis temperature) are sufficiently reliable for the water association energy.

The global minima for the 2-5 water clusters (Figure 102) with the same level of theory used here, are the same as those reported by other authors[134-137]. However the $(H_2O)_6$ cluster in some work is found to be a single 6-ring structure and in others a double-4-ring. In this work, the single 6-ring structure is found. The main feature

Table 42 Association electronic energies (ΔE) and enthalpies (ΔH) in $kJmol^{-1}$, for water clusters in the gas phase and in COSMO solvation at 0, 298 and 375K (indicated as a subscript). The first column does not include the Zero Point Energy. The water clusters are shown in Figure 102.

	Reaction	ΔE	ΔE_0	ΔH_{298}	ΔH_{375}
	$2H_2O \rightarrow (H_2O)_2$	-20	-11	-14	-13
		-22.8[a]	-10.5[b]	-14.6[b]	-15.0[c]
Gas	$3H_2O \rightarrow (H_2O)_3$	-54	-36	-47	-48
Gas	$4H_2O \rightarrow (H_2O)_4$	-98	-71	-87	-87
Gas	$5H_2O \rightarrow (H_2O)_5$	-155	-112	-126	-125
Gas	$6H_2O \rightarrow (H_2O)_6$	-114	-68	-81	-78
	$2H_2O \rightarrow (H_2O)_2$	-20	-8	-12	-11
	$3H_2O \rightarrow (H_2O)_3$	-22	-5	-15	-15
Sol.	$4H_2O \rightarrow (H_2O)_4$	-52	-25	-42	-44
Sol.	$5H_2O \rightarrow (H_2O)_5$	-105	-57	-73	-71
Sol.	$6H_2O \rightarrow (H_2O)_6$	-108	-51	-70	-68

[a] Experimental result according with Curtiss[131], Kim[132] and Jursic[133].
[b] Theoretical result at the high level of theory G3B3MP2[140].
[c] Experimental result according with Curtiss[131].

exhibited by the water clusters in Figure 102 is the gradual shortening of the H-bond distance with increasing cluster size (from 1.98 to 1.76Å). Thus, shorter H-bond distances are, in general, associated with stronger interaction energies.

The effects of vibrations even at 0K (ZPE) are important for all the water clusters, as can be seen by comparing ΔE with ΔE_0 (first and second column in Table 42). However raising the temperature from 0 to 298K and above the boiling point of bulk liquid water, 375K, has only a small effect on the enthalpies, which increase of only a few $kJmol^{-1}$. Thus, we can consider that the enthalpy changes for water interactions at the zeolite synthesis temperature (around 450K) will be very close to the value shown here at 375K.

The energy of interaction increases steadily with the cluster size (Figure 102 and Table 42). We note that for every water molecule added, a new H-bond is formed. Subsequently, the water clusters size can be associated with (approximately) the number of H-bonds and thus a specific energy release per H-bond. However, this is not the case for silicates, (see section 4.2 and 5.3). However, there are a number of anomalies: the

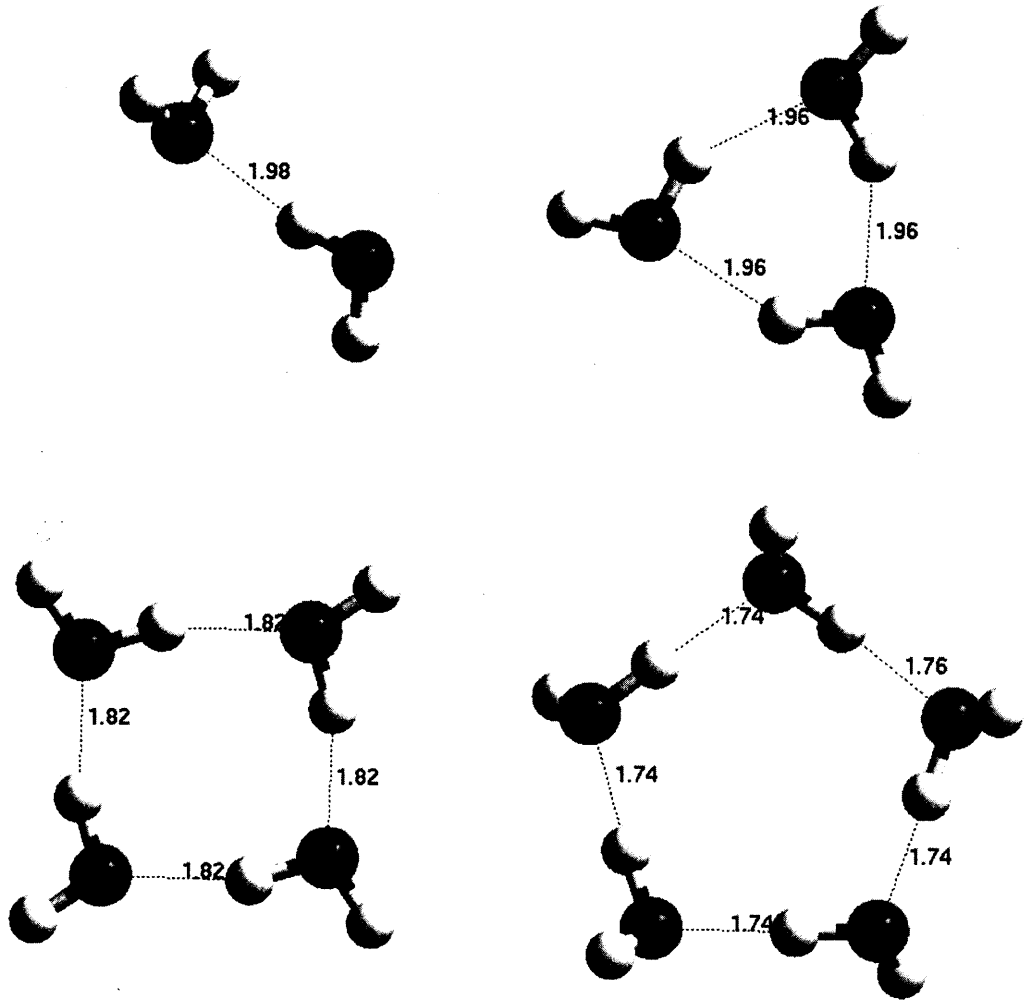

Figure 102 Water clusters for $(H_2O)_n$ for n=2-5. The dotted lines represent the H-bonds and their lengths are in angstroms.

cluster with three water molecules in COSMO solvation has almost the same interaction energy as the dimer. In addition, the cluster with six water molecules shows a strange behaviour increasing the energy with respect to the five-water cluster. A more stable conformation for the six-water cluster is suggested by the latter observation. Thus, even in pure water clusters it proves difficult to give a general "strength of an H-bond".

In spite of the good agreement between experiment and DFT calculations, the main purpose here is to compare the water-water interaction with that of the silicate-water. We report the calculated electronic energy and the enthalpy and not the entropy change, because the aim is to compare the relative strengths of the H-bonds in different

aggregates. The results with the COSMO solvation are only an approximation to the water-water interactions in the real liquid. However, they provide an improved model compared to the gas phase, as shown in particular by the alteration to the structures of the silicate clusters when COSMO solvation is included.

In the condensation reactions of silicates, a water molecule is also produced. The solvation of that molecule could be modelled approximately as the inclusion of a water molecule into the water clusters given in Figure 102. The energy associated with the process is obtained from Table 42 (taking the difference of two rows). For example, the inclusion of a water molecule into a four-water-cluster under the COSMO solvation model (forming a five-water-cluster), releases 27 $kJmol^{-1}$ at 375K.

The most important result from the water clusters is dimer formation, since it gives the energy for the formation of a single H-bond between two water molecules. Thus, we consider the enthalpy change of -12 $kJmol^{-1}$ in solvation and -14 $kJmol^{-1}$ in the gas phase to be indicative of the strength of a water-water H-bond. These values can now be compared with those found for water-silicate H-bonds presented in the next section.

5.2 Solvation of monomers and dimers including explicit water molecules

5.2.1 Monomer solvation

The hydrophobicity of silicates cannot arise from poor interactions with the water molecules surrounding a cluster: the hanging hydroxyls have a positive interaction with water molecules. Rather we must consider the relative interaction with respect to H_2O-H_2O interaction. Furthermore, as the silicate cluster grows, the structure tends to be very compact; which reduces the extent to which a cluster can interact with the solvent. Similarly, the proportion of hydrogen atoms decreases with the size of the clusters and bridging oxygen atoms have less strong interaction with the water molecules than those in hydroxyl groups.

The solvation of silicate species is an important problem and has been addressed by other authors using explicit water molecules[64, 94, 100], with polarizable continuum methods [141] and the COSMO solvation method [60]. However a detailed account, such as presented here, of the progressively hydration of neutral and particularly charged silicates using both explicit water and COSMO solvation is not found in the literature.

Furthermore, the aim in this work is to identify the relative "strength" of a variety of H-bonds.

In all cases, a maximum of four explicit water molecules are used. In the case of the monomer, this number of molecules is approximately enough to cover a first shell surrounding the monomer. When the anionic clusters are explored, the contribution of the counterion is not taken into account, as a first approximation; primarily because the interest here is to obtain a pure H-bond interaction and the presence of the cation will modify the local geometry and the energy change. The cation effect was studied previously in section 4.1.3 page 90, whilst the present section is dedicated to the analysis of the effect of water on the solvation process of silicate anions.

Each water molecule takes up a consistent geometry with respect to the monomer, with the degree of solvation making little change to the geometry, as can be appreciated in Figure 103 where the monomer is solvated by one to four water molecules. In the case of the monomer with two water molecules, two different conformations are possible: one where a single Si-OH hydroxyl is interacting with two water molecules, and that which is shown in Figure 103; both conformations have the same energy. These homogeneous geometrical interactions are reflected in the uniform energy association seen in Table 43, for every water molecule added (the results in Table 43 are per

Table 43 The energy and enthalpy ($kJmol^{-1}$ per H_2O) of association of water and the $Si(OH)_4$ (M) silicate, in the gas phase and in COSMO solvation at 0 and 298K.

	Gas			Sol.		
Reaction	ΔE	ΔE_0	ΔH_{298}	ΔE	ΔE_0	ΔH_{298}
$M + H_2O \rightarrow M(H_2O)$	-33	-23	-25	-19	-8	-11
$M + 2H_2O \rightarrow M(H_2O)_2$	-33	-23	-26	-20	-9	-12
$M + 3H_2O \rightarrow M(H_2O)_3$	-36	-25	-28	-21	-10	-13
$M + 4H_2O \rightarrow M(H_2O)_4$	-36	-25	-28	-22	-10	-13
$M + (H_2O)_2 \rightarrow M(H_2O)_2$	-23	-17	-19	-10	-5	-6
$M + (H_2O)_3 \rightarrow M(H_2O)_3$	-18	-12	-12	-14	-8	-8
$M + (H_2O)_4 \rightarrow M(H_2O)_4$	-12	-8	-7	-9	-4	-3
$M^{-1} + H_2O \rightarrow M(H_2O)^{-1}$	-80	-72	-75	-43	-32	-36
$M^{-1} + 2H_2O \rightarrow M(H_2O)_2^{-1}$	-76	-66	-70	-38	-27	-31
$M^{-1} + 4H_2O \rightarrow M(H_2O)_4^{-1}$	-60	-49	-52	-30	-19	-23
$M^{-2} + 4H_2O \rightarrow M(H_2O)_4^{-2}$	-118	-109	-112	-42	-32	-36

molecule of water). When more than four explicit water molecules are solvating the monomer, the water molecules form H-bonds between themselves (not shown), and no further water-silica H-bonds are formed. The eight H-bonds shown by the cluster $Si(OH)_4(H_2O)_4$, are probably the maximum number of interactions with the solvent possible for the monomer.

The H-bonds in the water-monomer aggregates are approximately 1.9 and 2Å for all the neutral clusters considered. The shortest H-bond is always the SiO-H···OH_2. The slightly elongated SiO-H bond suggests some proton transfer, which may be indicative of the acidic character of the silicate hydrogen.

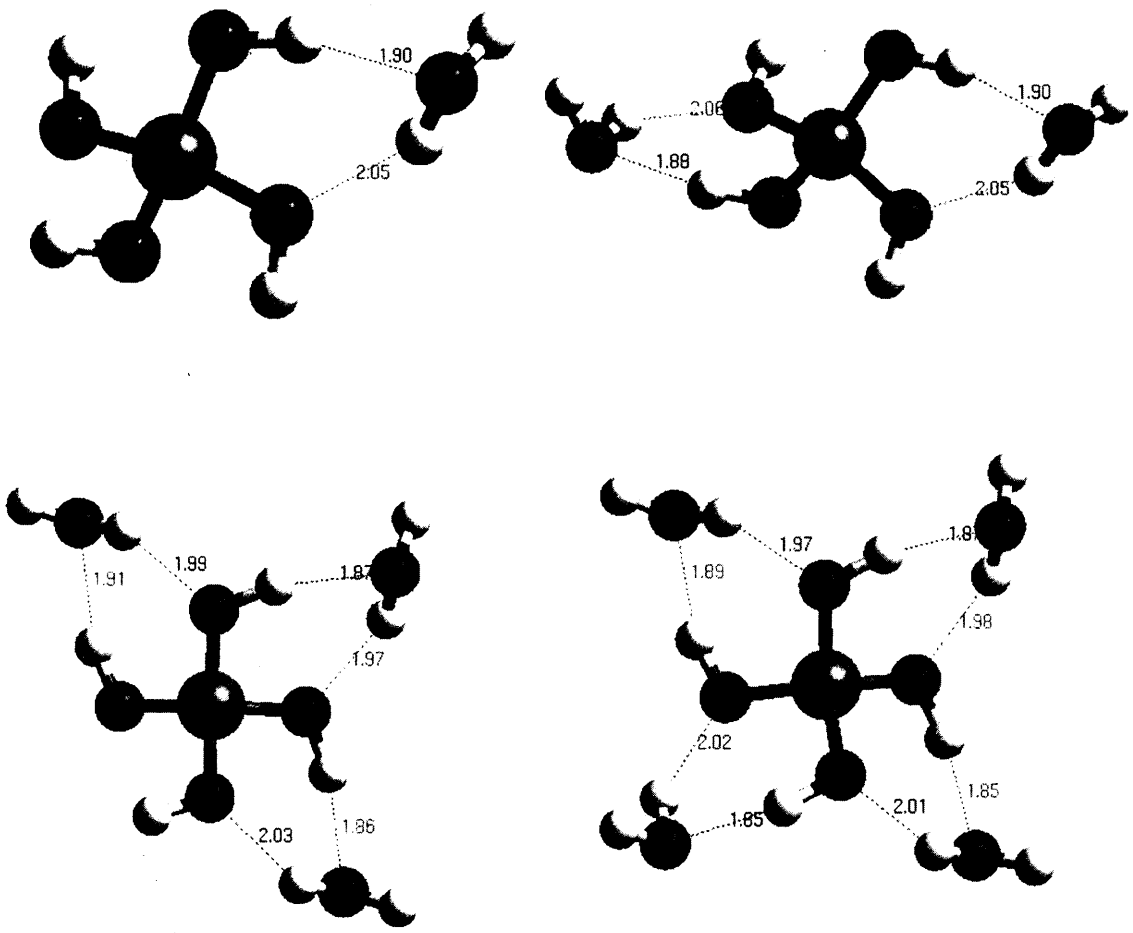

Figure 103 The optimized structures for the association of water on monomer, $Si(OH)_4(H_2O)_n$ for n=1-4. The bigger spheres are the Si and the smallest the H.

One final remark on the geometries shown in Figure 103 is that the silicon atom is spatially "free", because the Si does not form part of any H-bonding, and is therefore susceptible to nucleophilic attack by an anion. In the case of the monomer, with four water molecules, it is clear than an attack perpendicular to the plane of the paper in Figure 103, will be most successful.

The enthalpy released at 298K, associated with explicit water solvation, is approximately 25-28 $kJmol^{-1}$ in the gas phase, and around 11-13 $kJmol^{-1}$ in COSMO solvation (Table 43), for all the clusters analysed, which is a very homogeneous result. The equivalent results for the water dimer are 14 and 12 $kJmol^{-1}$ in gas and COSMO respectively. These results show that in the dielectric COSMO solvation a water molecule will be equally energetically stable bonded to another water molecule as with the $Si(OH)_4$. However, note that for water the $H_2O\cdots H_2O$ interaction has one H-bond while the $Si(OH)_4\cdots H_2O$ has two H-bonds; but both results in the same solvation enthalpy.

Another way to analyse the solvation of the monomer is to consider the insertion of the monomer into a preformed water clusters shown in Figure 102. Rows 4-6 in Table 43 show the results for this process. This is certainly a more realistic model for the solvation of the monomer and the monomer cluster with a complete first shell with explicit four water molecules (Figure 103) will be the most accurate representation. According to this process it is found that the monomer has a weak interaction with the water ($\Delta H \approx$ -3 $kJmol^{-1}$) in COSMO and only slightly strong in the gas phase ($\Delta H \approx$ -7 $kJmol^{-1}$). Note that four water-water H-bonds are broken and eight water-monomer H-bonds are formed by the process. This result can be interpreted as the first factor contributing to the low solubility ($2x10^{-3}$ M[15]) of the monomer.

The anionic monomer (present at high pH hydrothermal synthesis) will have a stronger interaction with the surrounding water. The deprotonated oxygen in the charged monomer forms an H-bond that is 0.3-0.4Å shorter to the water molecule than that calculated for the neutral monomer (Figure 104). However, the $SiOH\cdots OH_2$ interactions are slightly weaker in the anionic cluster. The strong water interaction with the anionic monomer is reflected in the energy of association, (Table 43) which is roughly double that for the neutral monomer.

The importance of incorporating solvation explicitly around the anionic species is seen when a doubly charged monomer is optimized. Unless four water molecules are included when optimizing the $Si(OH)_2O_2^{2-}$ anion, a water molecule will transfer a proton to the anion. As a result, a full first shell solvation of water is necessary to stabilize a $Si(OH)_2O_2^{2-}$ anion. This latter result is of key importance because it provides an adequate model for the doubly deprotonate monomer, when the counterion is not present.

However, inside a gel or sol particle the low water content may not be enough to provide such a minimum solvation shell. Furthermore, with the ratio $OH^-/Si < 0.5$ (Figure 43) present in the zeolite synthesis, the environment may not support the

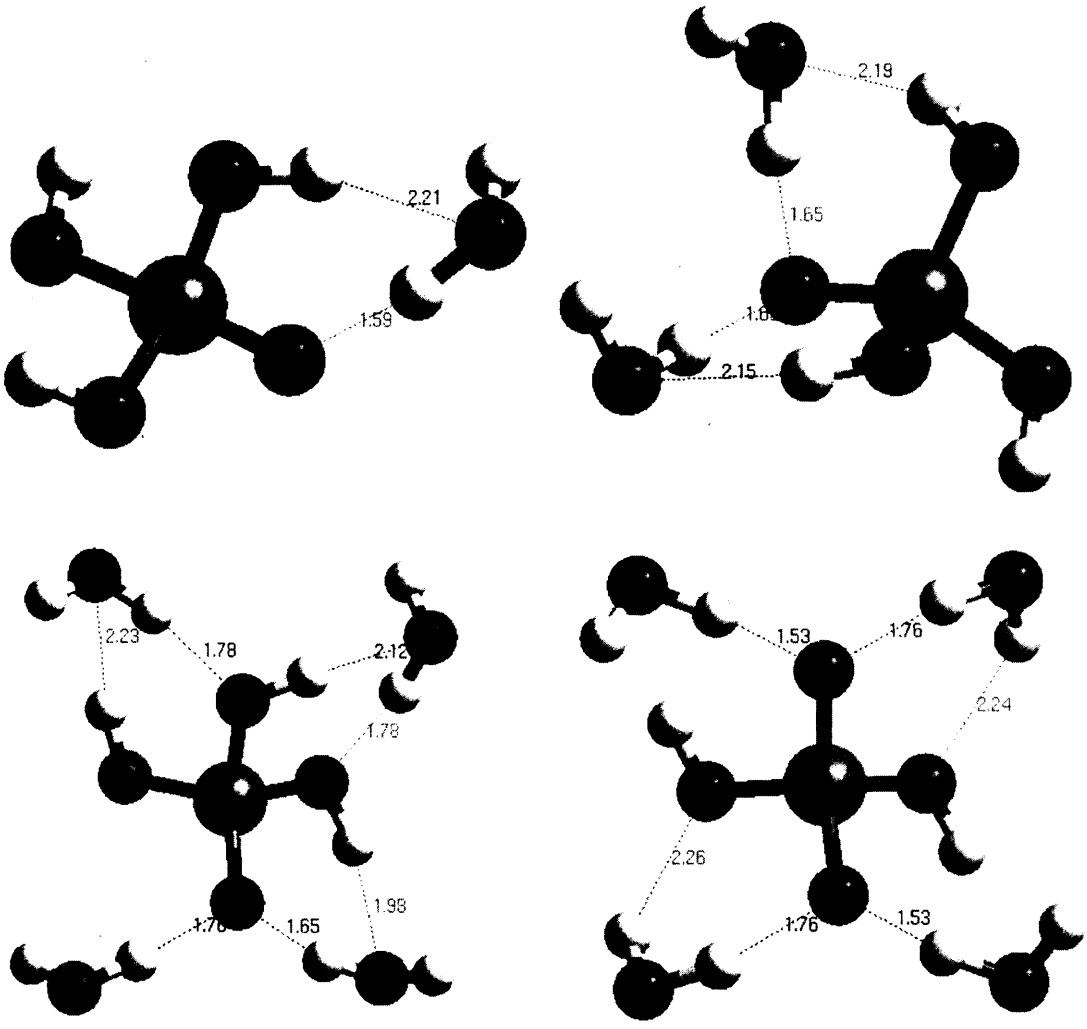

Figure 104 The optimized structures of the solvated anionic monomer with various degrees of explicit solvation.

formation of the very reactive $Si(OH)_2O_2^{2-}$ anion. However, here the likely stabilization effect of the cation is yet to be considered.

The doubly charged monomer is the most strongly deprotonated anion that can be modelled. This is because when the monomer with three and four protons removed is considered, optimization leads to a geometry where the monomer is doubly charged with proton transfer from the water molecule. These theoretical results are in excellent agreement with experiment[93] (Figure 105), where only above pH 14 is there evidence for $Si(OH)O_3^{3-}$.

In concluding this section, it is important to reiterate the constant interaction of water with the neutral monomer, which is independent of the extent of solvation. This result could enable the development of a good model for larger neutral silicates, where the same functional group SiOH, is found, *i.e.* in bigger clusters, only a few explicit water molecules at the site of reaction may be needed to represent the water-silicate interactions. The interaction of the monomer with a water cluster (rows 5 to 7 in Table 43) in COSMO solution reveals a low solvation energy, which could be interpreted as a first insight into the silica low solubility[15]. However, it is also clear that solvation of the bare oxygen in the anionic species is very important, and to model quantitatively the monomer deprotonation (section 4.1.3.1) inclusion of explicit water is necessary.

In spite of our success in describing the solvation of the monomer, it is the simplest species and lacks a key feature of larger oligomers; namely internal H-bonds. Solvation

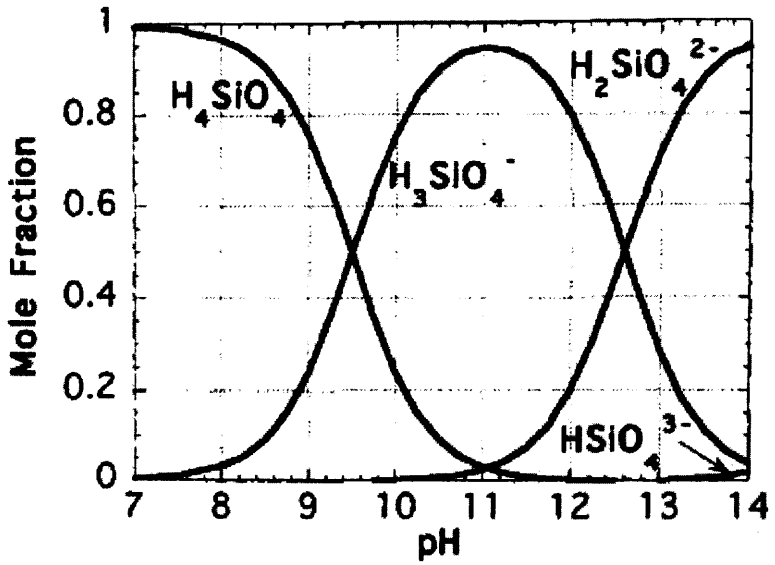

Figure 105 Experimental distribution for the monosilicic acid, $Si(OH)_4$ at different pH. Taken from the work of Sefcik and McCormick[93].

of the dimer considered now, provides an analysis of the contribution of such a feature to the chemistry of aqueous silica.

5.2.2 Dimer Solvation

An analysis of the explicit water solvation of the dimer will provide us with a general picture of the solvation characteristics of larger silicate oligomers, featuring as it does the interaction between hydroxyls on different silicon atoms through H-bonds.

Essentially, there are two distinct sites on the dimer where a water molecule can interact. One interaction is in a position that resembles the monomer-water cluster and in the other; the water molecule links two non-adjacent hydroxyls (HO···SiOSi···OH) as can be seen in the upper part of Figure 106. There are two possible configurations of

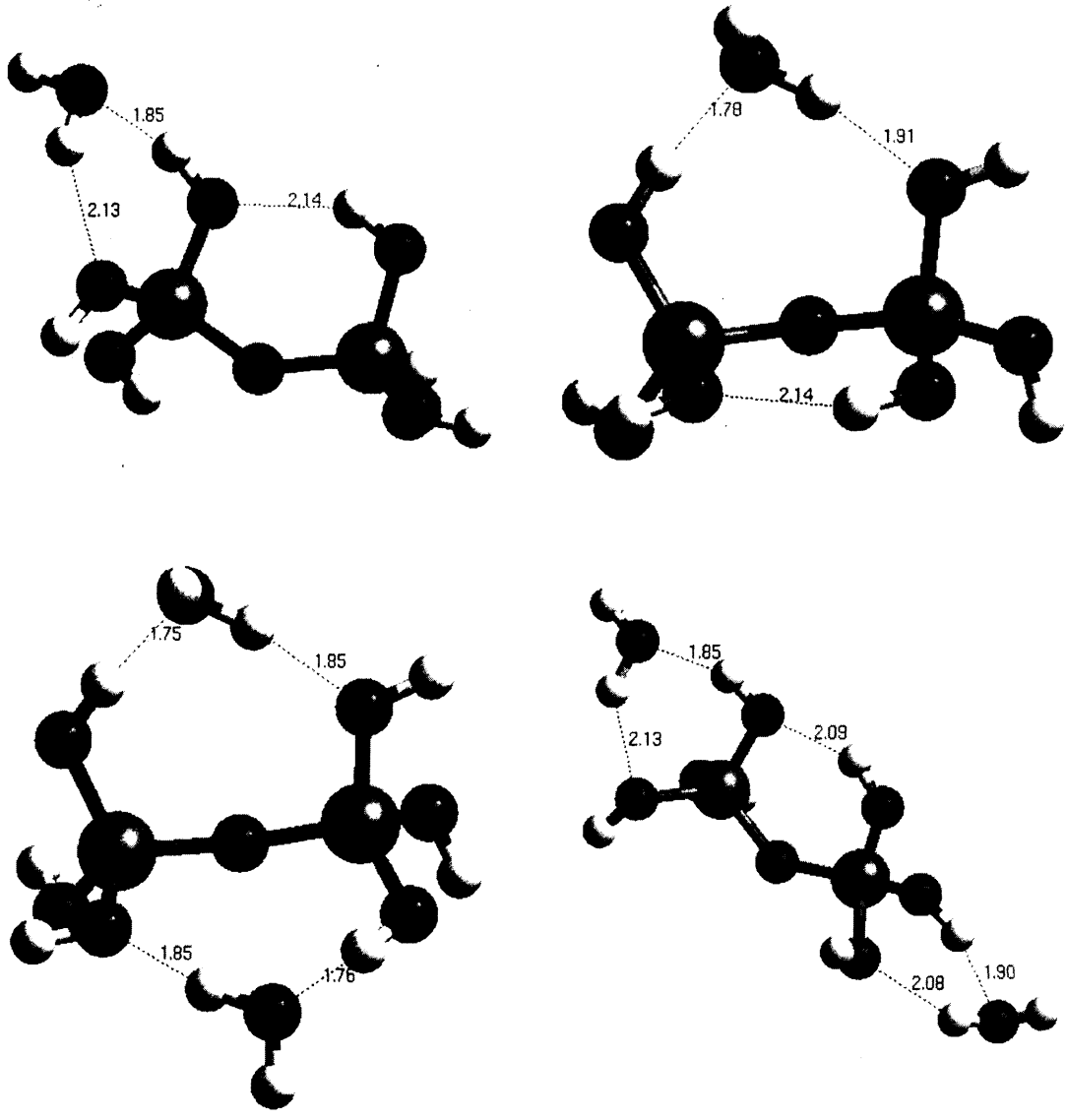

Figure 106 The optimized structures for the association of water on the neutral dimer.

this latter site, but there are at least six sites equivalent to the monomer configuration (lower part of Figure 106). Therefore, the more probable interaction will be the monomer-like site. Figure 106 reveals a shorter H-bond length for the two non-adjacent hydroxyl sites, compared with the other site type: consequently, a stronger interaction is expected, as is indeed calculated (Table 44).

The interactions of water with two adjacent hydroxyls in the dimer are very similar as in the monomer. The H-bond distances are the same: 1.9 Å and 2.1Å, and the energies are within 2 $kJmol^{-1}$. Adding a second water molecule to the dimer near two adjacent hydroxyls has again a similar effect as for the monomer (see Figure 106 and Table 44). Thus, further solvation of the dimer is expected to follow the same trend found for the monomer.

The enthalpy released at 298K when a water molecule binds with two non-adjacent hydroxyls, is twice than that for the single hydroxyl site (22 and 11 $kJmol^{-1}$ respectively) in COSMO solvation (although the difference is less in the gas phase, see Table 44). The higher energy interaction in the first site could be attributed to the ease with which the dimer can accommodate the water molecule. The higher flexibility comes from the flexible Si-O-Si bond and the hydroxyls are non-adjacent. It is very interesting to note the destruction of the internal H-bond in the dimer when two water molecules bridge two non-adjacent hydroxyl sites (Figure 106). However, this

Table 44 The energy and enthalpy ($kJmol^{-1}$ per molecule of water) of association of water and the dimer (D, $SiO_2(OH)_6$) silicate, in the gas phase and in COSMO solvation at 0 and 298K. The dimer D* represents the second and more stable conformation described in the text and shown in Figure 106.

	Gas			Sol.		
Reaction	ΔE	ΔE_0	ΔH_{298}	ΔE	ΔE_0	ΔH_{298}
$D + H_2O \rightarrow D(H_2O)$	-34	-24	-27	-21	-10	-11
$D + H_2O \rightarrow D^*(H_2O)$	-49	-37	-41	-33	-21	-22
$D + 2H_2O \rightarrow D(H_2O)_2$	-33	-23	-26	-22	-10	-12
$D + 2H_2O \rightarrow D^*(H_2O)_2$	-46	-35	-38	-32	-20	-24
$D^{-1} + H_2O \rightarrow D(H_2O)^{-1}$	-63	-53	-55	-30	-18	-22
$D^{-1} + 2H_2O \rightarrow D(H_2O)_2{}^{-1}$	-52	-41	-44	-25	-13	-17
$D^{-2} + 2H_2O \rightarrow D(H_2O)_2{}^{-2}$	-100	-92	-95	-41	-32	-35

configuration remains more stable than the alternative configuration, which retains the internal H-bond (Table 44).

The charged dimers have stronger interactions with the water molecules than the neutral ones, analogous to that found earlier for the monomer (Figure 107). However, in the dimer, the internal H-bond plays a key role in stabilizing the excess charge on the bare oxygen. As a result, the interaction of the water molecule with the charged dimer is weaker than that for the corresponding monomer. In larger clusters, the internal H-bonding stabilizing function could be even more effective, particularly if a chain of H-bonds is formed, as in the 4-ring. In addition, the larger silicate clusters can more readily redistribute the excess negative charge.

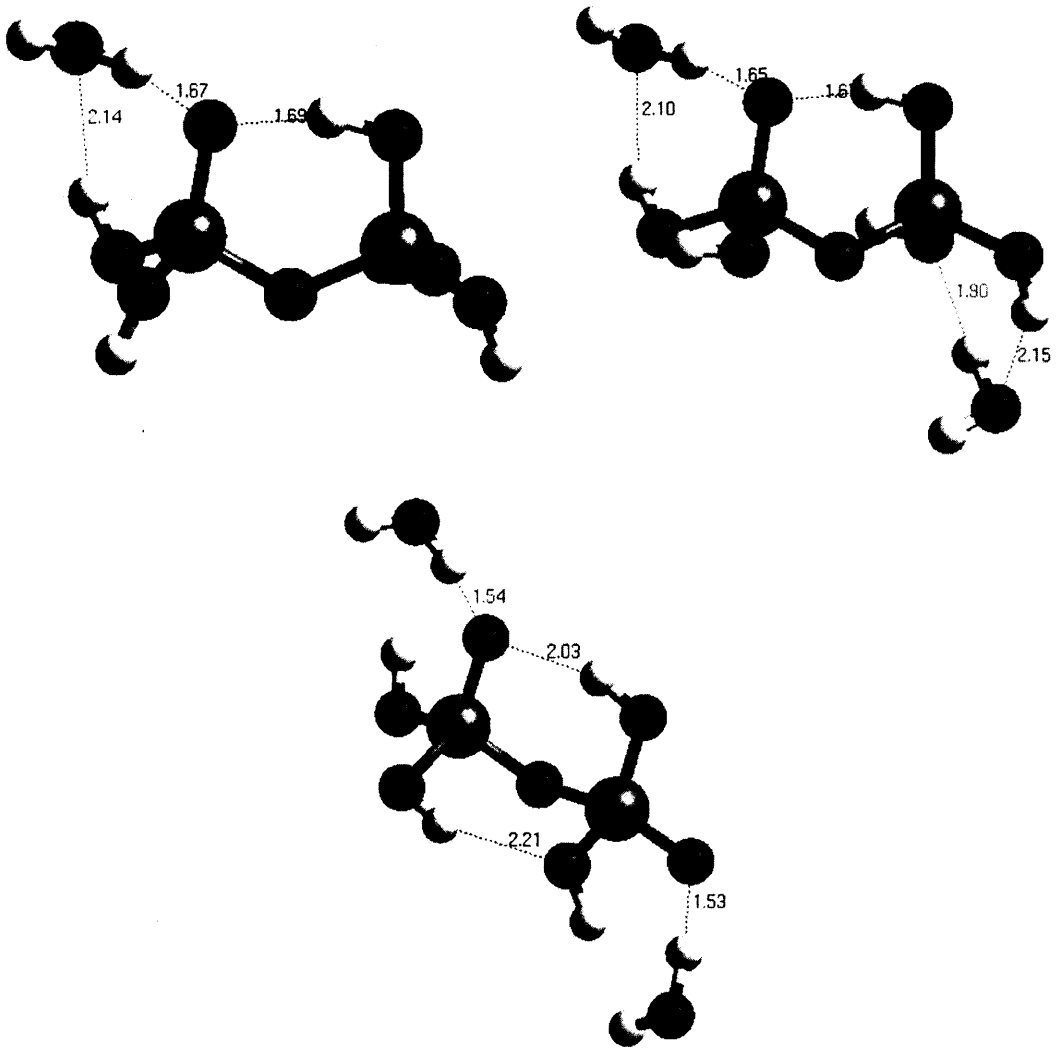

Figure 107 The optimized structures for the association of water on the anionic dimer.

The strong interaction of the internal H-bond to the bare oxygen is confirmed by the shorter H-bond distance (1.69 Å), compared with the neutral dimer (2.14 Å) (Figure 107). Adding a second water molecule to the monocharged dimer does not change the geometry, although there is a slight effect on the energy.

Considering now the doubly deprotonated dimer, we see again, as in the monomer, significant changes. We saw earlier how the doubly charged monomer undergoes a contraction to create a second H-bond to distribute the excess charge (Figure 107). However, a significant difference is that the dimer^{2-} is able to stabilize itself with only two water molecules (with no proton transfer from the water) in contrast to the monomer^{2-}, which requires further solvation.

To summarize, an analysis of the solvation of the dimer shows the importance of flexible angles Si-O-Si in increasing favourable interactions with water. Two different kinds of "water sites" are identified for the dimer. Finally, for this larger cluster, the anionic form stabilizes itself through the formation of internal H-bonds.

5.3 Different electrostatic interactions between two siliceous monomers

During the synthesis of zeolites, it is clear that the interactions between silicates will determine the direction of the synthesis. The low water content prevailing in the synthesis will ensure favourable silicate-silicate interactions, as explained earlier. Furthermore, in sol particles or in a gel structure, the physical interactions between silicates will dominate the properties such as diffusion, water content and the chemical reactions taking place inside them.

This section will present an analysis of the physical interactions between two siliceous monomers, neutral and charged, through H-bonding (Table 45). This interaction will play an important role in the chemical reaction of two monomers; indeed this interaction may be minor when neutral species are reacting, but major in the case of charged species.

The physical interaction between silicate species has not been reported in the literature until now. However, the importance of the study is demonstrated by the results of previous sections. The present study also shows a full comparison of the three main interactions, water-water, water-silicate and silicate-silicate.

Two monomers can interact in three different ways. The first two conformations are shown in the upper part of Figure 108 with three and two H-bonds, respectively. The total energy for these two conformations with different number of H-bonds, are surprisingly similar (≈ -38 $kJmol^{-1}$). Such behaviour could be explained by the H-bond geometries. Two of the H-bonds in the triple H-bonded conformer (Figure 108) are approximately 2.01Å while in the doubly bonded conformer; the distance is only 1.86Å, suggesting a stronger interaction. The third conformation (not shown), where a single hydroxyl (Si-OH) from a monomer interacts with two in the second monomer, is 8.5 $kJmol^{-1}$ less stable. Whilst similar in energy to the double H-bonded conformer, the triple H-bonded conformer is more likely to be dynamically more stable.

An important conclusion can be drawn from these results: a higher number of H-bonds do not necessarily imply a cluster with lower energy (*i.e.* more stable). In other words, different silicate-silicate H-bonds cannot be considered as being equal in energy when two clusters interact, or possibly even when they occur in an intramolecular manner in larger oligomers.

The H-bond lengths in the neutral monomer agglomerate (Figure 108) are very similar to those found between a water with either a monomer or a dimer (Figure 103 and Figure 106, respectively): between 1.85 and 2.1Å. However, the energetics of the interaction between the neutral monomers are significantly stronger; being (approximately 9 $kJmol^{-1}$) more stable than the water-water and monomer-water interactions (Table 45). Thus, we may conclude from this finding that the silicate hydroxyl (Si-OH) forms stronger H-bonds with another silicate than it does with the water hydroxyl (H-OH).

Table 45 The energy and enthalpy ($kJmol^{-1}$) of association of two monomers (M, $Si(OH)_4$), in the gas phase and in COSMO solvation at 0 and 298K.

	Gas			Sol.		
Reaction	ΔE	ΔE_0	ΔH_{298}	ΔE	ΔE_0	ΔH_{298}
$M + M \rightarrow M^{\cdots}M$	-38	-29	-31	-30	-19	-21
$M + M^{-1} \rightarrow M^{\cdots}M^{-1}$	-134	-130	-132	-71	-61	-65
$M + M^{-2} \rightarrow M^{\cdots}M^{-2}$	-356	-350	-350	-124	-122	-122
$M^{-1} + M^{-1} \rightarrow M^{\cdots}M^{-2}$	149	157	154	-66	-61	-63

In a previous section (4.2.1.1), the high reactivity of the singly charged monomer was demonstrated. We now consider the interaction between two monomers, one of which is deprotonated, to give a better insight into the reactions where anionic silicate species participate. The optimized structure is shown in the lower part of Figure 108. A very strong interaction can be observed from the short H-bond between the two species (1.4Å). Indeed, this is the shortest of all the H-bond distances observed in this section. The strong interaction for this agglomerate is confirmed by the more favourable interaction energy, which is approximately four times than that for the neutral monomers.

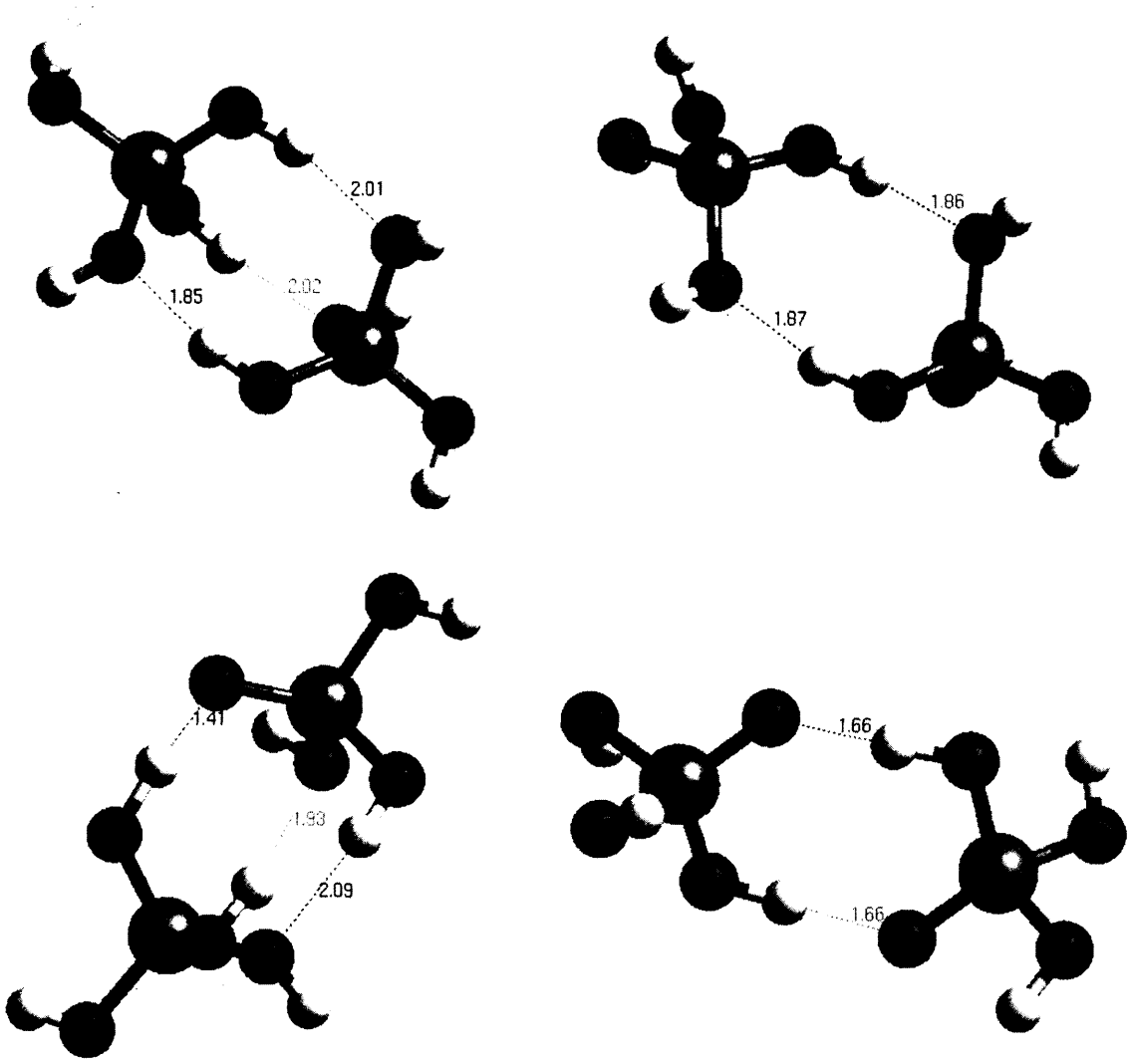

Figure 108 The optimized structures for the association of two neutral monomers (upper part of the figure) and anionic monomers (lower part of the figure).

A more detailed analysis of the geometry for the singly charged monomer-monomer agglomerate (Figure 108), reveals a meta-stable position for the proton with the shortest H-bond. This proton is only slightly off the bisector of the two oxygen atoms, and consequently an easy (and possibly a rapid) proton transfer can be expected. This result has important implications for the stability (equilibrium) of the silicates when anionic species are formed. For example, a $Si(OH)_3O^-$ can easily accept a proton from a larger cluster, where the subsequent increase in anionic charge can be better distributed through the structure. Hence, the importance of the results given in Table 3 (page 119) is emphasised and confirmed here: close approach between an anionic silicate and a neutral species, is likely to facilitate proton transfer.

It is clear from Table 45 that the already strong interactions between neutral silicates are enhanced by the presence of charge. However, when both monomers are deprotonated further, the interaction is electrostatically repulsive, as expected. However, solvation (COSMO only here) allows the monomers to overcome that repulsion, creating a net attractive interaction between two single charged monomers. This result confirms, once again, the importance of solvation in controlling the nucleation of zeolites.

The results for the association of two monomers where only charged clusters are involved, suggest that a reaction is almost inevitable, which is in agreement with the results shown previously (section 4.2.1.1). Finally, a further important conclusion that can be drawn from the results shown here, is that silicate species (even two monomers) are expected to coalesce forming agglomerates, which can be directly correlated with the low $Si(OH)_4$ solubility.

5.4 Final remarks on H-bond relative strength

From our detailed analysis of the different physical interactions that take place in a silica solution, it is possible to derive the relative strengths of the various interactions. Water-water interactions are similar to water-monomer interactions, whilst monomer-monomer interactions are stronger. However, when the multiplicity of sites possible for the interaction of water with (here dimer) larger silicate species takes place, we believe the relative strength of interspecies interactions to be: water-water < silicate-water < silicate-silicate. Certainly, when anionic clusters are present at high pH, then this trend is likely.

Finally, for all silicates where a water molecule interacts with a single hydroxyl (Si-OH), the interaction is expected to be the same as found for a monomer, whilst if water interacts with non-adjacent hydroxyls (HO···SiOSi···OH) the interaction is stronger. In anionic silicates, the monomer will present the strongest silicate-water and silicate-silicate interaction, and we expect a general decrease in these interactions with the size of the silicate.

Perhaps the most important conclusion of this section is, however, that the strength of the interactions between silicate clusters will provide a strong driving force for their aggregation, which will play a major role in zeolite synthesis.

6 CONCLUSIONS

The models studied in this work are a new attempt to understand better the nucleation mechanisms of zeolites. The following conclusions are obtained from the results and their analysis.

- The theoretical methods devised are able to reproduce experimental results accurately. We found that with a few water molecules representing the local solvation together with the COSMO approach, it is possible to obtain high accuracy in the modelling of silicate clusters, even with a relatively low level of theory (basis set and functional). Furthermore, our results show that the COSMO solvation alone is enough to reproduce the trend of the deprotonation reactions.
- pH drives chain condensation reactions. Without the presence of anionic silicate species, some key reactions in the early stages of nucleation are not favourable. The formation of anionic silicate species is possible with the presence of the strong base OH^- (high pH)[xix]. Therefore, the role of pH is to create species that can condense and later form larger clusters.
- Solvation is important in stabilizing more anionic silicate clusters. Water is necessary to stabilize the high charged silicate anions, which in turn are necessary for or produced in some reactions (see previous paragraph).
- Entropy is the main driving force for cyclization. The change of electronic energy by itself is not favourable for these important reactions, but the large positive change in entropy drives internal condensations, forming rings. Our results show that solvation and entropy have some cooperative function in the

[xix] In the fluoride route for zeolite synthesis, this could also be the role of the base F^-.

cyclization; however, the most important contribution in forming rings comes from the change in entropy.

- Ring formation is more favourable than linear condensation under conditions typical of synthesis. From our results, it is evident that there is a tendency to condense internally to form rings, rather than continuing to polymerize to form larger clusters. These results suggest that large linear oligomer silicates will not be present in solution and the formation of large rings will be from other smaller rings, and not directly from linear oligomers.
- pH and temperature selectively control some silicate condensation reactions, *i.e.* allowing some reaction pathways to take place and preventing others.
- Which specific rings are formed (in high concentrations) during nucleation depends on the precise pH and temperature. However, significantly, the 4-ring is unique in being produced under a broad range of pH and temperature conditions. This result could explain why the 4-ring is the most common ring structure in zeolite frameworks.
- 3-ring, 5-ring, 6-ring and d4-ring comprise an important set of cyclic structures in zeolite synthesis. This thesis suggests that all of them are formed favourably thermodynamically. 3-ring and d4-ring are observed experimentally in solution while 5-ring and 6-ring are part of zeolitic frameworks. The d4-ring can be reopened by changing the pH and temperature conditions. The calculated 5-ring has the same geometry as that in the crystalline MFI structure, indicating an early definition of this ring. We suggest that 6-rings are formed from the joining of smaller rings or the opening of the fused4-ring.
- The study of the interactions of water and silicates reveal the importance in the formation of aggregates, which could dictate the future condensation reactions during zeolite nucleation and growth. Experimentally, there is a growing body of evidence that such aggregates are crucial in the early stages of nucleation.

6.1 Future work

This thesis has mainly considered the geometric and thermodynamic properties of key species and reactions. Kinetics have not been considered and clearly knowledge of reaction barriers is necessary and would be very valuable.

The main focus has been on condensation reactions. However, a detailed study of the reactions leading to the dissolution of silicates will help us to understand better this important process involved in the zeolite nucleation.

Only pure silica chemistry has been considered here. However, a similar survey of the role of aluminium is needed to extend the general conclusion from high silica zeolites to low silica systems, where the aluminium has such an important role in directing the structure.

REFERENCES

[1] Cundy, C. S., Cox, P. A., The Hydrothermal Synthesis of Zeolites: History and Development from the Earliest Days to the Present Time *Chem. Rev.* **2003**, *103*, 663.

[2] D. P. Serrano, R. van Grieken, Heterogenous events in the crystallization of zeolites *J. Mater. Chem.* **2001**, *11*, 2391.

[3] C. T. G. Knight, S. D. Kinrade, Comment on Identification of Precursor Species in the Formation of MFI Zeolite in the TPAOH-TEOS-H_2O System *J. Phys. Chem. B* **2002**, *106*, 3329.

[4] C. E. A. Kirschhock, R. Ravishankar, F. Verspeurt, P. J. Grobet, P. A. Jacobs, J. A. Martens, Reply to the Comment on Identification of Precursor Species in the Formation of MFI Zeolite in the TPAOH-TEOS-H_2O System *J. Phys. Chem. B* **2002**, *106*, 3333.

[5] M. Haouas, F. Taulelle, Revisiting the identification of structural units in aqueous silicate solutions by two-dimensional silicon-29 INADEQUATE *J. Phys. Chem. B* **2006**, *110*, 3007.

[6] A. R. Felmy, H. Cho, J. R. Rustad, M. J. Mason, An Aqueous Thermodynamic Model for Polymerized Silica Species to High Ionic Stregth *J. Solution Chem.* **2001**, *30*, 509.

[7] P.-P. E. A. de Moor, T. P. M. Beelen, R. A. van Santen, L. W. Beck, M. E. Davis, Si-MFI Crystallization Using a Dimer and Trimer of TPA Studied with Small-Angle X-ray Scattering *J. Phys. Chem. B* **2000**, *104*, 7600.

[8] P.-P. E. A. de Moor, T. P. M. Beelen, R. A. van Santen, K. Tsuji, M. E. Davis, SAXS and USAXS Investigation on Nanometer-Scaled Precursors in Organic-Mediated Zeolite Crystallization from Gelating Systems *Chem. Mater.* **1999**, *11*, 36.

[9] C. E. A. Kirschhock, R. Ravishankar, F. Verspeurt, P. J. Grobet, P. A. Jacobs, J. A. Martens, Identification of Precursor Species in the Formation of MFI Zeolite in the TPAOH-TEOS-H_2O System *J. Phys. Chem. B* **1999**, *103*, 4965.

[10] D. D. Kragten, J. M. Fedeyko, K. R. Sawant, J. D. Rimer, D. G. Vlachos, R. F. Lobo, M. Tsapatsis, Structure of the silica phase extracted from silica/(TPA)OH solutions containing nanoparticles *J. Phys. Chem. B* **2003**, *107*, 10006.

[11] J. R. Agger, N. Hanif, C. S. Cundy, A. P. Wade, S. Dennison, P. A. Rawlinson, M. W. Anderson, Silicalite crystal growth investigated by atomic force microscopy *J. Am. Chem. Soc.* **2003**, *125*, 830.

[12] C. S. Cundy, P. A. Cox, The hydrothermal synthesis of zeolites: Precursors, intermediates and reaction mechanism *Microporous Mesoporous Mater.* **2005**, *82*, 1.

[13] R. M. Barrer, *Hydrothermal chemistry of zeolites*, Academic Press 1982, London, **1982**.

[14] C. J. Brinker, G. W. Scherer, *Sol-gel science: the physics and chemistry of sol-gel processing*, Harcourt Brace Jovanovich, Boston, **1990**.

[15] R. K. Iler, *The chemistry of silica : solubility, polymerization, colloid and surface properties, and biochemistry*, Wiley, New York, **1979**.

[16] C. Baerlocher, W. M. Meier, D. H. Olson, 5th ed., Elsevier - International Zeolite Association, Amsterdam, **2001**, p. 302.

[17] D. W. Breck, *Zeolite molecular sieves : structure, chemistry and use*, Wiley-Interscience 1974, New York ; London, **1974**.

[18] G. Gottardi, E. Galli, *Natural Zeolites*, Springer-Verlag, Heidelberg, **1985**.

[19] H. Robson, *Verified Syntheses of Zeolitic Materials*, 2nd ed., Elsevier - International Zeolite Association, Amsterdam, **2001**.

[20] R. G. Bell, M. D. Foster, A. Simperler, J. Klinowski, in *Recent Advances in the Science and Technology of Zeolites and Related Materials, Pts a - C, Vol. 154*, **2004**, pp. 1222.

[21] D. J. Earl, M. W. Deem, Toward a database of hypothetical zeolite structures *Ind. Eng. Chem. Res.* **2006**, *45*, 5449.

[22] M. D. Foster, O. D. Friedrichs, R. G. Bell, F. A. A. Paz, J. Klinowski, Chemical evaluation of hypothetical uninodal zeolites *J. Am. Chem. Soc.* **2004**, *126*, 9769.

[23] M. M. J. Treacy, I. Rivin, E. Balkovsky, K. H. Randall, M. D. Foster, Enumeration of periodic tetrahedral frameworks. II. Polynodal graphs *Microporous Mesoporous Mater.* **2004**, *74*, 121.

[24] S. A. Wells, M. D. Foster, M. M. J. Treacy, A simple geometric structure optimizer for accelerated detection of infeasible zeolite graphs *Microporous Mesoporous Mater.* **2006**, *93*, 151.

[25] A. Corma, From microporous to mesoporous molecular sieve materials and their use in catalysis *Chem. Rev.* **1997**, *97*, 2373.

[26] M. E. Davis, Ordered porous materials for emerging applications *Nature* **2002**, *417*, 813.

[27] A. F. Cronstedt, *Akad. Handl. Stockholm* **1756**, *17*, 120.

[28] R. M. Barrer, Synthesis of a Zeolitic Mineral with Chabazite-Like Sorptive Properties *Journal of the Chemical Society* **1948**, 127.

[29] A. K. Cheetham, G. Ferey, T. Loiseau, Open-framework inorganic materials *Angewandte Chemie-International Edition* **1999**, *38*, 3269.

[30] V. Nikolakis, D. G. Vlacho, M. Tsapatsis, Modeling of zeolite crystallization: the role of gel microstructure *Microporous Mesoporous Mater.* **1998**, *21*, 337.

[31] S. D. Kinrade, J. C. H. Donovan, A. S. Schach, C. T. G. Knight, Two substituted cubic octameric silicate cages in aqueous solution *J. Chem. Soc., Dalton Trans.* **2002**, *7*, 1250.

[32] S. D. Kinrade, C. T. G. Knight, D. L. Pole, R. T. Syvitski, Silicon-29 NMR Studies of Tetraalkylammonium Silicate Solutions. 2. Polymerization Kinetics *Inorg. Chem.* **1998**, *37*, 4278.

[33] S. D. Kinrade, C. T. G. Knight, D. L. Pole, R. T. Syvitski, Silicon-29 NMR Studies of Tetraalkylammonium Silicate Solutions. 1. Equilibria, ^{29}Si Chemical Shifts, and ^{29}Si Relaxation *Inorg. Chem.* **1998**, *37*, 4272.

[34] P. Bussian, F. Sobott, B. Brutschy, W. Schrader, F. Schuth, Speciation in solution: Silicate oligomers in aqueous solutions detected by mass spectrometry *Angewandte Chemie-International Edition* **2000**, *39*, 3901.

[35] R. Ravishankar, C. Kirschhock, B. J. Schoeman, P. Vanoppen, P. J. Grobet, S. Storck, W. F. Maier, J. A. Martens, F. C. De Schryver, P. A. Jacobs, Physicochemical Characterization of Silicalite-1 Nanophase Material *J. Phys. Chem. B* **1998**, *102*, 2633.

[36] R. Ravishankar, C. E. A. Kirschhock, P.-P. Knops-Gerrits, E. J. P. Feijen, P. J. Grobet, P. Vanoppen, F. C. De Schryver, G. Miehe, H. Fuess, B. J. Schoeman, P. A. Jacobs, J. A. Martens, Characterization of Nanosized Material Extracted from Clear Suspensions for MFI Zeolite Synthesis *J. Phys. Chem. B* **1999**, *103*, 4960.

[37] S. P. B. Kremer, C. E. A. Kirschhock, A. Aerts, K. Villani, J. A. Martens, O. I. Lebedev, G. Van Tendeloo, Tiling silicalite-1 nanoslabs into 3D mosaics *Advanced Materials* **2003**, *15*, 1705.

[38] F. Schuth, Nucleation and crystallization of solids from solution *Curr.Opin. Sol. State Mater. Sci.* **2001**, *5*, 389.

[39] J. C. G. Pereira, C. R. A. Catlow, G. D. Price, Ab Initio Studies of Silica-Based Clusters. Part II. Structures and Energies of Complex Clusters *J. Phys. Chem. A* **1999**, *103*, 3268.

[40] J. C. G. Pereira, C. R. A. Catlow, G. D. Price, Ab Initio Studies of Silica-Based Clusters. Part I. Energies and Conformations of Simple Clusters *J. Phys. Chem. A* **1999**, *103*, 3252.

[41] D. W. Lewis, C. R. A. Catlow, J. M. Thomas, Application of computer modelling to the mechanisms of synthesis of microporous catalytic materials *Faraday Discuss.* **1997**, 451.

[42] Klamt, A., Jonas, V., Burger, T., Lohrenz, J. C. W., Refinement and Parametrization of COSMO-RS *J. Phys. Chem. A* **1998**, *102*.

[43] A. Klamt, Conductor-like Screening Model for Real Solvents: A New Approach to the Quantitative Calculation of Solvation Phenomena *J. Phys. Chem.* **1995**, *99*, 2224.

[44] A. Klamt, V. Jonas, Treatment of the outlying charge in continuum solvation models *J. Chem. Phys.* **1996**, *105*, 9972.

[45] R. J. Francis, D. O'Hare, The kinetics and mechanisms of the crystallisation of mesoporous materials *J. Chem. Soc., Dalton Trans.* **1998**, 3133.

[46] P.-P. E. A. de Moor, T. P. M. Beelen, B. U. Komanschek, O. Diat, R. A. van Santen, In Situ Investigation of Si-TPA-MFI Crystallization Using (Ultra-) Small- and Wide-Angle X-ray Scattering *J. Phys. Chem. B* **1997**, *101*, 11077.

[47] P.-P. E. A. d. Moor, T. P. M. Beelen, R. A. v. Santen, SAXS/WAXS study on the formation of precursors and crystallization of silicalite *Microporous Mater.* **1997**, *9*, 117.

[48] P. de Moor, T. P. M. Beelen, B. U. Komanschek, R. A. van Santen, Nanometer scale precursors in the crystallization of Si-TPA-MFI *Microporous Mesoporous Mater.* **1998**, *21*, 263.

[49] P.-P. E. A. de Moor, T. P. M. Beelen, R. A. van Santen, In situ Observation of Nucleation and Crystal Growth in Zeolite Synthesis. A Small-Angle X-ray Scattering Investigation on Si-TPA-MFI *J. Phys. Chem. B* **1999**, *103*, 1639.

[50] C. E. A. Kirschhock, R. Ravishankar, P. A. Jacobs, J. A. Martens, Aggregation Mechanism of Nanoslabs with Zeolite MFI-Type Structure *J. Phys. Chem. B* **1999**, *103*, 11021.

[51] C. E. A. Kirschhock, R. Ravishankar, L. V. Looveren, P. A. Jacobs, J. A. Martens, Mechanism of Transformation of Precursors into Nanoslabs in the Early Stages of MFI and MEL Zeolite Formation from TPAOH-TEOS-H_2O and TBAOH-TEOS-H_2O Mixtures *J. Phys. Chem. B* **1999**, *103*, 4972.

[52] C. E. A. Kirschhock, S. P. B. Kremer, P. J. Grobet, P. A. Jacobs, J. A. Martens, New Evidence for Precursor Species in the Formation of MFI Zeolite in the Tetrapropylammonium Hydroxide-Tetraethyl Orthosilicate-Water System *J. Phys. Chem. B* **2002**, *106*, 4897.

[53] R. K. Harris, C. T. G. Knight, Si-29 Nuclear Magnetic-Resonance Studies of Aqueous Silicate Solutions .5. 1st-Order Patterns in Potassium Silicate Solutions Enriched with Si-29 *Journal of the Chemical Society-Faraday Transactions Ii* **1983**, *79*, 1525.

[54] R. K. Harris, C. T. G. Knight, Si-29 Nuclear Magnetic-Resonance Studies of Aqueous Silicate Solutions .6. 2nd-Order Patterns in Potassium Silicate Solutions Enriched with Si-29 *Journal of the Chemical Society-Faraday Transactions Ii* **1983**, *79*, 1539.

[55] C. T. G. Knight, A Two-Dimensional Si-29 Nuclear Magnetic-Resonance Spectroscopic Study of the Structure of the Silicate Anions Present in an Aqueous Potassium Silicate Solution *Journal of the Chemical Society-Dalton Transactions* **1988**, 1457.

[56] S. D. Kinrade, K. Marat, C. T. G. Knight, Longitudinal ^{29}Si Nuclear Magnetic Relaxation in Aqueous Alkali-Metal Silicate Solutions Revisited *J. Phys. Chem.* **1996**, *100*, 18351.

[57] C. S. Gittleman, K. Watanabe, A. T. Bell, C. J. Radke, A mechanistic study of the synthesis of zeolite SSZ-24 *Microporous Mater.* **1996**, *6*, 131.

[58] P. D. Lickiss, in *The Chemistry of organic silicon compounds, Vol. 3* (Eds.: Z. Rappoport, Y. Apeloig), John Wiley & Sons, **2001**.

[59] L. J. Broadbelt, R. Q. Snurr, Applications of molecular modeling in heterogeneous catalysis research *Applied Catalysis a-General* **2000**, *200*, 23.

[60] C. R. A. Catlow, D. S. Coombes, D. W. Lewis, J. C. G. Pereira, Computer Modeling of Nucleation, Growth, and Templating in Hydrothermal Synthesis *Chem. Mater.* **1998**, *10*, 3249.

[61] P. Ugliengo, V. Saunders, E. Garrone, Silanol as a Model for the Free Hydroxyl of Amorphous Silica - Ab Initio Calculations of the Interaction with Water *J. Phys. Chem.* **1990**, *94*, 2260.

[62] J. Sauer, Molecular-Models in Ab Initio Studies of Solids and Surfaces - from Ionic-Crystals and Semiconductors to Catalysts *Chem. Rev.* **1989**, *89*, 199.

[63] J. R. Hill, J. Sauer, Molecular Mechanics Potential for Silica and Zeolite Catalysts Based on Ab-Initio Calculations .1. Dense and Microporous Silica *J. Phys. Chem.* **1994**, *98*, 1238.

[64] V. Moravetski, J. R. Hill, U. Eichler, A. K. Cheetham, J. Sauer, Si-29 NMR chemical shifts of silicate species: Ab initio study of environment and structure effects *J. Am. Chem. Soc.* **1996**, *118*, 13015.

[65] B. Slater, C. R. A. Catlow, Z. Liu, T. Ohsuna, O. Terasaki, M. A. Camblor, Surface Structure and Crystal Growth of Zeolite Beta C *Angew. Chem., Int. Ed. Engl.* **2002**, *41*, 1235.

[66] J. C. G. Pereira, C. R. A. Catlow, G. D. Price, Silica condensation reaction: an ab initio study *Chem. Commun.* **1998**, 1387.

[67] A. A. Sokol, C. R. A. Catlow, J. M. Garces, A. Kuperman, Local States in Microporous Silica and Aluminum Silicate Materials. 1. Modeling Structure, Formation, and Transformation of Common Hydrogen Containing Defects *J. Phys. Chem. B* **2002**, *106*, 6163.

[68] J. B. Foresman, A. Frisch, *Exploring chemistry with electronic structure methods*, 2nd ed., Gaussian, Pittsburgh, PA, **1996**.

[69] P. W. Atkins, J. De Paula, *Atkins' Physical chemistry*, 7th ed., Oxford University Press, Oxford, **2002**.

[70] P. W. Atkins, R. S. Friedman, *Molecular quantum mechanics*, 4th ed., Oxford University Press, Oxford, **2004**.

[71] I. N. Levine, *Physical chemistry*, 4th ed., McGraw-Hill, New York ; London, **1995**.

[72] I. N. Levine, *Quantum chemistry*, 5th ed., Prentice Hall, Upper Saddle River, N.J., **2000**.

[73] F. Jensen, *An introduction to computational chemistry*, Wiley, Chichester, **1999**.

[74] M. P. Allen, D. J. Tildesley, *Computer Simulation of Liquids*, Claredon Press, Oxford, **1994**.

[75] A. R. Leach, *Molecular Modelling Principles and Applications*, 2nd ed., Prentice Hall, Harlow, **2001**.

[76] G. H. Grant, W. G. Richards, *Computational Chemistry*, Oxford University Press, Oxford, **1995**.

[77] P. Hohenberg, W. Kohn, Inhomogeneous Electron Gas *Physical Review B* **1964**, *136*, B864.

[78] C. T. Lee, W. T. Yang, R. G. Parr, Development of the Colle-Salvetti Correlation-Energy Formula into a Functional of the Electron-Density *Physical Review B* **1988**, *37*, 785.

[79] A. D. Becke, A New Mixing of Hartree-Fock and Local Density-Functional Theories *J. Chem. Phys.* **1993**, *98*, 1372.

[80] A. D. Becke, Density-Functional Exchange-Energy Approximation with Correct Asymptotic-Behavior *Phys. Rev. A* **1988**, *38*, 3098.

[81] W. Kohn, L. J. Sham, Self-Consistent Equations Including Exchange and Correlation Effects *Physical Review* **1965**, *140*, 1133.

[82] B. Delley, An All-Electron Numerical-Method for Solving the Local Density Functional for Polyatomic-Molecules *J. Chem. Phys.* **1990**, *92*, 508.

[83] B. Delley, From molecules to solids with the $DMol^3$ approach *J. Chem. Phys.* **2000**, *113*, 7756.

[84] Y. Inada, M. Mori, T. Morisato, H. Orita, On the efficiency of numerical basis sets in $DMol^3$ for predicting the binding energies of hydrogen bonded complexes: Evidence of small basis set superposition error compared to Gaussian basis sets *Conference Poster*.

[85] B. Delley, J. Behler, in *FHI Workshop*, Berlin, **2003**.

[86] J. Tomasi, M. Persico, Molecular-Interactions in Solution - an Overview of Methods Based on Continuous Distributions of the Solvent *Chem. Rev.* **1994**, *94*, 2027.

[87] A. Klamt, G. Schuurmann, Cosmo - a New Approach to Dielectric Screening in Solvents with Explicit Expressions for the Screening Energy and Its Gradient *Journal of the Chemical Society-Perkin Transactions 2* **1993**, 799.

[88] Accelrys Inc. $Cerius^2$, release 4.6 ed., San Diego, USA, **2001**.

[89] K. Baldridge, A. Klamt, First principles implementation of solvent effects without outlying charge error *J. Chem. Phys.* **1997**, *106*, 6622.

[90] G. Schuurmann, Quantum chemical analysis of the energy of proton transfer from phenol and chlorophenols to H_2O in the gas phase and in aqueous solution *J. Chem. Phys.* **1998**, *109*, 9523.

[91] D. A. McQuarrie, J. D. Simon, *Molecular Thermodynamics*, University Science Books, Sausalito, CA, **1999**.

[92] Biosym/MSI, *DMol USER GUIDE*, San Diego, **1995**.

[93] J. Sefcik, A. V. McCormick, Thermochemistry of Aqueous Silicate Solution Precursors to Ceramics *AIChE J.* **1997**, *43*, 2773.

[94] J. A. Tossell, Theoretical study on the dimerization of $Si(OH)_4$ in aqueous solution and its dependence on temperature and dielectric constant *Geochim. Cosmochim. Acta* **2005**, *69*, 283.

[95] A. V. McCormick, A. T. Bell, C. J. Radke, Evidence from Alkali-Metal Nmr-Spectroscopy for Ion-Pairing in Alkaline Silicate Solutions *J. Phys. Chem.* **1989**, *93*, 1733.

[96] Chen, B., Ivanov, I., Park, J. M., Parrinello, M., Klein, M. L., Solvation Structure and Mobility Mechanism of OH-: A Car-Parrinello Molecular Dynamics Investigation of Alkaline Solutions *J. Phys. Chem. B* **2002**, *106*.

[97] J. Sefcik, A. V. McCormick, Prediction of crystallization diagrams for synthesis of zeolites *Chem. Eng. Sci.* **1999**, *54*, 3513.

[98] M. J. S. Dewar, E. G. Zoebisch, E. F. Healy, J. J. P. Stewart, The Development and Use of Quantum-Mechanical Molecular-Models .76. AM1 - a New General-Purpose Quantum-Mechanical Molecular-Model *J. Am. Chem. Soc.* **1985**, *107*, 3902.

[99] R. G. Pearson, Ionization-Potentials and Electron-Affinities in Aqueous-Solution *J. Am. Chem. Soc.* **1986**, *108*, 6109.

[100] J. A. Tossell, N. Sahai, Calculating the acidity of silanols and related oxyacids in aqueous solution *Geochim. Cosmochim. Acta* **2000**, *64*, 4097.

[101] D. H. Aue, H. M. Webb, M. T. Bowers, Thermodynamic Analysis of Solvation Effects on Basicities of Alkylamines - Electrostatic Analysis of Substituent Effects *J. Am. Chem. Soc.* **1976**, *98*, 318.

[102] M. Tuckerman, K. Laasonen, M. Sprik, M. Parrinello, Ab-Initio Molecular-Dynamics Simulation of the Solvation and Transport of Hydronium and Hydroxyl Ions in Water *J. Chem. Phys.* **1995**, *103*, 150.

[103] M. E. Tuckerman, D. Marx, M. Parrinello, The nature and transport mechanism of hydrated hydroxide ions in aqueous solution *Nature* **2002**, *417*, 925.

[104] M. J. Mora-Fonz, C. R. A. Catlow, D. W. Lewis, The role of solvation and pH in the nucleation of the pure silica zeolites *Stud. Surf. Sci. Catal.* **2005**, *158*, 295.

[105] P. Caullet, J. L. Guth, in *Zeolite Synthesis* (Eds.: M. L. Occelli, H. E. Robson), American Chemical Society, Washington DC, **1989**.

[106] L. L. Hench, J. K. West, Molecular-Orbital Models of Silica *Annual Review of Materials Science* **1995**, *25*, 37.

[107] L. L. Hench, J. K. West, The Sol-Gel Process *Chem. Rev.* **1990**, *90*, 33.

[108] B. T. Luke, An Ab-Initio Investigation of the Lowest Potential-Energy Surface of Disiloxane *J. Phys. Chem.* **1993**, *97*, 7505.

[109] J. R. Hill, J. Sauer, Molecular Mechanics Potential for Silica and Zeolite Catalysts Based on Ab-Initio Calculations .2. Aluminosilicates *J. Phys. Chem.* **1995**, *99*, 9536.

[110] S. T. Bromley, M. A. Zwijnenburg, T. Maschmeyer, Fully coordinated silica nanoclusters: $(SiO_2)_N$ molecular rings *Phys. Rev. Lett.* **2003**, *90*, 035502.

[111] S. T. Bromley, M. A. Zwijnenburg, T. Maschmeyer, Two-ring vibrational modes on silica surfaces investigated via fully coordinated nanoclusters *Surf. Sci.* **2003**, *539*, L554.

[112] S. T. Bromley, M. A. Zwijnenburg, E. Flikkema, T. Maschmeyer, Comment on "Fully coordinated silica nanoclusters: $(SiO_2)_N$ molecular rings" - Reply *Phys. Rev. Lett.* **2004**, *92*.

[113] M. W. Zhao, R. Q. Zhang, S. T. Lee, Stable tetrahedral structure of the silica cluster $(SiO_2)_{10}$ *Physical Review B* **2004**, *70*, 205404.

[114] D. J. Zhang, M. W. Zhao, R. Q. Zhang, Two- and three-membered-ring hybrid structures of silica nanoclusters *J. Phys. Chem. B* **2004**, *108*, 18451.

[115] M. W. Zhao, R. Q. Zhang, S. T. Lee, Stable and extendable cage containing nanosize silica clusters based on three-membered rings *Physical Review B* **2004**, *69*.

[116] S. L. Lawton, W. J. Rohrbaugh, The Framework Topology of Zsm-18, a Novel Zeolite Containing Rings of 3 (Si,Al)-O Species *Science* **1990**, *247*, 1319.

[117] A. D. McNaught, A. Wilkinson, *Compendium of chemical terminology : IUPAC recommendations.*, Second ed., Blackwell Science, Oxford, **1997**.

[118] M. T. Melchior, D. E. W. Vaughan, C. F. Pictroski, Local Environment Fine-Structure in the Si-29 Nmr-Spectra of Faujasite Zeolites *J. Phys. Chem.* **1995**, *99*, 6128.

[119] S. Caratzoulas, D. G. Vlachos, M. Tsapatsis, On the role of tetramethylammonium cation and effects of solvent dynamics on the stability of the cage-like silicates $Si_6O_{15}^{6-}$ and $Si_8O_{20}^{8-}$ in aqueous solution. A molecular dynamics study *J. Am. Chem. Soc.* **2006**, *128*, 596.

[120] S. Sugiyama, S. Yamamoto, O. Matsuoka, H. Nozoye, J. Yu, G. Zhu, S. Qiu, O. Terasaki, AFM observation of double 4-rings on zeolite LTA crystals surface *Microporous Mesoporous Mater.* **1999**, *28*, 1.

[121] G. Sastre, J. A. Vidal-Moya, T. Blasco, J. Rius, J. L. Jorda, M. T. Navarro, F. Rey, A. Corma, Preferential location of Ge atoms in polymorph C of beta zeolite (ITQ-17) and their structure-directing effect: A computational, XRD, and NMR spectroscopic study *Angewandte Chemie-International Edition* **2002**, *41*, 4722.

[122] T. Blasco, A. Corma, M. J. Diaz-Cabanas, F. Rey, J. A. Vidal-Moya, C. M. Zicovich-Wilson, Preferential location of Ge in the double four-membered ring units of ITQ-7 zeolite *J. Phys. Chem. B* **2002**, *106*, 2634.

[123] M. A. Zwijnenburg, S. T. Bromley, J. C. Jansen, T. Maschmeyer, Computational insights into the role of Ge in stabilising double-four ring containing zeolites *Microporous Mesoporous Mater.* **2004**, *73*, 171.

[124] B. Slater, J. O. Titiloye, F. M. Higgins, S. C. Parker, Atomistic simulation of zeolite surfaces *Current Opinion in Solid State & Materials Science* **2001**, *5*, 417.

[125] S. Dumrul, S. Bazzana, J. Warzywoda, R. R. Biederman, A. S. Jr., Imaging of crystal growth-induced fine surface features in zeolite A by atomic force microscopy *Microporous Mesoporous Mater.* **2002**, *54*, 79.

[126] E. R. Cooper, C. D. Andrews, P. S. Wheatley, P. B. Webb, P. Wormald, R. E. Morris, Ionic liquids and eutectic mixtures as solvent and template in synthesis of zeolite analogues *Nature* **2004**, *430*, 1012.

[127] M. Matsukata, M. Ogura, T. Osaki, P. Rao, M. Nomura, E. Kikuchi, Conversion of dry gel to microporous crystals in gas phase *Top. Catal.* **1999**, *9*, 77.

[128] M. J. Mora-Fonz, C. R. A. Catlow, D. W. Lewis, Oligomerization and Cyclisation Processes in the Nucleation of Microporous Silicas *Angew. Chem., Int. Ed. Engl.* **2005**, *44*, 3082.

[129] H. Lechert, in *Verified Syntheses of Zeolitic Materials*, 2nd ed. (Ed.: H. Robson), Elsevier - International Zeolite Association, Amsterdam, **2001**, p. 266.

[130] W. Y. Xu, J. X. Dong, J. P. Li, J. Q. Li, F. Wu, A Novel Method for the Preparation of Zeolite Zsm-5 *Journal of the Chemical Society-Chemical Communications* **1990**, 755.

[131] L. A. Curtiss, D. J. Frurip, M. Blander, Studies of Molecular Association in H_2O and D_2O Vapors by Measurement of Thermal-Conductivity *J. Chem. Phys.* **1979**, *71*, 2703.

[132] K. S. Kim, B. J. Mhin, U. S. Choi, K. Lee, Ab Initio Studies of the Water Dimer Using Large Basis-Sets - the Structure and Thermodynamic Energies *J. Chem. Phys.* **1992**, *97*, 6649.

[133] B. S. Jursic, Computational study of water and ammonia dimers with density functional theory methods *Journal of Molecular Structure-Theochem* **1998**, *434*, 29.

[134] D. J. Wales, M. P. Hodges, Global minima of water clusters $(H_2O)_n$, n <= 21, described by an empirical potential *Chem. Phys. Lett.* **1998**, *286*, 65.

[135] Y. C. Choi, C. Pak, K. S. Kim, Electric field effects on water clusters (n=3-5): Systematic ab initio study of structures, energetics, and transition states *J. Chem. Phys.* **2006**, *124*.

[136] T. James, D. J. Wales, J. Hernandez-Rojas, Global minima for water clusters $(H_2O)_n$, n <= 21, described by a five-site empirical potential *Chem. Phys. Lett.* **2005**, *416*, 302.

[137] H. Kabrede, R. Hentschke, Global minima of water clusters $(H_2O)_N$, N <= 25, described by three empirical potentials *J. Phys. Chem. B* **2003**, *107*, 3914.

[138] A. A. Vostrikov, S. V. Drozdov, V. S. Rudnev, L. I. Kurkina, Molecular dynamics study of neutral and charged water clusters *Computational Materials Science* **2006**, *35*, 254.

[139] M. E. Dunn, E. K. Pokon, G. C. Shields, The ability of the Gaussian-2, Gaussian-3, Complete Basis Set-QB3, and Complete Basis Set-APNO model chemistries to model the geometries of small water clusters *Int. J. Quantum Chem.* **2004**, *100*, 1065.

[140] A. G. Baboul, L. A. Curtiss, P. C. Redfern, K. Raghavachari, Gaussian-3 theory using density functional geometries and zero-point energies *J. Chem. Phys.* **1999**, *110*, 7650.

[141] J. Sefcik, W. A. Goddard, Thermochemistry of silicic acid deprotonation: Comparison of gas-phase and solvated DFT calculations to experiment *Geochim. Cosmochim. Acta* **2001**, *65*, 4435.

APPENDIX A TOTAL ENERGIES OF SILICATE CLUSTERS

The following tables show the electronic energy (including the ZPE), the entropy, enthalpy and free energy for all the clusters analysed in this thesis. All results are in Hartrees (1 Ha = 2625.5 $kJmol^{-1}$). The clusters were optimized and the energy calculated with BLYP/DNP as described in the section 3.1 (page 48). Some clusters were not calculated in the COSMO solvation but the row is left in blank, so the order is the same as in the table for the gas phase.

a. Calculation on species in gas phase

	E+ZPE	TS		H		G	
T (K) ->	0	298	450	298	450	298	450
NaOH	-238.15945	0.027	0.044	-238.15503	-238.15233	-238.18226	-238.19671
OH^-	-75.791471	0.02	0.032	-75.788166	-75.786483	-75.807759	-75.818108
H_2O	-76.431242	0.022	0.036	-76.427463	-76.4255	-76.449576	-76.461267
monomer	-593.07253	0.038	0.067	-593.0644	-593.05701	-593.10261	-593.12363
$monomer^-$	-592.51638	0.038	0.066	-592.50844	-592.50162	-592.54685	-592.56786
$monomer^{2-}$	-591.76728	0.036	0.062	-591.76019	-591.75401	-591.79656	-591.81639
$monomer^{3-}$	-590.81486	0.036	0.061	-590.80824	-590.80264	-590.84386	-590.8632
$monomer^{4-}$	-589.64936	0.034	0.058	-589.64335	-589.63826	-589.67781	-589.69645
monomerNa	-754.83735	0.041	0.072	-754.82822	-754.82018	-754.86967	-754.89249
$monomerNa_2$	-916.59242	0.044	0.078	-916.58228	-916.57356	-916.62678	-916.6513
$monomerNa_3$	-1078.3529	0.047	0.083	-1078.3419	-1078.3325	-1078.389	-1078.415
$monomerNa_4$	-1240.1085	0.049	0.086	-1240.0967	-1240.0867	-1240.1459	-1240.1731
dimer	-1109.7195	0.055	0.098	-1109.7056	-1109.6927	-1109.7605	-1109.7911
$dimer^-$	-1109.193	0.051	0.092	-1109.1801	-1109.1681	-1109.2313	-1109.26
$dimer^{2-}$	-1108.5071	0.049	0.088	-1108.495	-1108.4836	-1108.5443	-1108.5718
$dimer^{3-}$	-1107.6651	0.048	0.086	-1107.6534	-1107.6426	-1107.7018	-1107.7287
$dimer^{4-}$	-1106.6666	0.048	0.085	-1106.6553	-1106.645	-1106.7033	-1106.73
dimerNa	-1271.4909	0.055	0.099	-1271.4764	-1271.463	-1271.5314	-1271.5623
$dimerNa_2$	-1433.2486	0.059	0.106	-1433.233	-1433.219	-1433.2919	-1433.3249
trimer	-1626.3681	0.065	0.121	-1626.3489	-1626.3305	-1626.4143	-1626.4515
$trimer^-$	-1625.8604	0.061	0.113	-1625.8425	-1625.8253	-1625.9038	-1625.9386
$trimer^{2-}$	-1625.1985	0.06	0.11	-1625.1813	-1625.1647	-1625.2411	-1625.2751
$trimer^{3-}$	-1624.403	0.058	0.107	-1624.3867	-1624.3708	-1624.4451	-1624.4783
$trimer^{4-}$	-1623.4897	0.06	0.11	-1623.4732	-1623.4575	-1623.5336	-1623.5677
trimerNa	-1788.1541	0.066	0.123	-1788.1339	-1788.115	-1788.2004	-1788.2383
$trimerNa_2$	-1949.939	0.071	0.131	-1949.9176	-1949.898	-1949.9886	-1950.0289
3ring	-1549.9266	0.061	0.111	-1549.9095	-1549.8933	-1549.9701	-1550.0043
$3ring^-$	-1549.4037	0.055	0.102	-1549.3884	-1549.3734	-1549.4438	-1549.4751
$3ring^{2-}$	-1548.7403	0.054	0.099	-1548.7257	-1548.7113	-1548.7797	-1548.8103
$3ring^{3-}$	-1547.9484	0.054	0.098	-1547.9342	-1547.9204	-1547.9878	-1548.0181
$3ring^{4-}$	-1547.0066	0.05	0.092	-1546.9936	-1546.9806	-1547.044	-1547.0725
3ringNa	-1711.703	0.061	0.112	-1711.6852	-1711.6685	-1711.7459	-1711.7803
$3ringNa_2$	-1873.4809	0.063	0.116	-1873.4621	-1873.4447	-1873.5252	-1873.561

3-1ring	-2066.5825	0.071	0.132	-2066.5604	-2066.539	-2066.631	-2066.6714
3-1ring^{-}	-2066.0739	0.067	0.125	-2066.0533	-2066.0331	-2066.12	-2066.1582
3-1ring^{2-}	-2065.4375	0.065	0.123	-2065.4175	-2065.3979	-2065.483	-2065.5205
3-1ring^{3-}	-2064.6611	0.066	0.122	-2064.6414	-2064.6222	-2064.707	-2064.7444
3-1ring^{4-}	-2063.8099	0.066	0.122	-2063.7908	-2063.7722	-2063.8566	-2063.8941
d3ring	-2870.5613	0.077	0.146	-2870.5359	-2870.5107	-2870.6127	-2870.6571
d3ring^{-}	-2870.0432	0.074	0.141	-2870.0188	-2869.9943	-2870.0929	-2870.1358
d3ring^{2-}	-2869.4177	0.073	0.139	-2869.3938	-2869.37	-2869.4666	-2869.5087
d3ring^{3-}	-2868.6678	0.072	0.137	-2868.6446	-2868.6213	-2868.7164	-2868.7579
d3ring^{4-}	-2867.8132	0.071	0.135	-2867.7905	-2867.7677	-2867.8616	-2867.9026
fused3	-1990.1277	0.064	0.119	-1990.1084	-1990.0894	-1990.1722	-1990.2087
fused3^{-}	-1989.6178	0.061	0.114	-1989.5996	-1989.5815	-1989.6608	-1989.6959
fused3^{2-}	-1988.9593	0.06	0.113	-1988.9415	-1988.9239	-1989.002	-1989.0366
fused3^{3-}	-1988.2007	0.06	0.112	-1988.1834	-1988.1663	-1988.2438	-1988.2782
fused3^{4-}	-1987.3138	0.059	0.11	-1987.2972	-1987.2806	-1987.3566	-1987.3904
3-2ring	-2583.2304	0.084	0.159	-2583.2028	-2583.176	-2583.2869	-2583.3354
3-2ring^{-}	-2582.7275	0.082	0.156	-2582.7007	-2582.6748	-2582.7831	-2582.8305
3-2ring^{2-}	-2582.1151	0.081	0.153	-2582.089	-2582.0638	-2582.1702	-2582.2168
tetramer	-2143.019	0.077	0.144	-2142.9945	-2142.9708	-2143.071	-2143.115
tetramer^{-}	-2142.5221	0.074	0.139	-2142.4988	-2142.4762	-2142.5725	-2142.6148
tetramer^{2-}	-2141.8848	0.071	0.134	-2141.8624	-2141.8407	-2141.9339	-2141.9749
tetramer^{3-}	-2141.1208	0.072	0.135	-2141.0986	-2141.0772	-2141.1707	-2141.212
tetramer^{4-}	-2140.2475	0.072	0.134	-2140.2261	-2140.2055	-2140.2981	-2140.3391
tetramerNa	-2304.8058	0.078	0.147	-2304.7805	-2304.7564	-2304.8585	-2304.9033
tetramerNa$_2$	-2466.5868	0.079	0.149	-2466.5608	-2466.5362	-2466.6401	-2466.6857
tetrahedron	-1913.6646	0.058	0.108	-1913.6481	-1913.6315	-1913.7063	-1913.7395
tetrahedron^{-}	-1913.1441	0.054	0.101	-1913.1291	-1913.1137	-1913.1835	-1913.2144
tetrahedron^{2-}	-1912.5026	0.054	0.1	-1912.4877	-1912.4724	-1912.5416	-1912.5723
tetrahedron^{3-}	-1911.7345	0.052	0.096	-1911.7204	-1911.7058	-1911.7726	-1911.8022
tetrahedron^{4-}	-1910.8391	0.051	0.093	-1910.8258	-1910.8118	-1910.8764	-1910.9051
4ring	-2066.5795	0.076	0.14	-2066.5573	-2066.5363	-2066.6331	-2066.6762
4ring^{-}	-2066.0773	0.068	0.127	-2066.0566	-2066.0364	-2066.1243	-2066.163
4ring^{2-}	-2065.4323	0.067	0.125	-2065.4121	-2065.3925	-2065.479	-2065.5173
4ring^{3-}	-2064.6568	0.068	0.126	-2064.6367	-2064.6174	-2064.7044	-2064.743
4ring^{4-}	-2063.7679	0.065	0.121	-2063.7485	-2063.7297	-2063.8138	-2063.851
4ringNa	-2228.3541	0.074	0.138	-2228.3311	-2228.3093	-2228.4047	-2228.4468
4ringNa$_2$	-2390.1519	0.073	0.138	-2390.1282	-2390.1055	-2390.2016	-2390.2438
4-one-ring	-2506.7898	0.079	0.149	-2506.7645	-2506.7399	-2506.8433	-2506.8887

4-one-ring^{-}	-2506.2895	0.076	0.143	-2506.265	-2506.2413	-2506.3411	-2506.3848
4-one-ring^{2-}	-2505.6504	0.076	0.142	-2505.6264	-2505.6034	-2505.7021	-2505.7456
4-one-ring^{3-}	-2504.8909	0.074	0.139	-2504.8676	-2504.8451	-2504.9416	-2504.984
4-one-ring^{4-}	-2504.0263	0.073	0.138	-2504.0035	-2503.9815	-2504.0769	-2504.119
4-three-ring	-2506.7926	0.077	0.145	-2506.7676	-2506.7432	-2506.8441	-2506.8883
4-three-ring^{-}	-2506.2991	0.073	0.139	-2506.2753	-2506.252	-2506.3486	-2506.3909
4-three-ring^{2-}	-2505.6457	0.07	0.133	-2505.6233	-2505.601	-2505.6935	-2505.7339
4-three-ring^{3-}	-2504.8971	0.071	0.134	-2504.8746	-2504.8523	-2504.9454	-2504.9861
4-three-ring^{4-}	-2504.0452	0.07	0.132	-2504.0233	-2504.0015	-2504.0932	-2504.1334
4-1-ring	-2583.2267	0.086	0.163	-2583.1987	-2583.1717	-2583.2852	-2583.335
4-1-ring^{-}	-2582.7328	0.08	0.151	-2582.7069	-2582.6813	-2582.7867	-2582.8328
4-1-ring^{2-}	-2582.104	0.078	0.147	-2582.0789	-2582.054	-2582.1565	-2582.2013
4-1-ring^{3-}	-2581.354	0.075	0.143	-2581.3299	-2581.3057	-2581.4051	-2581.4486
4-1-ring^{4-}	-2580.5285	0.078	0.147	-2580.5039	-2580.4799	-2580.582	-2580.6268
4-2-ring	-3099.8877	0.095	0.182	-3099.8545	-3099.8223	-3099.9492	-3100.0043
4-2-ring^{-}	-3099.4048	0.094	0.179	-3099.373	-3099.3423	-3099.4671	-3099.5215
4-2-ring^{2-}	-3098.7815	0.092	0.176	-3098.7499	-3098.7195	-3098.8419	-3098.8952
fused4_ring	-3023.4375	0.081	0.157	-3023.4099	-3023.381	-3023.4905	-3023.5377
fused4_ring^{1-}	-3022.96	0.086	0.164	-3022.931	-3022.9027	-3023.0167	-3023.0664
fused4_ring^{2-}	-3022.3345	0.089	0.168	-3022.3049	-3022.2765	-3022.3937	-3022.4449
fused4_ring^{3-}	-3021.5967	0.083	0.159	-3021.5688	-3021.5412	-3021.6522	-3021.7006
fused4_ring^{4-}	-3020.7458	0.082	0.156	-3020.7185	-3020.6914	-3020.8002	-3020.8476
pentamer	-2659.6697	0.088	0.168	-2659.6397	-2659.6106	-2659.728	-2659.7791
pentamerNa	-2821.4548	0.088	0.168	-2821.4248	-2821.3958	-2821.513	-2821.5641
pentamer^{-}	-2659.1881	0.083	0.158	-2659.1604	-2659.1331	-2659.2433	-2659.2914
pentamer^{2-}	-2658.5654	0.085	0.16	-2658.5374	-2658.5102	-2658.6219	-2658.6707
pentamer^{3-}	-2657.8283	0.084	0.159	-2657.8005	-2657.7739	-2657.8845	-2657.9328
pentamer^{4-}	-2656.9699	0.084	0.159	-2656.9429	-2656.9168	-2657.027	-2657.0754
5ring	-2583.2297	0.086	0.163	-2583.2012	-2583.1741	-2583.2875	-2583.3371
5ring^{-}	-2582.7416	0.079	0.151	-2582.7154	-2582.6897	-2582.7945	-2582.8402
5ring^{2-}	-2582.122	0.077	0.146	-2582.097	-2582.0726	-2582.1738	-2582.2181
5ring^{3-}	-2581.3587	0.077	0.146	-2581.3336	-2581.3091	-2581.4104	-2581.4547
5ring^{4-}	-2580.4982	0.076	0.144	-2580.4737	-2580.4497	-2580.5496	-2580.5933
5ringNa	-2745.0167	0.085	0.161	-2744.9884	-2744.9611	-2745.0731	-2745.122
5ringNa$_2$	-2906.8058	0.086	0.163	-2906.7767	-2906.7489	-2906.8624	-2906.912
5-2-ring	-3540.0952	0.106	0.204	-3540.058	-3540.0223	-3540.1642	-3540.2259
hexamer	-3176.3246	0.101	0.194	-3176.2891	-3176.2547	-3176.3899	-3176.4485
hexamer^{-}	-3175.8405	0.099	0.189	-3175.806	-3175.7727	-3175.9049	-3175.9622
hexamer^{2-}	-3175.2472	0.096	0.184	-3175.2139	-3175.1816	-3175.3096	-3175.3652

hexamer^{3-}	-3174.5164	0.094	0.18	-3174.484	-3174.4523	-3174.5781	-3174.6327
hexamer^{4-}	-3173.7023	0.09	0.173	-3173.6715	-3173.6406	-3173.7614	-3173.8137
6ring	-3099.8814	0.097	0.185	-3099.8483	-3099.8162	-3099.9455	-3100.0017
6ring^{-}	-3099.3884	0.093	0.178	-3099.3568	-3099.3258	-3099.45	-3099.504
6ring^{2-}	-3098.7899	0.09	0.172	-3098.7594	-3098.7293	-3098.8491	-3098.9011
6ring^{3-}	-3098.0689	0.088	0.168	-3098.0394	-3098:0101	-3098.1274	-3098.1785
6ring^{4-}	-3097.2565	0.085	0.162	-3097.2281	-3097.1996	-3097.3127	-3097.3618
d4ring	-3827.4414	0.097	0.187	-3827.4071	-3827.3733	-3827.5036	-3827.56
d4ring^{-}	-3826.9239	0.09	0.175	-3826.8918	-3826.8594	-3826.9816	-3827.0342
d4ring^{2-}	-3826.3077	0.089	0.173	-3826.2758	-3826.2436	-3826.3647	-3826.4168
d4ring^{3-}	-3825.5844	0.087	0.17	-3825.5534	-3825.5218	-3825.6404	-3825.6914
d4ring^{4-}	-3824.7634	0.085	0.166	-3824.7332	-3824.7023	-3824.8182	-3824.8679
d4-1-ring	-4344.0898	0.114	0.219	-4344.0489	-4344.0093	-4344.1625	-4344.2288
d4-1-ring^{-}	-4343.5919	0.108	0.21	-4343.5526	-4343.5141	-4343.6607	-4343.7239
d4-1-ring^{2-}	-4342.9864	0.106	0.206	-4342.9478	-4342.91	-4343.0538	-4343.1158
4-4-ring	-4056.7387	0.116	0.224	-4056.6972	-4056.6566	-4056.813	-4056.8806
tri4-ring	-3980.3199	0.109	0.211	-3980.2803	-3980.2419	-3980.3894	-3980.4531
tri4-ring^{-}	-3980.0543	0.065	0.12	-3979.9086	-3979.9704	-3980.0543	-3980.0543
tri4-ring^{2-}	-3979.2344	0.101	0.196	-3979.1977	-3979.1614	-3979.2984	-3979.3573
tri4-ring^{3-}	-3978.7093	0.062	0.116	-3978.5799	-3978.6383	-3978.7093	-3978.7093
tri4-ring^{4-}	-3977.8858	0.061	0.114	-3977.7645	-3977.8208	-3977.8858	-3977.8858
open-d4ring	-3903.8794	0.105	0.202	-3903.842	-3903.8056	-3903.9467	-3904.0077
open-d4ring^{-}	-3903.3816	0.102	0.196	-3903.3454	-3903.3104	-3903.4474	-3903.5068
open-d4ring^{2-}	-3902.7641	0.102	0.196	-3902.728	-3902.6931	-3902.8299	-3902.8892
open-d4ring^{3-}	-3902.0561	0.096	0.187	-3902.0217	-3901.9878	-3902.1182	-3902.1745
open-d4ring^{4-}	-3901.2398	0.095	0.183	-3901.2061	-3901.1727	-3901.3008	-3901.3561
d6ring	-5741.1748	0.121	0.241	-5741.1271	-5741.0787	-5741.2479	-5741.3197
d6ring^{-}	-5740.6716	0.133	0.26	-5740.6209	-5740.5712	-5740.7536	-5740.8316
d6ring^{2-}	-5740.0899	0.125	0.249	-5740.0411	-5739.9921	-5740.1664	-5740.2406
d6ring^{3-}	-5739.4119	0.121	0.241	-5739.3645	-5739.3165	-5739.4859	-5739.5579
d6ring^{4-}	-5738.645	0.116	0.232	-5738.5994	-5738.5524	-5738.7155	-5738.7846
$(H_2O)_2$	-152.86671	0.033	0.055	-152.86009	-152.85555	-152.89273	-152.91034
$(H_2O)_3$	-229.30762	0.036	0.061	-229.30045	-229.29481	-229.33611	-229.35548
$(H_2O)_4$	-305.75193	0.042	0.072	-305.74281	-305.73534	-305.78445	-305.80725
$(H_2O)_5$	-382.19883	0.052	0.092	-382.18542	-382.17418	-382.23737	-382.26623
$(H_2O)_6$	-458.61346	0.065	0.115	-458.59553	-458.58135	-458.66022	-458.69621
$(H_2O)_{10}$	-764.41203	0.075	0.141	-764.38748	-764.36517	-764.46268	-764.50573
H_3O^+	-76.686506	0.023	0.037	-76.682723	-76.680712	-76.705631	-76.717736
$H_3O(H_2O)_3^-$	-306.09865	0.047	0.083	-306.08693	-306.07758	-306.13432	-306.16046

$OH(H_2O)^-$	-152.28292	0.029	0.048	-152.27793	-152.27417	-152.30669	-152.32214
$OH(H_2O)_4^-$	-381.65623	0.05	0.089	-381.64362	-381.63303	-381.69376	-381.72155
$OH(H_2O)_5^-$	-458.10768	0.053	0.095	-458.09348	-458.08094	-458.14616	-458.17565
$NaOH(H_2O)_3$	-467.53989	0.046	0.081	-467.52866	-467.51919	-467.57441	-467.59973
$monomerOH^-$	-668.97318	0.047	0.083	-668.96224	-668.95302	-669.00966	-669.03578
$monomerOH^{2-}$	-668.24898	0.043	0.075	-668.23944	-668.23109	-668.28238	-668.30602
$monomer(H_2O)$	-669.51234	0.045	0.079	-669.50157	-669.49184	-669.54638	-669.57127
$monomer(H_2O)^-$	-668.97498	0.045	0.079	-668.96451	-668.95552	-669.00986	-669.03487
$monomer(H_2O)_2$	-745.95235	0.052	0.093	-745.93876	-745.92667	-745.99072	-746.01975
$monomer(H_2O)_2^-$	-745.42368	0.052	0.092	-745.41055	-745.39909	-745.4621	-745.4908
$monomer(H_2O)_2^-$	-745.4279	0.052	0.093	-745.41475	-745.40335	-745.46712	-745.49622
$monomer(H_2O)_2^{2-}$	-744.73246	0.047	0.083	-744.72132	-744.71128	-744.76798	-744.79388
$monomer(H_2O)_3$	-822.39437	0.057	0.104	-822.37844	-822.36411	-822.43583	-822.46811
$monomer(H_2O)_4$	-898.83597	0.063	0.116	-898.81742	-898.80082	-898.88089	-898.91675
$monomer(H_2O)_6$	-1051.7269	0.077	0.141	-1051.7033	-1051.6822	-1051.7799	-1051.8234
$monomer(H_2O)_4^-$	-898.31656	0.066	0.118	-898.29815	-898.28215	-898.36368	-898.40046
$monomer(H_2O)_4^{2-}$	-897.65799	0.063	0.113	-897.64072	-897.62558	-897.70364	-897.7389
$monomerNa(H_2O)_3$	-984.19269	0.063	0.114	-984.17483	-984.15949	-984.23782	-984.27317
$monomerNa_2(H_2O)_6$	-1375.3238	0.084	0.155	-1375.2967	-1375.2735	-1375.3805	-1375.4281
$dimerH_2O$	-1186.165	0.058	0.105	-1186.1489	-1186.1337	-1186.2065	-1186.239
dimerH2O	-1186.1599	0.06	0.109	-1186.1434	-1186.1281	-1186.2032	-1186.2369
$dimerH_2O^-$	-1185.6443	0.058	0.105	-1185.6286	-1185.6143	-1185.687	-1185.7197
$dimer(H_2O)_2$	-1262.6084	0.065	0.119	-1262.5895	-1262.5721	-1262.6543	-1262.6911
$dimer(H_2O)_3$	-1262.5993	0.066	0.122	-1262.58	-1262.5624	-1262.6465	-1262.684
$dimer(H_2O)_2^-$	-1262.0867	0.064	0.116	-1262.0688	-1262.0522	-1262.1325	-1262.1685
$dimer(H_2O)_2^{2-}$	-1261.4395	0.061	0.111	-1261.4226	-1261.4069	-1261.4838	-1261.5183
$dimer(H_2O)_7$	-1644.8244	0.09	0.171	-1644.7938	-1644.7652	-1644.8839	-1644.9359
$trimer(H_2O)^-$	-1702.3101	0.068	0.126	-1702.2896	-1702.2701	-1702.3573	-1702.3959
$dimerNa(H_2O)_3$	-1500.8452	0.073	0.134	-1500.8227	-1500.8023	-1500.8954	-1500.9368
$dimerNa_2(H_2O)_6$	-1891.9649	0.098	0.183	-1891.9326	-1891.9042	-1892.031	-1892.0872
$trimerNa(H_2O)_3$	-2017.5068	0.086	0.162	-2017.4783	-2017.4521	-2017.5647	-2017.6143
$trimerNa_2(H_2O)_4$	-2408.6281	0.11	0.207	-2408.5898	-2408.5557	-2408.6994	-2408.7625
$3ring(H_2O)^-$	-1625.8556	0.061	0.113	-1625.8379	-1625.8207	-1625.8992	-1625.934
$3ringNa(H_2O)_3$	-1941.0548	0.078	0.146	-1941.0296	-1941.0061	-1941.1077	-1941.1524
$3ringNa_2(H_2O)_4$	-2332.1757	0.102	0.192	-2332.1411	-2332.1098	-2332.2432	-2332.3019
$tetramer(H_2O)^-$	-2218.9696	0.08	0.15	-2218.9438	-2218.9189	-2219.0235	-2219.0694
$tetramerNa(H_2O)_3$	-2534.1605	0.098	0.187	-2534.1262	-2534.0945	-2534.2246	-2534.2815
$tetramerNa_2(H_2O)_4$	-2925.2922	0.117	0.225	-2925.2496	-2925.2105	-2925.367	-2925.4351
$4ring(H_2O)^-$	-2142.5261	0.074	0.139	-2142.5029	-2142.4804	-2142.5766	-2142.6189

4ring$Na(H_2O)_3$	-2457.7086	0.092	0.174	-2457.6776	-2457.6485	-2457.7695	-2457.8225
4ring$Na_2(H_2O)_4$	-2848.8411	0.112	0.214	-2848.801	-2848.7643	-2848.9131	-2848.9779
fused3ring$Na(H_2O)_3$	-2381.255	0.083	0.156	-2381.2277	-2381.2018	-2381.3105	-2381.3582
fused3ring$Na_2(H_2O)_4$	-2772.3928	0.109	0.206	-2772.3549	-2772.3203	-2772.4636	-2772.5263

b. Calculation on species with COSMO solvation

	E+ZPE	TS		H		G	
T (K) ->	0	298	450	298	450	298	450
NaOH	-238.19943	0.028	0.045	-238.19498	-238.19226	-238.22259	-238.23724
OH^-	-75.962814	0.02	0.032	-75.95951	-75.957827	-75.979109	-75.989461
H_2O	-76.433501	0.022	0.036	-76.429723	-76.427761	-76.451882	-76.463596
monomer	-593.06788	0.038	0.067	-593.05972	-593.05234	-593.09801	-593.11907
$monomer^-$	-592.61813	0.038	0.066	-592.61018	-592.60333	-592.64836	-592.66927
$monomer^{2-}$	-592.14532	0.036	0.063	-592.1382	-592.132	-592.17466	-592.19455
$monomer^{3-}$	-591.64689	0.036	0.061	-591.64026	-591.63466	-591.67585	-591.69517
$monomer^{4-}$	-591.12366	0.034	0.057	-591.11784	-591.11295	-591.15195	-591.17036
monomerNa	-754.85498	0.041	0.07	-754.84679	-754.83985	-754.8874	-754.90957
$monomerNa_2$	-916.63944	0.046	0.08	-916.62873	-916.61982	-916.67447	-916.69968
$monomerNa_3$	-1078.4133	0.048	0.085	-1078.4016	-1078.392	-1078.4499	-1078.4766
$monomerNa_4$	-1240.1774	0.05	0.089	-1240.165	-1240.1547	-1240.2154	-1240.2433
dimer	-1109.7055	0.053	0.095	-1109.6923	-1109.6798	-1109.7449	-1109.7744
$dimer^-$	-1109.269	0.051	0.091	-1109.2561	-1109.244	-1109.3069	-1109.3353
$dimer^{2-}$	-1108.8079	0.047	0.085	-1108.7962	-1108.7848	-1108.8436	-1108.8701
$dimer^{3-}$	-1108.34	0.049	0.087	-1108.3282	-1108.3174	-1108.377	-1108.4041
$dimer^{4-}$	-1107.861	0.045	0.079	-1107.8508	-1107.8409	-1107.8953	-1107.92
dimerNa	-1271.5053	0.055	0.1	-1271.4904	-1271.477	-1271.5459	-1271.577
$dimerNa_2$	-1433.2903	0.059	0.106	-1433.2743	-1433.2601	-1433.333	-1433.3659
trimer	-1626.3467	0.064	0.118	-1626.3278	-1626.3096	-1626.3914	-1626.4277
$trimer^-$	-1625.9156	0.059	0.11	-1625.8985	-1625.8816	-1625.9578	-1625.9916
$trimer^{2-}$	-1625.4661	0.059	0.109	-1625.4491	-1625.4326	-1625.508	-1625.5415
$trimer^{3-}$	-1624.9939	0.058	0.107	-1624.9775	-1624.9615	-1625.0358	-1625.0689
$trimer^{4-}$	-1624.5258	0.058	0.106	-1624.5099	-1624.4945	-1624.5677	-1624.6004
trimerNa	-1788.1522	0.066	0.122	-1788.1322	-1788.1134	-1788.198	-1788.2355
$trimerNa_2$	-1949.9534	0.072	0.133	-1949.9314	-1949.9116	-1950.0035	-1950.0444
3ring	-1549.9092	0.061	0.112	-1549.8921	-1549.8759	-1549.953	-1549.9875
$3ring^-$	-1549.4656	0.055	0.101	-1549.4505	-1549.4355	-1549.5051	-1549.5361
$3ring^{2-}$	-1549.0168	0.054	0.099	-1549.0021	-1548.9877	-1549.0559	-1549.0864
$3ring^{3-}$	-1548.5614	0.053	0.096	-1548.5474	-1548.5336	-1548.6	-1548.6297
$3ring^{4-}$	-1548.0918	0.05	0.091	-1548.0789	-1548.0661	-1548.1289	-1548.157
3ringNa	-1711.7081	0.06	0.111	-1711.6905	-1711.6738	-1711.7508	-1711.785
$3ringNa_2$	-1873.5031	0.064	0.118	-1873.4841	-1873.4666	-1873.5479	-1873.5842
3-1ring	-2066.5528	0.069	0.131	-2066.5311	-2066.5098	-2066.6005	-2066.6404

3-1ring$^-$	-2066.1187	0.065	0.122	-2066.0988	-2066.079	-2066.1637	-2066.201
3-1ring^{2-}	-2065.683	0.067	0.126	-2065.6625	-2065.6427	-2065.7299	-2065.7685
3-1ring^{3-}	-2065.1963	0.065	0.122	-2065.1766	-2065.1574	-2065.2419	-2065.2792
3-1ring^{4-}	-2064.7483	0.064	0.119	-2064.7295	-2064.711	-2064.7938	-2064.8304
d3ring	-2870.5228	0.075	0.144	-2870.4976	-2870.4724	-2870.5729	-2870.6166
d3ring$^-$	-2870.0841	0.075	0.143	-2870.0595	-2870.0353	-2870.1349	-2870.1784
d3ring^{2-}	-2869.6403	0.073	0.14	-2869.6162	-2869.5922	-2869.6894	-2869.7318
d3ring^{3-}	-2869.1866	0.074	0.14	-2869.1628	-2869.1393	-2869.2366	-2869.2792
d3ring^{4-}	-2868.7287	0.07	0.132	-2868.7065	-2868.6841	-2868.776	-2868.8162
fused3	-1990.1077	0.063	0.118	-1990.0887	-1990.0698	-1990.1515	-1990.1875
fused3$^-$	-1989.6766	0.061	0.114	-1989.6584	-1989.6403	-1989.7194	-1989.7543
fused3^{2-}	-1989.2258	0.06	0.111	-1989.2083	-1989.1907	-1989.2679	-1989.302
fused3^{3-}	-1988.7643	0.06	0.111	-1988.7469	-1988.7298	-1988.8069	-1988.8411
fused3^{4-}	-1988.3051	0.063	0.115	-1988.2879	-1988.2713	-1988.3511	-1988.3867
3-2ring	-2583.1886	0.081	0.155	-2583.1616	-2583.1349	-2583.2429	-2583.29
3-2ring$^-$	-2582.7624	0.081	0.154	-2582.7359	-2582.7099	-2582.8168	-2582.8635
3-2ring^{2-}	-2582.325	0.078	0.148	-2582.2996	-2582.2745	-2582.3772	-2582.422
tetramer	-2142.9849	0.075	0.141	-2142.9609	-2142.9375	-2143.0355	-2143.0785
tetramer$^-$	-2142.5597	0.074	0.139	-2142.5363	-2142.5136	-2142.6102	-2142.6526
tetramer^{2-}	-2142.118	0.071	0.133	-2142.0958	-2142.074	-2142.1666	-2142.2072
tetramer^{3-}	-2141.6575	0.07	0.131	-2141.636	-2141.6151	-2141.7057	-2141.7457
tetramer^{4-}	-2141.1903	0.068	0.128	-2141.1696	-2141.1491	-2141.238	-2141.2772
tetramerNa							
tetramerNa$_2$	-2466.5914	0.079	0.15	-2466.5653	-2466.5408	-2466.6447	-2466.6903
tetrahedron	-1913.6502	0.057	0.106	-1913.6338	-1913.6172	-1913.6906	-1913.723
tetrahedron$^-$	-1913.2163	0.055	0.102	-1913.2007	-1913.1848	-1913.2558	-1913.2872
tetrahedron^{2-}	-1912.7747	0.055	0.102	-1912.7593	-1912.744	-1912.8147	-1912.8462
tetrahedron^{3-}	-1912.3266	0.053	0.099	-1912.3121	-1912.2974	-1912.3656	-1912.3959
tetrahedron^{4-}	-1911.8714	0.051	0.094	-1911.8578	-1911.8438	-1911.909	-1911.9381
4ring	-2066.5469	0.068	0.126	-2066.5267	-2066.5068	-2066.5944	-2066.6331
4ring$^-$	-2066.1199	0.068	0.127	-2066.0992	-2066.0789	-2066.1669	-2066.2056
4ring^{2-}	-2065.674	0.066	0.124	-2065.6539	-2065.6342	-2065.72	-2065.7578
4ring^{3-}	-2065.2136	0.065	0.121	-2065.1941	-2065.175	-2065.2591	-2065.2963
4ring^{4-}	-2064.7477	0.064	0.119	-2064.7287	-2064.7102	-2064.7928	-2064.8293
4ringNa							
4ringNa$_2$	-2390.1512	0.075	0.141	-2390.127	-2390.1042	-2390.2021	-2390.2452
4-one-ring	-2506.7544	0.072	0.138	-2506.731	-2506.7074	-2506.8034	-2506.8453
4-one-ring$^-$	-2506.3243	0.077	0.145	-2506.2995	-2506.2756	-2506.3764	-2506.4206
4-one-ring^{2-}	-2505.8747	0.073	0.137	-2505.8517	-2505.8293	-2505.9244	-2505.9662
4-one-ring^{3-}							

4-one-ring^{4-}	-2504.9571	0.072	0.135	-2504.9349	-2504.9134	-2505.0068	-2505.048
4-three-ring	-2506.755	0.075	0.142	-2506.7304	-2506.7061	-2506.805	-2506.8481
4-three-ring^{-}	-2506.3333	0.072	0.137	-2506.3098	-2506.2863	-2506.3818	-2506.4235
4-three-ring^{2-}	-2505.8782	0.071	0.134	-2505.8556	-2505.8331	-2505.9263	-2505.9671
4-three-ring^{3-}	-2505.4228	0.071	0.134	-2505.4001	-2505.3778	-2505.4711	-2505.512
4-three-ring^{4-}	-2504.9683	0.07	0.132	-2504.9463	-2504.9246	-2505.0161	-2505.0562
4-1-ring	-2583.1852	0.084	0.16	-2583.1575	-2583.1305	-2583.2417	-2583.2902
4-1-ring^{-}	-2582.7572	0.08	0.152	-2582.7311	-2582.7053	-2582.8108	-2582.8569
4-1-ring^{2-}	-2582.3141	0.079	0.149	-2582.2888	-2582.2638	-2582.3674	-2582.4127
4-1-ring^{3-}	-2581.8581	0.072	0.138	-2581.8348	-2581.8111	-2581.9071	-2581.9489
4-1-ring^{4-}	-2581.3993	0.077	0.145	-2581.3751	-2581.3513	-2581.4519	-2581.4961
4-2-ring							
4-2-ring^{-}	-3099.414	0.092	0.177	-3099.3821	-3099.3508	-3099.474	-3099.5274
4-2-ring^{2-}	-3098.9749	0.089	0.171	-3098.9439	-3098.9135	-3099.033	-3099.0847
fused4_ring	-3023.3964	0.09	0.171	-3023.366	-3023.3364	-3023.4558	-3023.5078
fused4_ring^{1-}	-3022.9755	0.085	0.163	-3022.9462	-3022.9173	-3023.0312	-3023.0805
fused4_ring^{2-}	-3022.5317	0.085	0.162	-3022.5031	-3022.4751	-3022.5882	-3022.6374
fused4_ring^{3-}	-3022.0775	0.084	0.16	-3022.0493	-3022.0216	-3022.1328	-3022.1812
fused4_ring^{4-}	-3021.6162	0.083	0.158	-3021.5885	-3021.5613	-3021.6712	-3021.7191
pentamer	-2659.6262	0.086	0.164	-2659.5971	-2659.5685	-2659.683	-2659.7329
pentamerNa	-2821.4367	0.09	0.171	-2821.4059	-2821.3765	-2821.4958	-2821.5478
pentamer^{-}	-2659.2053	0.086	0.164	-2659.1764	-2659.1485	-2659.2627	-2659.3125
pentamer^{2-}	-2658.7643	0.083	0.159	-2658.7364	-2658.7092	-2658.8196	-2658.8677
pentamer^{3-}	-2658.3233	0.083	0.157	-2658.2957	-2658.269	-2658.3785	-2658.4263
pentamer^{4-}	-2657.8453	0.079	0.15	-2657.8195	-2657.794	-2657.8985	-2657.9441
5ring	-2583.1906	0.083	0.158	-2583.1628	-2583.1358	-2583.2458	-2583.2939
5ring^{-}	-2582.7697	0.08	0.152	-2582.7432	-2582.7173	-2582.823	-2582.8692
5ring^{2-}	-2582.3281	0.071	0.134	-2582.3061	-2582.284	-2582.3773	-2582.4182
5ring^{3-}	-2581.8727	0.076	0.144	-2581.8478	-2581.8233	-2581.9238	-2581.9676
5ring^{4-}	-2581.4103	0.075	0.142	-2581.386	-2581.3621	-2581.4611	-2581.5044
5ringNa	-2745.002	0.086	0.164	-2744.973	-2744.9457	-2745.0595	-2745.1093
5ringNa$_2$	-2906.8062	0.087	0.164	-2906.7767	-2906.7489	-2906.8632	-2906.9132
5-2-ring	-3540.0326	0.102	0.197	-3539.9967	-3539.9615	-3540.0989	-3540.1584
hexamer	-3176.266	0.101	0.195	-3176.2302	-3176.1957	-3176.3314	-3176.3903
hexamer^{-}	-3175.85	0.096	0.185	-3175.8163	-3175.783	-3175.9119	-3175.9676
hexamer^{2-}	-3175.4209	0.096	0.184	-3175.3875	-3175.3549	-3175.483	-3175.5385
hexamer^{3-}	-3174.9649	0.09	0.174	-3174.9336	-3174.9025	-3175.0239	-3175.0764
hexamer^{4-}	-3174.5062	0.09	0.173	-3174.4753	-3174.4444	-3174.565	-3174.6172
6ring	-3099.8282	0.092	0.177	-3099.7963	-3099.7651	-3099.8884	-3099.9419
6ring^{-}	-3099.3994	0.091	0.174	-3099.3683	-3099.3376	-3099.4589	-3099.5116
6ring^{2-}	-3098.9683	0.087	0.167	-3098.939	-3098.9097	-3099.0259	-3099.0764

6ring^{3-}	-3098.5231	0.087	0.166	-3098.4939	-3098.4645	-3098.5804	-3098.6306
6ring^{4-}	-3098.075	0.082	0.157	-3098.0479	-3098.0203	-3098.1301	-3098.1777
d4ring	-3827.3684	0.095	0.184	-3827.3345	-3827.3009	-3827.4295	-3827.485
d4ring^{-}	-3826.9264	0.091	0.178	-3826.8935	-3826.8605	-3826.9846	-3827.038
d4ring^{2-}	-3826.4806	0.089	0.174	-3826.4485	-3826.416	-3826.5377	-3826.5901
d4ring^{3-}	-3826.0275	0.089	0.172	-3825.9959	-3825.964	-3826.0844	-3826.1363
d4ring^{4-}	-3825.5689	0.087	0.169	-3825.5381	-3825.5073	-3825.6255	-3825.6766
d4-1-ring	-4344.0075	0.111	0.215	-4343.9668	-4343.9271	-4344.0775	-4344.1423
d4-1-ring^{-}							
d4-1-ring^{2-}							
4-4-ring	-4056.6689	0.114	0.221	-4056.6279	-4056.5877	-4056.7418	-4056.8083
tri4-ring	-3980.2436	0.106	0.207	-3980.2044	-3980.1659	-3980.3107	-3980.373
tri4-ring^{-}	-3979.8257	0.105	0.204	-3979.7873	-3979.7497	-3979.8925	-3979.9541
tri4-ring^{2-}	-3979.3868	0.1	0.196	-3979.3501	-3979.3135	-3979.4505	-3979.5094
tri4-ring^{3-}	-3978.9284	0.099	0.193	-3978.8924	-3978.8564	-3978.9912	-3979.0491
tri4-ring^{4-}							
open-d4ring	-3903.8083	0.101	0.197	-3903.7712	-3903.7348	-3903.8724	-3903.9317
open-d4ring^{-}	-3903.3777	0.1	0.194	-3903.3412	-3903.3056	-3903.4413	-3903.4998
open-d4ring^{2-}	-3902.9297	0.099	0.192	-3902.8941	-3902.8595	-3902.9932	-3903.051
open-d4ring^{3-}	-3902.4836	0.096	0.185	-3902.4503	-3902.4175	-3902.5466	-3902.6025
open-d4ring^{4-}	-3902.0264	0.094	0.182	-3901.9933	-3901.9607	-3902.0874	-3902.1423
d6ring	-5741.0566	0.123	0.245	-5741.0079	-5740.959	-5741.1311	-5741.2041
d6ring^{-}	-5740.6266	0.131	0.259	-5740.5755	-5740.5251	-5740.7066	-5740.7841
d6ring^{2-}	-5740.1922	0.124	0.247	-5740.1434	-5740.0941	-5740.2676	-5740.3412
d6ring^{3-}							
d6ring^{4-}							
$(H_2O)_2$	-152.86987	0.031	0.052	-152.86385	-152.8595	-152.89503	-152.91185
$(H_2O)_3$	-229.3023	0.037	0.062	-229.29481	-229.2891	-229.33137	-229.35122
$(H_2O)_4$	-305.74342	0.039	0.068	-305.73499	-305.72809	-305.77418	-305.79562
$(H_2O)_5$	-382.18912	0.05	0.09	-382.17626	-382.16521	-382.22669	-382.25473
$(H_2O)_6$	-458.62055	0.058	0.104	-458.60496	-458.59165	-458.66291	-458.69527
$(H_2O)_{10}$	-764.38446	0.073	0.137	-764.36064	-764.33864	-764.43382	-764.47576
H_3O^+	-76.807149	0.023	0.037	-76.803365	-76.801352	-76.826297	-76.838415
$H_3O(H_2O)_3^-$	-306.15712	0.045	0.078	-306.14647	-306.13759	-306.19116	-306.21582
$OH(H_2O)^-$	-152.41507	0.028	0.047	-152.41026	-152.40683	-152.43876	-152.454
$OH(H_2O)_4^-$	-381.73577	0.049	0.086	-381.72368	-381.71381	-381.77273	-381.79982
$OH(H_2O)_5^-$	-458.17238	0.054	0.096	-458.15794	-458.14526	-458.21144	-458.24138
$NaOH(H_2O)_3$	-467.5416	0.046	0.081	-467.53026	-467.52074	-467.57598	-467.60131
monomerOH$^-$	-669.06317	0.047	0.082	-669.05229	-669.04304	-669.09901	-669.12477
monomerOH^{2-}	-668.59299	0.043	0.074	-668.58349	-668.57509	-668.6261	-668.64958
monomer(H_2O)	-669.50457	0.045	0.08	-669.49372	-669.48398	-669.53868	-669.56365
monomer(H_2O)$^-$	-669.06363	0.043	0.076	-669.0536	-669.04464	-669.09709	-669.12113

monomer$(H_2O)_2$	-745.94151	0.052	0.093	-745.92801	-745.91594	-745.97967	-746.00854
monomer$(H_2O)_2^-$	-745.49906	0.05	0.089	-745.48643	-745.47531	-745.5365	-745.56437
monomer$(H_2O)_2^-$	-745.50494	0.052	0.092	-745.49186	-745.48043	-745.54355	-745.57231
monomer$(H_2O)_2^{2-}$	-745.04459	0.046	0.082	-745.03364	-745.0237	-745.07988	-745.10553
monomer$(H_2O)_3$	-822.37954	0.057	0.103	-822.36384	-822.34963	-822.4207	-822.45268
monomer$(H_2O)_4$	-898.81727	0.063	0.115	-898.79913	-898.7827	-898.86192	-898.89739
monomer$(H_2O)_6$	-1051.701	0.072	0.134	-1051.679	-1051.6587	-1051.7512	-1051.7922
monomer$(H_2O)_4^-$	-898.38067	0.061	0.111	-898.36369	-898.34834	-898.42506	-898.45958
monomer$(H_2O)_4^{2-}$	-897.92861	0.063	0.113	-897.9114	-897.8962	-897.97428	-898.00954
monomer$Na(H_2O)_3$	-984.18875	0.062	0.112	-984.17127	-984.15602	-984.23323	-984.26804
monomer$Na_2(H_2O)_6$	-1375.3071	0.083	0.153	-1375.2806	-1375.2578	-1375.3638	-1375.4111
dimerH_2O	-1186.1468	0.058	0.105	-1186.1307	-1186.1155	-1186.1884	-1186.221
dimerH2O	-1186.1428	0.06	0.11	-1186.126	-1186.1107	-1186.1864	-1186.2204
dimerH_2O^-	-1185.7096	0.057	0.104	-1185.694	-1185.6796	-1185.7515	-1185.7838
dimer$(H_2O)_2$	-1262.5878	0.063	0.115	-1262.5696	-1262.5527	-1262.6321	-1262.6676
dimer$(H_2O)_3$	-1262.5801	0.067	0.123	-1262.5609	-1262.5434	-1262.6282	-1262.6661
dimer$(H_2O)_2^-$	-1262.146	0.063	0.115	-1262.1281	-1262.1116	-1262.191	-1262.2266
dimer$(H_2O)_2^{2-}$	-1261.6994	0.06	0.11	-1261.6825	-1261.6668	-1261.7429	-1261.777
dimer$(H_2O)_7$	-1644.7829	0.088	0.166	-1644.7533	-1644.7252	-1644.8409	-1644.8915
trimer$(H_2O)^-$	-1702.3552	0.066	0.123	-1702.3353	-1702.3161	-1702.4015	-1702.4392
dimer$Na(H_2O)_3$	-1500.8322	0.072	0.134	-1500.8098	-1500.7894	-1500.8822	-1500.9234
dimer$Na_2(H_2O)_6$	-1891.9525	0.095	0.178	-1891.9208	-1891.8926	-1892.0159	-1892.0703
trimer$Na(H_2O)_3$	-2017.4763	0.084	0.158	-2017.4483	-2017.4222	-2017.5322	-2017.5805
trimer$Na_2(H_2O)_4$	-2408.5955	0.108	0.203	-2408.558	-2408.5247	-2408.666	-2408.7281
3ring$(H_2O)^-$	-1625.9066	0.061	0.113	-1625.8888	-1625.8716	-1625.9498	-1625.9845
3ring$Na(H_2O)_3$	-1941.0369	0.078	0.147	-1941.0117	-1940.9882	-1941.09	-1941.1349
3ring$Na_2(H_2O)_4$	-2332.16	0.096	0.181	-2332.1272	-2332.0968	-2332.2229	-2332.278
tetramer$(H_2O)^-$	-2218.9985	0.08	0.151	-2218.9726	-2218.9476	-2219.0525	-2219.0985
tetramer$Na(H_2O)_3$	-2534.1193	0.097	0.185	-2534.0854	-2534.0538	-2534.1823	-2534.2384
tetramer$Na_2(H_2O)_4$	-2925.2472	0.115	0.22	-2925.2057	-2925.1672	-2925.3205	-2925.3872
4ring$(H_2O)^-$	-2142.5592	0.071	0.134	-2142.5368	-2142.5147	-2142.6081	-2142.6491
4ring$Na(H_2O)_3$	-2457.6765	0.091	0.173	-2457.6455	-2457.6163	-2457.7368	-2457.7894
4ring$Na_2(H_2O)_4$	-2848.8028	0.11	0.21	-2848.7634	-2848.7267	-2848.8732	-2848.937
fused3ring$Na(H_2O)_3$	-2381.2312	0.085	0.16	-2381.2029	-2381.1763	-2381.2878	-2381.3366
fused3ring$Na_2(H_2O)_4$	-2772.3614	0.109	0.207	-2772.3234	-2772.2888	-2772.4326	-2772.4956